



TAMPEREEN TEKNILLINEN YLIOPISTO
TAMPERE UNIVERSITY OF TECHNOLOGY

Lijo George

**Light-Activated Antimicrobial Materials Based on
Perylene Imides and Phthalocyanines**



Julkaisu 1554 • Publication 1554

Tampere 2018

Tampereen teknillinen yliopisto. Julkaisu 1554
Tampere University of Technology. Publication 1554

Lijo George

Light-Activated Antimicrobial Materials Based on Perylene Imides and Phthalocyanines

Thesis for the degree of Doctor of Science in Technology to be presented with due permission for public examination and criticism in Festia Building, Auditorium Pieni Sali 1, at Tampere University of Technology, on the 6th of June 2018, at 12 noon.

Tampereen teknillinen yliopisto - Tampere University of Technology
Tampere 2018

Doctoral candidate: Lijo George
Laboratory of Chemistry and Bioengineering
Faculty of Natural Sciences
Tampere University of Technology
Finland

Supervisor: Dr. Alexander Efimov
Laboratory of Chemistry and Bioengineering
Faculty of Natural Sciences
Tampere University of Technology
Finland

Pre-examiners: Professor Marjo Yliperttula
Division of Pharmaceutical Biosciences
Faculty of Pharmacy
University of Helsinki
Finland

Dr. Nathalie Solladie
Group of Synthesis of Porphyrinic Systems
Laboratory of Coordination Chemistry, CNRS
France

Opponent: Professor Mark Wainwright
School of Pharmacy and Biomolecular Sciences
Faculty of Science
Liverpool John Moores University
United Kingdom

ISBN 978-952-15-4156-8 (printed)
ISBN 978-952-15-4159-9 (PDF)
ISSN 1459-2045

Abstract

In the era of globalization, the spread of infectious diseases is a serious concern. The emergence of drug resistant bacteria and healthcare associated infections in particular, poses a great danger to human health. Self-disinfecting surfaces may play a significant role in controlling the spread of pathogenic diseases. Photodynamic antimicrobial chemotherapy (PACT) can be a very efficient way of inactivation of drug resistant bacteria and biofilms. However, making a self-disinfecting surface based on PACT principles requires novel photosensitizers, which can efficiently generate reactive oxygen species, and are stable and accessible. In this thesis, attempts are undertaken to synthesize novel photosensitizers based on peryleneimides and phthalocyanines. We propose a novel efficient method for the direct and regioselective amination of peryleneimides. The substitution occurs with high yields exclusively at 1,6- and 7,12-positions of the bay region of perylenediimide and perylenemonoimide diester. We also report the synthesis of novel cationic peryleneimides, which can be potentially used as photosensitizers in PACT. Phthalocyanines are known to be efficient photosensitizers. In this thesis we present the synthesis of novel pyridinyl-substituted phthalocyanine and its tetracationic derivatives. As a unique synthetic approach, pyridinyl groups are connected to α -phthalo positions of the macrocycle via direct C-C bonds. Prototype self-disinfecting materials are prepared by impregnating filter paper with the synthesized dyes. Binding of the dyes occurs via electrostatic interactions and does not require any special chemical modification. A fast and simple setup for the evaluation of antimicrobial efficacies of dyed papers is proposed. The setup employs bioluminescent bacteria and allows for a fast screening of a large number of dyes. According to the screening results, tetracationic phthalocyanines are the most efficient antimicrobial photosensitizers. The antimicrobial efficacies of phthalocyanine derivatives are evaluated quantitatively with the help of colony forming unit (CFU) counting method. The papers impregnated with as little as 80 mg/m² of cationic zinc phthalocyanine exhibit 2.7 and 3.4 log reduction in CFU against *Escherichia coli* (*E. coli*) and *Acinetobacter baylyi* (*A. baylyi*), respectively after illumination with the light intensity 18 mW/cm² in a solar simulator. Similar antimicrobial efficacies are achieved under illumination with consumer light emitting diode (LED) lights. Phthalocyanine-impregnated papers show very good stability. Incubation of the dye-impregnated papers in phosphate-buffered saline demonstrates superior binding ability of phthalocyanine, with basically no detectable leaching of the dye. Photostability of the dyed paper is also high. Continuous illumination with 42 mW/cm² LED light for 64 h decreases the absorbance of dyed papers only by 10%.

Preface

The research work presented in this thesis was carried out in the Laboratory of Chemistry and Bioengineering, Tampere university of Technology from January 2015 to December 2017. The financial support from the Graduate School of Tampere University of Technology is gratefully acknowledged.

First of all, I would like to express my heartfelt gratitude to my supervisor, Dr. Alexander Efimov for giving me the opportunity to conduct research under his guidance. I truly indebted to him for his immense support and encouragement throughout the entire period. This work would not have been possible without his guidance, involvement and motivation. I appreciate him for giving me valuable suggestions and feedbacks to improve the quality of research work. I am very grateful to Assistant Prof. Ville Santala for allowing me to conduct experiments in his laboratory and for teaching the basic techniques in microbiology. I appreciate him for being co-author in our publications. I gratefully acknowledge Prof. Nikolai Tkancheko for introducing me to Synthetic Team2 group and teaching spectroscopy methods. I convey my thanks to Prof. Emeritus Helge Lemmetyinen for giving me the opportunity to work in his group. I am thankful to all the lecturers, professors and other staff at the department for creating a pleasant work atmosphere. I am particularly thankful to Mr. Arto Hiltunen, Dr. Elena Efimova, Dr. Essi Sariola-Leikas, Mr. Heikki Tirkonnen and Dr. Zafar Ahmed for the support during the years.

I would like to convey my sincere thanks to all my friends in Finland and abroad especially Mr. Ajit Kutty, Dr. Bobin George Abraham, Dr. Jinto Antony and Dr. Rahul Mangayil, for your thoughts, advice and being there whenever I needed a help. I am also grateful to Dr. Anish Philip, Mr. Ciljo Joseph, Mr. Jibin Joseph, Mr. Joby Jacob and Mr. Shaji Kumar, for their invaluable friendship. I would like to express my sincere gratitude to my parents (C.V George and Rosily George) for their love, support and prayers throughout my life. I am grateful to for my parents-in-law (A.J Poulouse and Elsy Poulouse) for their unfailing support during these years. I thank my brother Mr. Linto George, sister Mrs. Lincy George, sister-in-law Mrs. Nimi Poulouse and their families for supporting me during my doctoral studies. I express my deep gratitude to my beloved wife, Simi Poulouse for her love, care, understanding and prayers. Her support and encouragement is an important factor in the completion of this thesis. I also thank my lovely children, Lizbeth Mariam and Joanna Mariam, for giving me much happiness and joy in my life. Above all, I thank Jesus Christ for all his blessings bestowed upon me.

Lijo George

Contents

ABSTRACT	I
PREFACE.....	III
CONTENTS.....	V
LIST OF SYMBOLS AND ABBREVIATIONS	VII
LIST OF PUBLICATIONS	XI
AUTHOR'S CONTRIBUTION	XII
1. INTRODUCTION	13
2. BACKGROUND	15
2.1. Mechanism of PACT	15
2.2. Criteria of photosensitizers.....	17
2.3. Perylene diimides.....	18
2.3.1. Preparation of PDI derivatives.....	19
2.3.1.1. Imidization	19
2.3.1.2. Modification at perylene core.....	22
2.3.2. Strategies to improve the formation of triplet excited state in PDIs.....	24
2.4. Phthalocyanines.....	27
2.4.1. Synthesis of phthalocyanines.....	28
2.4.2. Mechanism of phthalocyanine's formation.....	29
2.4.3. Modifications	30
2.4.4. Constitutional isomers.....	31
2.5. Photoactive self-disinfecting materials and surfaces	33

3.	RESEARCH OBJECTIVES.....	37
4.	MATERIALS AND METHODS.....	39
4.1.	Characterization of substances.....	39
4.2.	Light sources.....	39
4.3.	Antimicrobial test.....	40
5.	RESULTS AND DISCUSSION.....	43
5.1.	Synthesis of perylenes.....	43
5.1.1.	Regioselective 1,6-amination of perylenes.....	43
5.1.2.	Synthesis of perylene imide dyes with anchoring groups.....	51
5.1.3.	Synthesis of cationic perylene diimide dyes.....	53
5.2.	Synthesis of phthalocyanine photosensitizers.....	57
5.3.	Antimicrobial studies.....	60
5.3.1.	Screening test for the efficiency of dyes.....	61
5.3.3.	Antimicrobial efficacy using consumer LED lamp.....	66
5.3.3.1.	Lamp profile and light dose calculation.....	67
5.3.3.2.	Photostability and leaching test of dyed filter papers.....	68
5.3.3.3.	Comparison of antimicrobial efficacy by CFU counting.....	70
6.	CONCLUSIONS.....	73
6.1.	Future Perspectives.....	73
	REFERENCES.....	75
	APPENDIX.....	93

List of Symbols and Abbreviations

a	absorptance
A	absorbance
<i>A. baumannii</i>	<i>Acinetobacter baumannii</i>
<i>A. baylyi</i>	<i>Acinetobacter baylyi</i>
ASM	American Society of Microbiology
BODIPY	boron-dipyrromethene
CFU	colony forming unit
COSY	correlation spectroscopy
CuPc	copper phthalocyanine
DBB	o-dibenzoyl benzene
DBU	1,8-diazabicyclo[5.4.0]undec-7-ene
DMAE	2-(dimethylamino)-ethanol
DMF	dimethylformamide
DMSO	dimethyl sulfoxide
DPBF	1,3-diphenylisobenzofuran
<i>E. coli</i>	<i>Escherichia coli</i>
ET	electron transfer
gHMBC	gradient-selected heteronuclear multiple-bond correlation spectroscopy
gHSQC	gradient-selected heteronuclear single quantum coherence spectroscopy

HAI	hospital acquired infection, healthcare associated infection
HRMS	high-resolution mass spectrometry
ICU	intensive care unit
IS	integrating sphere
ISC	intersystem crossing
LB	lysogeny broth
LED	light emitting diode
MCPc	monocarboxy phthalocyanine
MPc	metal phthalocyanine
NMR	nuclear magnetic resonance
MRSA	methicillin-resistant <i>Staphylococcus aureus</i>
<i>P. aeruginosa</i>	<i>Pseudomonas aeruginosa</i>
<i>P. vulgaris</i>	<i>Proteus vulgaris</i>
PACT	photodynamic antimicrobial chemotherapy
PBS	phosphate-buffered saline
PbTePyPc	Lead(II) N-Ethylpyridinyloxy-phthalocyanine tetraiodide
PDC	pyridinium dichromate
PDI	perylene-3,4,9,10-tetracarboxylic acid diimide
PDT	photodynamic therapy
PMI	perylene-3,4,9,10-tetracarboxylic acid-3,4-monoimide
ppm	parts per million

PTCDA	perylene-3,4,9,10-tetracarboxylic dianhydride
<i>p</i> -TSOH	<i>p</i> -toluenesulfonic acid
R	reflectance
ROS	reactive oxygen species
<i>S. aureus</i>	<i>Staphylococcus aureus</i>
SAPYR	(2-((4-pyridinyl)methyl)-1H-phenalen-1-one chloride)
SOC	spin-orbit coupling
T	transmittance
TLC	thin layer chromatography
TMPyP	5,10,15,20-tetrakis(1-methyl-4-pyridinyl)-porphyrin tetra-(<i>p</i> -toluenesulfonate)
<i>trans</i> -MePy ⁺ -NH ₂	<i>trans</i> -pyridinium aminoporphyrin
ZnMCsPc	Zinc(II) monocysteinyll phthalocyanine
ZnMPCPc	Zinc(II) monophenoxy-carboxyphthalocyanine
ZnPcS	Zinc(II) phthalocyanine tetrasulfonic acid tetrasodium salt
ZnTTQPc	zinc(II) (4)-tetra[2-thioquinoline]phthalocyanine
2D NMR	two-dimensional nuclear magnetic resonance spec- troscopy

List of Publications

The thesis is based on the work described in the following publications, which are hereafter be referred by their Roman numerals.

- I. Lijo George, Zafar Ahmed, Helge Lemmetyinen, Alexander Efimov. Controlled Regioselective Amination of Peryleneimides, *Eur. J. Org. Chem.* 2015, 584–590
- II. Zafar Ahmed, Lijo George, Arto Hiltunen, Helge Lemmetyinen, Terttu Hukka, Alexander Efimov. Synthesis and study of electrochemical and optical properties of substituted perylenemonoimides in solutions and on solid surfaces, *J. Mater. Chem. A*, 2015, 3, 13332-13339
- III. Lijo George, Alexander Müller, Beate Röder, Ville Santala, Alexander Efimov. Photodynamic self-disinfecting surface using pyridinium phthalocyanine, *Dyes and Pigments*, 2017, 147, 334-342
- IV. Lijo George, Arto Hiltunen, Ville Santala, Alexander Efimov. Photo-antimicrobial efficacy of zinc complexes of porphyrin and phthalocyanine activated by inexpensive consumer LED lamp. *J. Inorg. Biochem.* 2018, 183, 94-100

Author's Contribution

- I. Lijo George planned and carried out the synthesis and characterization of the compounds, interpreted the results and drafted the manuscript. Zafar Ahmed contributed in the synthesis and characterization of compounds especially the PMIs. Helge Lemmetyinen participated in the design of experiments and the interpretation of results. Alexander Efimov supervised the work and contributed into design of experiments and interpretation of the results. All co-authors contributed to writing of the manuscript.
- II. Lijo George's contribution was the synthesis and characterization of the compounds. Zafar Ahmed is the first author of the manuscript, planned the work, and contributed to the synthesis, characterization, preparation of Self-assembling monolayers, optical measurements and interpretation of the results. Arto Hiltunen performed the DPV measurements. Helge Lemmetyinen contributed to design of experiments and interpretation of the results. Terttu Hukka performed molecular modelling calculations. Alexander Efimov supervised the work and contributed into design of experiments and interpretation of the results. All co-authors contributed to writing of the manuscript.
- III. Lijo George planned and carried out the synthesis and characterization of the compounds, prepared the dye-impregnated papers, conducted the antimicrobial tests, interpreted the results and drafted the manuscript. Alexander Müller and Beate Roeder measured the quantum yield of singlet oxygen and cell viability assays. Ville Santala supervised the antimicrobial studies at TUT. Alexander Efimov supervised the work and contributed into design of experiments and interpretation of the results. All co-authors contributed to writing of the manuscript.
- IV. Lijo George planned and carried out the synthesis and characterization of the compounds, prepared the dye-impregnated papers, conducted the antimicrobial tests, interpreted the results and drafted the manuscript. Arto Hiltunen performed the measurement of the lamp profile, light intensities and absorptance of the dye-impregnated papers. Ville Santala supervised the antimicrobial studies at TUT. Alexander Efimov supervised the work and contributed into design of experiments and interpretation of the results. All co-authors contributed to writing of the manuscript.

1. Introduction

The rapid spread of infectious diseases due to the increased human mobility poses a serious risk to the human health.¹⁻³ This is evident from the recent outbreaks of deadly diseases such as SARS, H1N1 flu, MERS and Ebola hemorrhagic fever that claimed many lives.⁴⁻⁹ Another major concern is Nosocomial or Healthcare Associated Infections (HAIs) that lead to serious morbidity and mortality among the patients across the world. HAIs cause longer hospital stay and bring a financial burden to both patients and hospitals.¹⁰⁻¹⁴ Recent data published by European surveillance system indicated that in 2015, 8.3% of patients (11788 out of 141 955) admitted to intensive care unit (ICU) were affected by at least one HAI.¹⁵ HAIs are primarily caused by the microbial contamination of the surfaces or medical devices.¹⁶⁻¹⁸ The contamination eventually leads to the formation of biofilms, which facilitates microbial proliferation. The biofilm infections are extremely resistant to antibiotics treatment and require considerable efforts for their eradication.¹⁹ The emergence of antibiotic resistant bacteria such as ESKAPE pathogens (*Enterococcus faecium*, *Staphylococcus aureus*, *Klebsiella pneumoniae*, *Acinetobacter baumannii*, *Pseudomonas aeruginosa* and *Enterobacter* strains) increased the risk of HAIs several times.²⁰⁻²³ For example, methicillin-resistant *S. aureus* (MRSA) can cause infections in bones, artificial joints, surgical wounds, in the bloodstream, heart valves and lungs and often leads to life-threatening complications.²⁴⁻²⁸ The prevalence of deadly hospital acquired MRSA infections in developed countries like Canada between 1995 and 2014 is shown in Figure 1.1.²⁹ The extent of the spread of HAIs in underdeveloped and developing countries is much higher.³⁰

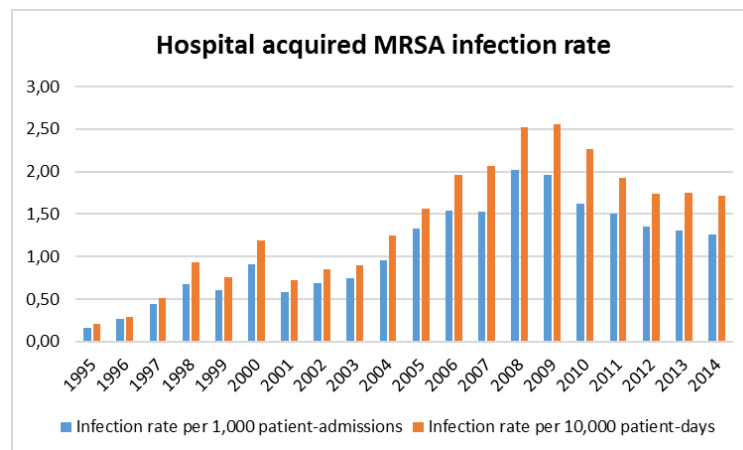


Figure 1.1: Infection rate of hospital acquired MRSA in Canada.²⁹

Self-disinfecting materials in the form of fabrics, facemasks, filters and paints or coatings play a key role in controlling the transmission of pathogenic microorganisms.³¹⁻³⁵ Generally, these materials utilize the chemotherapeutic effects of antibiotics or employ inorganic substances such as silver, copper and their oxides to reduce the microbial growth. However, for the effective functioning of these materials, the direct contact with the microbes is required.³⁶⁻⁴¹ Moreover, these materials induce resistance in bacteria thereby diminishing the effectiveness.^{42,43} Release of the active components into the environment is also a serious drawback of using the antibiotic-based self-disinfecting materials.⁴⁴⁻⁴⁶

An alternate method to circumvent the above-mentioned drawbacks is to fabricate self-disinfecting materials based on the principle of photodynamic antimicrobial chemotherapy (PACT).^{47,48} The pathogenic microorganisms are inactivated using reactive oxygen species (ROS) such as singlet oxygen, superoxide, hydroxyl radical produced by a dye (photosensitizer) upon light irradiation. The method is quite efficient and does not require a direct contact with microbes for inactivation. In addition, PACT is efficient against multi-drug resistant cultures and biofilms and does not induce resistance in pathogens.⁴⁹⁻⁵² Moreover, the applications of PACT can also be extended to prepare filters and membranes for air and water sanitization as singlet oxygen can diffuse through air and water.^{53,54}

Two important factors essentially required for the successful implementation of photoactivated self-disinfecting surface are (i) photosensitizers that can efficiently generate singlet oxygen; (ii) inexpensive and commercially available light sources. The main objective of our research work was to develop a prototype self-disinfecting material using a novel photosensitizer that can be activated under consumer LED lamp.

In this research work, efforts to develop novel photosensitizers based on perylene diimides (PDIs) and phthalocyanines were undertaken. Even though, PDIs are an industrially important class of organic chromophores, their role in PACT is very limited due to their low quantum yields in generation of singlet oxygen.⁵⁵ The quantum yield however can be improved by appropriate functionalization of PDIs. The Publications I and II used in the compilation of the thesis deal with the functionalization of PDIs. Synthesis of novel cationic PDIs and the preparation of prototype self-disinfecting surface by impregnating cationic PDIs into paper were not included in the publications and are presented in the thesis itself. In addition, a fast method to compare the antimicrobial efficacies of self-disinfecting surfaces using bioluminescent Gram-negative bacteria *E.coli* and *A. baylyi* is also described.

Synthesis of novel cationic phthalocyanine derivatives and the evaluation of the antimicrobial efficacies of phthalocyanine-impregnated papers were the subject of the Publication III. The Publication IV assesses the feasibility of using consumer LED lamp in the photoinactivation of microbes. Moreover, important parameters such as photostability and the stability against leaching of the dye-impregnated papers were also studied in this publication.

2. Background

In 1900 Oskar Raab was the first to report the ability of acridine orange to inactivate *Paramecium caudatum* under light.^{56,57} The term “photodynamic reaction” was used by his supervisor Hv Tappeiner to describe the process of inactivation of microbes by dyes in the presence of light. He also demonstrated the involvement of oxygen in the process.⁵⁸ The concept of photodynamic reaction was later successfully applied to the treatment of cancer and tumors and came to be known as Photodynamic Therapy (PDT).⁵⁶ Photodynamic antimicrobial chemotherapy (PACT) follows the same principle as that of PDT focusing on the treatment of infections caused by the pathogenic microbes.⁴⁷ The relevance of PACT, which was superseded by antibiotics since the discovery of penicillin, has increased recently with the emergence of multidrug resistant bacteria. It was demonstrated that PACT is able to inactivate multidrug resistant pathogens and biofilms.⁵⁹

2.1. Mechanism of PACT

PACT involves the inactivation of pathogenic microbes by the oxidative stress induced with the help of reactive oxygen species (ROS) such as singlet oxygen.⁶⁰ Molecular oxygen has three electronic states: a triplet ground state ($^3\Sigma_g^-$) and two singlet excited states ($^1\Delta_g$ and $^1\Sigma_g^+$) as shown in Figure 2.1. Due to the spin forbidden transition from the excited singlet state $^1\Delta_g$ to ground triplet state $^3\Sigma_g^-$, the $^1\Delta_g$ is a long-lived species whereas the spin-allowed transition $^1\Sigma_g^+ \rightarrow ^1\Delta_g$ makes the singlet excited $^1\Sigma_g^+$ short-lived.⁶¹ Due to the metastability of $^1\Delta_g$ state, the lifetime of oxygen in the singlet excited state is rather short, namely 86 ms in air and 3.5 μ s in water, respectively.⁵³ Singlet oxygen has more oxidizing power than ground state oxygen. It is highly electrophilic and could oxidize phenols, sulphides, and amines.⁶¹

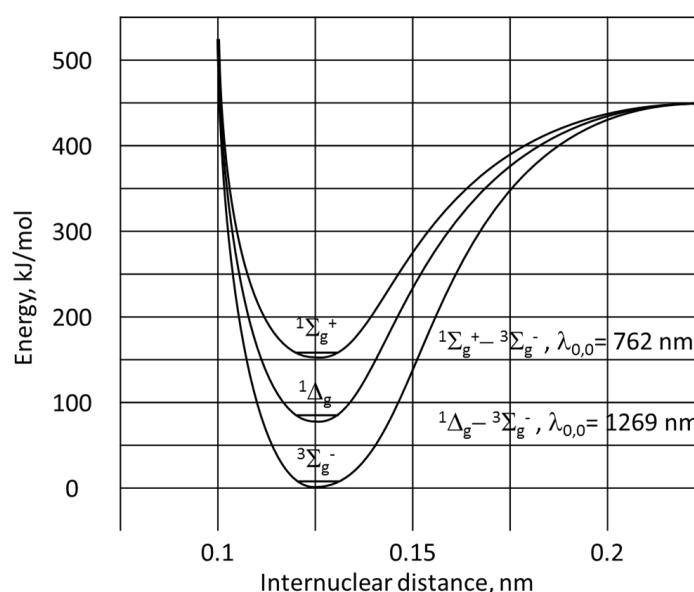


Figure 2.1: Potential energy curves for electronic states of molecular oxygen.⁶¹

Generation of singlet oxygen during the PACT process is commonly accepted to occur as follows. The dye (photosensitizer) is being excited to its singlet excited state by illumination with an appropriate wavelength. From there, the dye undergoes intersystem crossing to generate the triplet excited state. Since the lifetime of the triplet excited state is longer than that of the singlet excited state, it can undergo further a reaction in two ways, namely Type I (electron transfer) and Type II (energy transfer). Type I photo process involves a hydrogen atom abstraction or an electron transfer between the triplet state of the photosensitizer and the substrate molecule resulting in the formation of free radicals such as hydroxyl radicals, superoxide radical anions, etc. Type II mechanism generates the singlet oxygen ($^1\Delta_g$) by interaction of the triplet excited state with molecular oxygen. The process is explained in Jablonski diagram (Figure 2.2).⁶²

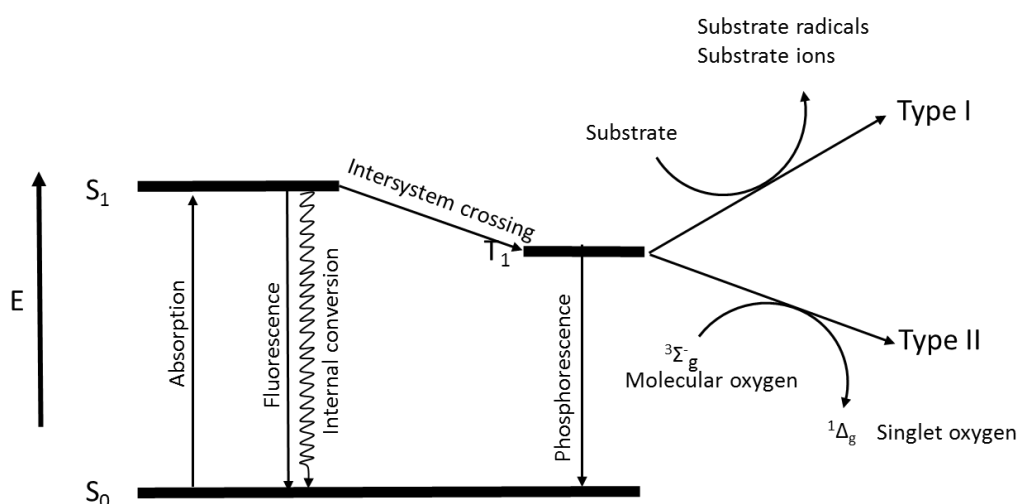


Figure 2.2: Jablonski diagram explaining the formation of singlet oxygen.⁶²

Singlet oxygen plays a major role in photooxidative damage to the microbial cells and in the destruction of molecules involved in the maintenance and structure of microbial cell walls.⁴⁷ Hydroxyl radical and superoxide radical resulting from Type I mechanism also can interact with biomolecules producing hydrogen peroxide *in situ*, thus leading to their degradation.^{60,63}

Microbes do have some defensive mechanisms against oxidative stress induced by PACT. Enzymes such as catalase, peroxidase or superoxide dismutase are able to neutralize ROS. However, these mechanisms were found to be inefficient against photodynamic action. The reason is that ROS have so short lifetime, high reactivity and so limited diffusion, that intercellular defence mechanisms could not have enough time to effectively neutralize the localized outburst of oxygen species at the outer membrane. Moreover, simultaneous photodamage at multiple sites of microbes make them less likely to survive.⁶⁰

2.2. Criteria of photosensitizers

As it was explained in the previous paragraph, photosensitizers generate ROS which induce oxidative stress in pathogenic microorganisms. An ideal candidate should meet the following criteria:⁶⁴⁻⁶⁶

- High singlet oxygen quantum yield
- Photostability
- Broad absorption wavelength and high extinction coefficient ($>20000 \text{ M}^{-1}\text{cm}^{-1}$).
- Antimicrobial action over a wide range of microorganisms such as bacteria, fungi and parasites
- High binding affinity for microorganism
- Low binding affinity for mammalian cells
- Low toxicity and low mutagenicity
- No dark toxicity
- Absorbance in the “Therapeutic window” 600-1000 nm

Antimicrobial efficiency of different photosensitizers varies greatly and depends not only on the singlet oxygen quantum yield, but also on other factors. According to the specification of American Society of Microbiology (ASM), the term “antimicrobial” or “antibacterial” can be used if a substance demonstrates an efficacy of 3 log reduction in CFU against microorganisms.⁶⁷ Studies have shown that the cell wall’s structure of various pathogens such as Gram-positive and Gram-negative bacteria and fungi can affect the susceptibility towards PACT. Gram-positive bacteria were found to be susceptible towards anionic and neutral photosensitizers, whereas Gram-negative bacteria were better inactivated by positively charged photosensitizers.^{68,69} Factors such as molecular weight, structure and pH of the photosensitizers influence the susceptibility toward PACT. At different pH, the charge on the functional groups of the photosensitizers could change thereby affecting the PACT.⁷⁰ The influence of molecular weight and structure was demonstrated by the difference in activity between porphyrin-based photosensitizer TMPyP (5,10,15,20-tetrakis(1-methyl-4-pyridinyl)-porphyrin tetra-(*p*-toluenesulfonate)) and 7-perinaphthenone-based photosensitizer SAPYR(2-((4-pyridinyl)methyl)-1H-phenalen-1-one chloride). Even though, TMPyP has 4.8 times higher singlet oxygen quantum yield than SAPYR, it was not able to inactivate *Enterococcus faecalis* biofilms, which were prone to SAPYR treatment. This was explained by the high molecular weight and large structure of TMPyP, which limited its diffusion through the extracellular matrix of biofilms thereby lowering its activity.⁷¹

The important classes of photosensitizers used for PACT are: 1) phenothiazines such as methylene blue, new methylene blue and toluidine blue O; 2) porphyrins and phthalocyanines; 3) fullerenes; 4) curcumin; 5) boron-dipyrromethenes (BODIPYs); 6) ruthenium complexes; 7) rose Bengal (Figure 2.3).^{48,62,65} Recently, other classes of stable industrial dyes such as perylene diimides are being under development as new photosensitizer for PACT application. In the following sections, chemistry of perylene diimide and phthalocyanine dyes will be discussed in detail.

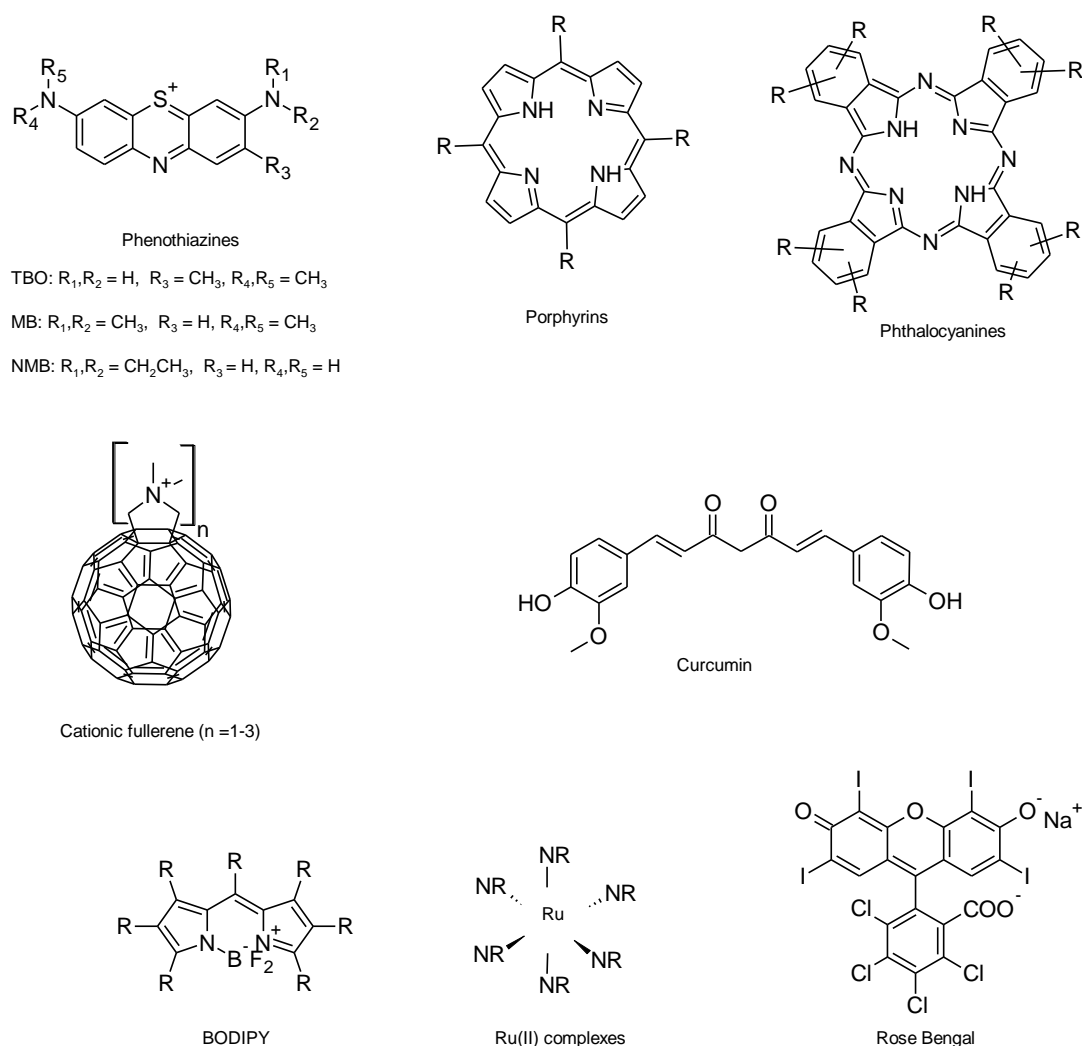


Figure 2.3: Important classes of photosensitizers used for PACT.

2.3. Perylene diimides

Perylene-3,4,9,10-tetracarboxylic acid diimide derivatives (commonly known as perylene diimides, PDIs) are an important class of organic dyes that have been utilized in industry for many decades. However, the use of PDIs in photodynamic therapy, particularly in PACT is largely unexplored. This is mainly because the triplet excited state of unsubstituted PDIs is poorly populated by photoexcitation.⁵⁵ The low triplet excitation, in turn significantly decreases the ability of PDI to generate singlet oxygen thereby hindering its usage for PACT applications. However, the photochemistry of perylene imides can change dramatically upon chemical modification, and an appropriate substitution can make PDIs efficient photosensitizers. In this section, general methods for the synthesis and functionalization of PDIs will be described. In addition, strategies to enhance the formation of triplet-excited state in PDIs thereby improving their capability to generate singlet oxygen will be reviewed.

Ever since the discovery by Kardos in 1913, PDIs were used as industrial colorants both as dyes and as pigments in paints, fibres and automobile industry because of their high chemical-, thermal-

and photo-stability.⁷² PDIs also have high fluorescence quantum yield, high photochemical stability, relatively high molar absorptions, excellent redox properties and strong electron-accepting nature.⁷³⁻⁷⁵ As it was mentioned, the properties of PDIs could be altered by appropriate functionalization depending on the requirements of the application. Notably, PDIs have found use in wide range of advanced applications such as sensors, laser dyes, n-type semiconductors, organic field effect transistors, electrophotography, fluorescent light collectors, organic photovoltaics and optical power limiters.⁷⁶⁻⁸¹

2.3.1. Preparation of PDI derivatives

2.3.1.1. Imidization

PDI derivatives are generally prepared by the condensation reaction between perylene-3,4,9,10-tetracarboxylic dianhydride (PTCDA) and a suitable amine.⁸² Industrially relevant PDIs such as Pigment Red 179 and Pigment Red 149 are shown in Figure 2.4.^{74,82}

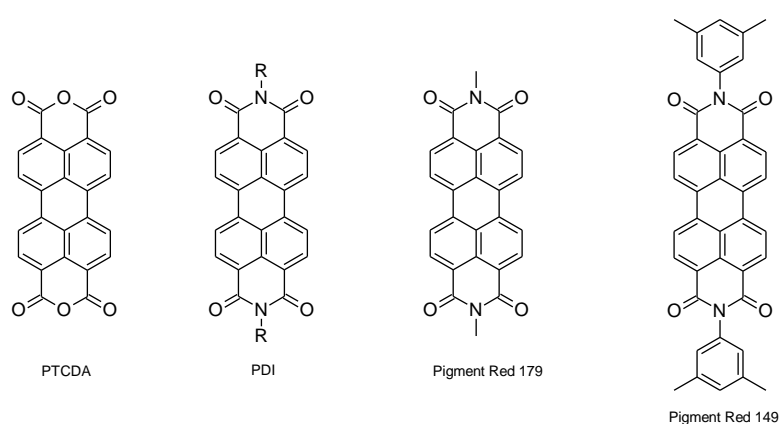


Figure 2.4: Chemical structures of PTCDA, PDI and commercially available PDIs.

Generally, substitution at imide position does not affect the electronic and optical properties of PDI.⁷⁵ However, it has much larger role in deciding the properties such as aggregation, solubility and molecular packing in the solid state.^{82,83} Depending on the type of substituents at the imide position, solubility of PDI can be controlled and tweaked for a particular solvent. For example, PDIs with reasonable solubility in non-polar organic solvents were synthesized by Langhals and co-workers using “swallowtail” substituents at PDI imide positions (Figure 2.5).⁸³ These bulky groups are protruding out of plane of the chromophore thereby disrupting the face-to-face π - π stacking of PDIs.

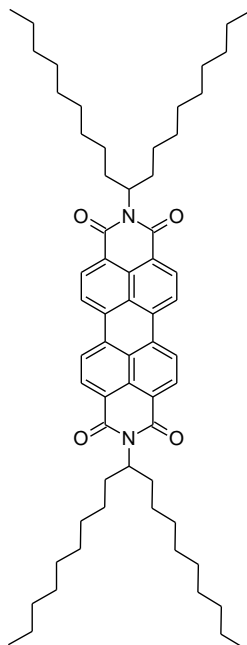
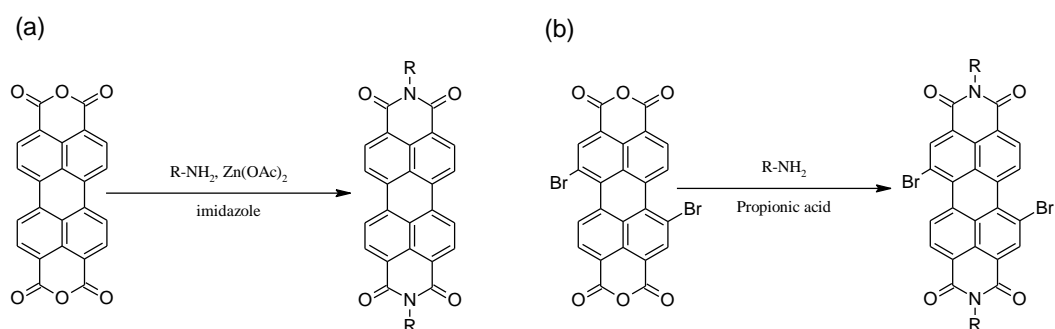


Figure 2.5: PDI with swallowtail substituent.

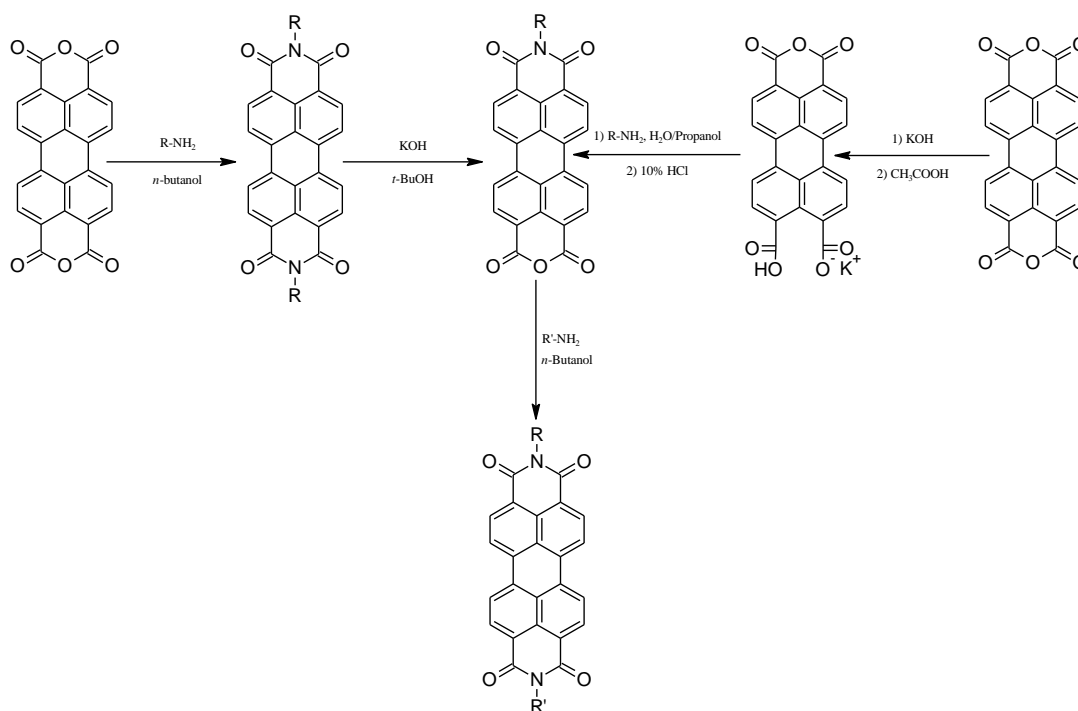
Symmetrically *N,N'*-substituted PDIs were prepared with high yields by the condensation reaction of unsubstituted PTCDA with aliphatic or aromatic amines in molten imidazole or quinoline in the presence of anhydrous zinc acetate.^{82,84} Alternatively, dibromo- or tetrachloro-substituted PTCDA were converted into corresponding PDIs with high yields by the reaction with primary amines in hot alcohols, in acetic or propionic acid, or in an alcohol/water mixture (Scheme 2.1).^{85,86}



Scheme 2.1: Synthetic routes for the preparation of symmetrical PDI.

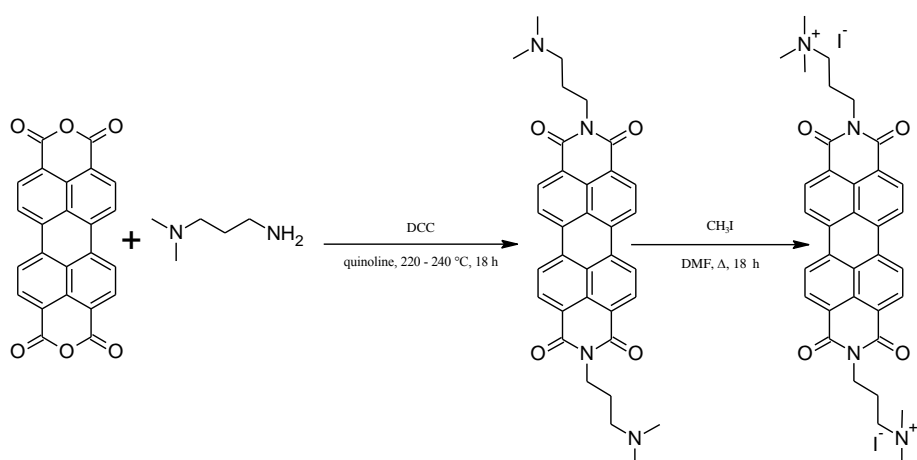
On the other hand, preparation of asymmetrical diimides of perylene with different substituents at imide nitrogens required a complex multi-step synthesis. Usually, a symmetrical diimide was partially hydrolysed to obtain perylene monoimide monoanhydride compound. The resultant mixed imide-anhydride was imidized with a second amine to yield asymmetrical PDI.⁸⁴ Attempts for a direct synthesis of perylene monoimide monoanhydride from PTCDA always resulted in the formation of symmetrical PDI as the predominant product. This is the reason why the partial hydrolysis of symmetrical PDI was established as a preferred route for the synthesis of asymmetrical PDI. Another possible

method is the partial hydrolysis of PTCDA into mixed anhydride-dicarboxylate salt. Successive imidization of anhydride-dicarboxylate salt provides desired asymmetrical PDI (Scheme 2.2).^{74,84}



Scheme 2.2: Synthetic methods for the preparation of asymmetrical PDIs.

PDIs which are soluble in aqueous solutions can also be prepared by imidization reaction. Hydrophilic substituents such as quaternary ammonium salts, carboxylate salts, phosphate residues, polyglycerol dendrons, and cyclodextrin moieties were incorporated at the imide site thus making perylene imides water-soluble (Scheme 2.3).⁸⁷⁻⁹¹



Scheme 2.3: Synthesis of water soluble PDI.

2.3.1.2. Modification at perylene core

Substitution at the imide position has negligible influence on the redox potential and absorption properties of PDI, since the imide substituents are not electronically connected to the perylene core.⁷⁵ However, modification at the PDI macrocycle itself alters these properties significantly. This provides a unique opportunity to tune the functional properties of PDI by core substitution, while maintaining its self-assembly properties or an ability for anchoring through imide substituents. Moreover, PDI core substitutions with appropriate groups also improve the solubility by several orders.⁷⁴ The functional positions in PDI core are shown in Figure 2.6.

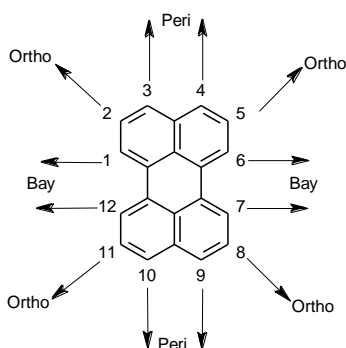
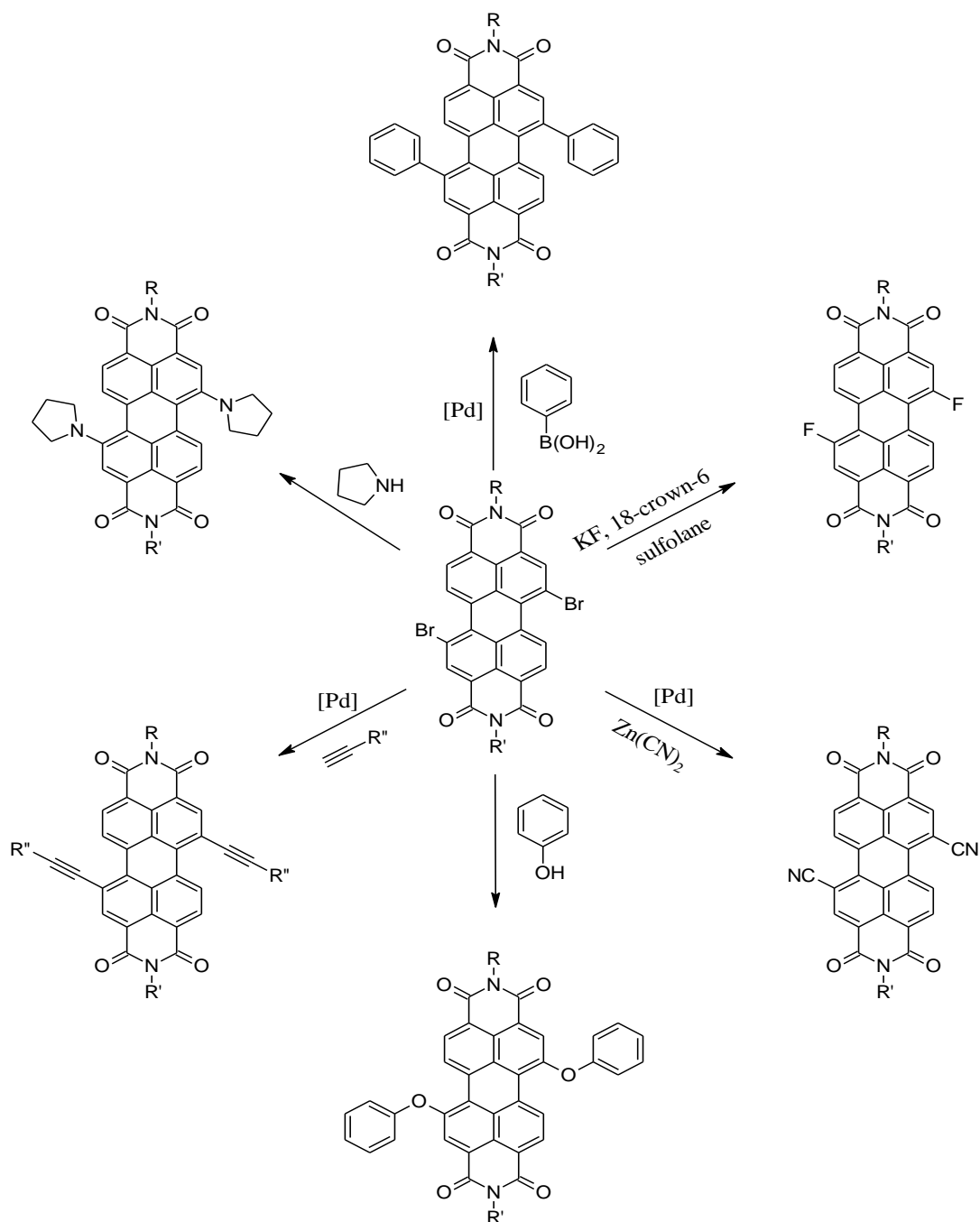


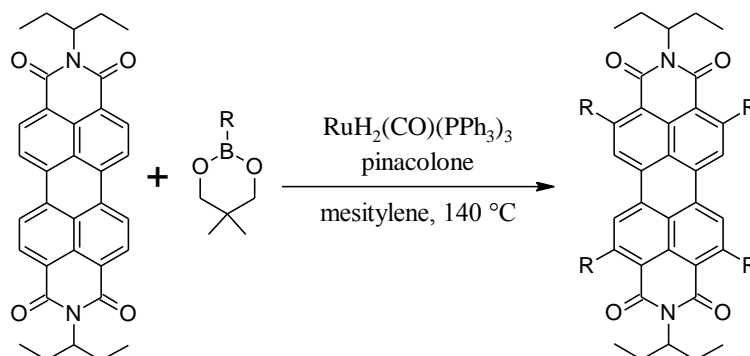
Figure 2.6: Structure of perylene core showing bay-, ortho- and peri- positions.

Most commonly, the functionalization of PDI core is done by modifying the peri- and bay-positions. However, functionalization of ortho positions were also reported.⁹² One important breakthrough in PDI core modification is the bay region bromination with further substitution, developed by Frank Wuerthner.^{75,86} The bromination reaction yielded predominantly 1,7- dibromo PDI in high yields. PDIs with different electronic and optical properties were synthesized by exchanging the bromo substituents in bay region with various nucleophiles.^{93–96} Moreover, various aryl-, heteroaryl-, and alkenyl functionalized PDIs were synthesized starting from dibromo-PDIs via Suzuki and Stille metal-catalysed cross-coupling reactions (Scheme 2.4).^{97–99} Direct core substitution of PDIs at bay positions without the use of bromine substitutions has also been reported recently.¹⁰⁰



Scheme 2.4: Some common methods for the bay-functionalization of PDIs.

Substitution at ortho positions of the PDI core is done by direct C-H bond functionalization. Nakazono and co-workers synthesized ortho-substituted tetraaryl PDIs from unsubstituted PDI using this approach (Scheme 2.5).^{92,101} Similarly, the modifications at ortho positions using bromine, chlorine, cyano, alkyl and various aryl substituents were also reported by different groups.^{92,101–103} Ortho-substitution of PDIs with alkyl groups significantly improves the solubility and emission in the solid state. Moreover, ortho-substitution with appropriate aryl groups significantly enhances the formation of the triplet excited state. Examples of ortho-substitution can be seen in the following section.



Scheme 2.5: Synthesis of ortho-substituted PDI.

2.3.2. Strategies to improve the formation of triplet excited state in PDIs

Effectiveness of PACT depends strongly on the ability of photosensitizers to generate reactive oxygen species such as singlet oxygen, hydroxyl radical etc. Efficient formation of a long-lived triplet excited state is an essential requirement for the production of ROS. The low formation of triplet excited state of PDIs by photoexcitation is the main reason behind the poor usage of PDIs in PACT applications.⁵⁵ However, there are different strategies to enhance the formation of PDI triplet state and some important methods are discussed in this section.

The most straightforward way to increase the triplet state formation of PDIs is to induce a strong spin-orbit coupling (SOC) by attaching “heavy atoms” to the molecule. These “heavy atoms” can be either large halogens such as Br and I, or transition metals such as Pt, Ru, Ir etc. This chemical modification is quite efficient. It was shown that perylene imides, which incorporate metals Pt, Ru and Ir in the structure, do demonstrate a high singlet oxygen quantum yield (Figure 2.7).^{104–107}

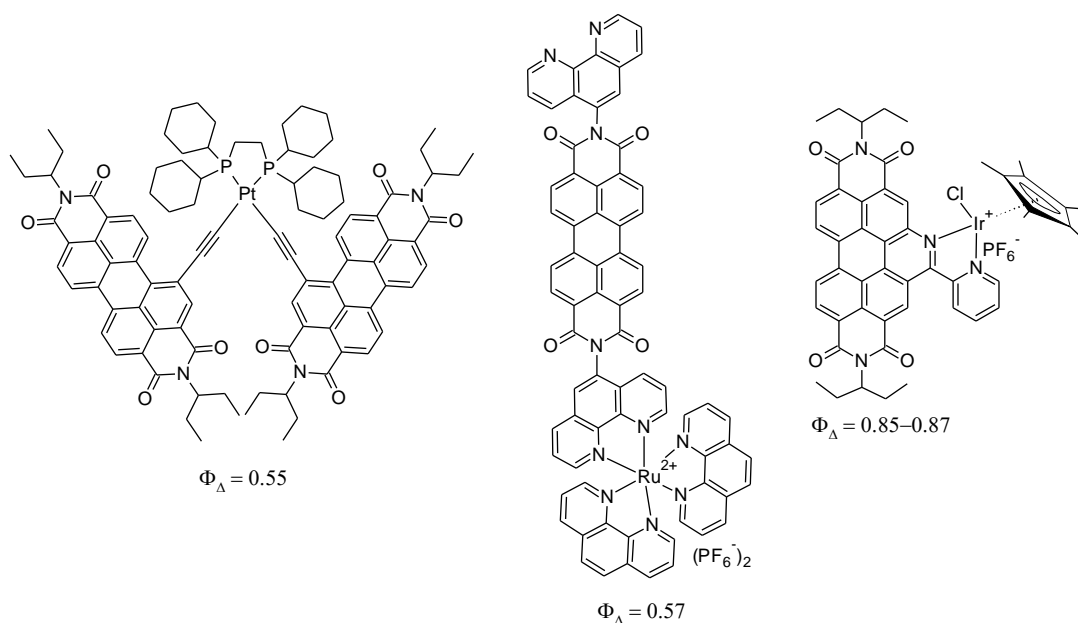


Figure 2.7: Structure of transition metal incorporated PDIs that generate singlet oxygen.

Alternatively, different methods were developed for heavy-atom-free PDIs that can efficiently generate triplet excited state. One such approach is to attach a spin converter such as fullerene to PDIs. Buckminsterfullerene C_{60} has very high yield of intersystem crossing ($\Phi_{ISC} \approx 1$).¹⁰⁸ PDI- C_{60} dyads that can generate singlet oxygen in high quantum yields were reported by Zhao and co-workers (Figure 2.8).¹⁰⁹

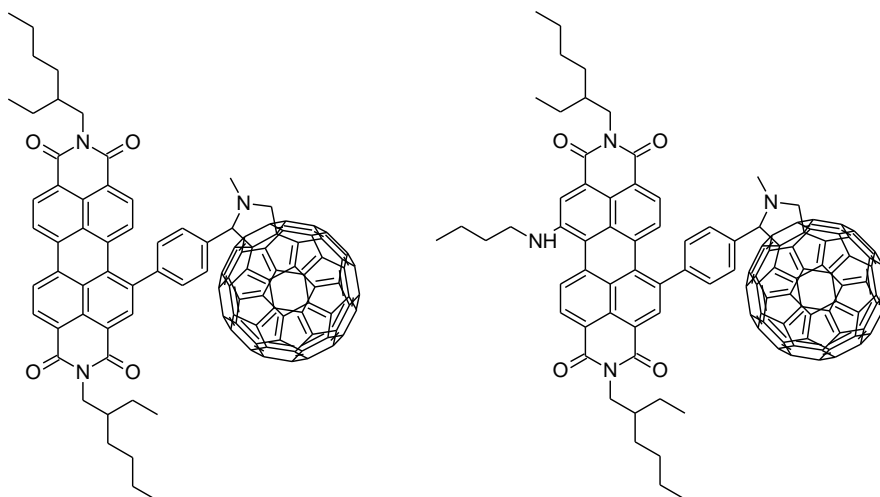


Figure 2.8: Structure of PDI- C_{60} dyads capable of generating singlet oxygen.

Substitution of bay positions with compounds such as pyrene and indole improves the overall singlet oxygen quantum yield of PDIs. Dinçalp and coworkers used this strategy to synthesize novel PDIs as shown in Figure 2.9.¹¹⁰ Singlet oxygen quantum yield for pyrene substituted PDI was found to be 0.93 and that for indole substituted PDI to be 0.33.

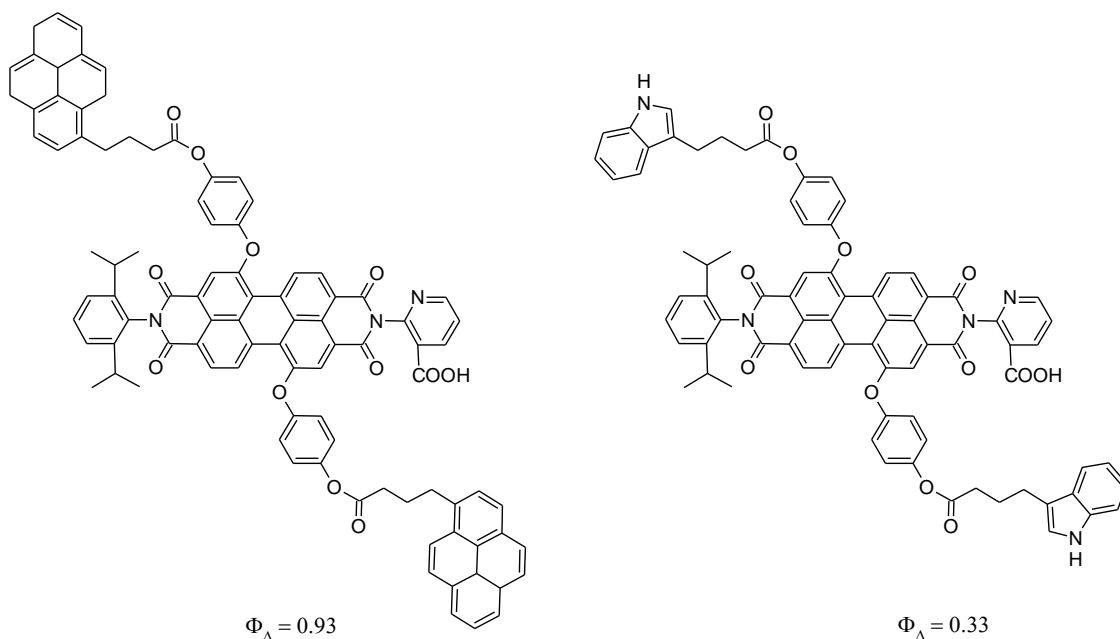


Figure 2.9: Pyrene and indole substituted PDIs.

Another method to improve the triplet state generation by perylene imides is to induce a twist in the perylene core. The distortion in core enhances the spin-orbital coupling resulting in higher intersystem crossing. PDIs with fused bay region substituents have a significant planar distortion in the core and hence are capable of generating singlet oxygen.^{111–113} The examples of core twisted PDIs with high singlet oxygen quantum yields are shown in Figure 2.10.

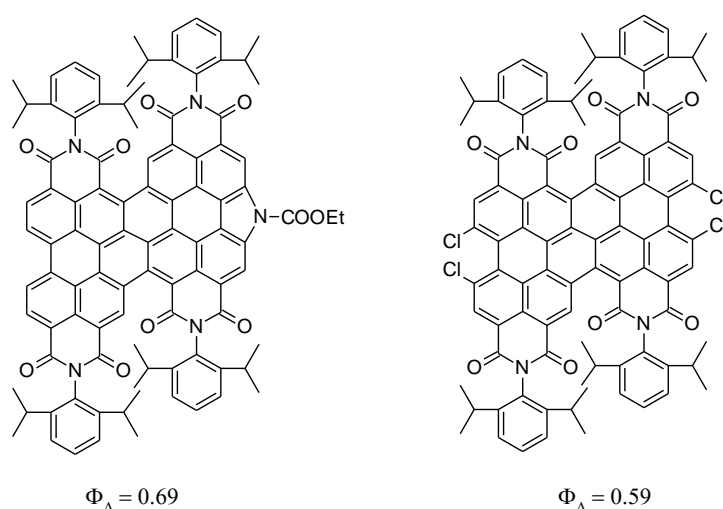


Figure 2.10: Structure of core twisted PDI showing high singlet oxygen quantum yield.

Efficient triplet state generation in heavy-atom-free PDIs can also be achieved without introducing a distortion in the molecular skeleton. Recent reports show that planar PDIs with four substituents at ortho positions can efficiently form the triplet excited state.⁹² The substituents such as phenylethynyl

group that can extend the π -conjugation framework of PDI core improve the triplet excited state formation (Figure 2.11).¹¹⁴ Similarly, PDIs with p-methoxyphenyl and p-methylthioxyphenyl substituents demonstrated a high singlet oxygen quantum yield of 0.50 and 0.80 respectively by enhancing spin orbital coupling (Figure 2.11).¹¹⁵

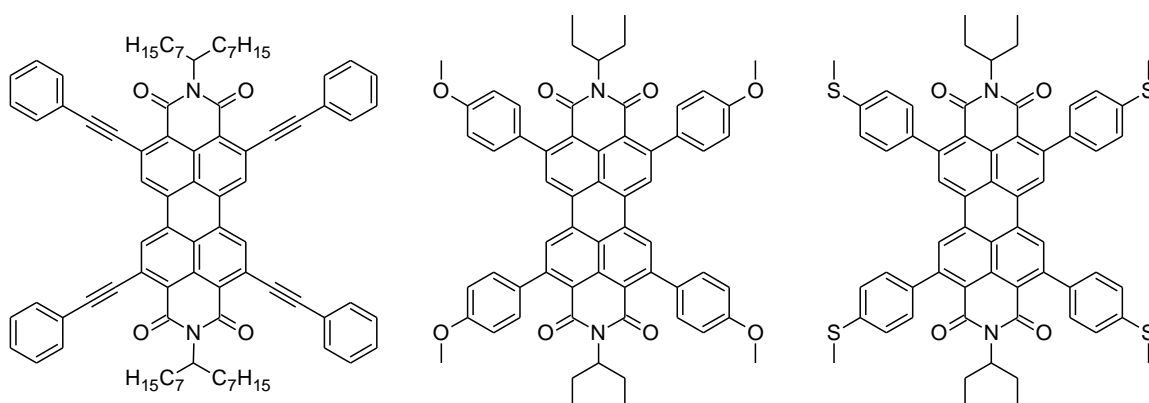


Figure 2.11: Structure of ortho-substituted PDIs capable of generating singlet oxygen.

Very efficient and fast generation of the triplet state is reported for PDIs modified by thionation of imide carboxyl groups. PDIs can be thionated without significant synthetic efforts and the products can be readily isolated by a column chromatography. Successive oxygen-sulfur substitution gives rise to five thionated PDI derivatives, which display a red shift in the absorption spectrum proportional to the degree of thionation. However, the rate of formation of the triplet state is not affected by the degree of thionation. The five thionated derivatives of PDI are shown in Figure 2.12.¹¹⁶

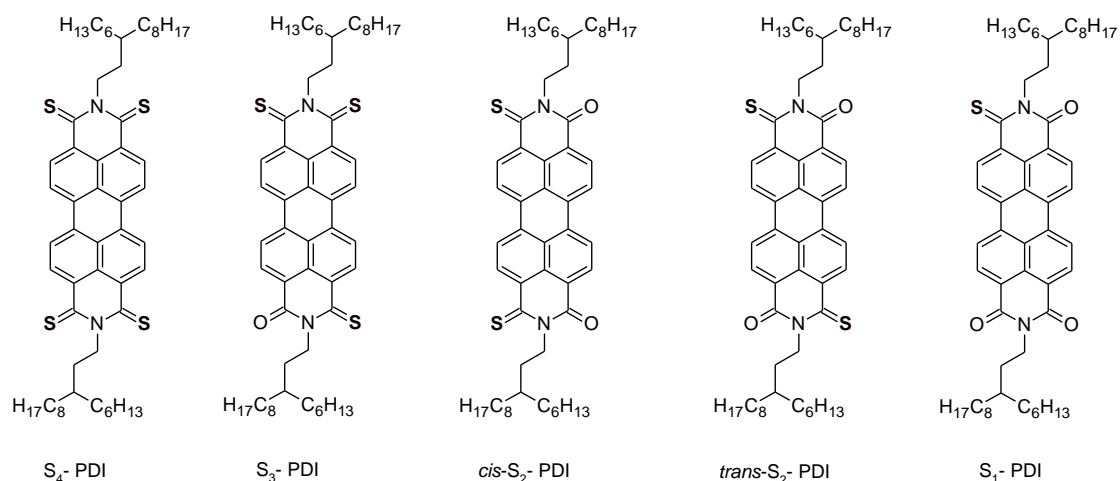


Figure 2.12: Structure of thionated derivatives of PDIs.

2.4. Phthalocyanines

Formation of phthalocyanine as a deep blue solid substance was first reported by Braun and Tcherniac in 1908.¹¹⁷ However, only after its serendipitous discovery by the employees of Scottish Dyes

in 1928, the structure of phthalocyanine was elucidated by Linstead.^{118,119} Phthalocyanine is a planar macrocyclic compound with 18 π electrons delocalized over the aromatic rings. It consists of four isoindole units connected together at their 1,3 positions through aza bridges. The deep blue-green colour of the compound is the result of its strong absorption in visible region of the solar spectrum, mostly around 620-700 nm.¹²⁰ Significant modification in the electronic and optical properties of phthalocyanines could be easily achieved by replacing two hydrogen atoms in the central cavity of the phthalocyanine's core with different metals, and/or by linking appropriate substituents at axial or peripheral positions of the macrocycle.¹²¹⁻¹²⁴ The basic structure of free-base and metal phthalocyanines along with potential sites for the modifications are shown in Figure 2.13. Phthalocyanines are highly versatile compounds that find application in various fields such as dyeing industry, photodynamic therapy, organic electronics etc.¹²⁰⁻¹²⁴

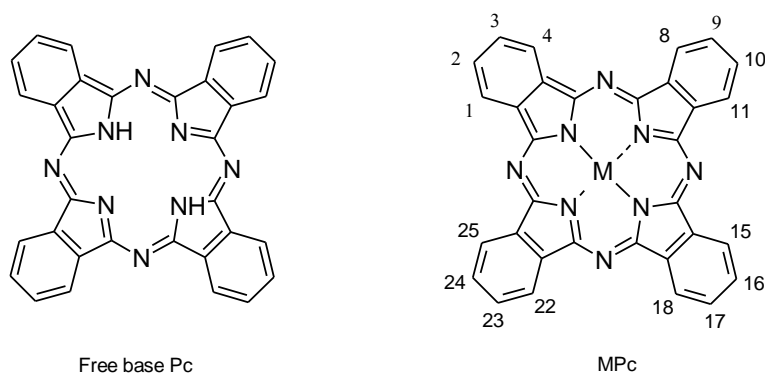


Figure 2.13: Structure of free base and metal phthalocyanine along with potential sites for substitution.

2.4.1. Synthesis of phthalocyanines

Phthalocyanines were synthesized by a metal-template assisted cyclotetramerization of aromatic *ortho*-dicarboxylic acid derivatives such as phthalic acid, phthalonitriles, phthalic anhydrides, phthalimides, phthalamides, diiminoisoindolines and *o*-cyanobenzamides (Figure 2.14).¹²⁴ The most common precursor for the synthesis of phthalocyanine in the laboratory scale is phthalonitrile. Phthalocyanines synthesized using phthalonitriles are characterized by clean tetramerization reaction, high purity and improved yields. As an extra benefit, many different synthetic routes are available for the preparation of phthalonitriles, which broadens their synthetic utility. However, their use is restricted to advanced technological applications where quality is preferred over the cost as phthalonitriles are expensive compounds.¹²⁴ Therefore, inexpensive phthalic acid is favoured for the large-scale industrial production of phthalocyanine. The preferred solvents for the phthalocyanine synthesis are high-boiling liquids such as chlorobenzene, quinolone and nitrobenzene, or high-boiling alcohols. In the case of alcohols, strong organic bases such as diazabicycloundecene (DBU), piperidine or cyclohexylamine are used in the reaction to assist the formation of alkoxyisoindoline units which rapidly undergo cyclotetramerization reaction. Most phthalocyanines synthesized industrially are metal phthalocyanines. Free base phthalocyanines are generally prepared by the demetalation

of phthalocyanine complexes of alkali and alkaline earth metals such as Li, Na and Mg. Alternatively, free-base phthalocyanines are also synthesized by reacting phthalonitriles with hydrogen in dioxane or with ammonia in 2-N,N-dimethylaminoethanol.^{124,125}

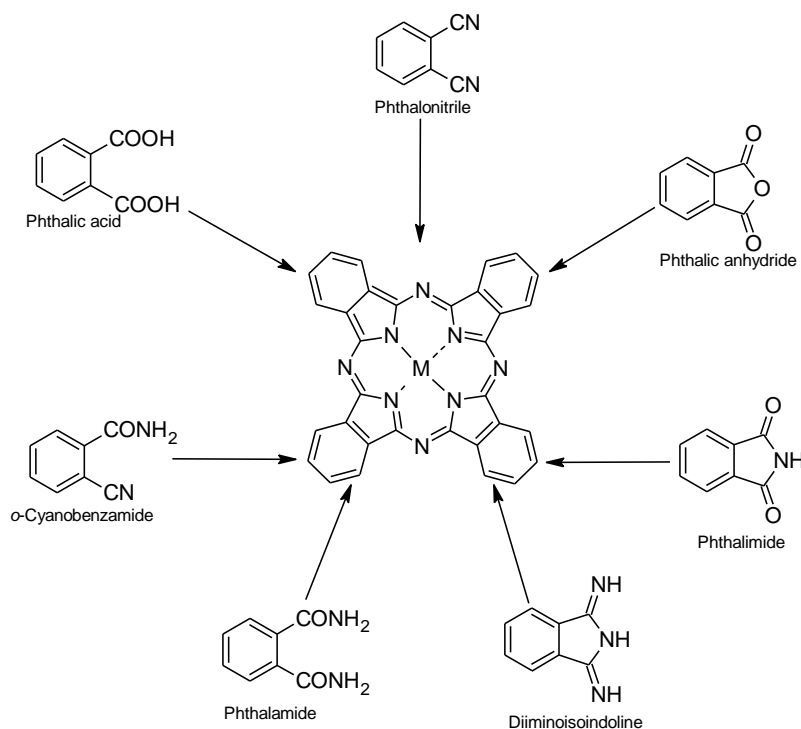


Figure 2.14: Main precursors for phthalocyanine synthesis.

2.4.2. Mechanism of phthalocyanine's formation

Phthalonitrile undergoes a metal-assisted stepwise polymerization and ring closure reaction to form a macrocycle. The resultant macrocycle is characterized by its high thermodynamic stability and added aromaticity, which is the driving force behind the tetramerization. The mechanism proposed by Christie and co-workers for the formation of copper phthalocyanine (CuPc) suggests that the metal coordination activates one of the cyano group, which subsequently undergoes a nucleophile attack.¹²⁶ The nucleophilic attack initiates a cyclization reaction to form an isoindolenine intermediate which acts as a nucleophile and carries out a further attack on another molecule of phthalonitrile. The steps are repeated until the tetramerization reaction yields phthalocyanine (Figure 2.15).

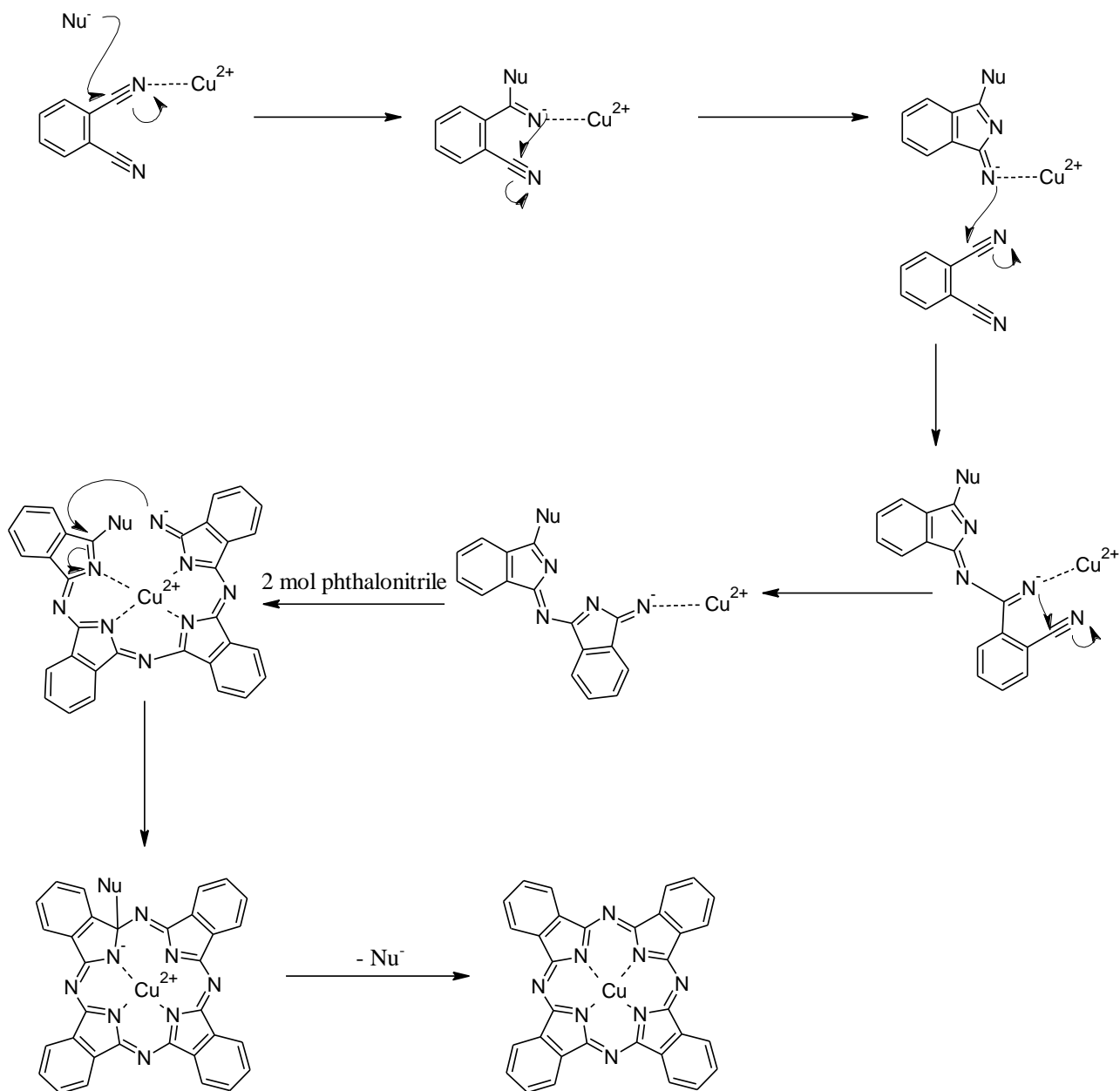


Figure 2.15: Mechanism proposed by Christie *et al* for the tetramerization reaction.¹²⁶

2.4.3. Modifications

Unsubstituted phthalocyanines are highly hydrophobic substances; they tend to form aggregates and are notoriously insoluble. Insolubility makes them unsuitable for such applications in organic electronics, optical devices and photodynamic therapy, where individual unclustered molecules are required to perform a function.^{123,124} Solubility and aggregation properties of phthalocyanines can be controlled by their chemical modification.^{124,127} One of the simplest, most common and efficient ways is to change the central atom and its axial ligands.¹²⁸ Another option is to control the peripheral substitution of the macrocycle core. Phthalocyanines can undergo substitution at both α and β

phthalo positions located at the periphery of the molecule (Figure 2.16). The appropriate substitution can significantly alter the physical, chemical and electronic properties of phthalocyanines. For example, substitution of α position with an electron rich group 16 elements such as S, Se and Te shifts the Q band to longer wavelength.¹²⁹ Peripheral substitution of phthalocyanines can be achieved by two basic methods.¹²⁴ The first method utilizes direct aromatic electrophilic substitution of the pre-existing phthalocyanine core as well as cycloaddition reactions. However, this method lack the control over the degree of substitution on phthalocyanine resulting in the formation of complex isomeric mixtures. The second basic method involves the use of already substituted phthalocyanines precursors such as substituted phthalonitriles, phthalic acids, phthalic anhydrides etc. The phthalocyanines synthesized using this approach have a better control over the degree of substitution, a criterion that is highly desirable for high-tech applications and photodynamic therapy.¹²⁴

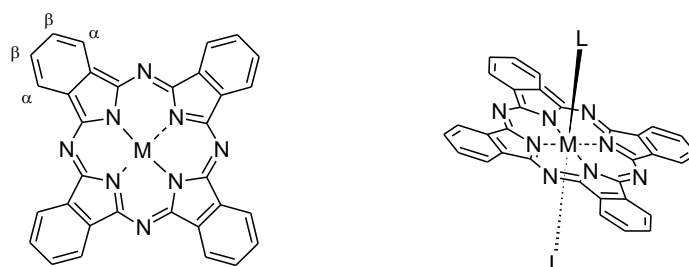


Figure 2.16: Structure of phthalocyanine showing α and β phthalo positions and axial substitution.

2.4.4. Constitutional isomers

Cyclotetramerization reaction using monosubstituted phthalonitriles leads to the formation of four constitutional isomers of phthalocyanines. According to the statistical distribution these structural isomers are found to be in the ratio $D_{2h}:C_s:C_{2v}:C_{4h} = 12.5:50:25:12.5$ (Figure 2.17).¹³⁰ Pure individual isomers generally exhibit interesting properties that the mixture of all four isomers cannot demonstrate.¹³¹

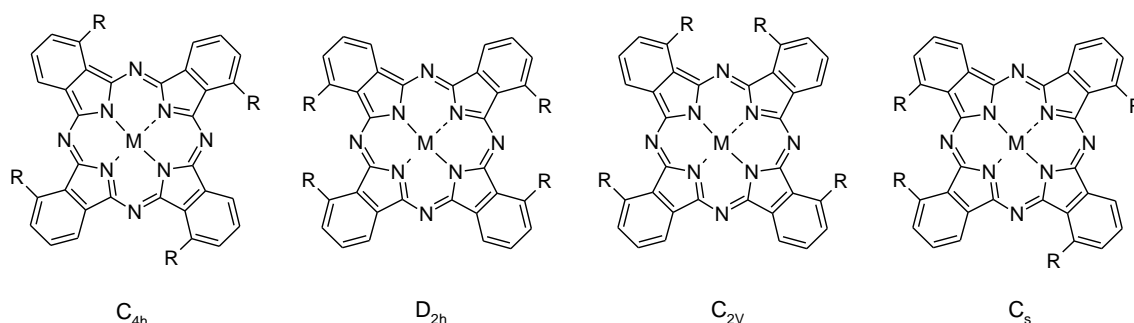


Figure 2.17: Four constitutional isomers of α -substituted metal phthalocyanine.

The separation and isolation of individual isomers is extremely laborious and difficult and requires chromatographic methods such as HPLC or MPLC.¹²⁷ Therefore, some approaches were developed

which allowed the formation of only one single isomer, exclusively or at least predominantly. The two proven methods for the selective synthesis are Statistical approach and Directed approach.¹²³

In the statistical approach, the selectivity of reaction towards a chosen isomer is improved by changing the substitution pattern of the precursor and by tuning the reaction conditions. For example, phthalocyanines synthesized from 4-substituted phthalonitrile bearing bulky alkoxy and thio moieties (Figure 2.18) yielded all the four constitutional isomers in the statistical ratio irrespective of the reaction conditions. However, when the substituent was located at 3-position of phthalonitrile, the isomer formation became dependent on the two factors, namely the temperature and the alcoholate used.¹³⁰ Leznoff and coworkers demonstrated that synthesis of phthalocyanines at low temperature (50 °C) and using Li/octanol as a base, favours the selective formation of C_{4h} isomer.¹³² Similarly, Kasuga and coworkers reported the formation of C_{4h} isomer with various 3-alkoxy substituted phthalonitriles at 80 °C and using Li/pentanol as a base. However, the phthalocyanine formation was not observed at temperatures below 80 °C.¹³³ This result shows that in the selective synthesis of phthalocyanine isomers, there is a considerable variation between the use of lithium pentonolate and lithium octano-

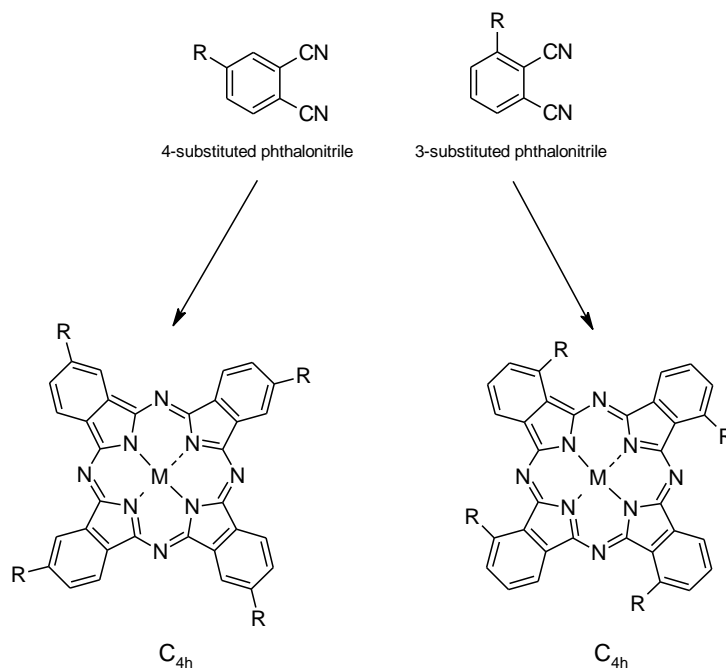


Figure 2.18: Structure of α and β substituted phthalocyanines prepared respectively from 3- and 4-substituted phthalonitriles.

Hanack and coworkers proposed two mechanisms for the difference in the selectivity of phthalocyanine formation based on the reaction conditions, position of substituents on the phthalonitrile and the central metal atoms.¹³⁰ The first mechanism works under basic conditions of lithium alcoholate and proceeds via the formation of an intermediate, 3-alkyloxy-1-imidoindoline. The difference in

charge distribution between two cyano groups is predominant in the case of 3-substituted phthalonitrile, which favours the selective formation of C_{4h} isomer. However, in the case of 4-substituted phthalonitrile, charge distribution is same on both cyano groups and therefore the reaction favours the statistical distribution of the four isomers.

The second mechanism operates in the presence of metal templates such as Zn, Ni or Cu. Four phthalonitrile units coordinates with the metal either before or during the cyclotetramerization reaction in a polar solvent. In this mechanism, there is no selectivity induced in the 3- or 4-substituted phthalonitriles and therefore the reaction favours the statistical distribution of all possible isomers.¹³⁰

In the directed approach to the synthesis of monoisomeric phthalocyanines, the precursors are designed in such a way that cyclotetramerization reaction yields only one constitutional isomer.¹²³ Using this approach, Kobayashi and coworkers prepared D_{2h} constitutional isomer by employing phthalonitrile dimers linked at their 4-positions with optically active 2,2'-dihydroxy-1,1'-binaphthyl (Figure 2.19a).¹³⁴ Similarly, Leznoff and co-workers synthesized D_{2h} isomer using phthalonitrile dimer linked at their 3-position with 2,2-disubstituted propan-1,3-diol spacer (Figure 2.19b).¹³⁵

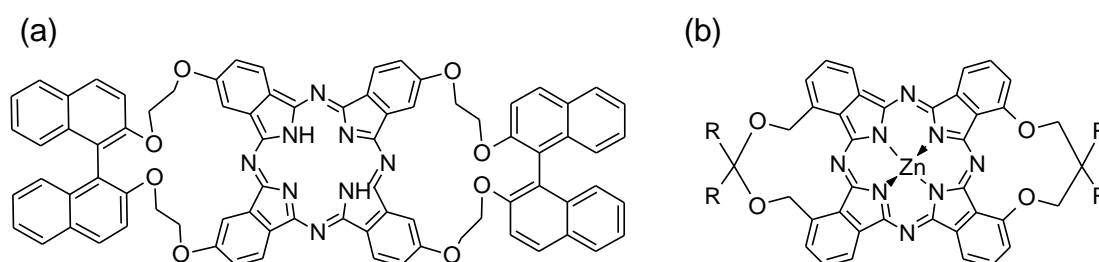


Figure 2.19: Structure of D_{2h} phthalocyanine isomers synthesized using directed approach.

2.5. Photoactive self-disinfecting materials and surfaces

The role of surfaces as potential sources of microbial infections is widely acknowledged. Self-disinfecting surfaces which utilize the concept of PACT can address this problem to a large extent. However, for successful implementation a reliable method for the immobilization of the photosensitizers on the surface is required. Successful immobilization of photosensitizers on materials such as films, paints, fabrics, filters, etc. are reported in the literature.^{48,62} The methods which are usually employed for the incorporation of photosensitizers onto surface are solvent facilitated dipping (swell-encapsulation-shrink approach), coating (deposition of a photosensitizer mixed with cellulose acetate), covalent attachment, vat dyeing, electrostatic interactions (layer by layer deposition), electrospinning (from a dye-doped polymer solution).^{136–143}

For example, efficient photoinactivation was reported with urinary catheter devices made from methylene blue (MB), toluidine blue (TBO) and gold nanoparticles-encapsulated medical grade polymer prepared by swell-encapsulation-shrink approach.¹³⁶ Inactivation rate of 2.8 log and 4.3 log reduction

in the growth of *Staphylococcus aureus* (*S. aureus*) was reported using MB- and TBO-impregnated polymers respectively after 24 h illumination with white light.

Antimicrobial activity of low symmetry phthalocyanine complexes such as Ge, Ti and Sn complexes of monocarboxy phthalocyanine, MCPc, zinc complexes of monocysteiny l phthalocyanine (ZnMCsPc), monophenoxy-carboxyphthalocyanine (ZnMPCPc) and symmetrically substituted phthalocyanines such as zinc tetraphenylcarboxyphthalocyanine, ZnTPCPc, unsubstituted zinc phthalocyanine (ZnPc) incorporated into electrospun polystyrene polymer fibers were investigated against *S. aureus*.¹⁴² The study revealed that low symmetry phthalocyanine complexes exhibited photo bactericidal effect whereas symmetrical ZnTPCPc and ZnPc did not show any activity. Similarly, polyamide nanofiber membranes with incorporated zinc(II) (4)-tetra[2-thioquinoline]phthalocyanine (ZnTTQPc) were prepared by the electrospinning method.¹⁴³ The polymer was able to generate singlet oxygen efficiently, which would make it useful as an antimicrobial surface. Furthermore, since the leaching of phthalocyanine was not detected during the stability tests, it was proposed that the material could be used as a water filtration membrane.

Modified polystyrene nanofiber impregnated with tetracationic porphyrin (TMpyP) through electrostatic interactions demonstrated significant antibacterial activity against *E. coli* under illumination.¹⁴⁰ Similarly, photobactericidal films prepared by the electrostatic interaction of TMpyP and regenerated cellulose exhibited photoinactivation against *E. coli*, *Proteus vulgaris* (*P. vulgaris*) and *S. aureus*.¹⁴¹

When compared to the noncovalent systems, covalent grafting allows permanent attachment of photosensitizers to the polymer substrate without losing the antibacterial properties over a long period. However, the protocol requires chemical modification of either substrate or photosensitizer. Ringot *et al* prepared photobacterial cotton fabrics by covalently attaching neutral aminoporphyrin (TPP-NH₂), anionic sulfonated aminoporphyrin(TPPS-NH₂) and cationic *trans*-pyridinium aminoporphyrin (*trans*-MePy⁺-NH₂) to the cellulose surface using 1,3,5-triazine linker.¹³⁸ The singlet oxygen quantum yields are 0.65, 0.59 and 0.82 for neutral, anionic and cationic porphyrins respectively. The photosensitizer grafted fabrics demonstrated phototoxicity against Gram-positive bacteria *S. aureus* with inactivation rate 93.7%, 37%, and 100% for neutral, anionic and cationic porphyrins respectively. However, all three photosensitizers failed to exhibit phototoxicity against Gram-negative bacteria *E. coli*. A compilation of antimicrobial efficacies of different porphyrins and phthalocyanines immobilized on solid substrates against various microbes is presented in Table 2.1.

Overall, the immobilization of photosensitizer on a solid substrate enhances the development of novel self-disinfecting materials that reduces the spread of pathogenic microorganisms. Immobilization of photosensitizers allows several cycles of photoinactivation of microbes without losing its efficiency. Reliable immobilization technique prevents the attached molecules from leaching thereby preventing the risk of pollution of the surroundings.⁴⁸

Table 2.1: Compilation of antimicrobial efficacies of porphyrins and phthalocyanines on surface.

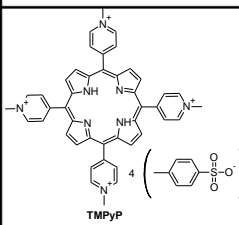
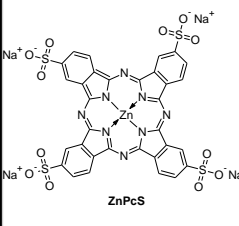
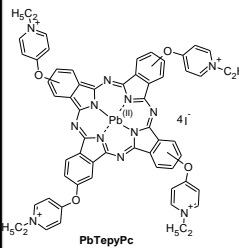
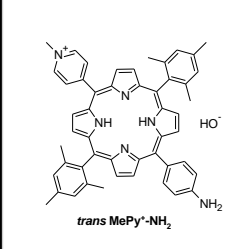
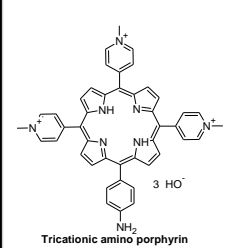
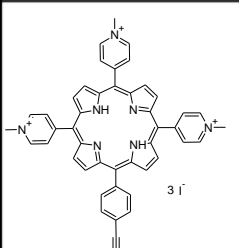
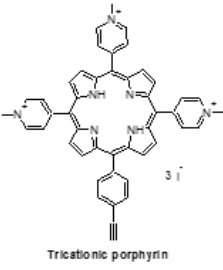
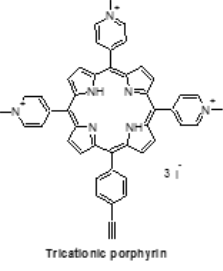
Support	Dye	Dye load	Light source	Light intensity	Duration	Light dose	Microbes	Inactivation rate
Regenerated cellulose (Cellophane film) ¹⁴¹	 TMPyP	$18 \times 10^{-3} \text{ mg/cm}^2$	Low power fluorescent lamp	8 W at a distance 30 cm	24 h		E. coli	No bacterial growth
							P. aeruginosa	Patchy growth
							P. vulgaris	No bacterial growth
							S. aureus	No bacterial growth
Chitosan ¹⁴⁴	 ZnPcS	$\sim 9 \mu\text{g/cm}^2$	Halogen lamp with water filters to remove IR radiations	500 W at 35 cm	30 min		E. coli	> 2 log reduction
Polystyrene ¹⁴⁵	 PbTepyPc	0.1 g to solution of the polymer 20% w/v	Quartz lamp with 600 nm glass (schott) and water filters to remove UV and IR radiations	300 W	30 min	$1.0 \times 10^{19} \text{ photons/cm}^2\text{s}$	E. coli	No bacterial growth
Cotton fabrics ¹³⁸	 trans MePy ⁺ -NH ₂	0.028 $\mu\text{mol/mg}$ of cotton	LED system-Luxeon Star white Lambertian LXHL-MW1D 5500K LED model	0.16 mW/cm^2	24 h	13.8 J/cm^2	S. aureus	100 %
							E.coli	No effect
Filter paper ¹⁴⁶	 Tricationic amino porphyrin	0.03 $\mu\text{mol/mg}$ of paper	LED model Luxeon® Star white Lambertian LXHL-MW1D 5500K LED model	0.16 mW/cm^2	24 h	13.8 J/cm^2	S.aureus	4 log reduction
							E. coli	2 log reduction
Cellulose nanocrystals (CNC) ¹⁴⁷	 Tricationic porphyrin	$0.16 \pm 0.03 \mu\text{mol/mg}$ of CNC	PDT light model LC122 (LumaCare, U.S.A.)	60 mW/cm^2	15 or 30 min	54 or 108 J/cm^2	E. coli	1-2 log reduction
							M. smegmatis	~ 4 log reduction
							S. aureus (after 15 min illumin)	> 5 log reduction

Table 2.1 (Continuation)

Support	Dye	Dye load	Light source	Light intensity	Duration	Light dose	Microbes	Inactivation rate
Cellulose nanocrystals (CNC) ¹⁴⁸	 <p>Tricationic porphyrin</p>	0.062 $\mu\text{mol/mg}$ of CNC	PDT light model LC122 (LumaCare, U.S.A.)	65 mW/cm^2	15 or 30 min	59 or 118 J/cm^2	Acinetobacter baumannii (A. baumannii) (after 15 min illumin)	4.5–5.5 log reduction
							multidrug resistant A. baumannii (MDRAB)	> 5 log reduction
							methicillin-resistant S. aureus	6 log reduction
							P. aeruginosa ATCC#97	2.5–3 log reduction
Cellulose paper ¹⁴⁹	 <p>Tricationic porphyrin</p>	12.4 nmol/mg of paper	PDT light model LC122 (LumaCare, U.S.A.) equipped with a LUM V fiber optic probe (400–700 nm band-pass filter) and an OSRAM Xenophot halogen lamp model 93653 ELC-3/X (24 V, 250 W)	65 \pm 5 mW/cm^2	30 min	118 J/cm^2	methicillin-susceptible S. aureus (MSSA) ATCC-2913	5 log reduction
							vancomycin-resistant Enterococcus faecium (VRE) strain ATCC-2320	4 log reduction
							A. baumannii ATCC- 19606	5 log reduction
							P. aeruginosa ATCC-9027	4 log reduction
							Klebsiella pneumoniaeA TCC-2146.	4.5 log reduction

3. Research objectives

The ultimate aim of this research was to develop a novel self-disinfecting material based on the principle of PACT. This material could find applications for example in textiles, coatings and filters for air and water sanitization. Successful implementation of the project required the synthesis of an efficient photosensitizer that can generate singlet oxygen in high quantum yields.

Generally, PDI-based photosensitizers are not employed in photodynamic therapy due to their low singlet oxygen quantum yield. One of the objectives of this work is to improve the singlet oxygen quantum yield of PDIs. Bay region functionalization of PDI using appropriate substituents could modify its properties. Methods for direct bay region modification of PDI should be investigated. Perylene imides with anchoring groups such as anhydrides and dicarboxylic acids, useful for the immobilization of dye onto the substrate, should be synthesized.

Synthesis of novel phthalocyanines which can generate singlet oxygen in high quantum yield is another objective of this research work. Synthesized phthalocyanines should be stable against bleaching and should provide high antimicrobial efficacy.

Cationic dyes are known to be efficient against both Gram-positive and Gram-negative bacteria. The presence of positive charge is useful in immobilizing the dyes onto the substrates through electrostatic interactions. Synthesis of cationic PDIs and phthalocyanines should be carried out and their singlet oxygen quantum yields and antimicrobial efficacies should be evaluated.

Antimicrobial tests are very time-consuming. A fast and efficient method to determine the antimicrobial efficacies of the surfaces for a large array of dyes should be developed. Finally, the possibility of using consumer LED lamp as a source of illumination for the photoinactivation of microbes should be confirmed.

4. Materials and Methods

All commercial reagents and solvents were purchased from TCI Europe, SigmaAldrich Co. or from VWR and were used without further purifications unless otherwise mentioned. The progress of the reactions was monitored by thin layer chromatography (TLC) using aluminium plates coated with silica gel 60 F₂₅₄ or neutral aluminium oxide 60 F₂₅₄ (Merck). Purification of the products was carried out either by column chromatography on Silica gel 60 or Silica gel 100 (Merck) or on preparative TLC plates coated with silica gel 60 F₂₅₄ or neutral aluminium oxide 60 F₂₅₄.

Prototype photoactive antimicrobial surfaces were prepared using qualitative filter paper 413 (medium filtration rate, particle retention 5-13 µm) purchased from VWR (cat. No. 516-0813). The filter paper (3.5 cm x 3.5 cm) pieces were soaked in an aqueous solution containing 0.1 mg of a dye and dried in the air. The dyed papers were stored in a plastic bag in a locker.

4.1. Characterization of substances

NMR spectra were recorded on Varian Mercury 300 MHz spectrometer using tetramethylsilane (TMS) as internal standard. Two-dimensional NMR measurements such as COSY, gHSQC, gHMBC were indispensable tools in assigning the structure of compounds accurately, particularly for the regioisomers of perylene imides.

High-resolution mass spectrometry (HRMS) measurements were done with Waters LCT Premier XE ESI-TOF benchtop mass spectrometer. Centering, calibration and lock-mass correction with Leucine Enkephaline as a reference compound were applied to the raw data to obtain the accurate mass. HRMS proved to be very useful for monitoring the formation of tetracationic dyes.

UV-Vis absorption spectra of solutions were recorded using Shimadzu UV-3600 UV-VIS-NIR spectrophotometer. Transmittance and reflectance spectra of dyed papers were recorded using the integrating sphere attachment ISR-3100. The absorbance **a**, which is the fraction of incident light absorbed by the paper was calculated according to equation $a = 1 - T - R$, where R is reflectance and T transmittance of the sample at given wavelength. The emission spectra were recorded on a Fluorolog Yobin Yvon-SPEX spectrofluorometer.

4.2. Light sources

The illumination source for photoinactivation of microbes were a solar simulator Luzchem and a consumer LED lamp. In the case of solar simulator, the UV and IR radiations were cut off using a combination of KG3 band pass filter (315-750 nm transmittance) and YG-17 filter (transmittance > 485 nm). The overall light intensity was regulated by adjusting the distance between the lamp and the microtitre plate. Intensity of the lamp emission was measured by Coherent LM10 power meter. Commercially available LED lamp OSRAM Star PAR16 80 W 575 lm GU10 was used as another

illumination source. Light intensity and spectral profile of the LED lamp were recorded with AvaSpec-2048 fibre optics spectrometer.

4.3. Antimicrobial test

All the solutions, culture mediums, vials and pipette tips used for microbial tests were sterilized before the experiments and all the operations were conducted inside the laminar hood to prevent contamination.

Microbial strains, *E. coli* MG1655 (*E. coli* Genetic Resources at Yale) and *A. baylyi* ADP1 (ATCC 33305) were used in determining antimicrobial efficacy. Microbial strains were inoculated in 5 mL of Lysogeny broth (LB) medium (10 g/l tryptone, 5 g/l yeast extract, 5 g/l NaCl) containing 1 % glucose and cultivated at 30 °C and 300 rpm in a temperature-controlled incubator shaker (IKA® KS 4000 i control). After overnight cultivation, 100 µL of the culture was diluted with 4.9 mL of LB medium containing 1 % glucose and cultivated for 3 h at 30 °C and 300 rpm in the temperature controlled incubator shaker (IKA® KS 4000 i control). The optical density of culture was recorded at 600 nm. The microbial solution was centrifuged for 5 min at 6500 rpm and the LB medium was decanted out from the vial. The residual microbes were suspended in 5 mL of PBS (phosphate-buffered saline) buffer.

Two sets (original and duplicate) of circular discs were cut from phthalocyanine-impregnated paper and control paper and placed in the wells of a microplate. Aliquots of 25 µL of microbial solution were pipetted over the disks. The microplate was covered with a transparent lid and was illuminated with an appropriate light source. Another microplate with the two sets of dyed and blank paper disks was used as a dark control. Aliquots of 25 µL of microbial solution were pipetted over each disk, the microplate was wrapped in aluminum foil and stored inside the laminar hood at room temperature. After 1 h of illumination or incubation, microbes were extracted from wells with 975 µL of PBS buffer and serial dilutions (up to 10^{-6}) were made from each extract. The dilutions were plated on LA agar plates (15 g/l agar, 10 g/l tryptone, 5 g/l yeast extract, 5 g/l NaCl, 0.2 % glucose) and incubated at 30 °C overnight in a laboratory incubator (Termaks). The colonies grown on the agar plates were counted and CFUs per milliliter were calculated to determine the antimicrobial efficacy. The scheme describing the procedure to determine the antimicrobial efficacy by CFU counting is presented in Figure 4.1. (Publications III and IV)

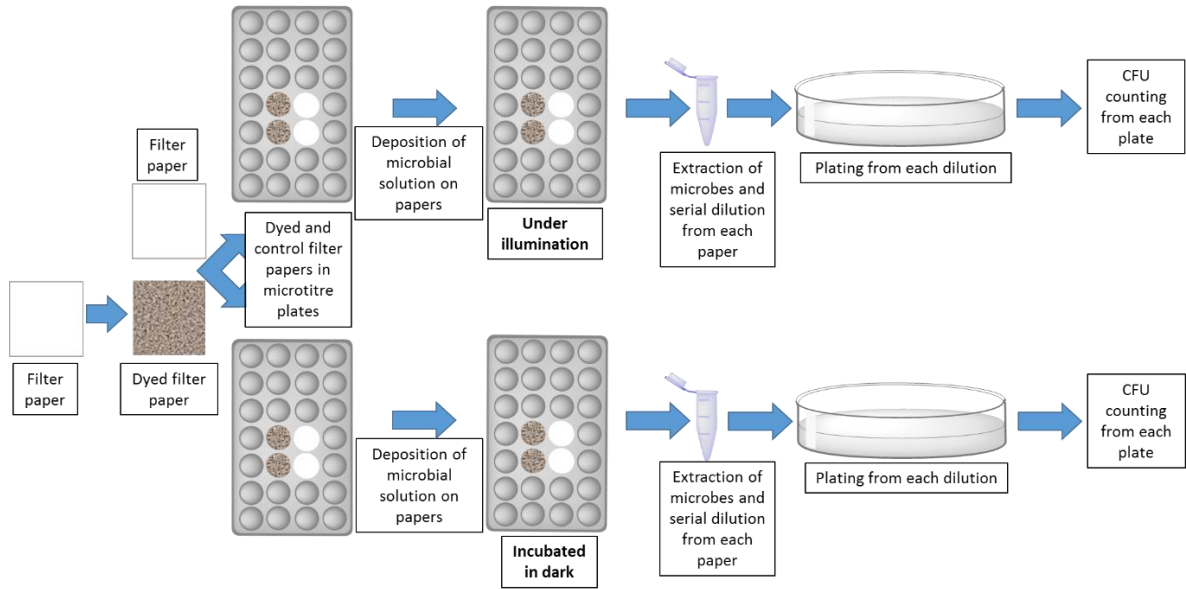


Figure 4.1: Scheme for the antimicrobial efficacy by CFU counting. (Publication IV)

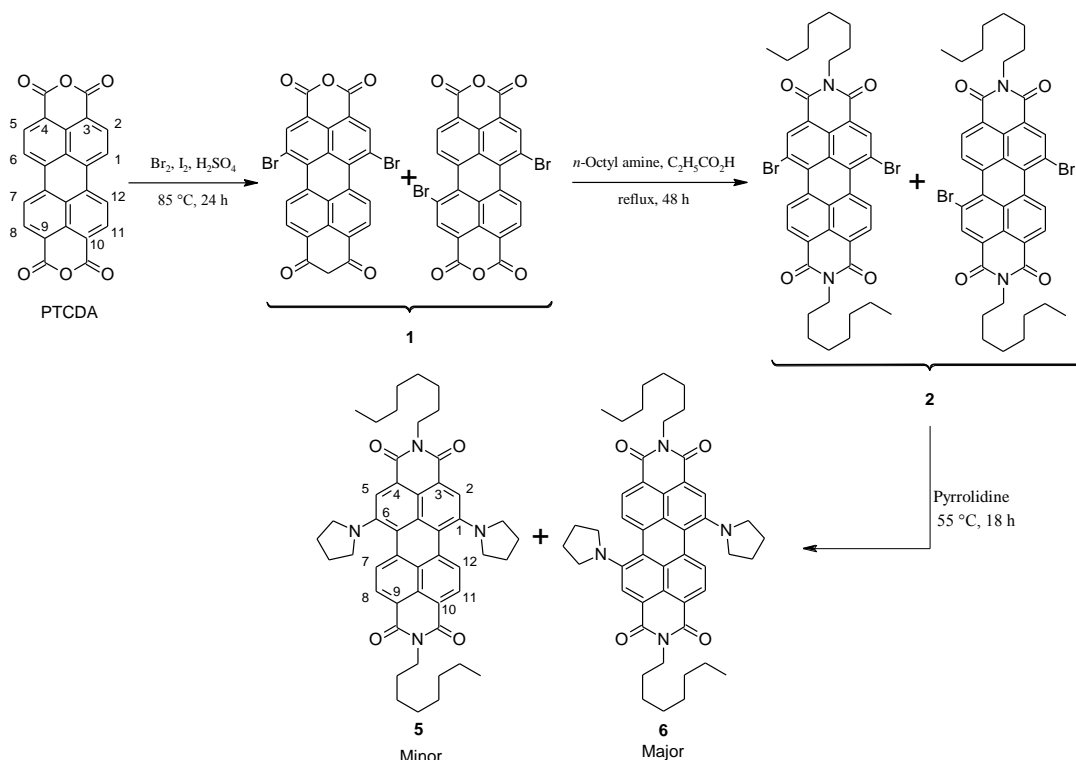
5. Results and discussion

5.1. Synthesis of perylenes

As mentioned in the previous chapter, photochemical properties of PDIs can be modified by appropriate functionalization. We have synthesized different perylene monoimides and diimides and studied their singlet oxygen quantum yields. Functionalization was carried out either to modify PDI's solubility or photochemical properties, or to introduce anchoring groups that would assure the immobilization of the photosensitizer on a substrate. Amination of perylene imides is an important substitution reaction as it can alter the redox properties and solubility and shifts the absorption to longer wavelengths.⁹⁶ Introduction of an amine group to PDI is also beneficial since the amines can be later converted into quaternary salts and provide cationic dyes for the photodynamic therapy.

5.1.1. Regioselective 1,6-amination of perylenes.

Generally, the bay region amination of perylene dimides is a multistep synthesis.^{75,85,86,96} The first reaction is the bromination of PTCDA using liquid bromine in concentrated H₂SO₄, which yields a mixture of mono-, di-, and tribromo PTCDA. Dibrominated product is the major component, however the reaction conditions can be tweaked up to tetrabromination. Imidiation of dibromo PTCDA and subsequent replacement of bay region bromines with amino groups such as pyrrolidine produce a mixture of two regioisomers, namely 1,6-dipyrrolidinyl **5** and 1,7-dipyrrolidinyl **6** PDIs. 1,7-Substituted isomer **6** forms in a higher proportion.⁸⁶ Though efficient, the method involves many purification steps, and isolation of pure regioisomers is cumbersome (Scheme 5.1).



Scheme 5.1: General synthesis of 1,6-dipyrrolidinyl **5** and 1,7-dipyrrolidinyl **6** PDIs.

The electrochemical and optical properties exhibited by 1,6- and 1,7-regioisomers are significantly different. For example, absorption maximum of 1,6-isomer **5** is at 680 nm with molar extinction coefficient $25000 \text{ L mol}^{-1} \text{ cm}^{-1}$ whereas that of 1,7-isomer **6** is at 698 nm with molar extinction coefficient $39960 \text{ L mol}^{-1} \text{ cm}^{-1}$ (Figure 5.1). Moreover, the absorption spectrum of 1,6-regioisomer **5** extends over a wide region of visible wavelengths when compared to that of 1,7-isomer **6**. This broader absorption band of 1,6-isomer **5** is particularly beneficial when utilizing the molecule for a light-triggered function. Since the general methods of substitution of perylene imides chiefly produce 1,7-regioisomers, in the present work we have undertaken attempts for the selective synthesis of 1,6-regioisomers.

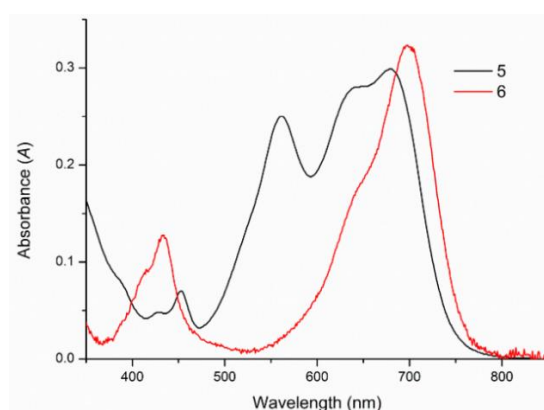
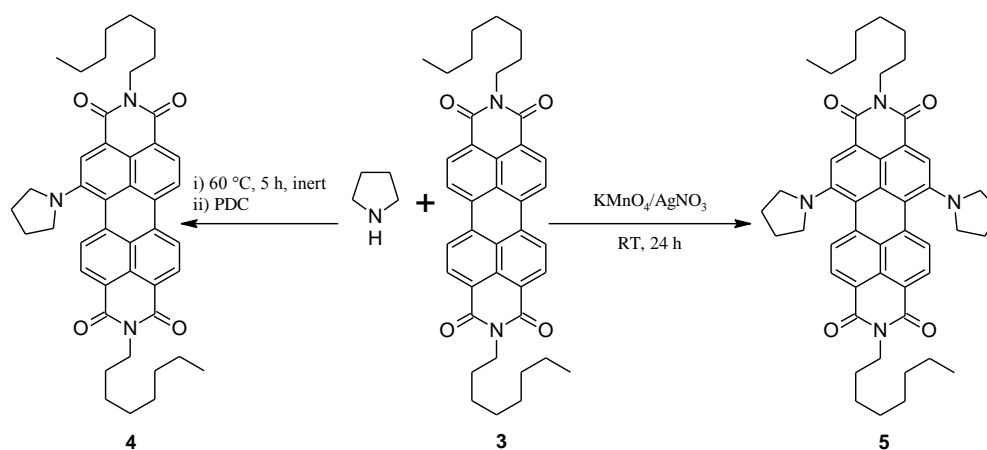


Figure 5.1: UV-Vis absorption spectra of 1,6-dipyrrolidinyl **5** and 1,7-dipyrrolidinyl **6** PDIs.

We have developed a direct bay region amination reaction for perylene diimides that yielded exclusively 1,6-regioisomer. The method does not require the bromine substitution, and hence unsubstituted PDIs **3** can be used for the amination reaction. The synthetic route is shown in Scheme 5.2.(Publication I)



Scheme 5.2: Synthesis of mono pyrrolidiny PDI **4** and 1,6-dipyrrolidiny PDI **5**.

The starting compound, unsubstituted dioctyl PDI **3**, was synthesized by the reaction of commercially available PTCDA with octyl amine in imidazole at elevated temperature. As other unsubstituted perylene imides, it is a deep red crystalline substance, and its solutions are usually red as well. However, we have noticed that when PDI **3** was incubated in a sealed vial in pyrrolidine at 60 °C under inert atmosphere, the solution became dark blue. We suggested that the change of the color was due to formation of a radical anion of PDI. The presence of this intermediate with distinct absorption maxima at 720 and 800 nm was evident from UV-Visible absorption spectra (Figure 5.2).¹⁵⁰⁻¹⁵⁴

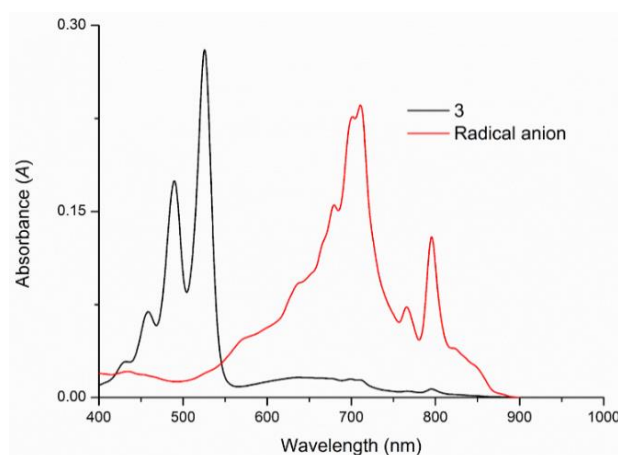


Figure 5.2: UV-Vis absorption spectra of starting material unsubstituted PDI **3** and reaction intermediate radical anion.

To be able to detect the anion radical, the absorption measurements were run in a sealed absorption cuvette equipped with a septum and thoroughly purged with argon. The chemical and electrochemical formation of radical anions of PDIs was already reported in literature and the UV-Vis spectrum of PDI **3** radical anion matched very well with that of reported ones. When the vial with this dark-blue solution was opened, the red color of original PDI was partly restored. To our surprise, a blue product was observed simultaneously, which was indentified as a pyrrolidinyl-substituted perylene diimide. We also noticed that the yield of the blue product was negligible if the residence time of PDI in pyrrolidine was short, and gradually increased with increase of the incubation time. As an explanation of such an unusual direct amination of the perylene core, we assumed a multistep mechanism with several reversible stages. At first, interaction of a strong base such as pyrrolidine with the electro-negative PDI π -system triggered an electron transfer (ET) process, and a radical anion of PDI formed, which was evident from the UV-Vis spectrum.¹⁵³ Formation of the radical anion in aprotic solvents under inert atmosphere was a reversible process, and upon exposing the blue solution of PDI radical anion to air, the radical anion disappeared and the absorption bands corresponding to the starting material (PDI **3**) restored. However, together with those a new broad absorption of monopyrrolidinyl PDI **4** appeared in the reaction. We proposed an explanation that with time the radical anion of perylene reacted with the molecule of pyrrolidine solvent and formed a PDI-pyrrolidine intermediate. When the vial was opened, this intermediate underwent a subsequent oxidation with oxygen from the air and produced the pyrrolidinated substance. (Publication I)

The tentative mechanism for the formation of mono pyrrolidinyl PDI is shown in Figure 5.3. We assumed that the use of a strong oxidant such as pyridinium dichromate (PDC) instead of air would improve the yield of pyrrolidinated product. To our delight, with such a modification we obtained monopyrrolidinyl PDI **4** in 70 % yield.

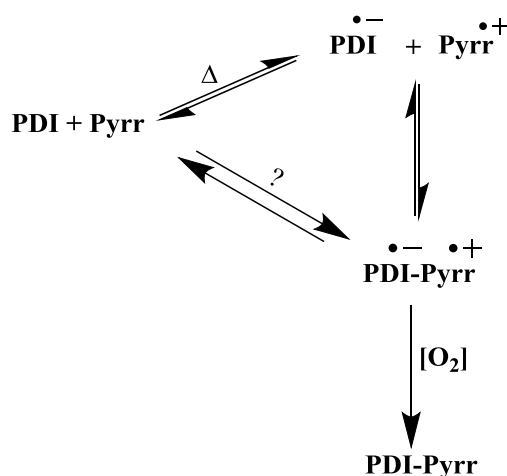


Figure 5.3: Tentative mechanism for the formation of mono pyrrolidinyl PDI.

Even more interesting results were obtained with modifications of the oxidant system. Pyrrolidination of PDI **3** through *in situ* oxidation using $\text{KMnO}_4/\text{AgNO}_3$ produced only one regioisomer, namely 1,6-dipyrrolidyl PDI **5** with high yield (Scheme 5.2). The monopyrrolidinyl substituted PDI **4** was isolated

by column chromatography and the structure was confirmed by the NMR spectroscopy. Monosubstitution actually happened at one of the bay positions of the PDI thus giving rise to two types of peaks in the aromatic region, namely two doublets and one singlet (Figure 5.4). The ortho-proton located next to the pyrrolidinated position of PDI could not couple with any other protons thus giving singlet signal at $\delta = 8.48$ ppm. The doublet signal at $\delta = 7.48$ ppm originates from another proton of the same bay, which is strongly shielded by the pyrrolidine group. This interpretation was derived from ^{13}C and 2D NMR measurements such as COSY, HSQC and HMBC. (Publication I)

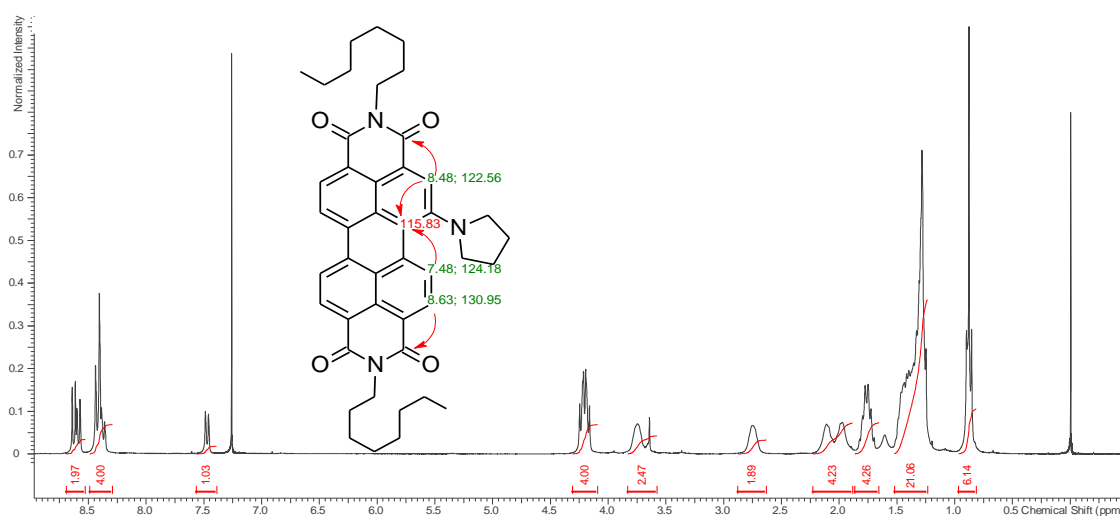


Figure 5.4: ^1H NMR spectrum for monopyrrolidinyl PDI **4**.

The proton NMR spectrum of compound **5** has two doublet signals at $\delta = 8.66$ ppm and $\delta = 7.87$ ppm and one singlet signal at $\delta = 8.34$ ppm with the integrals of 2 protons each. The pattern of singlet and doublet peaks in the aromatic area can be used to distinguish between 1,6- and 1,7-isomers. In the case of 1,7-isomer, these aromatic signals appear in the order of singlet, doublet and doublet while for 1,6-isomer, the order of signals in aromatic region is doublet, singlet and doublet as shown in Figure 5.5. Moreover, the structure was also confirmed by ^{13}C and 2D NMR measurements. (Publication I)

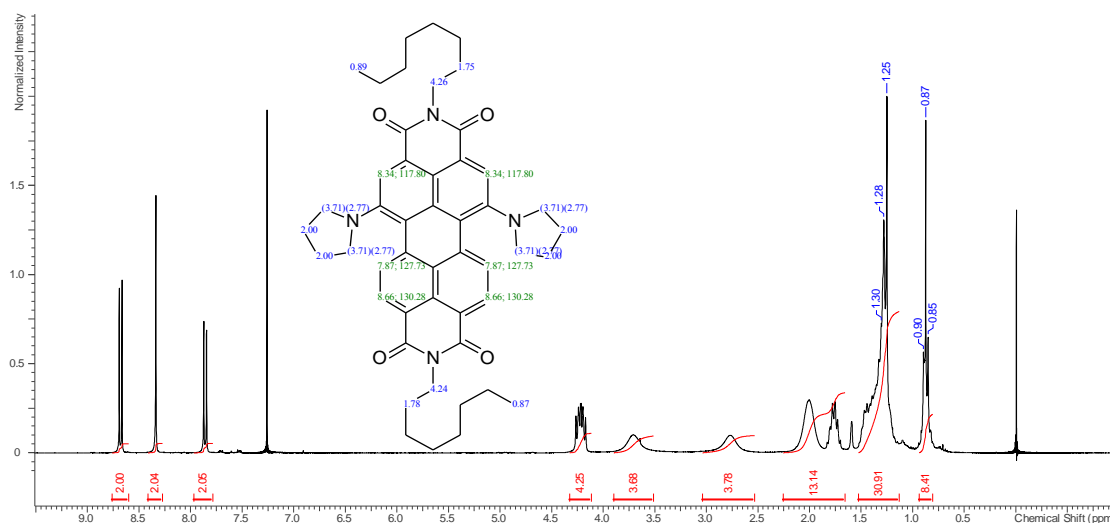


Figure 5.5: ^1H NMR spectrum for 1,6-dipyrrolidinyl PDI **5**.

The absorption spectra of unsubstituted perylene diimide, monopyrrolidinyl PDI and 1,6-dipyrrolidinyl PDI are shown in Figure 5.6. The mono-pyrrolidinyl PDI exhibits a broad absorption peak with a maximum at 672 nm. (Publication I)

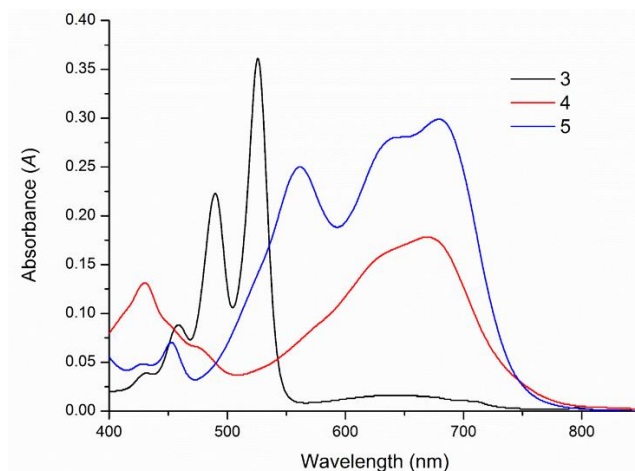


Figure 5.6: UV-Vis absorption spectra of unsubstituted PDI **3**, monopyrrolidinyl PDI **4** and 1,6-dipyrrolidinyl PDI **5**.

We extended the scope of the direct amino substitution of PDI core to perylene monoimides (PMIs). The reactions with perylene monoimides were highly regioselective and substitution occurred exclusively at bay 7- and 12-positions of the perylene ring, which are distant from the imide cycle. Moreover, the presence of imide cycle is also crucial for the reaction to occur. This was tested by the pyrrolidination of perylene tetracarboxylic ester **7** and perylene monoanhydride diester **8** (Figure 5.7) under the same reaction conditions. These compounds did not undergo the reaction, which underlined the importance of the imide moiety. (Publication I)

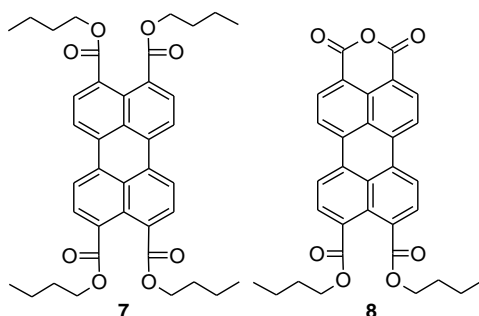
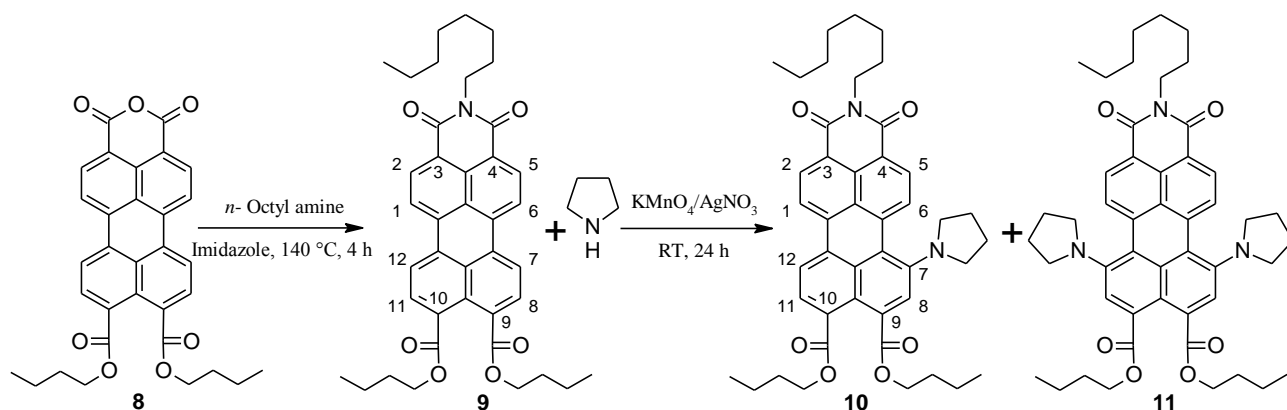


Figure 5.7: Chemical structure of perylene tetracarboxylic ester **7** and perylene monoanhydride diester **8**.

Perylene monoimide diester **9** was synthesized from monoanhydride **8** and octylamine in imidazole at higher temperature. Monoanhydride **8** was prepared from PTCDA according to the literature procedure. Pyrrolidination of PMI diester **9** using $\text{KMnO}_4/\text{AgNO}_3$ oxidation resulted in a mixture of monopyrrolidinated **10** and dipyrrolidinated **11** PMIs with 60 % and 20 % yields, respectively (Scheme 5.3). (Publication I)



Scheme 5.3: Synthesis of monopyrrolidiny and 7,12-dipyrrolidiny PMIs.

The regioselective substitution at bay 7- and 12-positions of perylene monoimide, positions which are distant from the imide cycle, was unambiguously established by NMR spectroscopy data. For pyrrolidinated PMI, a singlet signal at $\delta = 8.0$ ppm with one hydrogen could only arise in the case of mono substitution (Figure 5.8). Moreover, in gradient HMBC (gHMBC) measurement, this singlet signal shows a correlation with carbonyl carbon ($\delta = 168$ ppm) of the butyl ester. The identity of the carbonyl carbon was established with its correlation with α -butoxy protons at $\delta = 4.33$ ppm. This correlation was only possible if the bay substitution happened at the aromatic ring that was distant from the imide cycle. (Publication I)

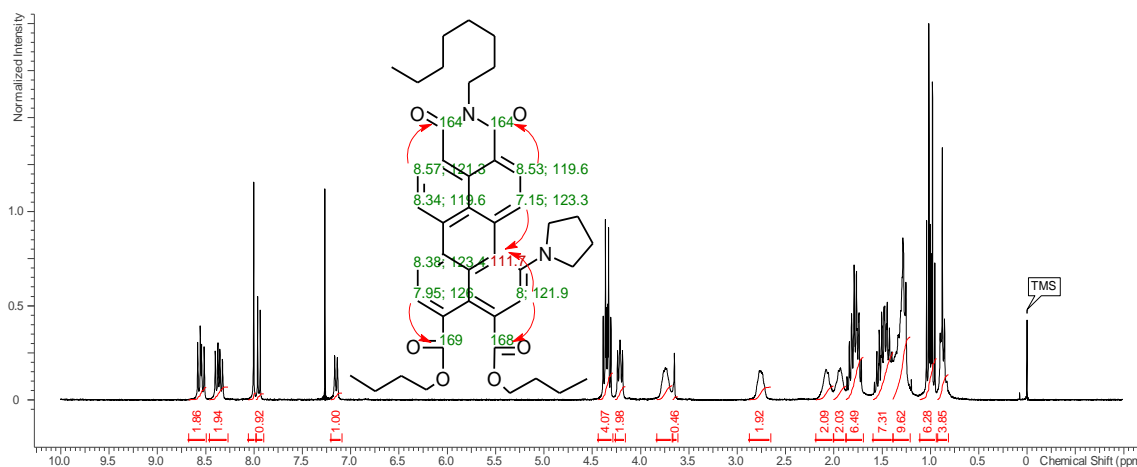


Figure 5.8: ^1H NMR spectrum for monopyrrolidinyl PDI **10**.

Similarly, proton NMR spectrum (Figure 5.9) of 7,12-disubstituted PMI **11** follows the same pattern of appearance of doublet and singlet signals in aromatic region as that of di-substituted PDI, with two hydrogens for each peak. The singlet signal at $\delta = 7.82$ ppm showed correlation with carbonyl carbon ($\delta = 168.48$ ppm) of butyl ester in gHMBC measurement. Again, the identity of carbonyl carbon was established by its correlation with α -butoxy protons at $\delta = 4.33$ ppm. (Publication I)

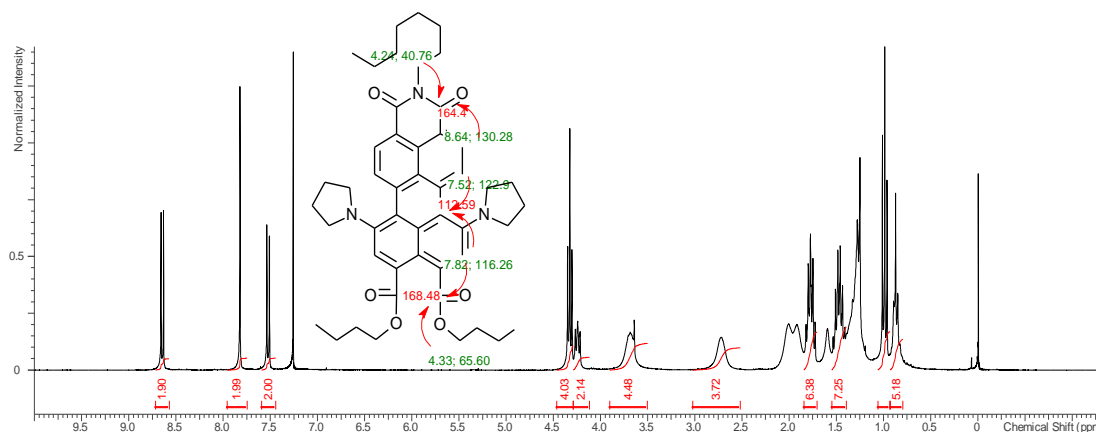


Figure 5.9: ^1H NMR spectrum for 7,12-dipyrrolidinyl PDI **11**.

The reactions of PMIs also proceeded through radical anion mechanism, which was evident from absorption peaks in the near IR region. The monopyrrolidinyl PMI **10** had a broad absorption peak similar to that of monopyrrolidinyl PDI **4** with absorption maximum blue shifted to 620 nm. The absorption spectrum of 7,12-dipyrrolidinyl PMI **11** was also similar to that of 1,6-dipyrrolidinyl PDI **5** with the wavelength of maximum absorption blue shifted to 642 nm with respect to PDI (Figure 5.10). (Publication I)

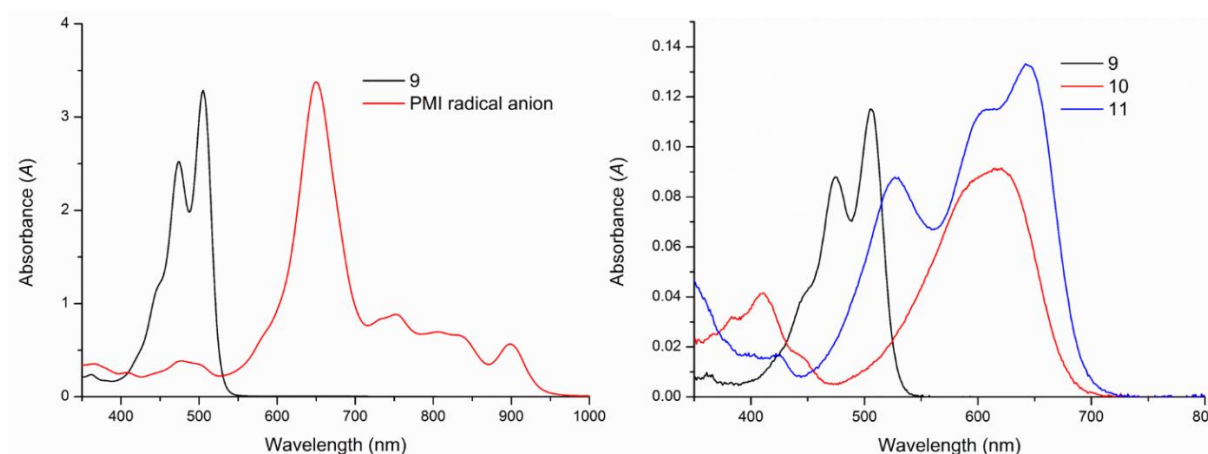
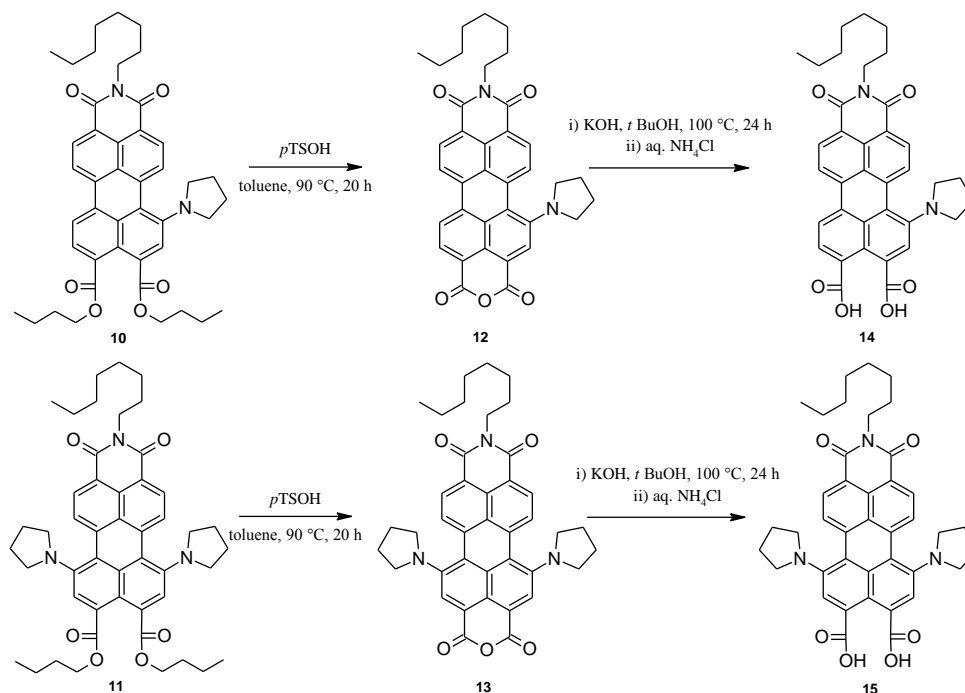


Figure 5.10: UV-Vis absorption spectra of unsubstituted PMI **9**, intermediate PMI radical anion, monopyrrolidinyl PMI **10** and 7,12-dipyrrolidinyl PMI **11**.

5.1.2. Synthesis of perylene imide dyes with anchoring groups

Surface immobilization of perylene imide dyes is possible only if appropriate anchoring groups are available. Perylene imides with carboxylic acid anchoring group could be immobilized on different surfaces such as polymers, films, coatings etc. either by electrostatic interactions or by a covalent bond formation.^{155–157} Direct attempts to synthesize dicarboxylic acid by hydrolysis of ester groups always ended up in the anhydride formation. Therefore, PMI diesters **10** and **11** were hydrolysed using *p*-toluenesulfonic acid (*p*-T₂SOH) to PMI monoanhydrides **12** and **13** in 93 % and 75 % yields, respectively. The anhydride group could be used directly as an anchoring group for immobilization of PMIs on oxide surfaces such as ZnO or TiO₂.^{157–159} PMI dicarboxylic acids could be synthesized from PMI monoanhydrides by heating with 2 equiv. of KOH in *t*BuOH at elevated temperature. The anhydride cycle opens at this reflux temperature, resulting in the formation of dicarboxylic acids. PMI monoanhydrides **12** and **13** were converted into corresponding dicarboxylic acids **14** and **15** with 70 % and 76 % yields, respectively (Scheme 5.4). (Publication II)



Scheme 5.4: Synthesis of PMI monoanhydrides (**12**, **13**) and corresponding dicarboxylic acids (**14**, **15**).

The UV-Vis absorption measurements of PMI monoanhydrides and PMI dicarboxylic acids (Figure 5.11) were carried out in ethanol. The absorption spectra of the compounds are similar to those of corresponding PMI diesters. However, the molar extinction coefficients for the PMI monoanhydrides and dicarboxylic acids were found to be higher than the corresponding diesters. The molar extinction coefficients for PMI monoanhydrides were 31665 L mol⁻¹ cm⁻¹ and 27600 L mol⁻¹ cm⁻¹ for **12** and **13** respectively. PMI dicarboxylic acids **14** and **15** have molar extinction coefficients 31900 L mol⁻¹ cm⁻¹ and 29700 L mol⁻¹ cm⁻¹ respectively, while that for PMI diesters **10** and **11** were 22847 and 22777 L mol⁻¹ cm⁻¹ respectively. (Publication II)

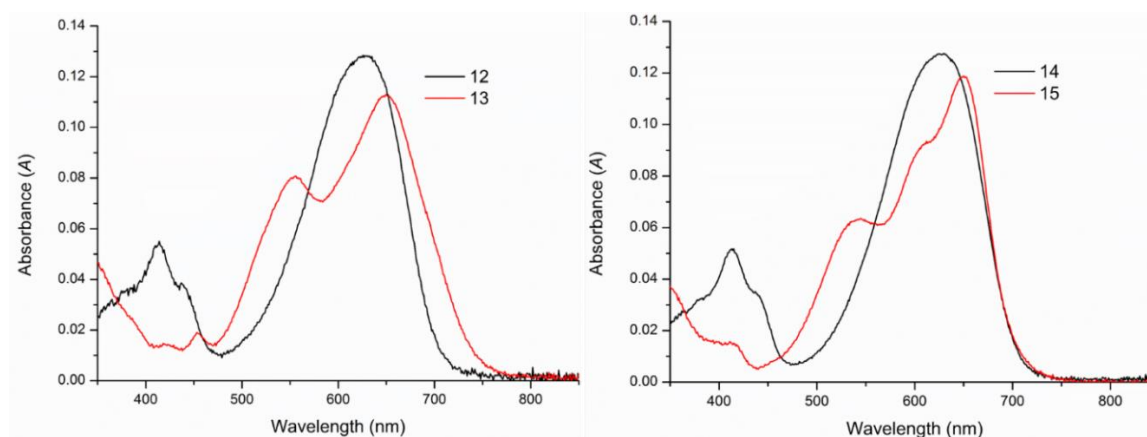


Figure 5.11: UV-Vis absorption spectra of PMI monoanhydrides (**12**, **13**) and dicarboxylic acids (**14**, **15**).

5.1.3. Synthesis of cationic perylene diimide dyes

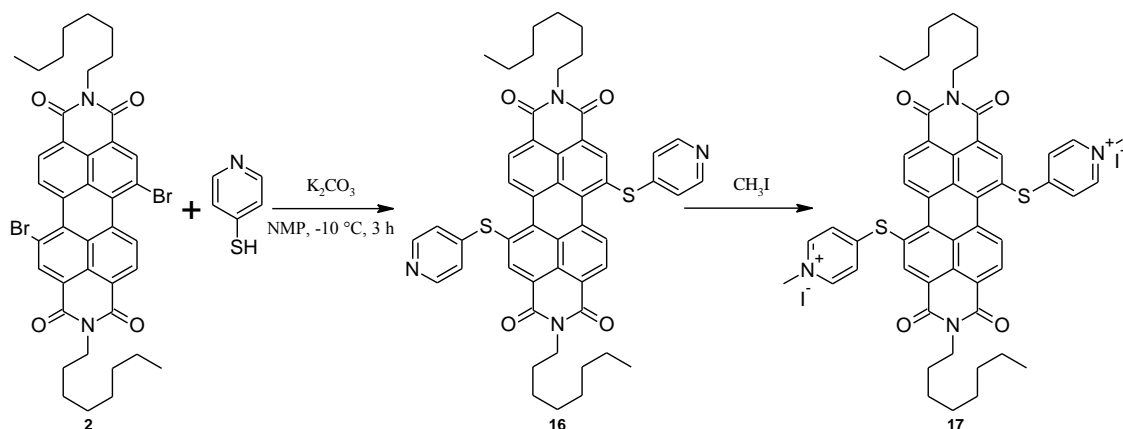
As a first step towards the usage of perylene imide dyes for photoinactivation of microbes, quantum yield of singlet oxygen formation from the synthesized perylene imides were determined. These measurements were conducted at Humboldt University of Berlin, in the group of Professor Beate Roeder. Time-resolved singlet oxygen measurements of the substances showed rather small singlet oxygen signals. The singlet oxygen quantum yields were calculated using Pheophorbide A ($\phi_{\Delta} = 56\%$) as a standard and are compiled in the Table 5.1.

Table 5.1: Singlet oxygen quantum yield for different PDIs and PMIs.

Compounds	Singlet oxygen quantum yield (ϕ_{Δ})
5	4 %
6	< 1 %
13	4 %
14	< 1 %
15	13 %

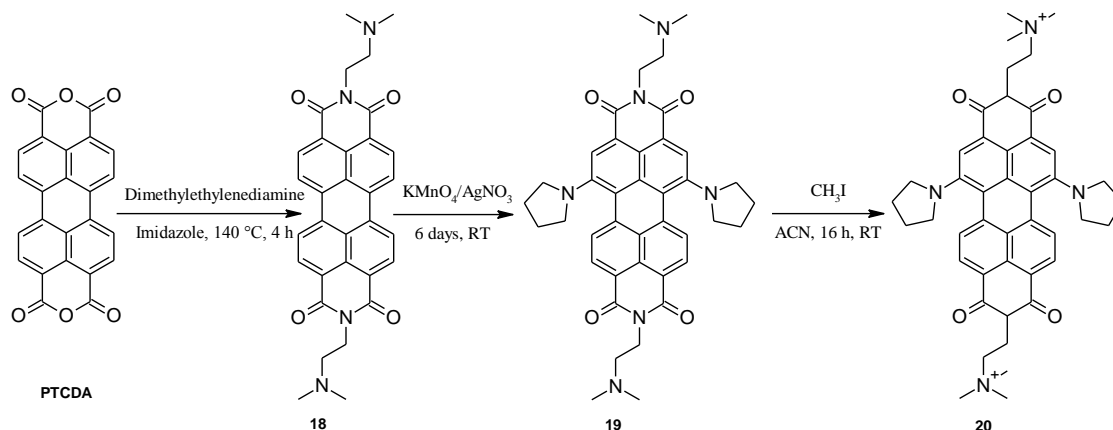
As can be seen from the table, the only potential candidate for PACT was the PMI dicarboxylic acid **15**. For the other compounds, the low values for singlet oxygen quantum yields made them unsuitable for photoantimicrobial applications. Therefore, we changed the synthetic strategy and we attempted to prepare another set of PDIs substituted at bay regions and at imide tail. We planned to prepare substances, which can be later converted to cationic salts. Cationic groups were chosen, as they are known to be effective against both Gram-positive and Gram-negative bacteria.^{68,69} Hence, PDIs with pyridine groups linked directly or through oxy- or thio-bridge on the bay region were synthesized. In addition to this, 1,6-dipyrroliidinyI PDI with amine groups at end position of imide tails was also prepared.

The novel cationic perylene diimide **17** was synthesized by following the synthetic route as summarized in Scheme 5.5. Coupling of a regioisomeric mixture of dibromo PDI **2** with mercaptopyridine resulted in the formation of 1,6- and 1,7-regioisomers of compound **16** in 55 % yield. Attempts to separate the isomers during the purification process were not successful and therefore the mixture was used as such for the next step. Methylation of **16** with methyl iodide yielded cationic bis(mercapto(N-methyl pyridinyl)) PDI **17** in 78 % yield.



Scheme 5.5: Synthesis of cationic bis(mercapto(N-methyl pyridinyl)) PDI **17** (mixture of 1,7 and 1,6-isomers, only 1,7-regioisomer is shown for clarity).

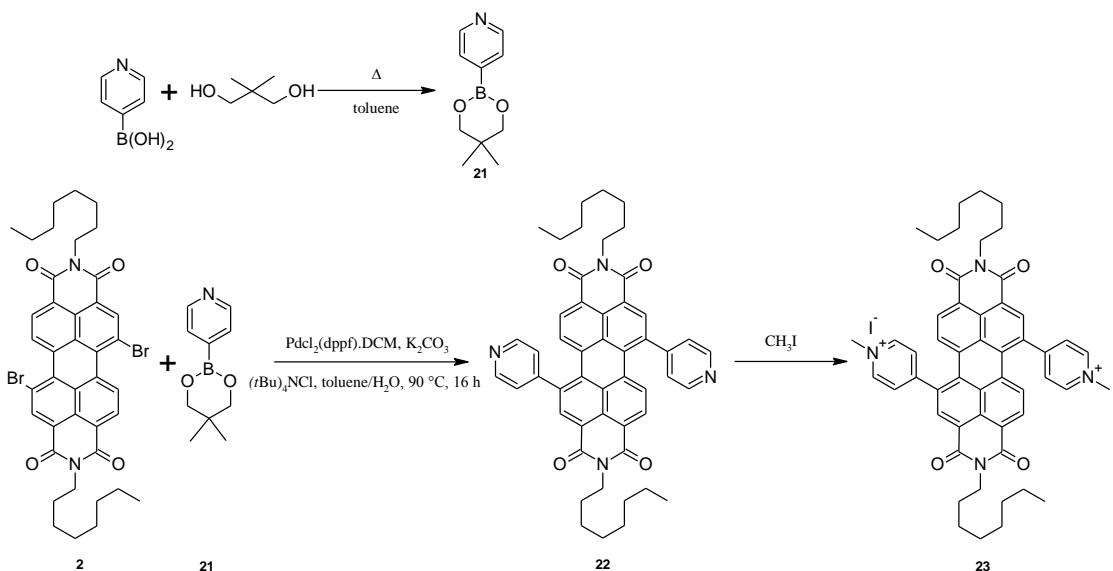
Novel perylene diimide **20** with cationic groups at imide tails was prepared as shown on the Scheme 5.6. The compound **18** was prepared by the procedure described by Langhal *et al.*⁸² Direct amination on bay regions using $\text{AgNO}_3/\text{KMnO}_4$ in pyrrolidine resulted in the formation of 1,6-bis pyrrolidine PDI **19**. The methylation of compound **19** in acetonitrile produced cationic PDI **20**.



Scheme 5.6: Synthesis of cationic dipyrrolidinyl PDI **20**.

Novel perylene diimide **22** with pyridinyl groups at the bay region was also synthesized. Suzuki coupling between regioisomeric mixture of dibromo PDI **2** and pyridine boronic acid produced a mixture of 1,6- and 1,7-isomers of **22** with 20 % yield. In order to improve the yield, pyridine boronic acid was converted into boronate ester **21** by reacting with neopentyl glycol. The reaction could be achieved by the removal of water generated during the reaction either by using molecular sieves or by azeotropic distillation. Boronate ester **21** precipitated upon cooling and its separation from the molecular sieves was difficult. Therefore, azeotropic distillation was preferred in the synthesis and allowed to obtain boronate ester **21** in 80 % yield. With the use of boronate ester, the yield of 1,6- and 1,7-isomers of PDI **22** from Suzuki coupling improved from 20 to 45 %. The 1,7-regioisomer of

22 was isolated by column chromatography. Novel cationic 1,7-PDI **23** was synthesized in 88 % yield by reacting 1,7-isomer of PDI **22** with methyl iodide (Scheme 5.7).



Scheme 5.7: Synthesis of cationic 1,7-dipyridinyl PDI **23**.

The cationic PDIs (**17**, **20** and **23**) were dissolved in ethanol and UV-Visible absorption spectra were measured (Figure 5.12). The molar extinction coefficient of the **17** was calculated using Beer-Lambert law and found to be $30000 \text{ L mol}^{-1} \text{ cm}^{-1}$ at maximum absorption wavelength 524 nm. Similarly PDI **20** exhibited broad absorption peak with maximum at 693 nm and molar extinction coefficient $14182 \text{ L mol}^{-1} \text{ cm}^{-1}$, while for PDI **23** the extinction coefficient was $24363 \text{ L mol}^{-1} \text{ cm}^{-1}$ at maximum absorption wavelength 539 nm.

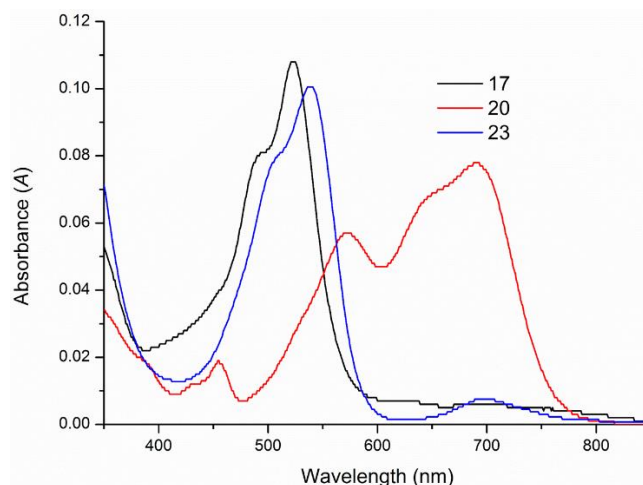
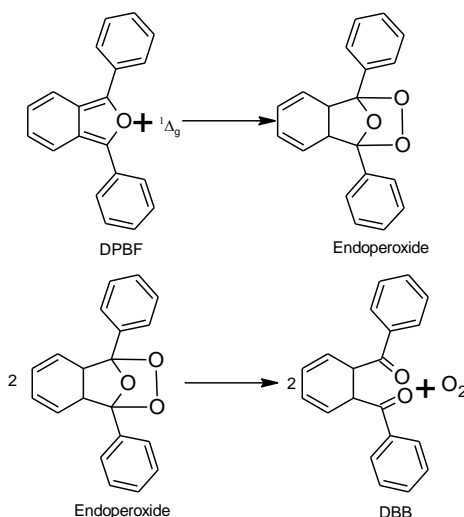


Figure 5.12: UV-Vis absorption spectra of cationic PDIs **17**, **20** and **23**.

The efficiency of the dye to generate singlet oxygen could be determined by photochemical method using 1,3-diphenylisobenzofuran (DPBF). DPBF reacts with singlet oxygen to form *o*-dibenzoyl benzene (DBB) (Scheme 5.8). Thus, the efficiencies for the generation of singlet oxygen of different dyes could be qualitatively compared by monitoring the disappearance of DPBF in the presence of dyes.^{160,161}



Scheme 8: Reaction for the quenching of singlet oxygen by DPBF.

The percentage decrease in the absorbance of DPBF at 411 nm in the presence of different dyes was calculated. The compound **17** was found to decrease 98 % of DPBF absorbance in 3 minutes, while compound **20** reduce 88 % of DPBF absorbance in 5 minutes and compound **23** lowered only 40 % of DPBF absorbance in 5 minutes. The graph (Figure 5.13) shows the decrease of efficiency in the order compound **17** > compound **20** > compound **23**.

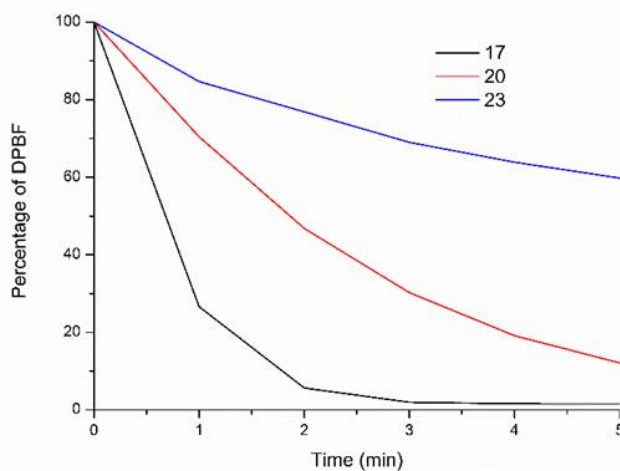


Figure 5.13: The graph showing the efficiency of cationic PDIs.

The graph for compound **17** revealed the disappearance of DPBF after 3 minutes. The constant value (2 %) seen in the graph is not from DPBF concentration. This is actually the absorbance of the dye at 411 nm remained in the solution after the photo oxidation of DPBF.

Time-resolved measurements of the singlet oxygen production of the compounds by luminescence method were done by our collaborator at Humboldt University of Berlin (group of Professor Beate Roeder) and gave matching results for the efficiency of singlet oxygen generation. The results are listed in Table 5.2.

Table 5.2: Singlet oxygen quantum yield for cationic PDIs.

Compounds	Singlet oxygen quantum yield (ϕ_{Δ})
17	19 %
20	12 %
23	5 %

Bay region modification of PDI dyes using pyridine moiety through thio-bridge increased the singlet oxygen quantum yield. However, the values were still too small to expect good antimicrobial efficacies. Different modifications to increase the formation of triplet states in PDIs that in turn could increase the singlet oxygen quantum yield were already mentioned in the previous chapter. However, their implementation would be quite laborious, and we therefore decided to change the core of the photosensitizer and proceed with phthalocyanines for a while.

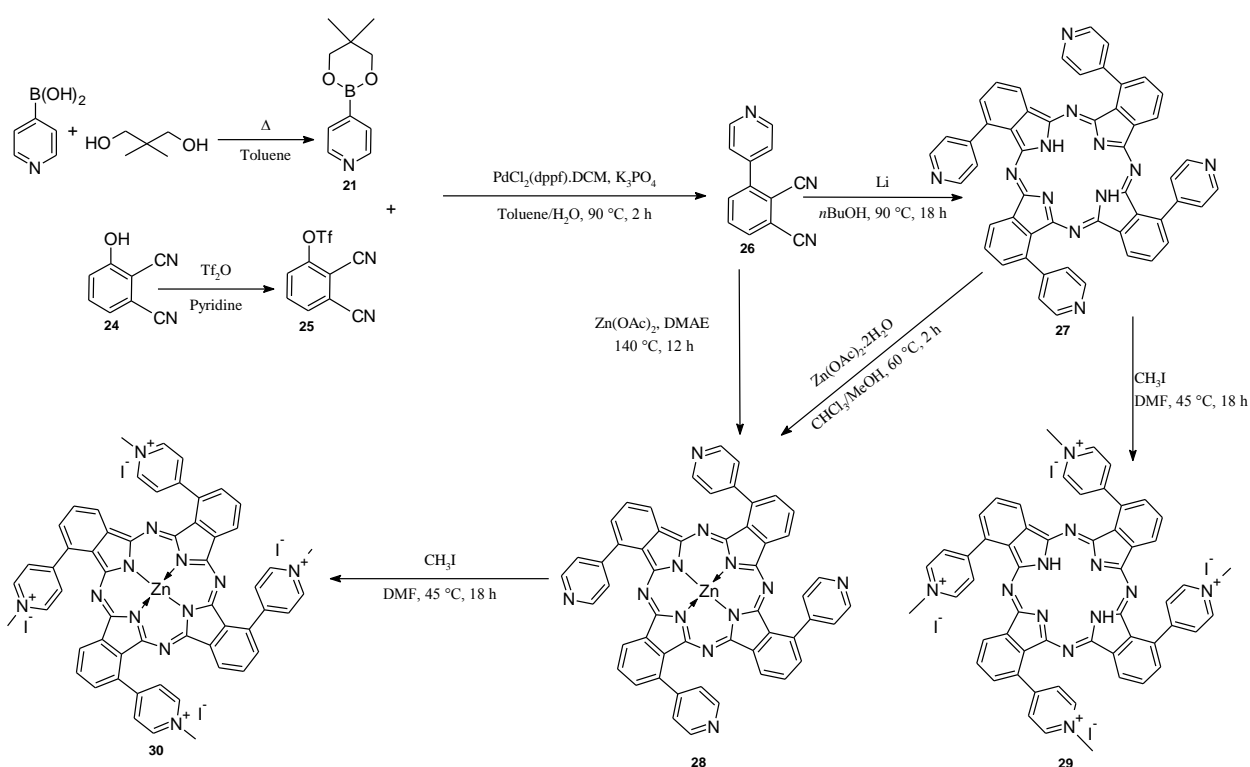
5.2. Synthesis of phthalocyanine photosensitizers.

Synthesis of novel phthalocyanine with direct C-C bond between α -phthalo position and pyridine unit will be described under this section. It should be noted that phthalocyanines with direct C-C- bond at α -position are rather rare.^{128,129,162–166} Most substitutions of phthalocyanines described in the literature are at β -positions and are either through oxy- or thio- linkage. This is also true for amino- and pyridinyl-substituted phthalocyanines. No pyridine substitution of phthalocyanines through direct C-C bond at α -phthalo position was reported before.^{145,167}

Synthesis of phthalocyanines from monosubstituted precursors was always burdened by the formation of regioisomers. Generally, C_{4h} isomer formation was favoured for tetrasubstituted phthalocyanines, synthesized in the presence of lithium alcoholates from phthalonitrile with a bulky group at 3-position. The presence of bulky groups such as aryl 3-position of phthalonitrile restricted the formation of other sterically constrained isomers. Moreover, in order to obtain C_{4h} isomer in a major proportion, the aryl group linked through direct C-C bond at 3-position of phthalonitrile was preferred

over aryloxy group. The aryloxy group would not stay in the plane of phthalocyanine macrocycle during tetramerization reaction because of the sp^3 -hybridization of oxygen atom thereby allowing the formation of other isomers. On the other hand, straight and rigid aryl substituents favoured the formation of C_{4h} isomer.¹⁶⁸ Thus, it was safe to assume that the C_{4h} phthalocyanine isomer's formation would be favoured when pyridine is attached to 3-position of phthalonitrile through direct C-C bond. Tetramerization reaction should be performed in the presence of Li alcoholates at moderate temperature. It must be however noticed that the formation of other isomers in minor amounts would still be possible in this case.

Novel pyridinyl-substituted phthalocyanine was synthesized from 3-pyridinyl phthalonitrile **26** according to Scheme 5.9. 3-Hydroxy phthalonitrile **24** was prepared from commercially available 3-nitrophthalonitrile according to the literature procedure and later converted to triflate salt **25** for Suzuki coupling with pyridine boronate ester **21**.¹⁶⁸ Phthalonitrile **26** can be tetramerized to free base phthalocyanine **27** or directly to phthalocyanine zinc complex **28**. In the first case, Zn(II) complex **28** was prepared by metalation of phthalocyanine **27** using zinc acetate in a mixture of chloroform and methanol with 85 % yield. The direct synthesis of **28** using anhydrous zinc acetate and DMAE is characterized by a very high yield (> 90 %) and proceeds as a single step reaction, which is very important for industrial scale applications. However, the direct synthesis of phthalocyanine using $Zn(OAc)_2$ at higher temperature might lead to the formation of higher proportion of constitutional isomers. Cationic salts **29** and **30** were synthesized from free base phthalocyanine **27** and phthalocyanine Zn(II) complex **28** respectively by reaction with methyl iodide in DMF. (Publication III)



Scheme 5.9: Synthesis of pyridinyl-substituted phthalocyanines **27**, **28**, **29** and **30**.

Formation of tetracationic phthalocyanine was confirmed by the high-resolution mass spectrometry data. The 0.25 Da separation between the peaks in MS signals confirmed the tetracationic charge of the molecule (Figure 5.14).

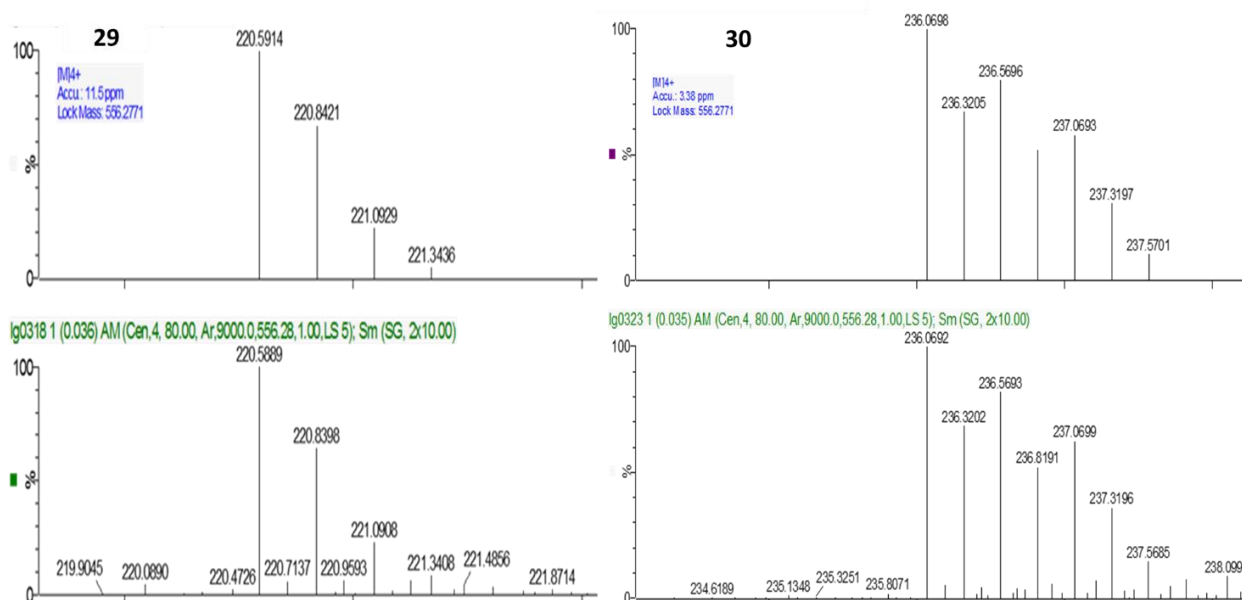


Figure 5.14: High-resolution mass spectra for tetracationic phthalocyanines **29** and **30**.

UV-Visible absorption spectra of the phthalocyanines were measured in chloroform and DMF according to their solubility (Figure 5.15). The spectra were rather broad probably because of the aggregation of the molecules which was also observed in the NMR spectra. The free base phthalocyanines **27** exhibited very high molar extinction coefficient of $100000 \text{ L mol}^{-1} \text{ cm}^{-1}$ at absorption maximum 715 nm. Its corresponding zinc phthalocyanine **28** has absorption maximum at 695 nm with the extinction coefficient $113077 \text{ L mol}^{-1} \text{ cm}^{-1}$. Zinc insertion into phthalocyanine **27** closes the splitting of Q-band peaks. The free base phthalocyanine consists of two type of isoindole nitrogens, one carrying hydrogen atoms and other involved in iminic type functions. Thus, the electronic transitions responsible for Q-band are polarized in x or y directions, giving rise to the split Q-band. The insertion of zinc into the macrocycle give a thermodynamically stable delocalized phthalocyanine dianion with higher symmetry and as a result only one absorption peak is observed in the Q-band.^{169,170} Free base cationic phthalocyanine **29** displayed a broad peak with absorption maximum at 702 nm and extinction coefficient $141250 \text{ L mol}^{-1} \text{ cm}^{-1}$. Phthalocyanine **30** exhibited absorption peak with maximum absorption at 692 nm and extinction coefficient $128500 \text{ L mol}^{-1} \text{ cm}^{-1}$. (Publication III)

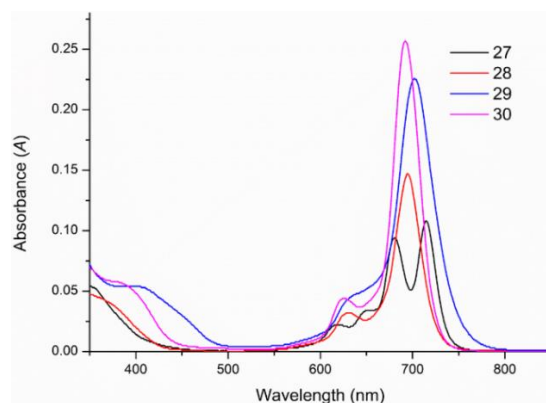


Figure 5.15: UV-Vis absorption spectra of phthalocyanines **27**, **28**, **29** and **30**.

Singlet oxygen quantum yields for cationic phthalocyanines **29** and **30** in water were measured by the group of Professor Beate Roeder at Humboldt University of Berlin using luminescence method. The quantum yield of singlet oxygen for phthalocyanine **30** was calculated to be $30 \pm 20\%$ by comparing the phosphorescence signal intensity at 1270 nm of with that of TMPyP as reference compound with quantum yield 74%. The observed signal had a low signal-to-noise ratio, and the standard bi-exponential model for singlet oxygen luminescence was hard to apply. Hence, quantum yield was determined with the error of the fitting procedure of the NIR luminescence signals that introduced large variation in the result. The value for singlet oxygen quantum yield for phthalocyanine **30** was reasonably good, considering that water is known to quench the singlet oxygen. On other hand, phthalocyanine **29** did not produce any signal for singlet oxygen in water. (Publication III)

5.3. Antimicrobial studies

Successful implementation of PACT depends on many factors such as the ability of a photosensitizer to generate singlet oxygen, immobilization of photosensitizer on a substrate and an accessible and economical light source. Photosensitizers could be reliably grafted onto a substrate by covalent bonding. However, immobilization of photosensitizers by covalent bonds is a laborious and challenging process. Such immobilization requires considerable synthetic work to modify both the substrate and photosensitizer and needs to use a linker between them. The other immobilization methods could be e.g. incorporation of photosensitizers into polymer matrix during electrospinning of polymer fiber, or binding of the dye through electrostatic interactions or by swell-encapsulation-shrink processes. We observed that cationic photosensitizers bound strongly to filter papers just by soaking the paper into a solution of photosensitizer. The filter papers used in laboratory are essentially pure cellulose and these materials have “highly hydrophilic and slight anionic character with a low negative surface charge density”.^{171,172} The cationic dyes therefore probably bind to the filter paper through electrostatic interactions thereby giving it a stable colour. The filter paper impregnated with dyes were stable under light and dyes did not wash out into water even after sonication. Filter paper was chosen as a substrate for testing the prototype photoactive antimicrobial materials owing to the simple procedure of immobilization of cationic photosensitizers. (Publications III and IV)

5.3.1. Screening test for the efficiency of dyes

Comparison of the antimicrobial efficacies of many different photosensitizers is a laborious and time consuming process. Therefore, a simple and fast method for screening of the antimicrobial efficacies using bioluminescent bacteria as reporter cells was developed. The efficiency of photodynamic inactivation of the microbes was estimated from the measurements of the bioluminescence. The intensity of bioluminescence arising from the bacteria on a surface is directly related to the metabolic status of bacteria. When a dye effectively inactivates bioluminescent bacteria, a sharp decrease in signal intensity is observed. Antimicrobial tests were conducted using two Gram-negative bacteria, *Escheria coli* (*E. coli*) and *Acinetobacter baylyi* (*A. baylyi*) ADP1 strains carrying bacterial luciferase genes. Gram-negative bacteria were selected particularly because they are more difficult to inactivate when compared to Gram-positive bacteria.^{68,69} The bioluminescence signal arising from the surface of filter paper soaked with bioluminescent microbes was measured before and after the illumination.

Photodynamic antimicrobial efficacies of cationic perylene dyes were evaluated at first. Small square pieces (area 0.49 cm²) were cut from the filter paper impregnated with cationic PDI dyes and pasted on an LA agar plate in a 3 x 3 grid as shown in Figure 5.16. Each column contained 3 paper pieces with dyes **17**, **20** and **23**. Using a dark screen with a square hole in the center, one column of dyes was protected from light while the other two columns of dyes were left accessible for the light. The whole set up was placed inside the solar simulator and was illuminated for 1 h with the light intensity 18 mW/cm². In order to eliminate the effects of UV and infrared radiations on the growth of microbes, optical filters were used to cut off these wavelengths.

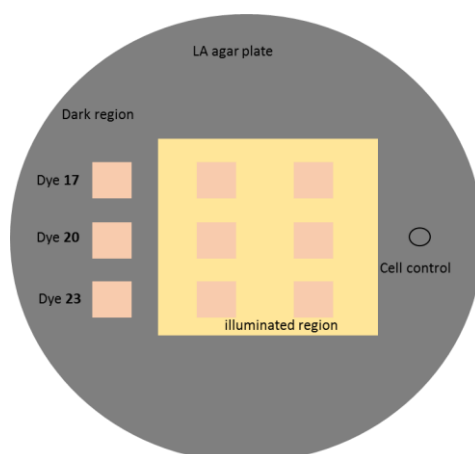


Figure 5.16: Schematic diagram of the setup for screening the antimicrobial dyes.

Photodynamic inactivation of microbes after 1 hour of illumination was negligibly low. Even though, a difference in intensity between samples and cell control was observed, the result were not convincing enough. The intensity of the signals in the illuminated and dark regions remained almost same, except for the dye **20** (Figure 5.17). Interestingly, PDI **23** with the lowest singlet oxygen quantum yield decreased the bioluminescence similarly as the other two PDIs.

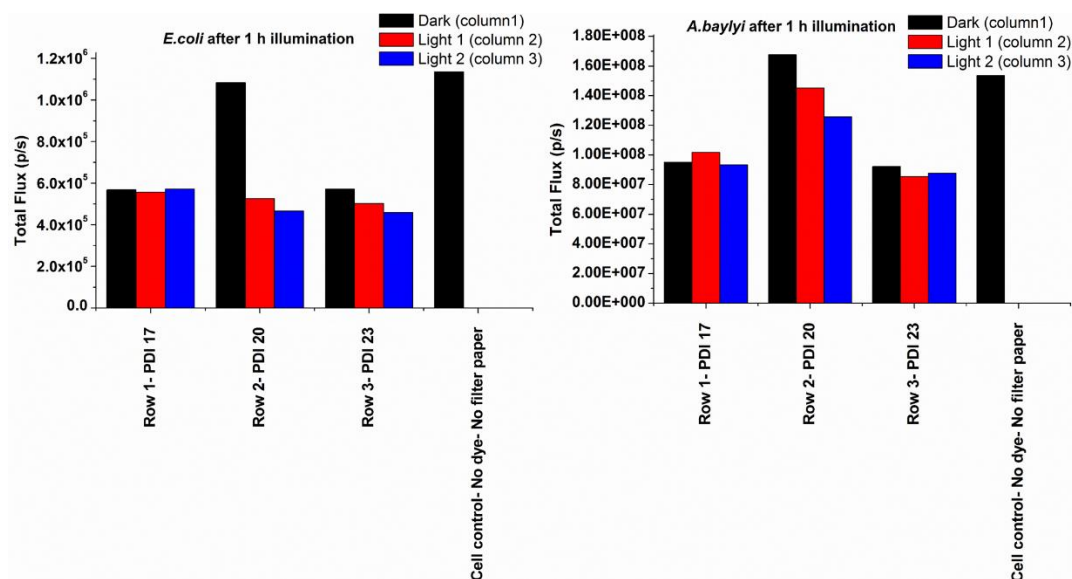


Figure 5.17: Bioluminescence from dark and illuminated PDI-dyed samples.

A slightly modified set up was used to improve the reproducibility of measurements during the evaluation of antimicrobial efficacies of filter papers dyed with phthalocyanines. Previously for the PDI dyes, square shaped papers were used for testing. In a new setup, paper discs of identical size were cut with the help of a hole puncher, since a slight difference in the size of the papers would strongly affect the total counted luminescence intensity. Moreover, the blank control filter papers both in the dark and illuminated regions were added to increase the credibility of the results. The modified setup is shown in Figure 5.18.

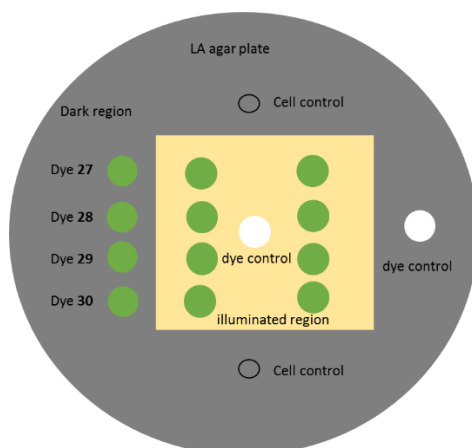


Figure 5.18: Schematic diagram of the modified setup for screening the dyes. (Publication III; reproduced with the permission from Elsevier)

The surfaces with cationic phthalocyanines **29** and **30** demonstrated antimicrobial efficacy higher than the neutral compounds against bioluminescent *E. coli*. Moreover, cationic zinc derivative **30** had shown higher efficacy than free base phthalocyanine **29**. The bioluminescence from the paper

dyed with **30** incubated in the dark region of the plate was also found to be low. This decrease might not be originated from the dark toxicity of the compound. Probably, the exposure to stray light could trigger photo inactivation of microbes, since incubation was done in the same plate. The results are shown in Figure 5.19. (Publication III)

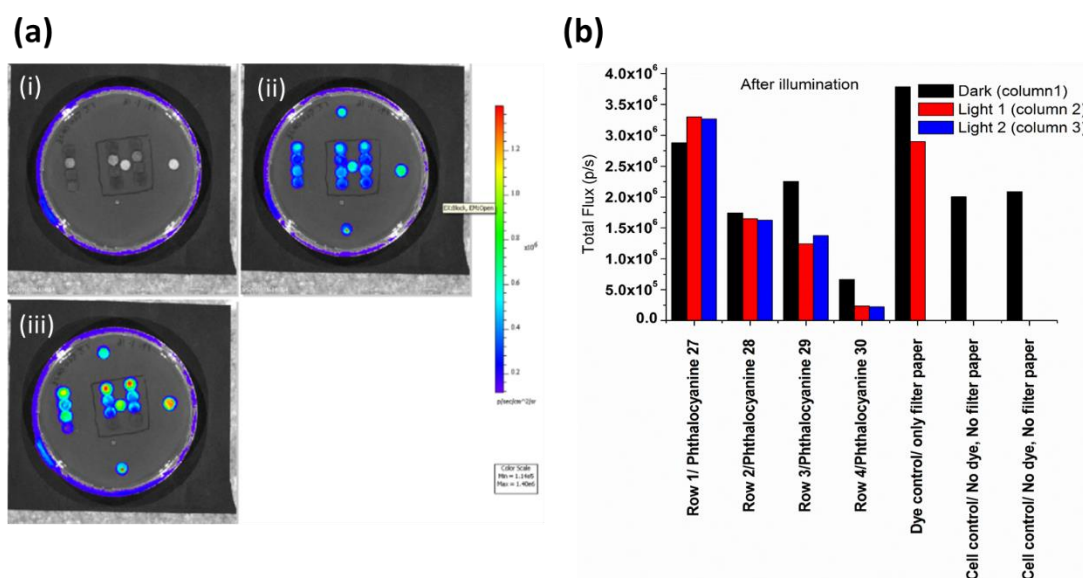


Figure 5.19: (a) Bioluminescent images of *E. coli* (carrying pBAV1C-T5-lux plasmid) on surface, before and after light exposure. (i) background image, (ii) before illumination, (iii) after illumination; (b) graph showing the antibacterial activity of the phthalocyanines after illumination. (Publication III; reproduced with the permission from Elsevier)

Antimicrobial tests using filter paper soaked with bioluminescent *A. baylyi* were also conducted. Dyes **28**, **29** and **30** demonstrated significant photoinactivation of microbes (Figure 5.20). Cationic phthalocyanines and zinc complex **30** in particular had shown higher activity. In this experiments signals from the dyed paper kept in the dark region were also absent due to the stray light exposure. The screening tests of surfaces impregnated with phthalocyanine dyes concluded that tetracationic derivatives and particularly zinc derivative **30** were more efficient than the neutral ones. The extra cationic charges of the molecule might had played an important role in binding the Gram-negative bacteria to the photosensitizer molecules thereby ensuring a better photodynamic inactivation. (Publication III)

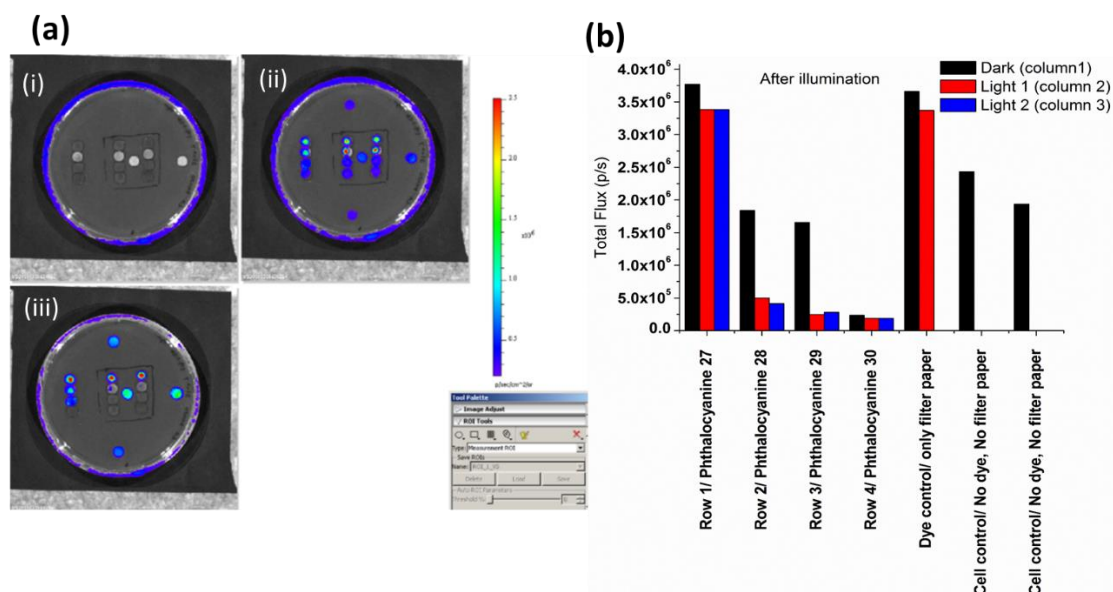


Figure 5.20: (a) Bioluminescent images of *A. baylyi* ADP1 (carrying plasmid pBAV1C-T5-lux) on surface, before and after light exposure. (i) background image, (ii) before illumination, (iii) after illumination; (b) graph showing the antibacterial activity of the phthalocyanines after illumination. (Publication III; reproduced with the permission from Elsevier)

5.3.2. Antimicrobial efficacy by CFU counting

The screening tests using bioluminescent bacteria demonstrated that the surface impregnated with tetracationic phthalocyanine **30** was the most potent material for further studies. Antimicrobial efficacy of filter paper impregnated with phthalocyanine **30** was quantitatively determined by CFU counting using wild type microbes. In order to control the growth of microbes during the illumination experiments and upon serial dilutions, the LB medium was replaced with PBS buffer before the deposition on the filter paper.

From the previous experiments, phthalocyanine **30** was found to be highly phototoxic towards both *E. coli* and *A. baylyi*. Since the inactivation experiments were conducted on the surface, the number of colonies from control samples were large, and the dye exhibited very high photoinactivation of microbes even at low concentrations, the half maximal inhibitory concentration (IC₅₀) value for the dye was not calculated. Instead, the minimal inhibitory dye loading at given light dose was estimated. Filter papers with different dye loading were prepared by soaking the filter papers into water solutions with different concentrations of dye **30** (Figure 5.21). The antimicrobial test using these papers were conducted using *A. baylyi*, and the number of colonies from the microbial extracts from each paper was counted to determine an optimum dye loading. (Publication III)

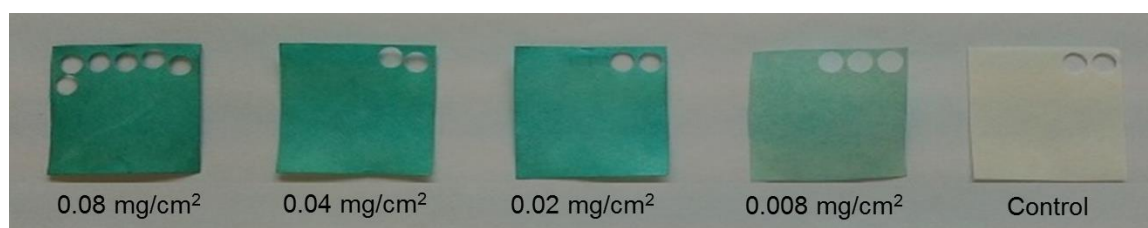


Figure 5.21: Filter papers impregnated with different concentrations of dye **30**. (Publication III; reproduced with the permission from Elsevier)

The papers with microbes were illuminated for 1 hour, the microbes were extracted with PBS buffer and plated onto LA agar plates. For papers with the dye load higher than 0.008 mg/cm², no colonies of bacteria could be found on LA plates incubated overnight. This implies that papers with higher dye loads were highly phototoxic, and the smallest dye load would be sufficient and necessary for quantitative testing of the antimicrobial efficacy. The results of these tests are compiled in Table 5.3.

Table 5.3: Photoinactivation of *A. baylyi* under illumination. (Publication III; reproduced with the permission from Elsevier)

Dye loading	Number of colonies	
	1 st dilution	2 nd dilution
0.08 mg/cm ²	0	0
0.04 mg/cm ²	0	0
0.02 mg/cm ²	0	0
0.008 mg/cm ²	20	1
Control	Too many to count	Too many to count

Hence, the filter paper with the dye load 0.008 mg/cm² was used for further antimicrobial tests. The optical densities of the microbial solutions measured before the deposition on the filter paper were 0.2 and 0.1 for *E. coli* and *A. baylyi* respectively. The higher number of colonies of *E. coli* compared to *A. baylyi* grown after the plating agrees with the optical measurements. The filter paper impregnated with phthalocyanine **30** demonstrated photoinactivation of 2.7 log reduction in CFU against *E. coli* and 3.4 log reduction in CFU against *A. baylyi* with the light intensity 18 mW/cm² (Figure 5.22).

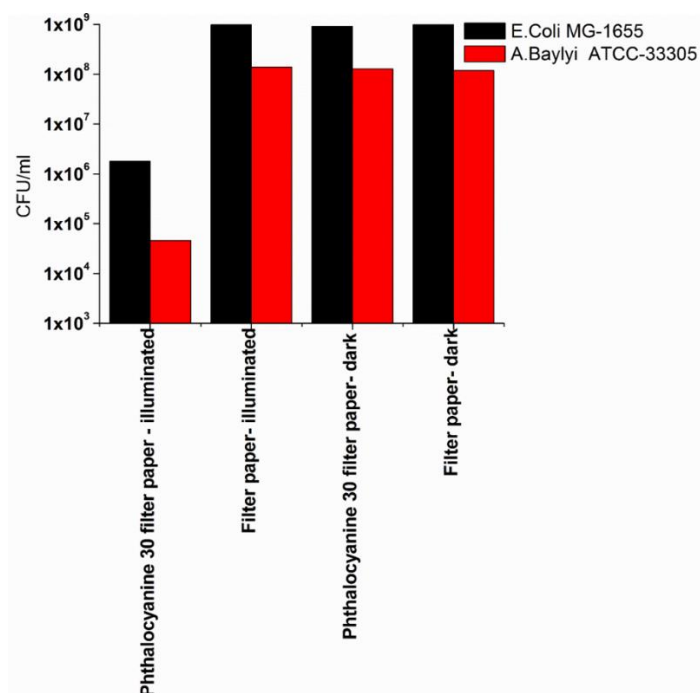


Figure 5.22: Antimicrobial efficacy of filter paper dyed with phthalocyanine **30** against *E. coli* and *A. baylyi*. (Publication III; reproduced with the permission from Elsevier)

5.3.3. Antimicrobial efficacy using consumer LED lamp

The successful implementation of PACT in everyday life requires an accessible and economical light source. However, our previous experiments were conducted using a solar simulator, which is inconvenient in practical applications. Therefore, as a next step of our research the photoinactivation of microbes was assessed using commercially available lighting system such as consumer LED lamp. The antimicrobial efficacy of paper impregnated with cationic zinc phthalocyanine **30** illuminated with a consumer LED lamp was calculated and evaluated against the paper dyed with an already known tetracationic photosensitizer, Zn(II) tetrakis(methylpyridinyl idonium) porhyrin **31** (Figure 5.23).^{173,174} During this study, important parameters such as photostability of the dye-impregnated paper and stability against leaching were also evaluated.

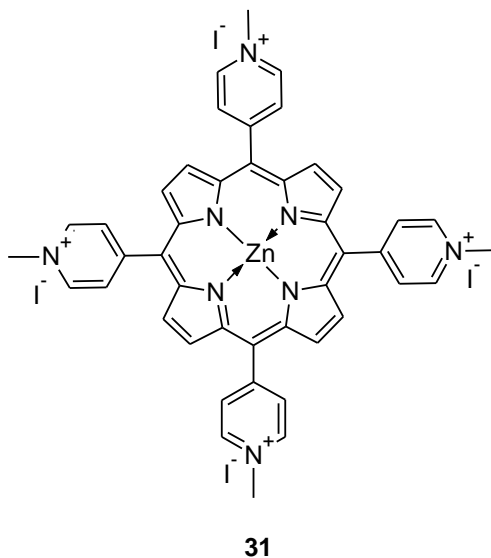


Figure 5.23: Chemical structure of Zn(II) tetrakis(methylpyridyl iodonium) porphyrin.

5.3.3.1. Lamp profile and light dose calculation

Selection and comparison of consumer bulbs for photodynamic therapy are rather difficult as the spectral data are not generally available. Therefore, the spectrum of LED lamp was measured prior to the experiments. The wavelength range of lamp emission was found to span from 400 nm to 750 nm with a maximum at 594 nm (Figure 5.24a). To make the photoinactivation experiments more precise, the power density of the lamp was also measured at different illumination distances. The absorbance profiles of the papers impregnated with phthalocyanine and porphyrin were recorded. Porphyrin-dyed paper exhibited a maximum absorption at 430 nm while phthalocyanine-dyed paper had a maximum absorption at 696 nm. The absorbance profiles of dyes were recalculated since, the both dyed papers absorbed at different wavelength, neither the lamp emission profile was uniform. Recalculated light absorbance at certain wavelength was determined using the equation $I(\lambda) = L(\lambda) \times a(\lambda) / 100$, where $I(\lambda)$ is the absorbed light dose, $L(\lambda)$ is the relative light intensity of the lamp, and $a(\lambda)$ is the absorbance value as measured with the integrating sphere. The recalculated spectra are shown in Figure 5.24b. The ratio of the area under the recalculated spectra for respective dyes to the total area of the lamp spectrum gives the absorbed light power densities for porphyrin and phthalocyanine dyed papers. The absorbed light power density for porphyrin-dyed paper was found to be 1.2 times higher than that of phthalocyanine-dyed material. Thus for the lamp intensity 35 mW/cm², the calculated light doses were 45 J/cm² and 37 J/cm² for porphyrin and phthalocyanine, respectively. This variation in the light doses was taken into account while setting up the illumination conditions for the phototreatment. Hence, for porphyrin-impregnated paper, the total light intensity of the lamp would be decreased to 29 mW/cm² to equal the light dose of phthalocyanine-impregnated paper. (Publication IV)

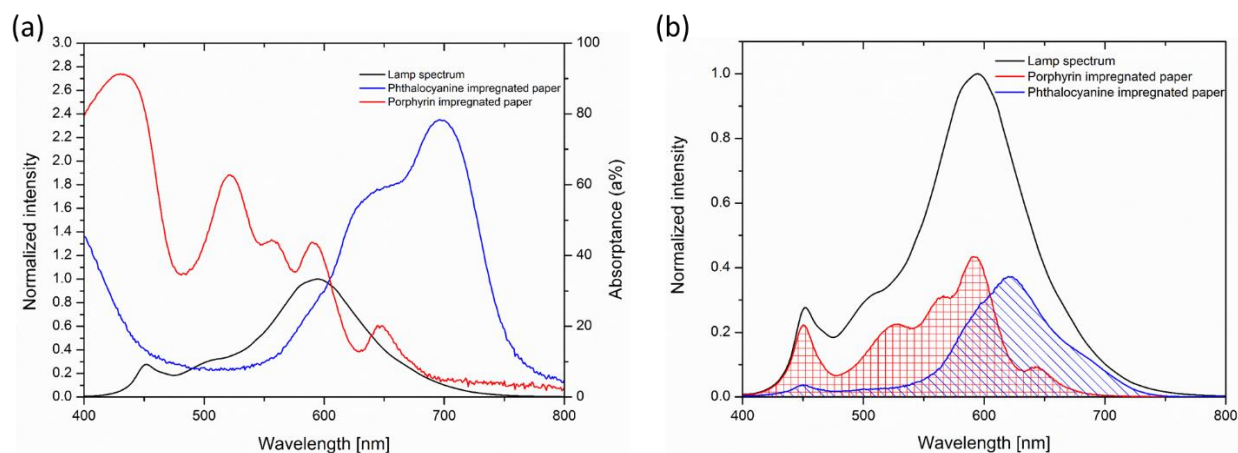


Figure 5.24: (a) The lamp spectrum and absorbance of zinc phthalocyanine and porphyrin impregnated papers (b) light dose calculated for phthalocyanine- and porphyrin-impregnated papers. (Publication IV)

5.3.3.2. Photostability and leaching test of dyed filter papers

The photostability of the filter papers impregnated with phthalocyanine **30** and porphyrin **31** was tested. The reflectance and transmittance measurements were used to calculate the absorbance of papers (Figure 5.25). The difference in the absorbance values before and after the illumination in air was used as the criterion. The absorption profile of phthalocyanine-dyed paper remained unchanged even after 64 hours of continuous illumination. The calculated absorbance at 696 nm before the illumination was 81.88 % and after illumination it was 71.30 %. The photodegradation for the phthalocyanine **30** impregnated on paper was calculated from the difference in the absorbance values, and it was found to be 12.9 %. In the case of the paper dyed with porphyrin **31**, the peaks around 520 nm and 590 nm disappeared almost completely after the exposure to light. The absorbance of the main peak around 430 nm for porphyrin-impregnated paper before illumination was 90.50 % and after illumination it was 81.28 %. Hence, the difference in the values give the photodegradation of porphyrin-dyed paper as high as 10.18 %, however with obvious degradation of the spectrum. These results demonstrated superior photostability of phthalocyanine-impregnated papers even after 64 h of continuous illumination with light intensity of 42 mW/cm². (Publication IV)

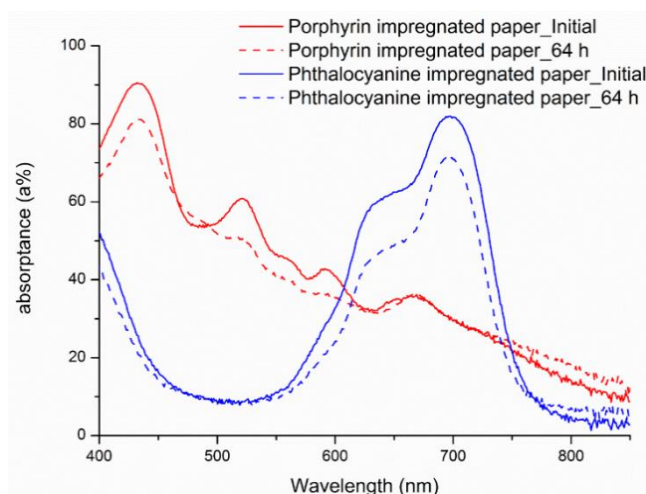


Figure 5.25: Absorbance of dye-impregnated papers before and after irradiation. (Publication IV)

Leaching of the dyes was tested by incubation of the dyed papers in PBS buffer with pH 7.4. The UV-Vis absorption spectra of the PBS extracts were measured to determine the amount of dye leached out from paper. The fluorescence measurements of the extracts were also done in order to detect the minute concentrations of dye that could not be observed by absorption measurements. The PBS extract of porphyrin paper had shown a strong absorption peak at 422 nm that confirmed the leaching of porphyrin **31** into the solution. A broad intense emission peak with the maximum around 720 nm was also observed during the emission measurement of the PBS extract excited at 422 nm. UV-Vis absorption measurement of the PBS extract of phthalocyanine paper did not show any peak even after 20 h of incubation at room temperature (Figure 5.26a). However, in the emission measurements, upon excitation at 694 nm, the extract produced a faint signal (Figure 5.26b) which indicated that only negligible amount of phthalocyanine **30** was extracted into buffer. It must be underlined that such a strong binding ability of cationic phthalocyanine **30** is much beneficial for practical applications. (Publication IV)

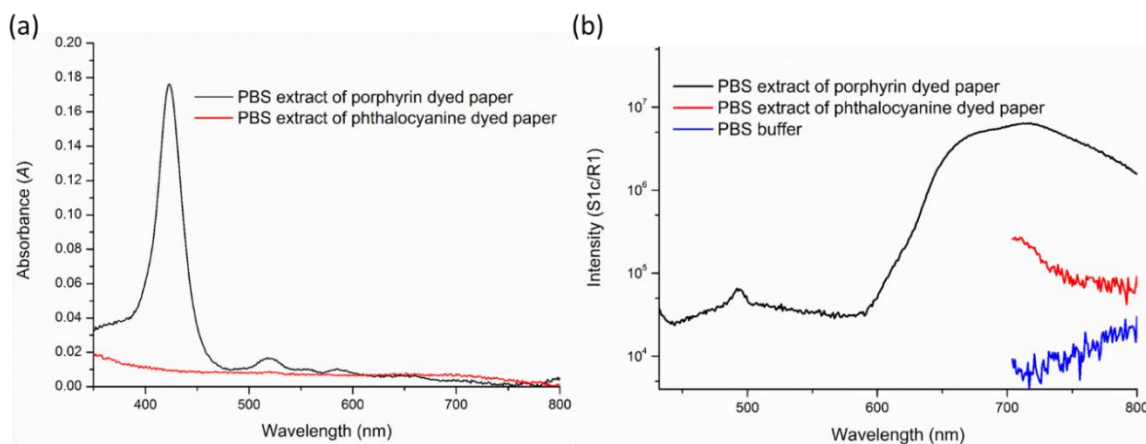


Figure 5.26. (a) Absorbance measurements (b) emission measurements of PBS extracts of dye-impregnated papers. (Publication IV)

5.3.3.3. Comparison of antimicrobial efficacy by CFU counting

The total light intensity of the LED lamp was set at 35 mW/cm² for the paper dyed with phthalocyanine **30**. From the absorbance profile it can be calculated that the phthalocyanine-dyed paper would be exposed to the absorbed light dose of 37 J/cm² after 1 hour of illumination. In order to obtain the same light dose for paper dyed with porphyrin **31**, the total light intensity of LED lamp was reduced to 29 mW/cm², which would give the absorbed light dose 37 J/cm². At this intensity, the microbes were found to be completely inactivated after 1 h of illumination. Such high efficacy can be explained by the leakage of immobilized porphyrin into PBS buffer, which created a considerable concentration of the photosensitizer in the solution thereby enhancing the inactivation of microbes. Therefore, in order to obtain a countable number of colonies of bacteria after illumination, the total light intensity of LED lamp was reduced to 4 mW/cm². The absorbed light dose was calculated to be 5.04 J/cm². Under these conditions, the antimicrobial efficacy of paper dyed with porphyrin **31** was 1.66 and 2.01 log reduction in CFU against *E. coli* and *A. baylyi* respectively. (Publication IV)

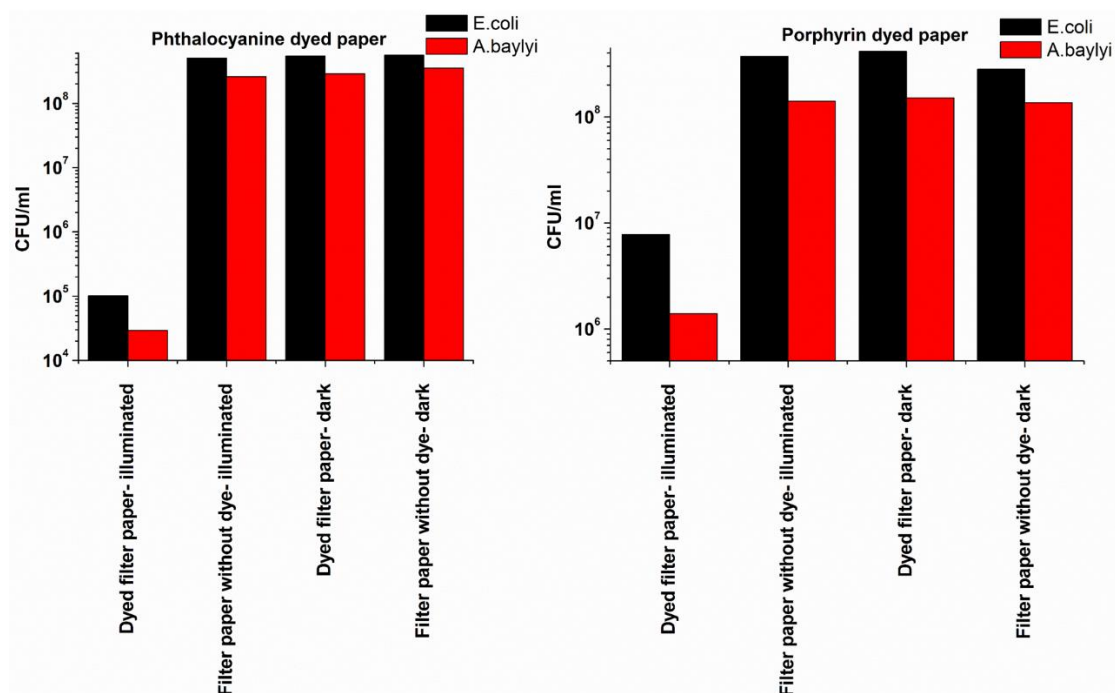


Figure 5.27: Antimicrobial efficacy of dye-impregnated papers against *E. coli* and *A. baylyi* after 1 h of light exposure. (Publication IV)

The paper dyed with phthalocyanine **30** demonstrated excellent antimicrobial efficacy of 3.72 and 4.01 log reduction in CFU units against *E. coli* and *A. baylyi*, respectively after 1 hour of illumination with the light dose 37 J/cm² (Figure 5.27). Comparison of the result with Table 2.1 shows that the photoinactivation achieved by cationic zinc phthalocyanine **30** is comparable to that of other efficient porphyrinoid photosensitizers on surfaces reported in the literature. However, in our studies we used obviously a smaller load of the photosensitizer. High photostability, strong binding ability and signif-

ificant photoinactivation of Gram-negative bacteria makes cationic zinc phthalocyanine **30** a right candidate for further photoantimicrobial studies using different microbes. Furthermore, studies using phthalocyanine **30** impregnated on different polymer substrates other than filter paper would also be conducted. Our results proved that consumer LED bulb can be used for the photodynamic inactivation of microbes. Use of consumer LED lamp as an illumination source dramatically enhances the applicability of PACT in everyday life, where an accessible and inexpensive illumination device is required.

6. Conclusions

A novel method for the direct amination of the bay region of perylene imides was developed. The method was found to be highly regioselective and produced 1,6- or 7,12-substituted perylene diimides and perylene monoimides, respectively as the major products. The reaction proceeded through a radical anion intermediate. The presence of imide cycle was crucial for the reaction to happen. Synthesis of novel 7-pyrrolidnyl and 7,12-bispyrrolidinyl perylene imides with the anhydride and dicarboxylic acid anchoring groups for immobilization on substrates was also developed. Three different perylene diimides with cationic groups were synthesized and immobilized on filter paper to study the photoantimicrobial effect.

Synthesis of novel phthalocyanine with pyridinyl substituents at α -positions via direct C-C bond and preparation of its zinc complexes and cationic derivatives was developed. Tetracationic zinc phthalocyanine was found to be the most efficient photosensitizer with the singlet oxygen quantum yield of 30 ± 20 % in water.

A fast and simple screening setup for testing the photodynamic antimicrobial substances using bioluminescent bacteria *E. coli* and *A. baylyi* was elaborated, and the synthesized dyes were screened for their antimicrobial activity. Tetracationic Zn(II) phthalocyanine was found to be the most efficient antimicrobial substance, and the quantitative measurements of the photodynamic effect were undertaken. The paper impregnated with the dye concentration as low as 80 mg/m^2 of tetra cationic zinc phthalocyanine demonstrated significant antimicrobial efficacy after 1 h illumination with 18 mW/m^2 light in a solar simulator. The paper impregnated with the dye achieved photoinactivation of 2.7 log CFU reduction against *E. coli* and 3.4 log CFU reduction against *A. baylyi*, respectively.

The possibility of using an economical and easily accessible light source was established after evaluating the antimicrobial efficacies of papers impregnated with tetracationic zinc phthalocyanine and tetracationic zinc porphyrin. Both dyed papers exhibited excellent photoinactivation of microbes upon illumination with consumer LED lamp. The paper impregnated with tetracationic zinc phthalocyanine demonstrated 3.72 and 4.01 log reduction in CFU against *E. coli* and *A. baylyi* respectively after 1h of illumination with consumer LED at 35 mW/cm^2 . Phthalocyanine-impregnated paper exhibited very high stability in the leaching test. The bleaching studies revealed that phthalocyanine-impregnated paper have very good photostability, with no significant degradation even after 64 h of continuous exposure to the light.

6.1. Future Perspectives

The phthalocyanine-impregnated paper served as a prototype substrate for testing the antimicrobial activity against antibiotic-resistant bacteria. The antimicrobial efficacy of the phthalocyanine-impregnated paper should be evaluated against the known antimicrobial materials such as silver- or copper-impregnated surfaces. Further improvements in the antimicrobial efficacy of pyridinyl phthalocyanine

could be achieved by changing the central metal atom with different elements. For example, introduction of elements such as phosphorous, silicon will alter the photochemical properties of phthalocyanines significantly. Moreover, the possibility of using the axial ligands of these elements as anchoring groups is an additional advantage for the immobilization on surfaces. The use of different metals such as aluminum and iron as central metal could also alter the properties of phthalocyanines. Efficiency of PDIs to generate singlet oxygen in high quantum yields could be improved by ortho-substitution and thionation reactions. These reactions could be performed without considerable synthetic effort. Another important method that could improve the efficiency of PDIs to generate singlet oxygen is by attaching to fullerenes. Comprehensive set of toxicity tests including genotoxicity, skin irritation and eye irritation of the developed photosensitizers should also be done before development of commercial self-disinfecting surfaces.

The newly developed photosensitizers impregnated into various solid substrates could be developed in future into self-disinfecting fibers and cloths, paints, films, filters for air and water sanitization and other photoactive antimicrobial materials. Another area of application is the development of photoactive antimicrobial biomedical surfaces such as hydrogel and adhesive bandages. Along with the efforts to develop novel photosensitizers, significant research should be dedicated to develop stable and efficient methods to incorporate photosensitizers on to substrates. Leaching of photosensitizers from the surface loses the antimicrobial efficiency of the modified surface thereby defeating the very purpose of self-disinfecting surfaces. With the use of inexpensive consumer LED light sources, the implementation of PACT into everyday life could be accelerated. Prospective customers are hospitals, healthcare industries, paint manufactures, manufacturers of air and water purification systems.

References

1. MacPherson DW, Gushulak BD, Baine WB, et al. Population mobility, globalization, and antimicrobial drug resistance. *Emerg Infect Dis.* 2009;15(11):1727-1732. doi:10.3201/eid1511.090419.
2. Gushulak BD, MacPherson DW. Globalization of Infectious Diseases: The Impact of Migration. *Clin Infect Dis.* 2004;38(12):1742-1748. doi:10.1086/421268.
3. Saker L, Lee K, Cannito B, Gilmore A, Campbell-Lendrum D. Globalization and infectious diseases: A review of the linkages. *Trop Med.* 2004;(3):63. doi:TDR/STR/SEB/ST/04.2.
4. Murray KA, Preston N, Allen T, Zambrana-Torrel C, Hosseini PR, Daszak P. Global biogeography of human infectious diseases. *Proc Natl Acad Sci.* 2015;112(41):12746-12751. doi:10.1073/pnas.1507442112.
5. Brockmann D. Global Connectivity and the Spread of Infectious Diseases. *Nov Acta Leopoldina NF Nr.* 2017;419(419):129-136. http://rocs.hu-berlin.de/papers/brockmann_2017b.pdf.
6. Morens DM, Fauci AS. Emerging Infectious Diseases: Threats to Human Health and Global Stability. *PLoS Pathog.* 2013;9(7):7-9. doi:10.1371/journal.ppat.1003467.
7. Allegranzi B, Kilpatrick C, Storr J, Kelley E, Park BJ, Donaldson L. Global infection prevention and control priorities 2018–22: a call for action. *Lancet Glob Heal.* 2017;5(12):e1178-e1180. doi:10.1016/S2214-109X(17)30427-8.
8. Connectivity and Emerging infectious diseases in southeast Asia. <http://www.irinnews.org/feature/2014/02/03>. Published 2014. Accessed March 14, 2018.
9. Belluz J. 4 Reasons Disease Outbreaks Are Erupting Around the World. Vox.com. <https://www.vox.com/2016/5/31/11638796/why-there-are-more-infectious-disease-outbreaks>. Published 2016.
10. WHO. *Guidelines on Core Components of Infection Prevention and Control Programmes at the National and Acute Health Care Facility Level.*; 2016. <http://www.wipo.int/amc/en/mediation/rules%0Ahttp://apps.who.int/iris/bitstream/10665/251730/1/9789241549929-eng.pdf?ua=1>. 10/06/2017.

11. Cassini A, Plachouras D, Eckmanns T, et al. Burden of Six Healthcare-Associated Infections on European Population Health: Estimating Incidence-Based Disability-Adjusted Life Years through a Population Prevalence-Based Modelling Study. *PLoS Med.* 2016;13(10):1-16. doi:10.1371/journal.pmed.1002150.
12. Hensley BJ, Monson JRT. Hospital-acquired infections. *Surg (United Kingdom)*. 2015;33(11):528-533. doi:10.1016/j.mpsur.2015.08.008.
13. Al-Tawfiq JA, Tambyah PA. Healthcare associated infections (HAI) perspectives. *J Infect Public Health.* 2014;7(4):339-344. doi:10.1016/j.jiph.2014.04.003.
14. Khan HA, Baig FK, Mehboob R. Nosocomial infections: Epidemiology, prevention, control and surveillance. *Asian Pac J Trop Biomed.* 2017;7(5):478-482. doi:10.1016/j.apjtb.2017.01.019.
15. ECDC. Annual Epidemiological Report 2016 – Healthcare-associated infections acquired in intensive care units. 2016;(May):22-25. https://ecdc.europa.eu/sites/portal/files/documents/AER-HCAI_ICU_3_0.pdf <https://ecdc.europa.eu/en/publications-data/healthcare-associated-infections-acquired-intensive-care-units-annual>.
16. Mitchell A, Spencer M, Edmiston C. Role of healthcare apparel and other healthcare textiles in the transmission of pathogens: A review of the literature. *J Hosp Infect.* 2015;90(4):285-292. doi:10.1016/j.jhin.2015.02.017.
17. Bravo Z, Chapartegui-González I, Lázaro-Díez M, Ramos-Vivas J. *Acinetobacter pittii* biofilm formation on inanimate surfaces after long-term desiccation. *J Hosp Infect.* 2018;98(1):74-82. doi:10.1016/j.jhin.2017.07.031.
18. Fijan S, Turk SŠ. Hospital textiles, are they a possible vehicle for healthcare-associated infections? *Int J Environ Res Public Health.* 2012;9(9):3330-3343. doi:10.3390/ijerph9093330.
19. Donlan RM. Biofilm formation: a clinically relevant microbiological process. *Clin Infect Dis.* 2001;33(8):1387-1392. doi:10.1086/322972.
20. Boucher HW, Talbot GH, Bradley JS, et al. Bad Bugs, No Drugs: No ESKAPE! An Update from the Infectious Diseases Society of America. *Clin Infect Dis.* 2009;48(1):1-12. doi:10.1086/595011.
21. van Wezel GP. Eliciting antibiotics active against the ESKAPE pathogens in a collection of actinomycetes isolated from mountain soils. *Microbiology.*

- 2014;160(2014):1714-1725. doi:10.1099/mic.0.078295-0.
22. Pendleton JN, Gorman SP, Gilmore BF. Clinical relevance of the ESKAPE pathogens. *Expert Rev Anti Infect Ther.* 2013;11(3):297-308. doi:10.1586/eri.13.12.
 23. Santajit S, Indrawattana N. Mechanisms of Antimicrobial Resistance in ESKAPE Pathogens. *Biomed Res Int.* 2016;2016. doi:10.1155/2016/2475067.
 24. Klein E, Smith DL, Laxminarayan R. Hospitalizations and deaths caused by methicillin-resistant *Staphylococcus aureus*, United States, 1999-2005. *Emerg Infect Dis.* 2007;13(12):1840-1846. doi:10.3201/eid1312.070629.
 25. Grundmann H, Aires-de-Sousa M, Boyce J, Tiemersma E. Emergence and resurgence of methicillin-resistant *Staphylococcus aureus* as a public-health threat. *Lancet.* 2006;368(9538):874-885. doi:10.1016/S0140-6736(06)68853-3.
 26. Centers for Disease Control and Prevention. General Information About MRSA in Healthcare Settings. <https://www.cdc.gov/mrsa/healthcare/index.html>. Accessed March 14, 2018.
 27. Huang S. Staph infections carry long-term risks. <https://medicalxpress.com/news/2008-07-staph-infections-long-term.html>. Published 2008. Accessed March 14, 2018.
 28. Mayo Clinic. MRSA infection. <https://www.mayoclinic.org/diseases-conditions/mrsa/symptoms-causes/syc-20375336>. Accessed March 14, 2018.
 29. Public Health Agency of Canada. *Canadian Antimicrobial Resistance Surveillance System Report 2016.*; 2016. <https://www.canada.ca/en/public-health/services/publications/drugs-health-products/canadian-antimicrobial-resistance-surveillance-system-report-2016.html>.
 30. Hawkey PM. Multidrug-resistant Gram-negative bacteria: A product of globalization. *J Hosp Infect.* 2015;89(4):241-247. doi:10.1016/j.jhin.2015.01.008.
 31. Weber DJ, Rutala WA. Self-disinfecting surfaces: Review of current methodologies and future prospects. *Am J Infect Control.* 2013;41(5 SUPPL.):S31-S35. doi:10.1016/j.ajic.2012.12.005.
 32. Hasan J, Crawford RJ, Ivanova EP. Antibacterial surfaces: The quest for a new

- generation of biomaterials. *Trends Biotechnol.* 2013;31(5):295-304. doi:10.1016/j.tibtech.2013.01.017.
33. Bazaka K, Jacob M V., Crawford RJ, Ivanova EP. Efficient surface modification of biomaterial to prevent biofilm formation and the attachment of microorganisms. *Appl Microbiol Biotechnol.* 2012;95(2):299-311. doi:10.1007/s00253-012-4144-7.
 34. Muller MP, MacDougall C, Lim M, et al. Antimicrobial surfaces to prevent healthcare-associated infections: A systematic review. *J Hosp Infect.* 2016;92(1):7-13. doi:10.1016/j.jhin.2015.09.008.
 35. Otter J. An overview of the options for antimicrobial surfaces in hospitals. <https://reflectionsipc.com/2014/02/12/an-overview-of-the-options-for-antimicrobial-surfaces-in-hospitals/>. Published 2014. Accessed March 14, 2018.
 36. Carmona-Ribeiro AM, de Melo Carrasco LD. Cationic antimicrobial polymers and their assemblies. *Int J Mol Sci.* 2013;14(5):9906-9946. doi:10.3390/ijms14059906.
 37. Tiller JC, Liao CJ, Lewis K, Klibanov a M. Designing surfaces that kill bacteria on contact. *Proc Natl Acad Sci U S A.* 2001;98(11):5981-5985. doi:10.1073/pnas.111143098.
 38. Siedenbiedel F, Tiller JC. Antimicrobial polymers in solution and on surfaces: Overview and functional principles. *Polymers (Basel).* 2012;4(1):46-71. doi:10.3390/polym4010046.
 39. O’Gorman J, Humphreys H. Application of copper to prevent and control infection. Where are we now? *J Hosp Infect.* 2012;81(4):217-223. doi:10.1016/j.jhin.2012.05.009.
 40. Bright KR, Gerba CP, Rusin PA. Rapid reduction of *Staphylococcus aureus* populations on stainless steel surfaces by zeolite ceramic coatings containing silver and zinc ions. *J Hosp Infect.* 2002;52(4):307-309. doi:10.1053/jhin.2002.1317.
 41. Grass G, Rensing C, Solioz M. Metallic copper as an antimicrobial surface. *Appl Environ Microbiol.* 2011;77(5):1541-1547. doi:10.1128/AEM.02766-10.
 42. Humphreys H. Self-disinfecting and microbicide-impregnated surfaces and fabrics: What potential in interrupting the spread of healthcare-associated infection? *Clin Infect Dis.* 2014;58(6):848-853. doi:10.1093/cid/cit765.

43. Cloutier M, Mantovani D, Rosei F. Antibacterial Coatings: Challenges, Perspectives, and Opportunities. *Trends Biotechnol.* 2015;33(11):637-652. doi:10.1016/j.tibtech.2015.09.002.
44. Singer AC, Shaw H, Rhodes V, Hart A. Review of antimicrobial resistance in the environment and its relevance to environmental regulators. *Front Microbiol.* 2016;7(NOV):1-22. doi:10.3389/fmicb.2016.01728.
45. Thomas K. The environmental fate and behaviour of antifouling paint booster biocides: A review. *Biofouling.* 2001;17(1):73-86. doi:10.1080/08927010109378466.
46. Finnie AA. Improved estimates of environmental copper release rates from antifouling products. *Biofouling.* 2006;22(5):279-291. doi:10.1080/08927010600898862.
47. Wainwright M. Photodynamic antimicrobial chemotherapy (PACT). *J Antimicrob Chemother.* 1998;42(1):13-28. doi:10.1093/jac/42.1.13.
48. Spagnul C, Turner LC, Boyle RW. Immobilized photosensitizers for antimicrobial applications. *J Photochem Photobiol B Biol.* 2015;150:11-30. doi:10.1016/j.jphotobiol.2015.04.021.
49. Pereira Rosa L, Silva FC da. Antimicrobial Photodynamic Therapy: A New Therapeutic Option to Combat Infections. *J Med Microbiol Diagnosis.* 2014;3(4):1-7. doi:10.4172/2161-0703.1000158.
50. Wainwright M. Photodynamic medicine and infection control. *J Antimicrob Chemother.* 2012;67(4):787-788. doi:10.1093/jac/dkr562.
51. Dai T, Huang Y-Y, Hamblin MR. Photodynamic therapy for localized infections—State of the art. *Photodiagnosis Photodyn Ther.* 2009;6(3-4):170-188. doi:10.1016/j.pdpdt.2009.10.008.
52. Sperandio FF, Huang Y-Y, Hamblin MR. Antimicrobial Photodynamic Therapy to Kill Gram-negative Bacteria. *Recent Pat Antiinfect Drug Discov.* 2013;8(2):1-23. doi:10.2174/1574891X113089990012.
53. Ogilby PR. Singlet oxygen: there is indeed something new under the sun. *Chem Soc Rev.* 2010;39(8):3181. doi:10.1039/b926014p.

54. Alves E, Faustino MAF, Neves MGPMS, Cunha Â, Nadais H, Almeida A. Potential applications of porphyrins in photodynamic inactivation beyond the medical scope. *J Photochem Photobiol C Photochem Rev.* 2014;22:34-57. doi:10.1016/j.jphotochemrev.2014.09.003.
55. Ford WE, Kamat P V. Photochemistry of 3,4,9,10-perylenetetracarboxylic dianhydride dyes. 3. Singlet and triplet excited-state properties of the bis(2,5-di-tert-butylphenyl)imide derivative. *J Phys Chem.* 1987;91(25):6373-6380. doi:10.1021/j100309a012.
56. MacDonald IJ, Dougherty TJ. Basic principles of photodynamic therapy. *J Porphyrins Phthalocyanines.* 2001;5(2):105-129. doi:10.1002/jpp.328.
57. Wainwright M, Maisch T, Nonell S, et al. Photoantimicrobials—are we afraid of the light? *Lancet Infect Dis.* 2016;3099(16):1-7. doi:10.1016/S1473-3099(16)30268-7.
58. Maisch T. Anti-microbial photodynamic therapy: useful in the future? *Lasers Med Sci.* 2007;22(2):83-91. doi:10.1007/s10103-006-0409-7.
59. Tim M. Strategies to optimize photosensitizers for photodynamic inactivation of bacteria. *J Photochem Photobiol B Biol.* 2015;150:2-10. doi:10.1016/j.jphotobiol.2015.05.010.
60. Maisch T. Resistance in antimicrobial photodynamic inactivation of bacteria. *Photochem Photobiol Sci.* 2015;14:1518-1526. doi:10.1039/c5pp00037h.
61. DeRosa MC, Crutchley RJ. Photosensitized singlet oxygen and its applications. *Coord Chem Rev.* 2002;233-234:351-371. doi:10.1016/S0010-8545(02)00034-6.
62. Noimark S, Dunnill CW, Parkin IP. Shining light on materials - A self-sterilising revolution. *Adv Drug Deliv Rev.* 2013;65(4):570-580. doi:10.1016/j.addr.2012.07.003.
63. Benov L. Photodynamic therapy: Current status and future directions. *Med Princ Pract.* 2015;24(suppl 1):14-28. doi:10.1159/000362416.
64. Castano AP, Demidova TN, Hamblin MR. Mechanisms in photodynamic therapy: Part two - Cellular signaling, cell metabolism and modes of cell death. *Photodiagnosis Photodyn Ther.* 2005;2(1 SPEC. ISS.):1-23. doi:10.1016/S1572-1000(05)00030-X.

65. Maisch T. Strategies to optimize photosensitizers for photodynamic inactivation of bacteria. *J Photochem Photobiol B Biol.* 2015;150:2-10. doi:10.1016/j.jphotobiol.2015.05.010.
66. Sharman WM, Allen CM, Van Lier JE. Photodynamic therapeutics: Basic principles and clinical applications. *Drug Discov Today.* 1999;4(11):507-517. doi:10.1016/S1359-6446(99)01412-9.
67. Cieplik F, Tabenski L, Buchalla W, Maisch T. Antimicrobial photodynamic therapy for inactivation of biofilms formed by oral key pathogens. *Front Microbiol.* 2014;5(405):1-17. doi:10.3389/fmicb.2014.00405.
68. Alves E, Costa L, Carvalho CMB, et al. Charge effect on the photoinactivation of Gram-negative and Gram-positive bacteria by cationic meso-substituted porphyrins. *BMC Microbiol.* 2009;9(1):70. doi:10.1186/1471-2180-9-70.
69. Carvalho CMB, Gomes ATPC, Fernandes SCD, et al. Photoinactivation of bacteria in wastewater by porphyrins: Bacterial β -galactosidase activity and leucine-uptake as methods to monitor the process. *J Photochem Photobiol B Biol.* 2007;88(2-3):112-118. doi:10.1016/j.jphotobiol.2007.04.015.
70. Huang L, Zhiyentayev T, Xuan Y, Azhibek D, Kharkwal GB, Hamblin MR. Photodynamic inactivation of bacteria using polyethylenimine-chlorin(e6) conjugates: Effect of polymer molecular weight, substitution ratio of chlorin(e6) and pH. *Lasers Surg Med.* 2011;43(4):313-323. doi:10.1002/lsm.21056.
71. Cieplik F, Späth A, Regensburger J, et al. Photodynamic biofilm inactivation by SAPYR - An exclusive singlet oxygen photosensitizer. *Free Radic Biol Med.* 2013;65:477-487. doi:10.1016/j.freeradbiomed.2013.07.031.
72. Herbst W, Hunger K, Wilker G, Ohleier H, Winter R. *Industrial Organic Pigments: Production, Properties, Applications: Third, Completely Revised Edition.*; 2005. doi:10.1002/3527602429.
73. Geissler G, Remy H. Ger.Pat. Appl., DE1130099. *Ger Pat Appl 1130099.* 1959.
74. Huang C, Barlow S, Marder SR. Perylene-3,4,9,10-tetracarboxylic acid diimides: synthesis, physical properties, and use in organic electronics. *J Org Chem.* 2011;76(8):2386-2407. doi:10.1021/jo2001963.
75. Würthner F. Perylene bisimide dyes as versatile building blocks for functional supramolecular architectures. *Chem Commun (Camb).* 2004;(14):1564-1579.

doi:10.1039/b401630k.

76. Siekierzycka JR, Hippus C, Würthner F, Williams RM, Brouwer AM. Polymer glass transitions switch electron transfer in individual molecules. *J Am Chem Soc.* 2010;132(4):1240-1242. doi:10.1021/ja905667c.
77. Qian G, Yang Y, Wang Z, Yang C, Yang Z, Wang M. Photostability of perylene orange, perylene red and pyrromethene 567 laser dyes in various precursors derived gel glasses. *Chem Phys Lett.* 2003;368(5-6):555-560. doi:10.1016/S0009-2614(02)01906-1.
78. Kim JY, Chung IJ, Lee C, Kim YC, Kim JK, Yu JW. Mobility of electrons and holes in an n-type organic semiconductor perylene diimide thin film. *Curr Appl Phys.* 2005;5(6):615-618. doi:10.1016/j.cap.2004.08.007.
79. Chen F-C, Liao C-H. Improved air stability of n-channel organic thin-film transistors with surface modification on gate dielectrics. *Appl Phys Lett.* 2008;93(10):103310. doi:10.1063/1.2980421.
80. Law KY. Organic photoconductive materials: recent trends and developments. *Chem Rev.* 1993;93(1):449-486. doi:10.1021/cr00017a020.
81. Kozma E, Catellani M. Perylene diimides based materials for organic solar cells. *Dye Pigment.* 2013;98(1):160-179. doi:10.1016/j.dyepig.2013.01.020.
82. Langhals H. Cyclic carboxylic imide structures as structure elements of high stability. Novel developments in perylene dye chemistry. *Heterocycles.* 1995;40(1):477-500. doi:10.3987/REV-94-SR2.
83. Wescott LD, Mattern DL. Donor- σ -Acceptor Molecules Incorporating a Nonadecyl-Swallowtailed Perylenediimide Acceptor. *J Org Chem.* 2003;68(26):10058-10066. doi:10.1021/jo035409w.
84. Nagao Y. Synthesis and properties of perylene pigments. *Prog Org Coatings.* 1997;31(1-2):43-49. doi:10.1016/S0300-9440(97)00017-9.
85. Böhm A, Arms H, Henning G, Blaschka P. BASF AG. 1997.
86. Würthner F, Stepanenko V, Chen Z, Saha-Möller CR, Kocher N, Stalke D. Preparation and characterization of regioisomerically pure 1,7-disubstituted perylene bisimide dyes. *J Org Chem.* 2004;69(23):7933-7939.

doi:10.1021/jo048880d.

87. Schnurpfeil G, Stark J, Wöhrle D. Syntheses of uncharged, positively and negatively charged 3,4,9,10-perylene-bis(dicarboximides). *Dye Pigment*. 1995;27(4):339-350. doi:10.1016/0143-7208(94)00075-D.
88. Backes C, Schmidt CD, Hauke F, Böttcher C, Hirsch A. High population of individualized SWCNTs through the adsorption of water-soluble perylenes. *J Am Chem Soc*. 2009;131(6):2172-2184. doi:10.1021/ja805660b.
89. Huang Y, Yan Y, Smarsly BM, Wei Z, Faul CFJ. Helical supramolecular aggregates, mesoscopic organisation and nanofibers of a perylenebisimide–chiral surfactant complex via ionic self-assembly. *J Mater Chem*. 2009;19(16):2356. doi:10.1039/b817838k.
90. Heek T, Fasting C, Rest C, Zhang X, Würthner F, Haag R. Highly fluorescent water-soluble polyglycerol-dendronized perylene bisimide dyes. *Chem Commun*. 2010;46(11):1884. doi:10.1039/b923806a.
91. Liu Y, Wang KR, Cuo DS, Jiang BP. Supramolecular assembly of perylene bisimide with B-cyclodextrin grafts as a solid-state fluorescence sensor for vapor detection. *Adv Funct Mater*. 2009;19(14):2230-2235. doi:10.1002/adfm.200900221.
92. Nakazono S, Imazaki Y, Yoo H, et al. Regioselective Ru-catalyzed direct 2,5,8,11-alkylation of perylene bisimides. *Chem - A Eur J*. 2009;15(31):7530-7533. doi:10.1002/chem.200901318.
93. Schmidt R, Ling MM, Oh JH, et al. Core-fluorinated perylene bisimide dyes: Air stable n-channel organic semiconductors for thin film transistors with exceptionally high on-to-off current ratios. *Adv Mater*. 2007;19(21):3692-3695. doi:10.1002/adma.200701478.
94. Ahrens MJ, Fuller MJ, Wasielewski MR. Cyanated perylene-3,4-dicarboximides and perylene-3,4:9,10-bis(dicarboximide): Facile chromophoric oxidants for organic photonics and electronics. *Chem Mater*. 2003;15(14):2684-2686. doi:10.1021/cm034140u.
95. Kohl C, Weil T, Qu J, Müllen K. Towards highly fluorescent and water-soluble perylene dyes. *Chem - A Eur J*. 2004;10(21):5297-5310. doi:10.1002/chem.200400291.

96. Zhao Y, Wasielewski MR. 3,4:9,10-Perylenebis(dicarboximide) chromophores that function as both electron donors and acceptors. *Tetrahedron Lett.* 1999;40(39):7047-7050. doi:10.1016/S0040-4039(99)01468-9.
97. Sivamurugan V, Kazlauskas K, Jursenas S, et al. Synthesis and photophysical properties of glass-forming bay-substituted perylenediimide derivatives. *J Phys Chem B.* 2010;114(5):1782-1789. doi:10.1021/jp907697f.
98. Zhan X, Tan Z, Domercq B, et al. A high-mobility electron-transport polymer with broad absorption and its use in field-effect transistors and all-polymer solar cells. *J Am Chem Soc.* 2007;129(23):7246-7247. doi:10.1021/ja071760d.
99. An Z, Odom SA, Kelley RF, et al. Synthesis and Photophysical Properties of Donor- and Acceptor-Substituted 1,7-Bis (arylalkynyl) perylene-3,4:9,10-bis (dicarboximide) s. 2009:5585-5593.
100. Rauch G, Höger S. N-Alkylated and N,N-dialkylated 1,6-diaminoperylene diimides synthesized via copper catalyzed direct aromatic amination. *Chem Commun.* 2014;50(42):5659. doi:10.1039/c4cc02124j.
101. Nakazono S, Easwaramoorthi S, Kim D, Shinokubo H, Osuka A. Synthesis of arylated perylene bisimides through C - H bond cleavage under ruthenium catalysis. *Org Lett.* 2009;11(23):5426-5429. doi:10.1021/ol902271b.
102. Battagliarin G, Zhao Y, Li C, Mullen K. Efficient tuning of LUMO levels of 2,5,8,11-substituted perylenediimides via copper catalyzed reactions. *Org Lett.* 2011;13(13):3399-3401. doi:10.1021/ol201144w.
103. Gao J, Xiao C, Jiang W, Wang Z. Cyano-substituted perylene diimides with linearly correlated LUMO levels. *Org Lett.* 2014;16(2):394-397. doi:10.1021/ol403250r.
104. Danilov EO, Rachford A a, Goeb S, Castellano FN. Evolution of the triplet excited state in Pt(II) perylenediimides. *J Phys Chem A.* 2009;113(19):5763-5768. doi:10.1021/jp9012762.
105. Maia PJS, de Aguiar I, dos Santos Velloso M, et al. Singlet oxygen production by a polypyridine ruthenium (II) complex with a perylene monoimide derivative: A strategy for photodynamic inactivation of *Candida albicans*. *J Photochem Photobiol A Chem.* 2018;353:536-545. doi:10.1016/j.jphotochem.2017.12.020.
106. Mari C, Huang H, Rubbiani R, et al. Evaluation of Perylene Bisimide-Based Rull

- and Ir(III) Complexes as Photosensitizers for Photodynamic Therapy. *Eur J Inorg Chem.* 2017;2017(12):1745-1752. doi:10.1002/ejic.201600516.
107. Sun J, Zhong F, Zhao J. Observation of the long-lived triplet excited state of perylenebisimide (PBI) in C^N cyclometalated Ir(III) complexes and application in photocatalytic oxidation. *Dalt Trans.* 2013;42(26):9595-9605. doi:10.1039/c3dt33036b.
 108. Zhao J, Wu W, Sun J, Guo S. Triplet photosensitizers: from molecular design to applications. *Chem Soc Rev.* 2013;42(12):5323. doi:10.1039/c3cs35531d.
 109. Liu Y, Zhao J. Visible light-harvesting perylenebisimide–fullerene (C₆₀) dyads with bidirectional “ping-pong” energy transfer as triplet photosensitizers for photooxidation of 1,5-dihydroxynaphthalene. *Chem Commun.* 2012;48(31):3751. doi:10.1039/c2cc30345k.
 110. Dinçalp H, Kızılok Ş, İçli S. Targeted singlet oxygen generation using different DNA-interacting perylene diimide type photosensitizers. *J Fluoresc.* 2014;24(3):917-924. doi:10.1007/s10895-014-1372-5.
 111. Wu Y, Zhen Y, Ma Y, Zheng R, Wang Z, Fu H. Exceptional intersystem crossing in Di(peryene bisimide)s: A structural platform toward photosensitizers for singlet oxygen generation. *J Phys Chem Lett.* 2010;1(17):2499-2502. doi:10.1021/jz1008328.
 112. Nagarajan K, Mallia AR, Reddy VS, Hariharan M. Access to Triplet Excited State in Core-Twisted Perylenediimide. *J Phys Chem C.* 2016;120(16):8443-8450. doi:10.1021/acs.jpcc.6b00755.
 113. Nagarajan K, Mallia AR, Muraleedharan K, Hariharan M. Enhanced intersystem crossing in core-twisted aromatics. *Chem Sci.* 2017;8(3):1776-1782. doi:10.1039/C6SC05126J.
 114. Yang W, Zhao J, Sonn C, et al. Efficient intersystem crossing in heavy-atom-free perylenebisimide derivatives. *J Phys Chem C.* 2016;120(19):10162-10175. doi:10.1021/acs.jpcc.6b01584.
 115. Yu Z, Wu Y, Peng Q, et al. Accessing the Triplet State in Heavy-Atom-Free Perylene Diimides. *Chem - A Eur J.* 2016;22(14):4717-4722. doi:10.1002/chem.201600300.
 116. Tilley AJ, Pensack RD, Lee TS, Djukic B, Scholes GD, Seferos DS. Ultrafast triplet

- formation in thionated perylene diimides. *J Phys Chem C*. 2014;118(19):9996-10004. doi:10.1021/jp503708d.
117. Braun A, Tcherniac J. Über die Produkte der Einwirkung von Acetanhydrid auf Phthalamid. *Berichte der Dtsch Chem Gesellschaft*. 1907;40(2):2709-2714. doi:10.1002/cber.190704002202.
118. Dent CE, Linstead RP, Lowe AR. 217. Phthalocyanines. Part VI. The structure of the phthalocyanines. *J Chem Soc*. 1934;(I):1033. doi:10.1039/jr9340001033.
119. Robertson JM, Woodward I. 7. An X-ray study of the phthalocyanines. Part IV. Direct quantitative analysis of the platinum compound. *J Chem Soc*. 1940;(36):36-48. doi:10.1039/jr9400000036.
120. Jiang J, ed. *Functional Phthalocyanine Molecular Materials*. Vol 135. Berlin, Heidelberg: Springer Berlin Heidelberg; 2010. doi:10.1007/978-3-642-04752-7.
121. Kobayashi N, Ogata H, Nonaka N, Luk'yanets EA. Effect of Peripheral Substitution on the Electronic Absorption and Fluorescence Spectra of Metal-Free and Zinc Phthalocyanines. *Chem - A Eur J*. 2003;9(20):5123-5134. doi:10.1002/chem.200304834.
122. Mack J, Kobayashi N. ChemInform Abstract: Low Symmetry Phthalocyanines and Their Analogues. *ChemInform*. 2011;42(20):no-no. doi:10.1002/chin.201120225.
123. de la Torre G, Claessens CG, Torres T. Phthalocyanines: The Need for Selective Synthetic Approaches. *European J Org Chem*. 2000;2000(16):2821-2830. doi:10.1002/1099-0690(200008)2000:16<2821::AID-EJOC2821>3.0.CO;2-2.
124. Sharman WM, Van Lier JE. *Synthesis of Phthalocyanine Precursors*. Vol 15. Elsevier Inc.; 2012. doi:10.1016/B978-0-08-092389-5.50007-9.
125. Wöhrle D, Schnurpfeil G, Knothe G. Efficient synthesis of phthalocyanines and related macrocyclic compounds in the presence of organic bases. *Dye Pigment*. 1992;18(2):91-102. doi:10.1016/0143-7208(92)80009-C.
126. Christie RM, Deans DD. An investigation into the mechanism of the phthalonitrile route to copper phthalocyanines using differential scanning calorimetry. *J Chem Soc Perkin Trans 2*. 1989;(2):193. doi:10.1039/p29890000193.
127. Hanack M, Meng D, Beck A, Sommerauer M, Subramanian LR. Separation of

- Structural Isomers of Tetra-tert-butylphthalocyaninatonicel (II). *J Chem Soc, Chem Commun.* 1993;(5):58-60.
128. Furuyama T, Harako R, Kobayashi N. Structural changes in non-planar octaaryl substituted phthalocyanine phosphorus complexes. *J Porphyr Phthalocyanines.* 2015;19(01-03):500-509. doi:10.1142/S1088424615500364.
129. Yoshida T, Furuyama T, Kobayashi N. Synthesis and optical properties of tetraazaporphyrin phosphorus(V) complexes with electron-rich heteroatoms. *Tetrahedron Lett.* 2015;56(13):1671-1674. doi:10.1016/j.tetlet.2015.02.033.
130. Rager C, Schmid G, Hanack M. Influence of Substituents , Reaction Conditions and Central Metals on the. *Chem Eur J.* 1999;5(1):280-288.
131. Sommerauer M, Rager C, Hanack M. Separation of 2(3),9(10),16(17),23(24)-tetrasubstituted phthalocyanines with newly developed HPLC phases. *J Am Chem Soc.* 1996;118(42):10085-10093. doi:10.1021/ja961009x.
132. Leznoff CC, Hu M, Nolan KJM. The synthesis of phthalocyanines at room temperature. *Chem Commun.* 1996;0(10):1245. doi:10.1039/cc9960001245.
133. Kasuga K, Asano K, Lin L, et al. Preparation and Some Properties of One Structural Isomer of Tetra-Substituted Phthalocyanine; 1,8,15,22-Tetrakis(pentan-3'-yloxy)phthalocyanine and Its Metal(II) Complexes. *Bull Chem Soc Jpn.* 1997;70(8):1859-1865. doi:10.1246/bcsj.70.1859.
134. Kobayashi N, Kobayashi Y, Osa T. Optically Active Phthalocyanines and Their Circular Dichroism. *J Am Chem Soc.* 1993;115(23):10994-10995. doi:10.1021/ja00076a069.
135. Drew DM, Leznoff CC. The Synthesis of Pure 1,11,15,25-Tetrasubstitutedphthalocyanines as Single Isomers Using Bisphthalonitriles. *Synlett.* 1994;1994(8):623-624. doi:10.1055/s-1994-22949.
136. Naik AJT, Ismail S, Kay C, Wilson M, Parkin IP. Antimicrobial activity of polyurethane embedded with methylene blue, toluidene blue and gold nanoparticles against Staphylococcus aureus; illuminated with white light. *Mater Chem Phys.* 2011;129(1-2):446-450. doi:10.1016/j.matchemphys.2011.04.040.
137. Decraene V, Pratten J, Wilson M. Cellulose acetate containing toluidine blue and rose bengal is an effective antimicrobial coating when exposed to white light. *Appl Environ Microbiol.* 2006;72(6):4436-4439. doi:10.1128/AEM.02945-05.

138. Ringot C, Sol V, Barrière M, et al. Triazinyl porphyrin-based photoactive cotton fabrics: Preparation, characterization, and antibacterial activity. *Biomacromolecules*. 2011;12(5):1716-1723. doi:10.1021/bm200082d.
139. Zhuo J, Sun G. Antimicrobial functions on cellulose materials introduced by anthraquinone vat dyes. *ACS Appl Mater Interfaces*. 2013;5(21):10830-10835. doi:10.1021/am403029w.
140. Henke P, Lang K, Kubát P, Sýkora J, Šlouf M, Mosinger J. Polystyrene nanofiber materials modified with an externally bound porphyrin photosensitizer. *ACS Appl Mater Interfaces*. 2013;5(9):3776-3783. doi:10.1021/am4004057.
141. Bonnett R, Galia A. Photobactericidal Films Based on Regenerated Cellulose. *Biotechnol Equip*. 1994;8(1):68-74. doi:10.1080/13102818.1994.10818756.
142. Masilela N, Kleyi P, Tshentu Z, Priniotakis G, Westbroek P, Nyokong T. Photodynamic inactivation of *Staphylococcus aureus* using low symmetrically substituted phthalocyanines supported on a polystyrene polymer fiber. *Dye Pigment*. 2013;96(2):500-508. doi:10.1016/j.dyepig.2012.10.001.
143. Goethals A, Mugadza T, Arslanoglu Y, et al. Polyamide nanofiber membranes functionalized with zinc phthalocyanines. *J Appl Polym Sci*. 2014;131(13):1-7. doi:10.1002/app.40486.
144. Bonnett R, Krysteva MA, Lalov IG, Artarsky S V. Water disinfection using photosensitizers immobilized on chitosan. *Water Res*. 2006;40(6):1269-1275. doi:10.1016/j.watres.2006.01.014.
145. Osifeko OL, Nyokong T. Applications of lead phthalocyanines embedded in electrospun fibers for the photoinactivation of *Escherichia coli* in water. *Dye Pigment*. 2014;111:8-15. doi:10.1016/j.dyepig.2014.05.010.
146. Mbakidi JP, Herke K, Alvès S, et al. Synthesis and photobiocidal properties of cationic porphyrin-grafted paper. *Carbohydr Polym*. 2013;91(1):333-338. doi:10.1016/j.carbpol.2012.08.013.
147. Feese E, Sadeghifar H, Gracz HS, Argyropoulos DS, Ghiladi RA. Photobactericidal porphyrin-cellulose nanocrystals: Synthesis, characterization, and antimicrobial properties. *Biomacromolecules*. 2011;12(10):3528-3539. doi:10.1021/bm200718s.

148. Carpenter BL, Feese E, Sadeghifar H, Argyropoulos DS, Ghiladi RA. Porphyrin-cellulose nanocrystals: A photobactericidal material that exhibits broad spectrum antimicrobial activity. *Photochem Photobiol.* 2012;88(3):527-536. doi:10.1111/j.1751-1097.2012.01117.x.
149. Carpenter BL, Scholle F, Sadeghifar H, et al. Synthesis, Characterization, and Antimicrobial Efficacy of Photomicrobicidal Cellulose Paper. *Biomacromolecules.* 2015;16(8):2482-2492. doi:10.1021/acs.biomac.5b00758.
150. Gosztola D, Niemczyk MP, Svec W, Lukas AS, Wasielewski MR. Excited doublet states of electrochemically generated aromatic imide and diimide radical anions. *J Phys Chem A.* 2000;104(28):6545-6551. doi:10.1021/jp000706f.
151. Marcon RO, Brochsztain S. Highly stable 3,4,9,10-perylenediimide radical anions immobilized in robust zirconium phosphonate self-assembled films. *Langmuir.* 2007;23(24):11972-11976. doi:10.1021/la702642h.
152. De Miguel M, Álvaro M, García H, Céspedes-Guirao FJ, Fernández-Lázaro F, Sastre-Santos Á. Selective photoinduced single or double electron reduction of perylenebisimides. *J Photochem Photobiol A Chem.* 2012;231(1):28-32. doi:10.1016/j.jphotochem.2012.01.008.
153. Goodson FS, Panda DK, Ray S, Mitra A, Guha S, Saha S. Tunable electronic interactions between anions and perylenediimide. *Org Biomol Chem.* 2013;11(29):4797. doi:10.1039/c3ob40703a.
154. Lu C, Fujitsuka M, Sugimoto A, Majima T. Unprecedented Intramolecular Electron Transfer from Excited Perylenediimide Radical Anion. *J Phys Chem C.* 2016;120(23):12734-12741. doi:10.1021/acs.jpcc.6b02454.
155. Hankins MG, Hayashita T, Kasprzyk SP, Bartsch RA. Immobilization of Crown Ether Carboxylic Acids on Silica Gel and Their Use in Column Concentration of Alkali Metal Cations from Dilute Aqueous Solutions. *Anal Chem.* 1996;68(17):2811-2817. doi:10.1021/ac951159a.
156. Demirci S, Emre FB, Ekiz F, et al. Functionalization of poly-SNS-anchored carboxylic acid with Lys and PAMAM: surface modifications for biomolecule immobilization/stabilization and bio-sensing applications. *Analyst.* 2012;137(18):4254. doi:10.1039/c2an35472a.
157. Choi SH, Kim MS, Ryoo JJ, et al. Immobilization of a cyclodextrin glucanotransferase (CGTase) onto polyethylene film with a carboxylic acid group

and production of cyclodextrins from corn starch using CGTase-immobilized PE film. *J Appl Polym Sci.* 2002;85(11):2451-2457. doi:10.1002/app.10879.

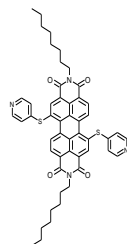
158. Sariola-Leikas E, Ahmed Z, Vivo P, et al. Color bricks: Building highly organized and strongly absorbing multicomponent arrays of terpyridyl perylenes on metal oxide surfaces. *Chem - A Eur J.* 2016;22(4):1501-1510. doi:10.1002/chem.201503738.
159. George L, Efimova E, Sariola-Leikas E, et al. Building Up Colors: Multilayered Arrays of Peryleneimides on Flat Surfaces and Mesoporous Layers. *Chempluschem.* 2017;82(5):705-715. doi:10.1002/cplu.201700061.
160. Wilkinson F, Helman WP, Ross AB. Quantum Yields for the Photosensitized Formation of the Lowest Electronically Excited Singlet State of Molecular Oxygen in Solution. *J Phys Chem Ref Data.* 1993;22(1):113-262. doi:10.1063/1.555934.
161. Zhang X-F, Li X. The photostability and fluorescence properties of diphenylisobenzofuran. *J Lumin.* 2011;131(11):2263-2266. doi:10.1016/j.jlumin.2011.05.048.
162. Kobayashi N, Fukuda T, Ueno K, Ogino H. Extremely non-planar phthalocyanines with saddle or helical conformation: Synthesis and structural characterizations [2]. *J Am Chem Soc.* 2001;123(43):10740-10741. doi:10.1021/ja0113753.
163. Fukuda T, Homma S, Kobayashi N. Deformed phthalocyanines: Synthesis and characterization of zinc phthalocyanines bearing phenyl substituents at the 1-, 4-, 8-, 11-, 15-, 18-, 22-, and/or 25-positions. *Chem - A Eur J.* 2005;11(18):5205-5216. doi:10.1002/chem.200500176.
164. Chambrier I, J. Cook M, T. Wood P. Conformationally stressed phthalocyanines: the non-planarity of the 1,4,8,11,15,18,22,25-octaisopentyl derivative. *Chem Commun.* 2000;(21):2133-2134. doi:10.1039/b006935n.
165. McKeown NB, Li H, Helliwell M. A non-planar, hexadeca-substituted, metal-free phthalocyanine. *J Porphyr Phthalocyanines.* 2006;9(9):841-845. doi:10.1142/S1088424605000964.
166. Ranta J, Kumpulainen T, Lemmetyinen H, Efimov A. Synthesis and characterization of monoisomeric 1,8,15,22-substituted (A3B and A2B2) phthalocyanines and phthalocyanine-fullerene dyads. *J Org Chem.* 2010;75(15):5178-5194. doi:10.1021/jo100766h.

167. Pereira JB, Carvalho EFA, Faustino MAF, et al. Phthalocyanine thio-pyridinium derivatives as antibacterial photosensitizers. *Photochem Photobiol.* 2012;88(3):537-547. doi:10.1111/j.1751-1097.2012.01113.x.
168. Ranta J, Kumpulainen T, Lemmetyinen H, Efimov A. Synthesis and Characterization of Monoisomeric 1,8,15,22-Substituted (A₃B and A₂B₂) Phthalocyanines and Phthalocyanine–Fullerene Dyads. *J Org Chem.* 2010;75(15):5178-5194. doi:10.1021/jo100766h.
169. Claessens CG, Hahn U, Torres T. Phthalocyanines: From outstanding electronic properties to emerging applications. *Chem Rec.* 2008;8(2):75-97. doi:10.1002/tcr.20139.
170. Rio Y, Salomé Rodríguez-Morgade M, Torres T. Modulating the electronic properties of porphyrinoids: a voyage from the violet to the infrared regions of the electromagnetic spectrum. *Org Biomol Chem.* 2008;6(11):1877. doi:10.1039/b800617b.
171. Pelton R. A model of the external surface of wood pulp fibers. *Nord Pulp Pap Res J.* 1993;8(1):113-119. doi:10.3183/NPPRJ-1993-08-01-p113-119.
172. Pelton R. Bioactive paper provides a low-cost platform for diagnostics. *TrAC Trends Anal Chem.* 2009;28(8):925-942. doi:10.1016/j.trac.2009.05.005.
173. Hamblin MR, Hasan T. Photodynamic therapy: a new antimicrobial approach to infectious disease? *Photochem Photobiol Sci.* 2004;3(5):436. doi:10.1039/b311900a.
174. Skwor TA, Klemm S, Zhang H, Schardt B, Blaszczyk S, Bork MA. Photodynamic inactivation of methicillin-resistant *Staphylococcus aureus* and *Escherichia coli*: A metalloporphyrin comparison. *J Photochem Photobiol B Biol.* 2016;165:51-57. doi:10.1016/j.jphotobiol.2016.10.016.

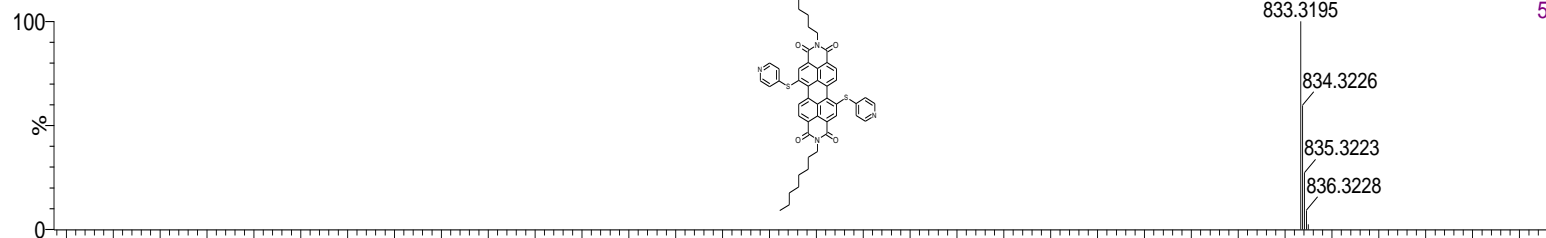
MS spectrum of compound 16

Ig0270posit in clf/MeOH

Ig0270posit (0.036) Is (1.00,1.00) C₅₀H₄₈N₄O₄S₂

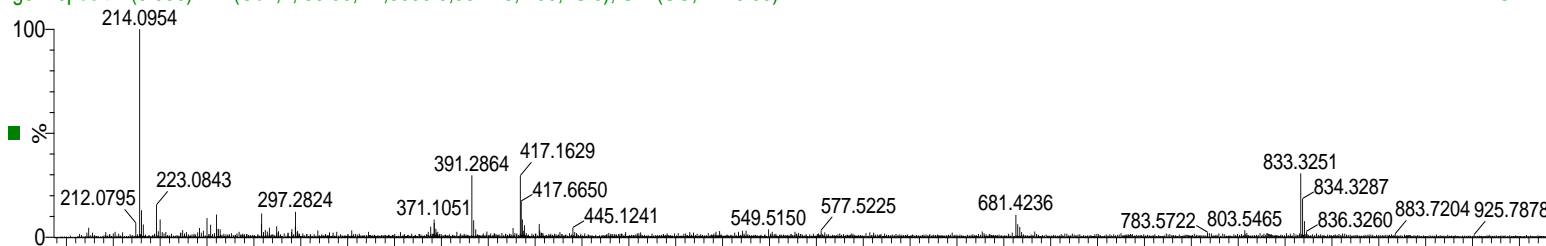


1: TOF MS ES+
5.03e12



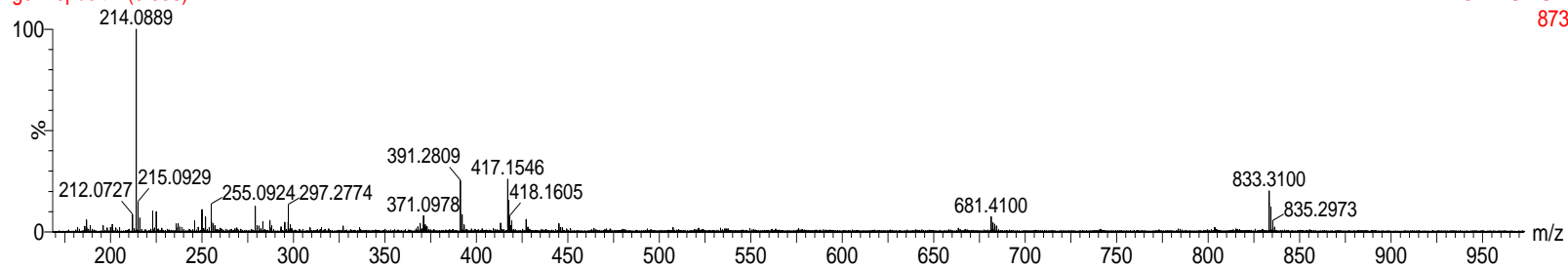
Ig0270posit 1 (0.036) AM (Cen,4, 80.00, Ar,8000.0,557.28,1.00,LS 5); Sm (SG, 2x10.00)

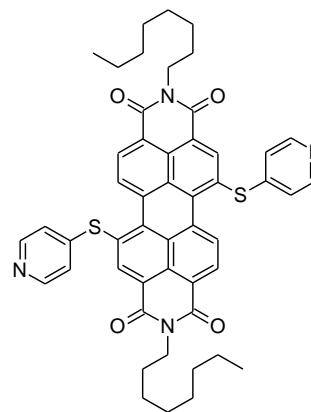
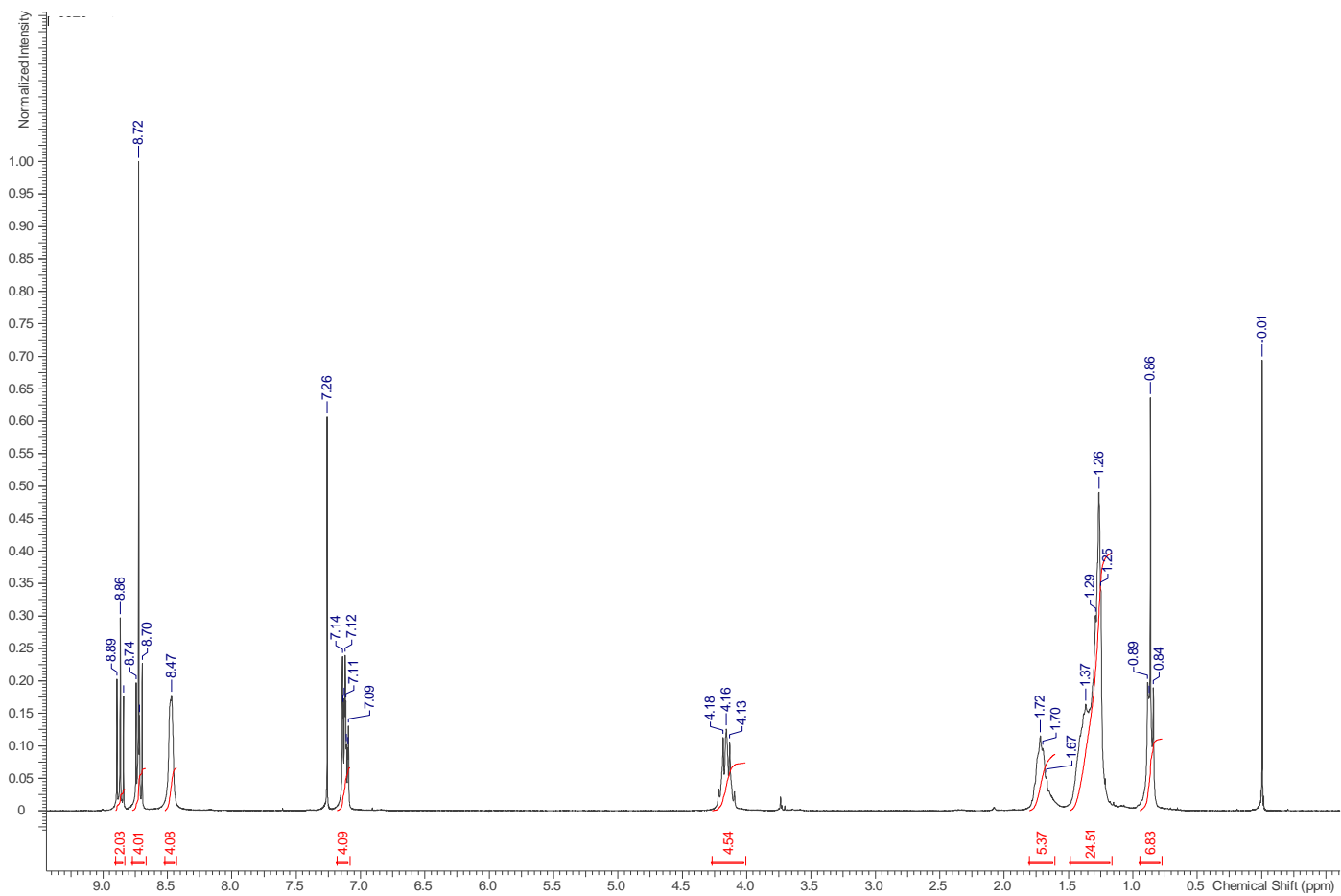
1: TOF MS ES+
6.08e3



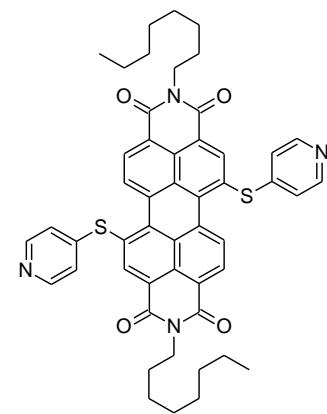
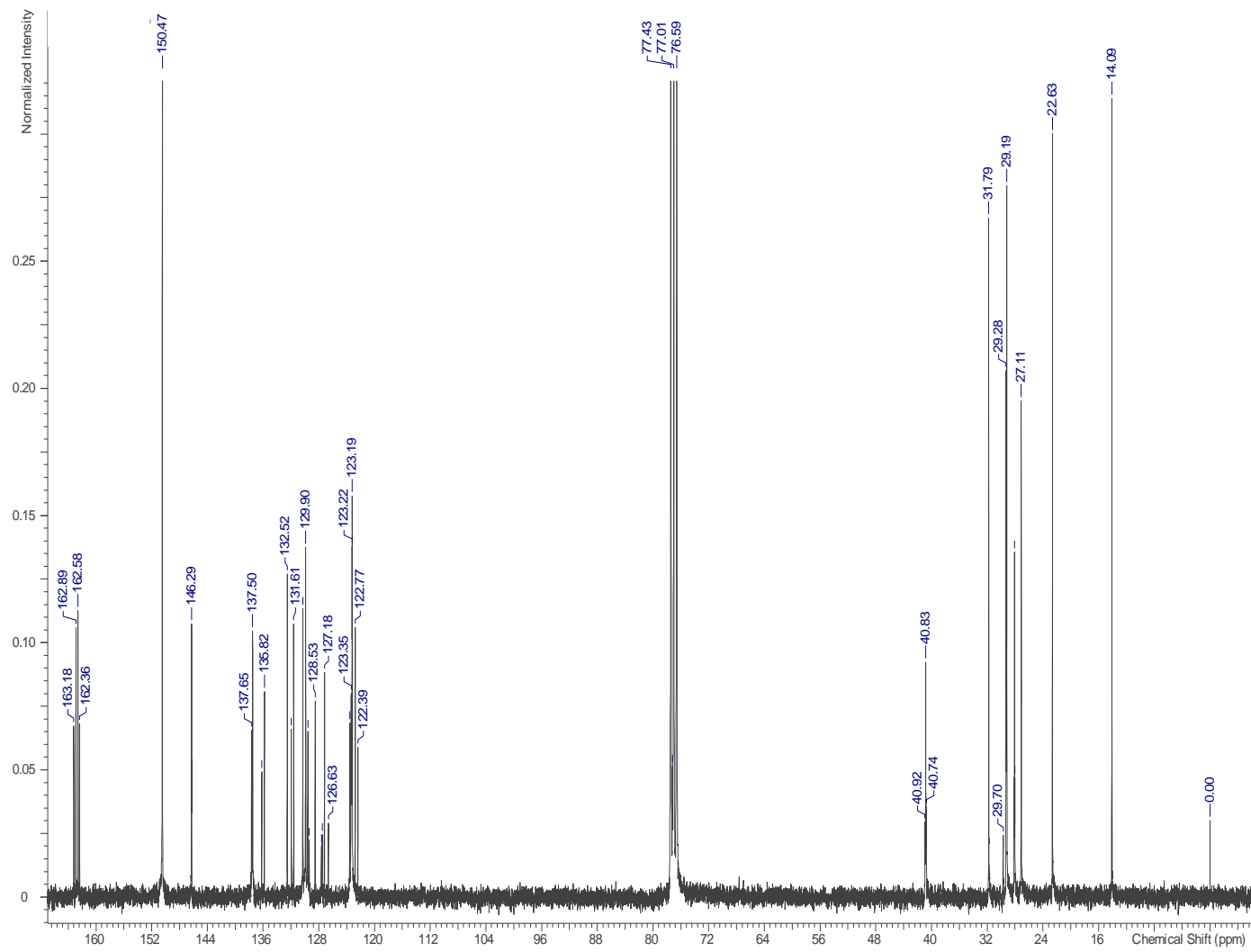
Ig0270posit 1 (0.036)

1: TOF MS ES+
873

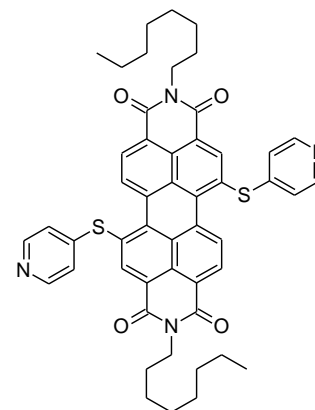
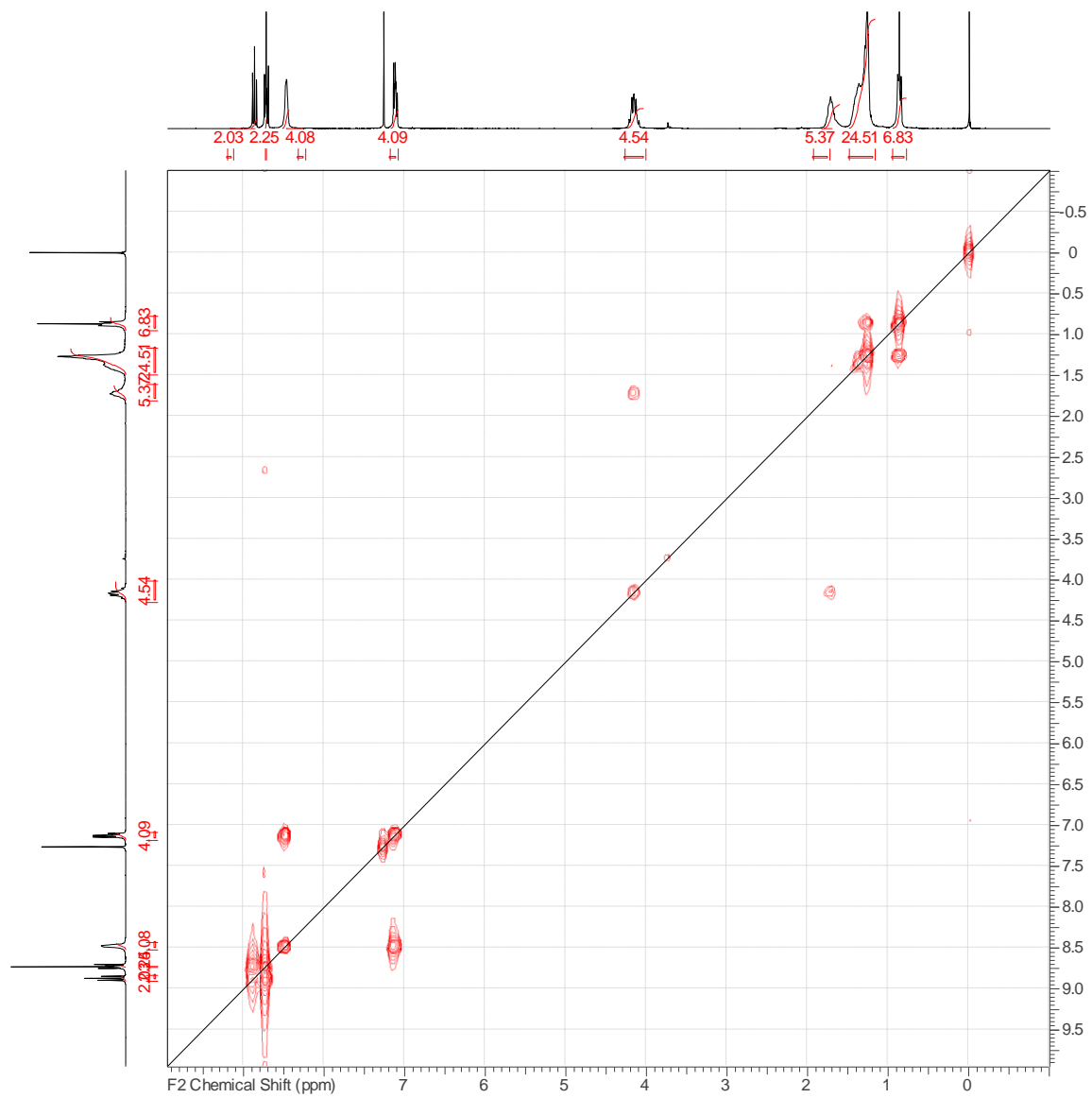


^1H NMR spectrum of compound 16

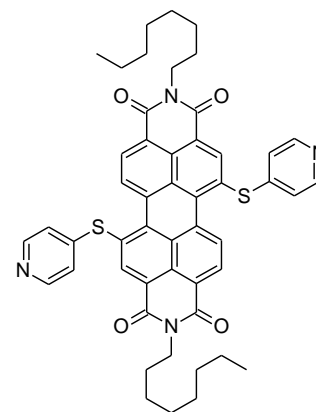
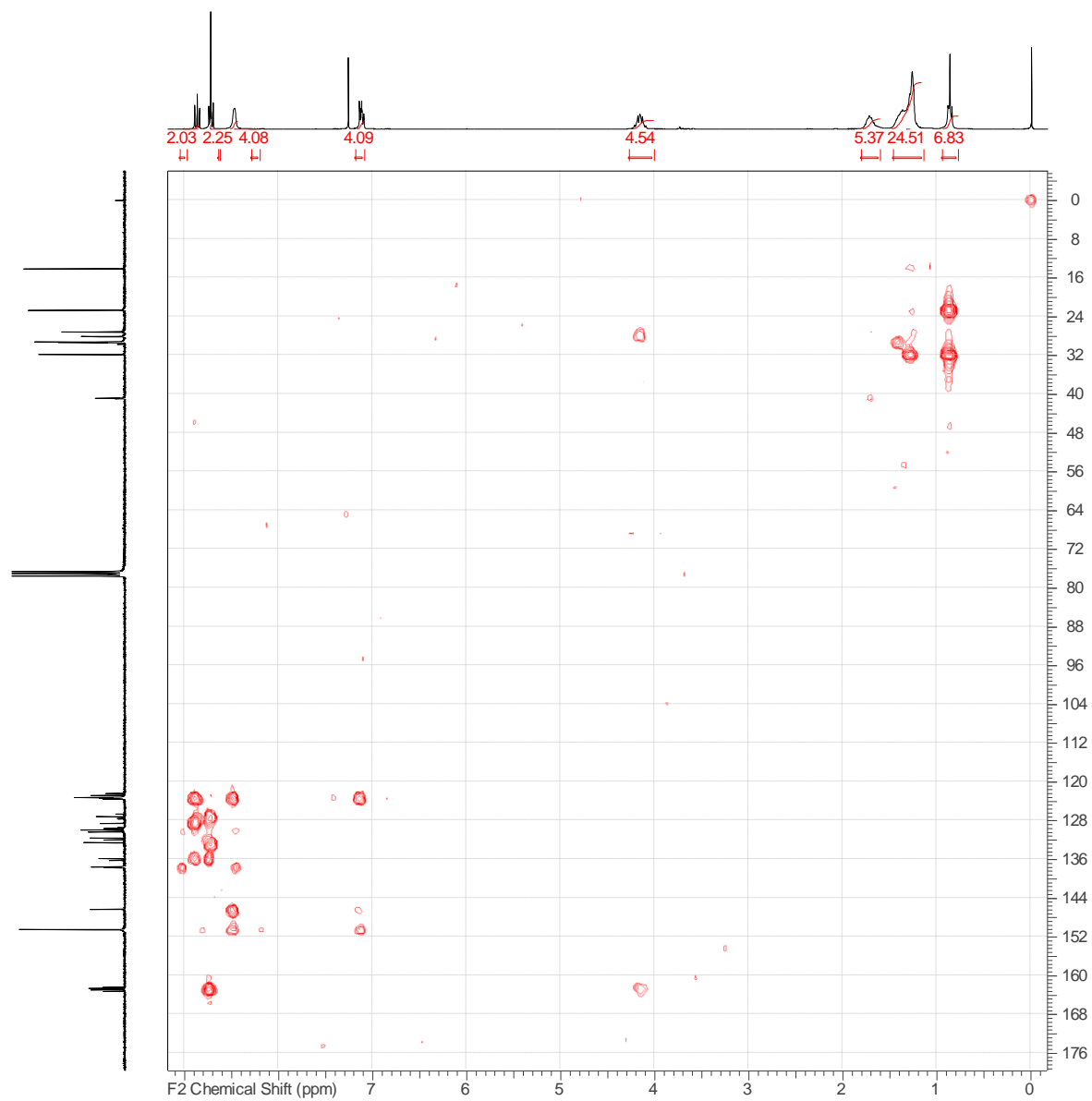
¹³C NMR Spectrum of compound 16

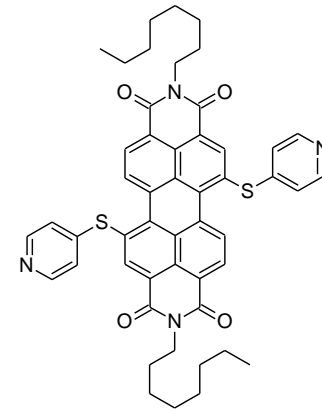
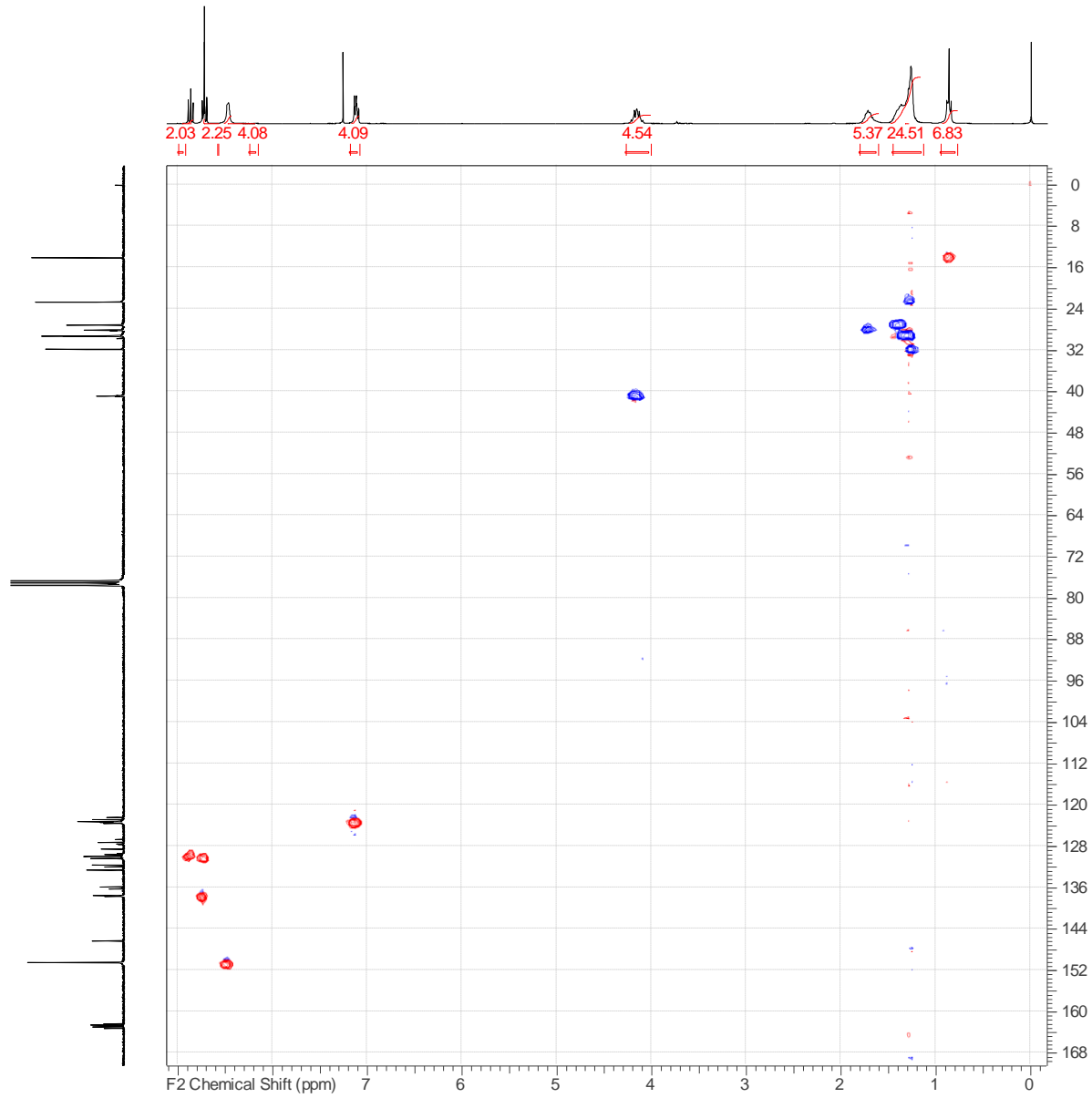


COSY spectrum of compound 16



gHMBC spectrum of compound 16



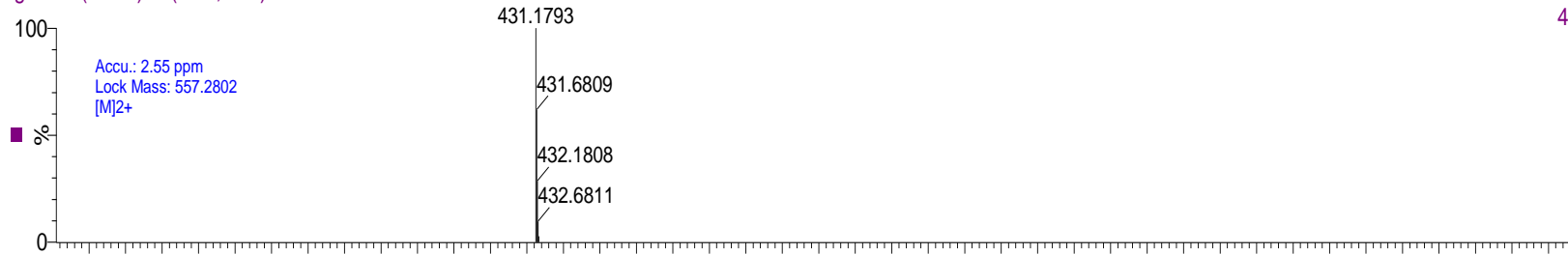
gHSQC spectrum of compound 16

MS spectrum of compound 17

Ig0271 in MeOH

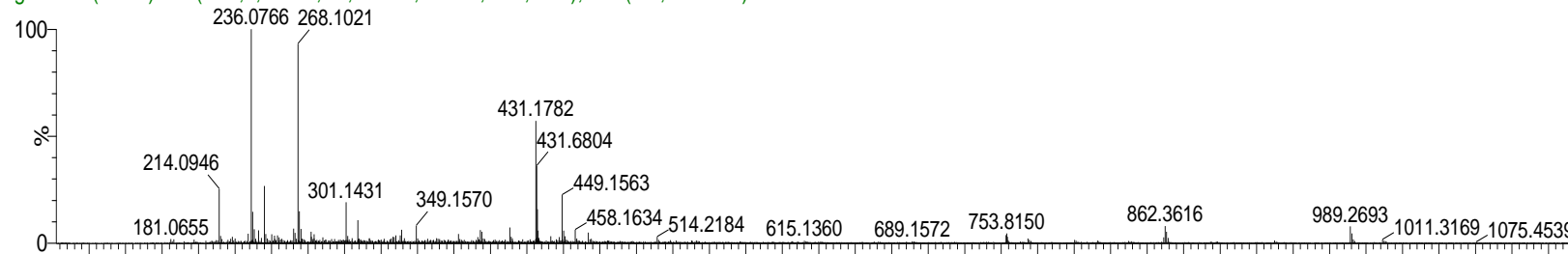
Ig0271 (0.035) Is (1.00,1.00) C₅₂H₅₂N₄O₄S₂

1: TOF MS ES+
4.92e12



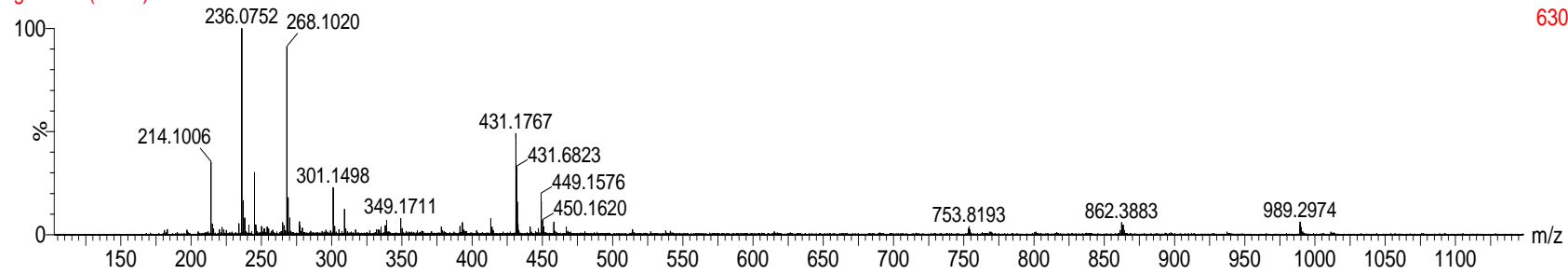
Ig0271 1 (0.035) AM (Cen,4, 80.00, Ar,8000.0,557.28,1.00,LS 5); Sm (SG, 2x10.00)

1: TOF MS ES+
4.69e3

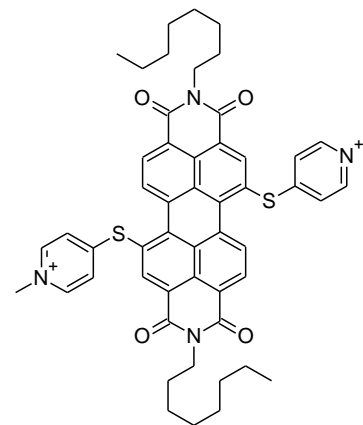
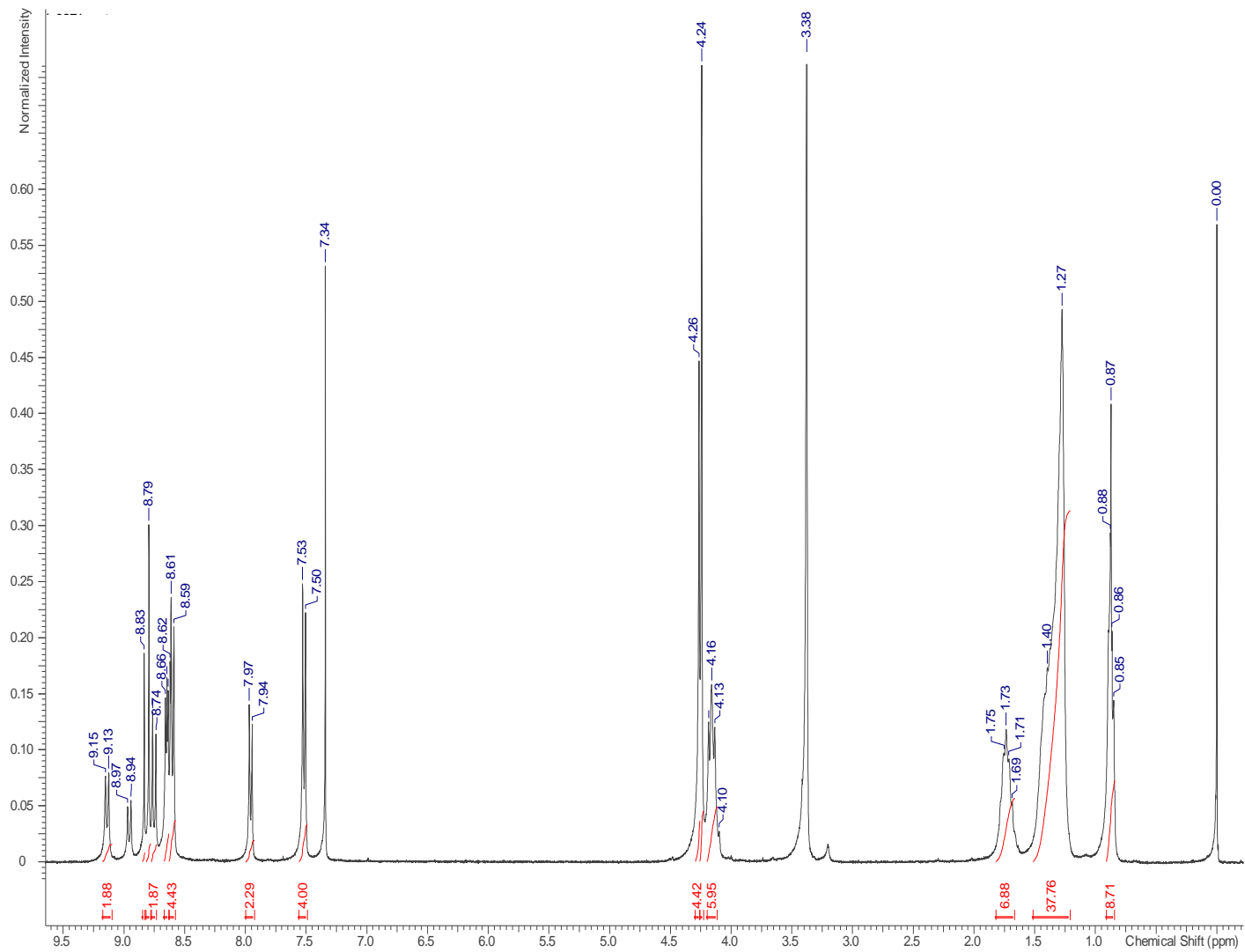


Ig0271 1 (0.035)

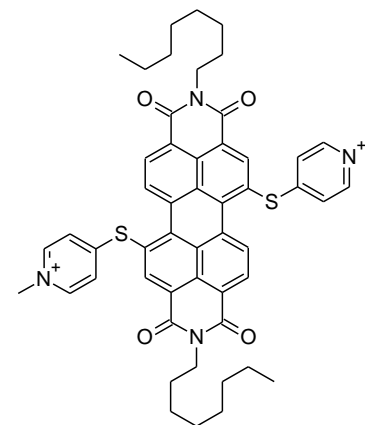
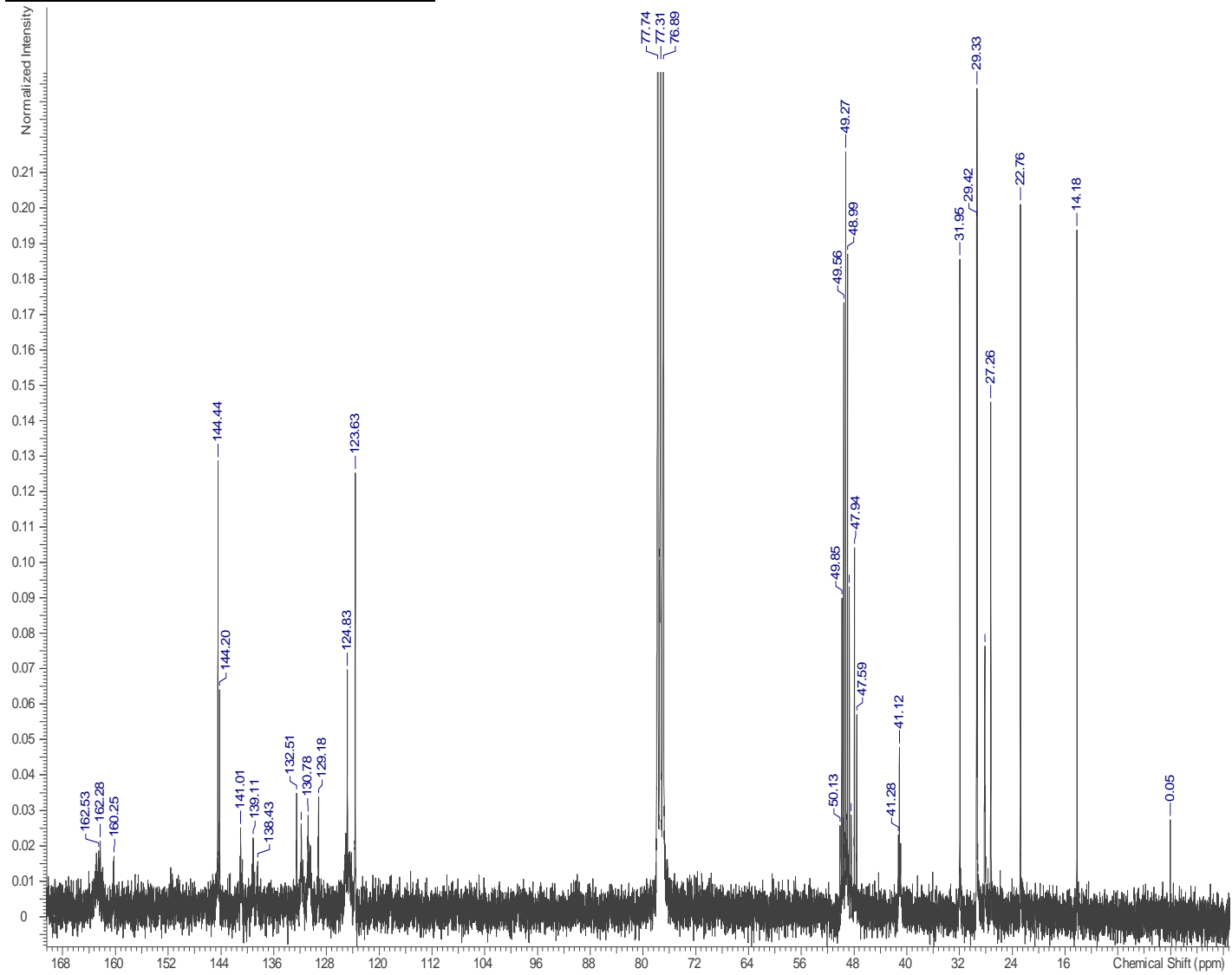
1: TOF MS ES+
630

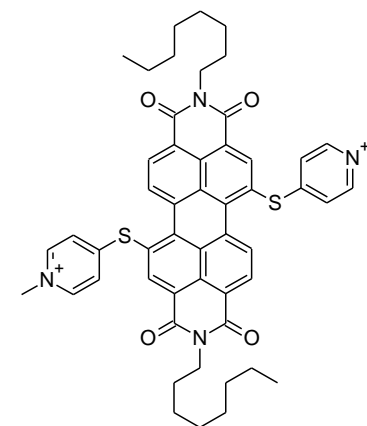
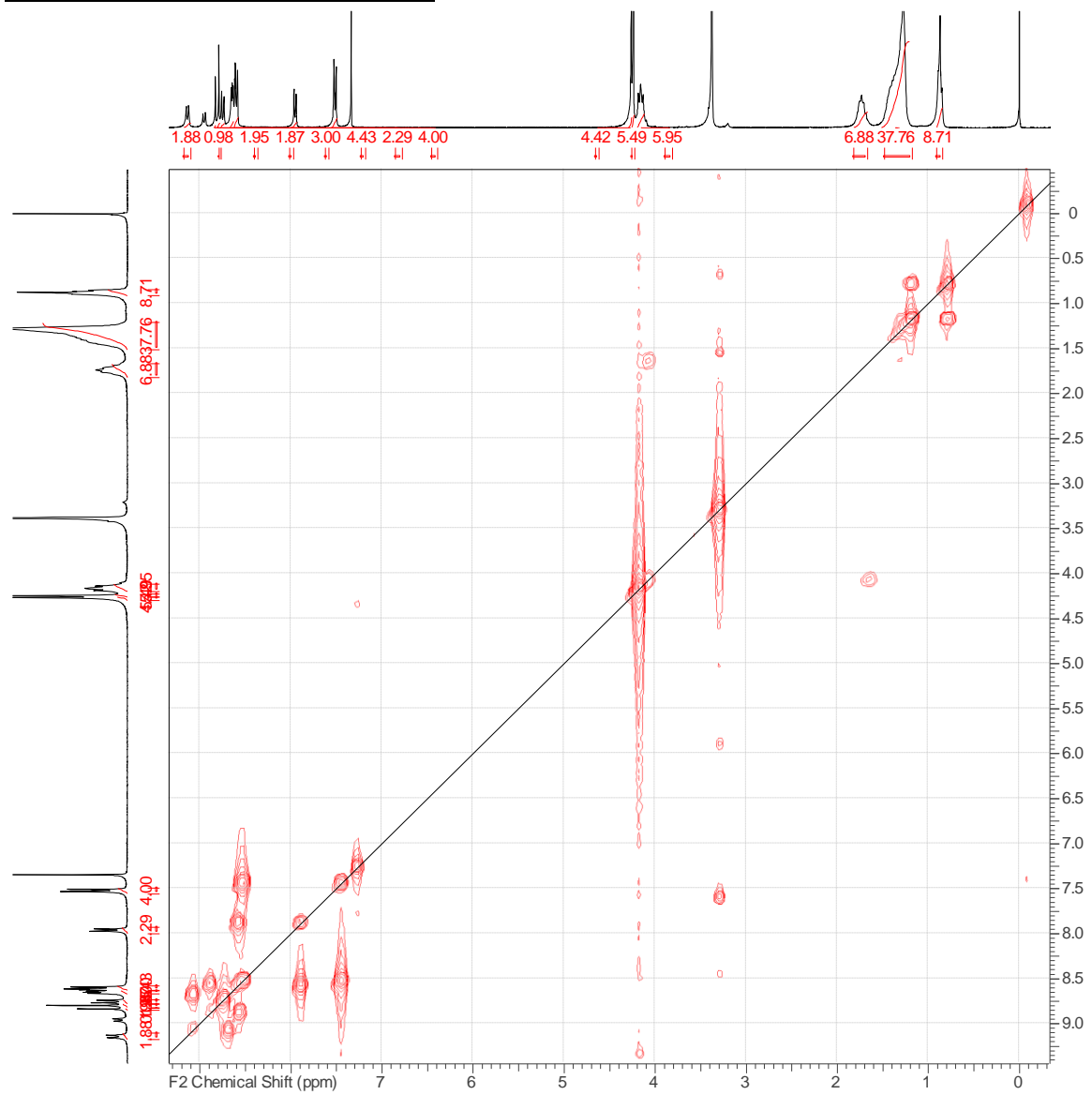


¹H NMR spectrum of compound 17

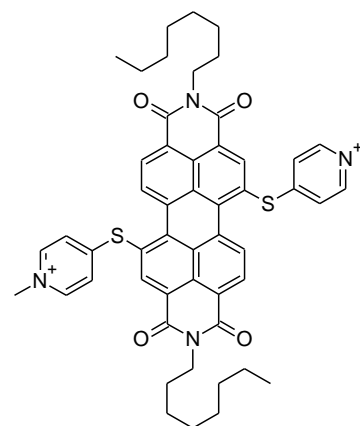
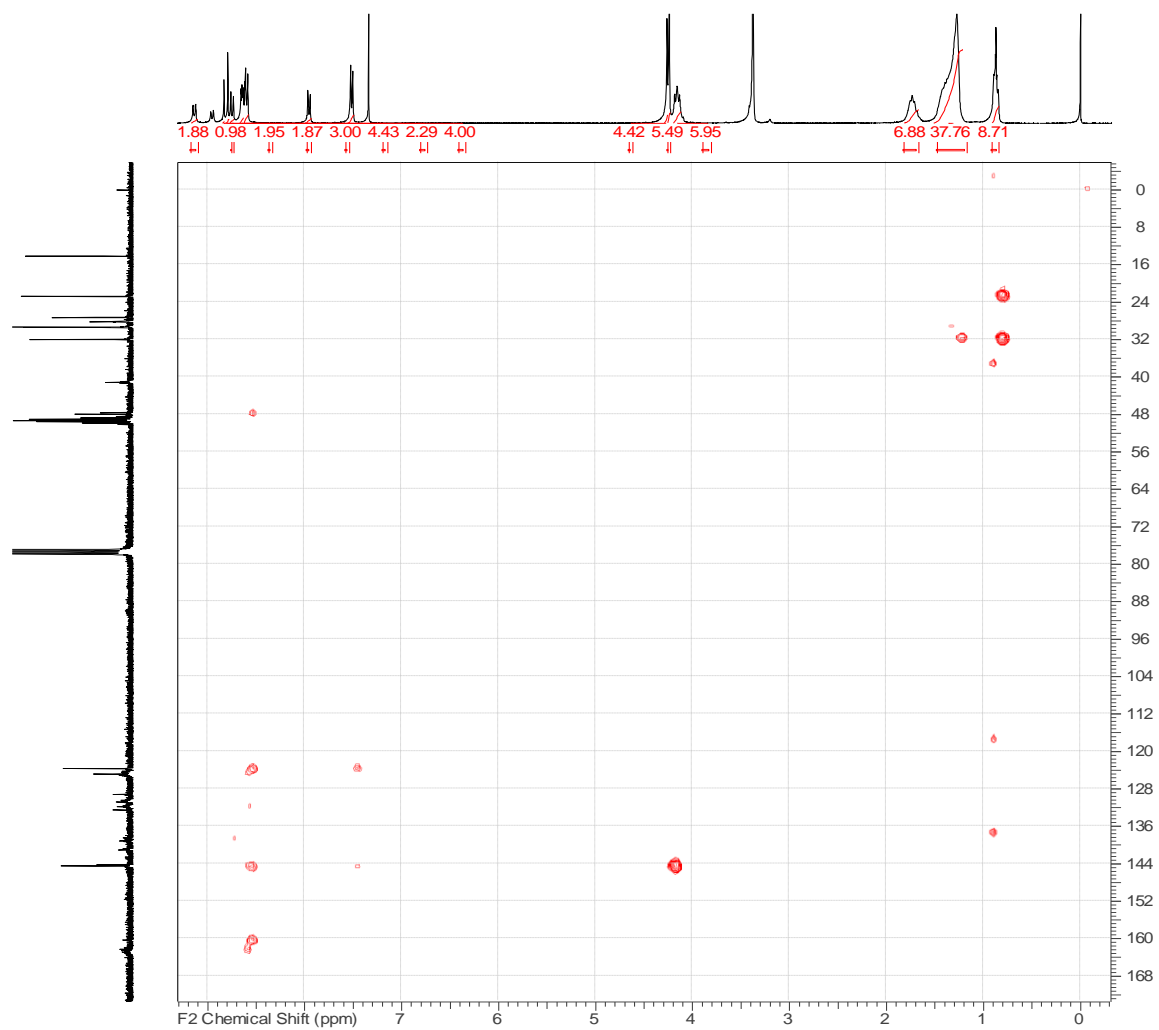


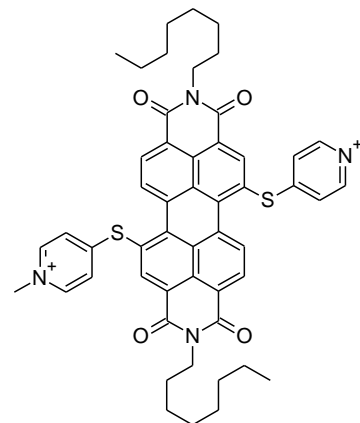
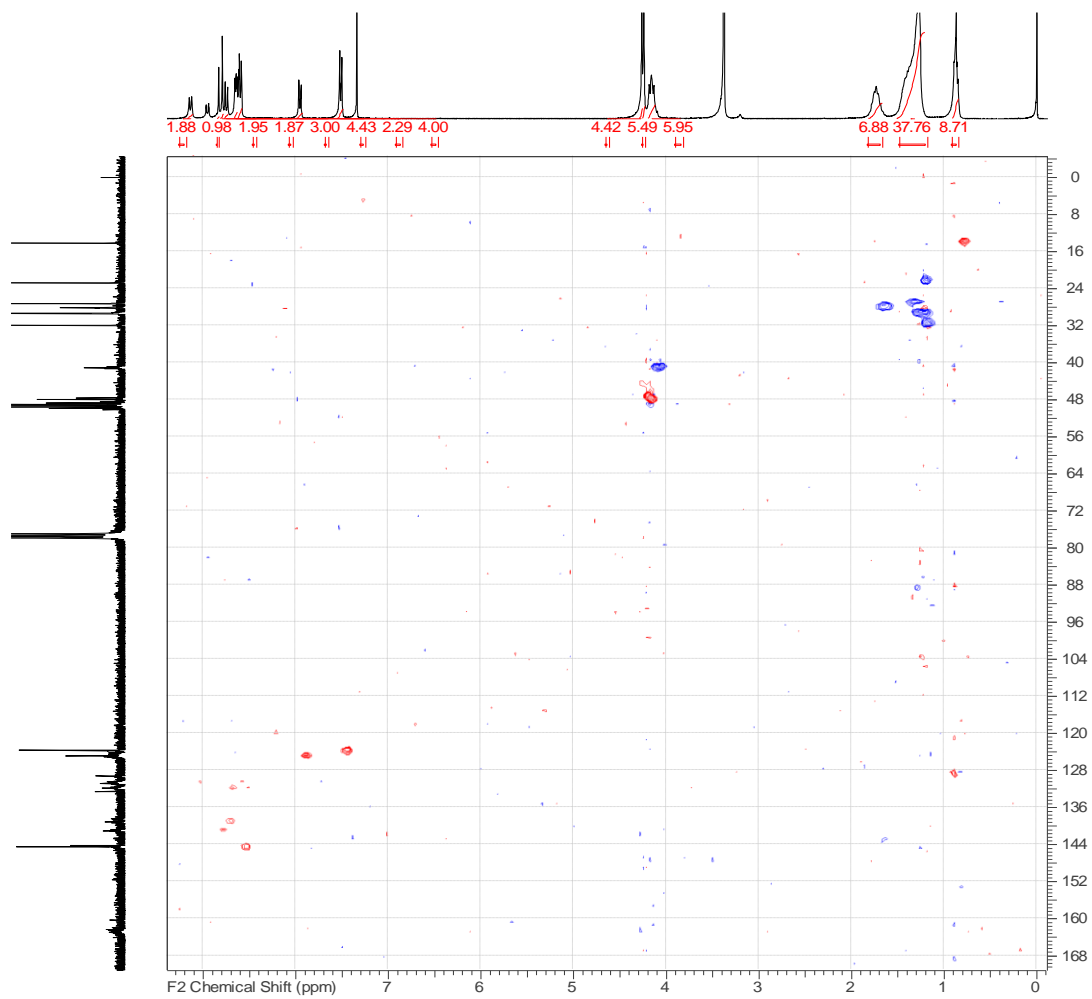
¹³C NMR Spectrum of compound 17



COSY spectrum of compound 17

gHMBC spectrum of compound 17



gHSQC spectrum of compound 17

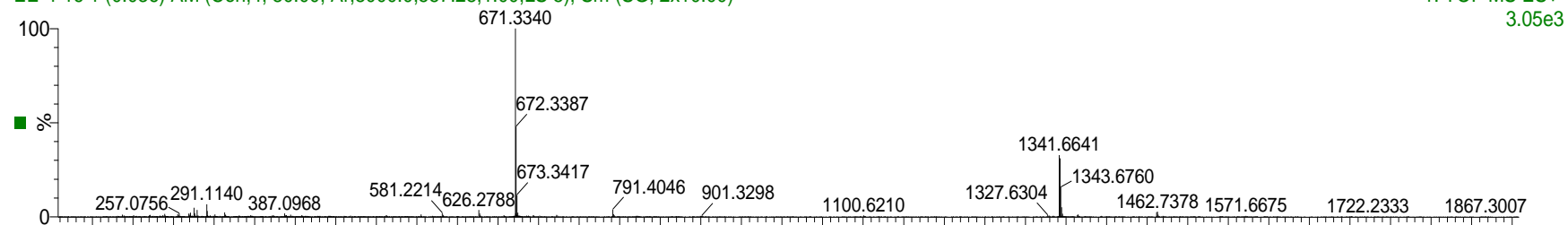
MS spectrum of compound 19

EE-4-16 in Chl/MeOH

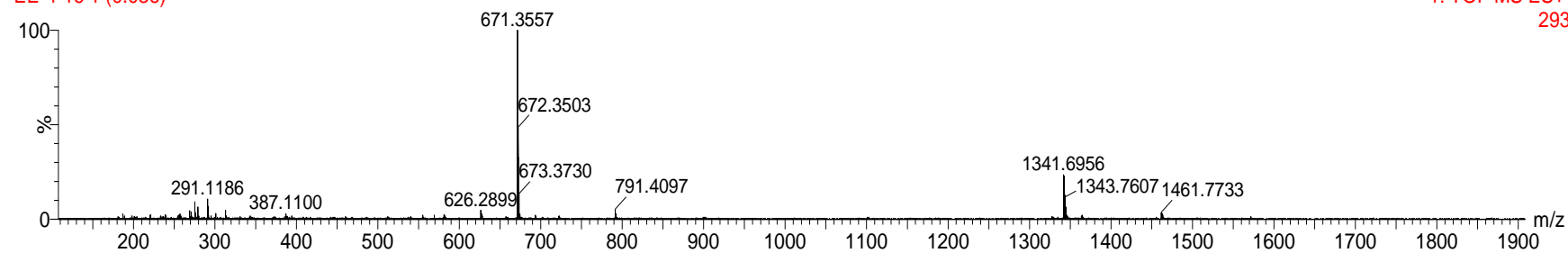
EE-4-16 (0.036) Is (1.00,1.00) C₄₀H₄₂N₆O₄



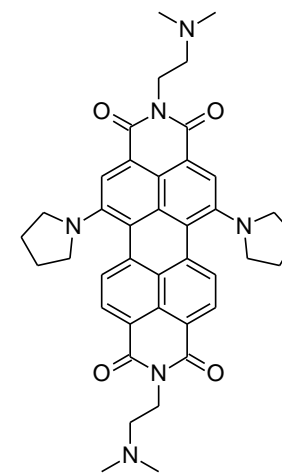
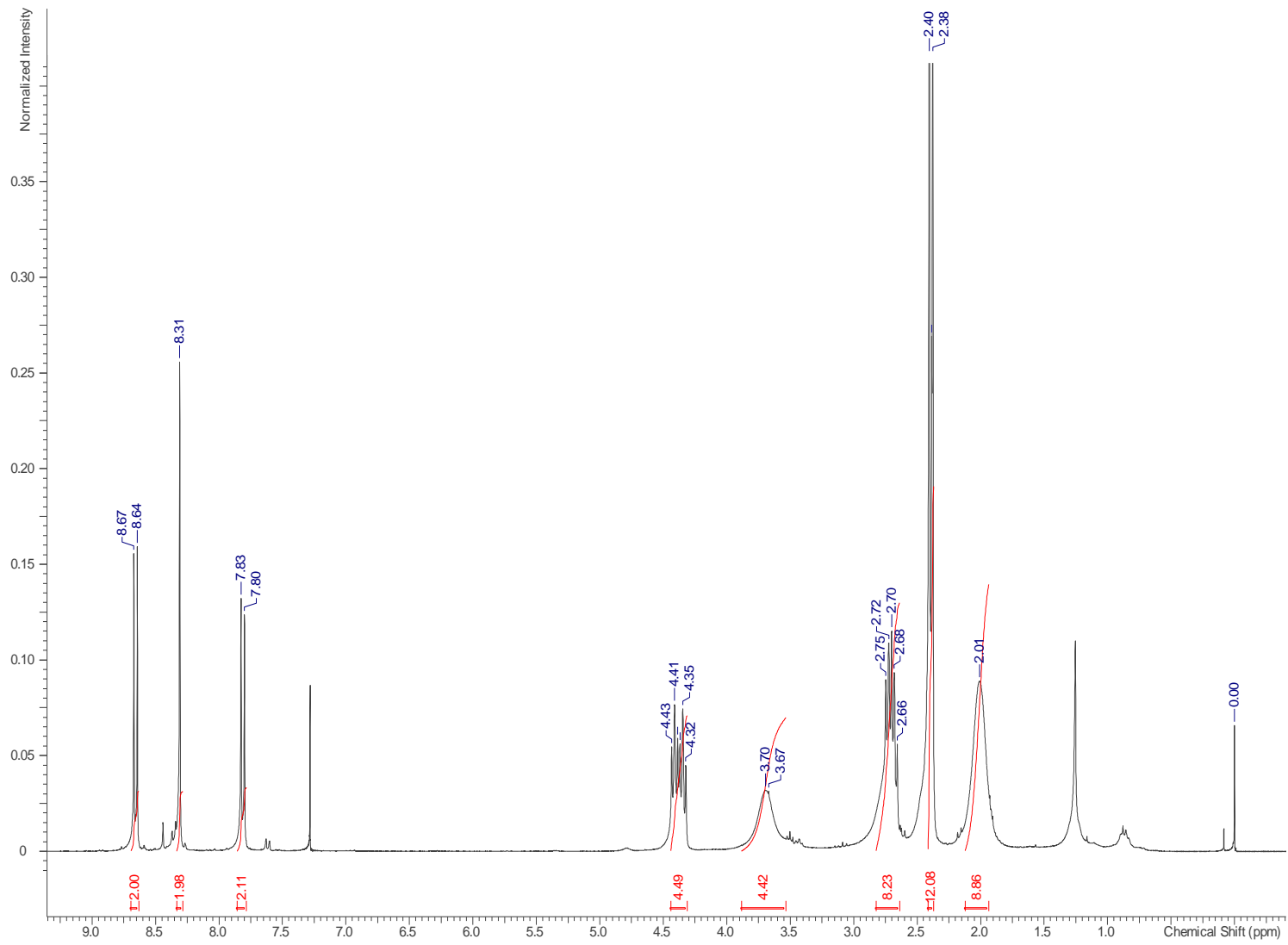
EE-4-16 1 (0.036) AM (Cen,4, 80.00, Ar,8000.0,557.28,1.00,LS 5); Sm (SG, 2x10.00)



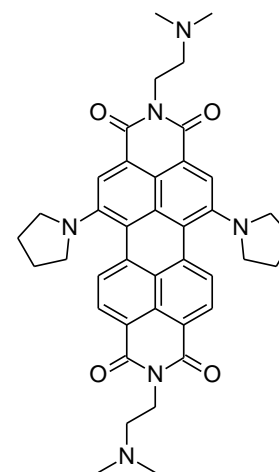
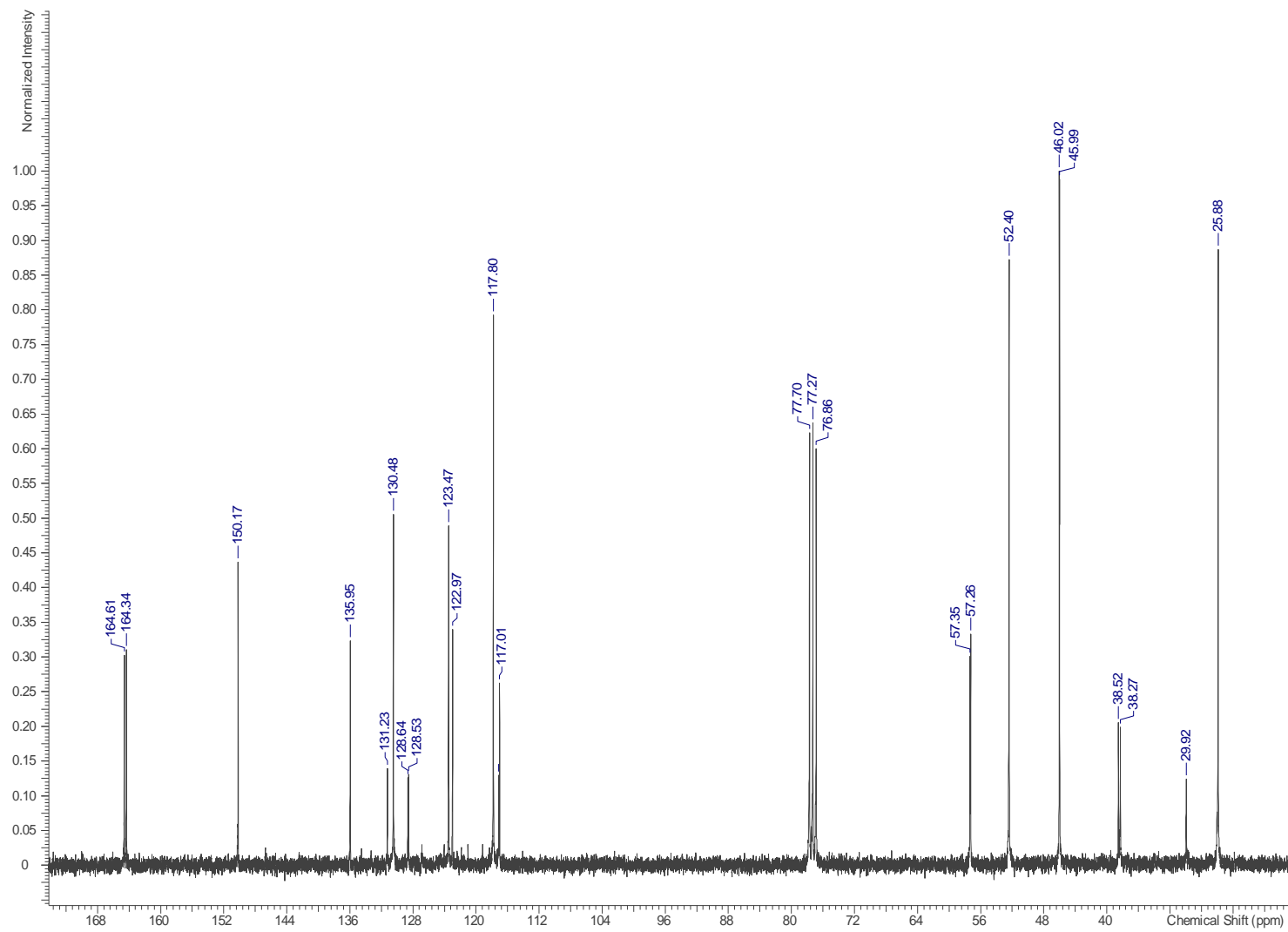
EE-4-16 1 (0.036)

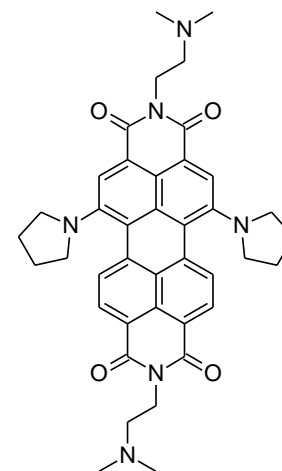
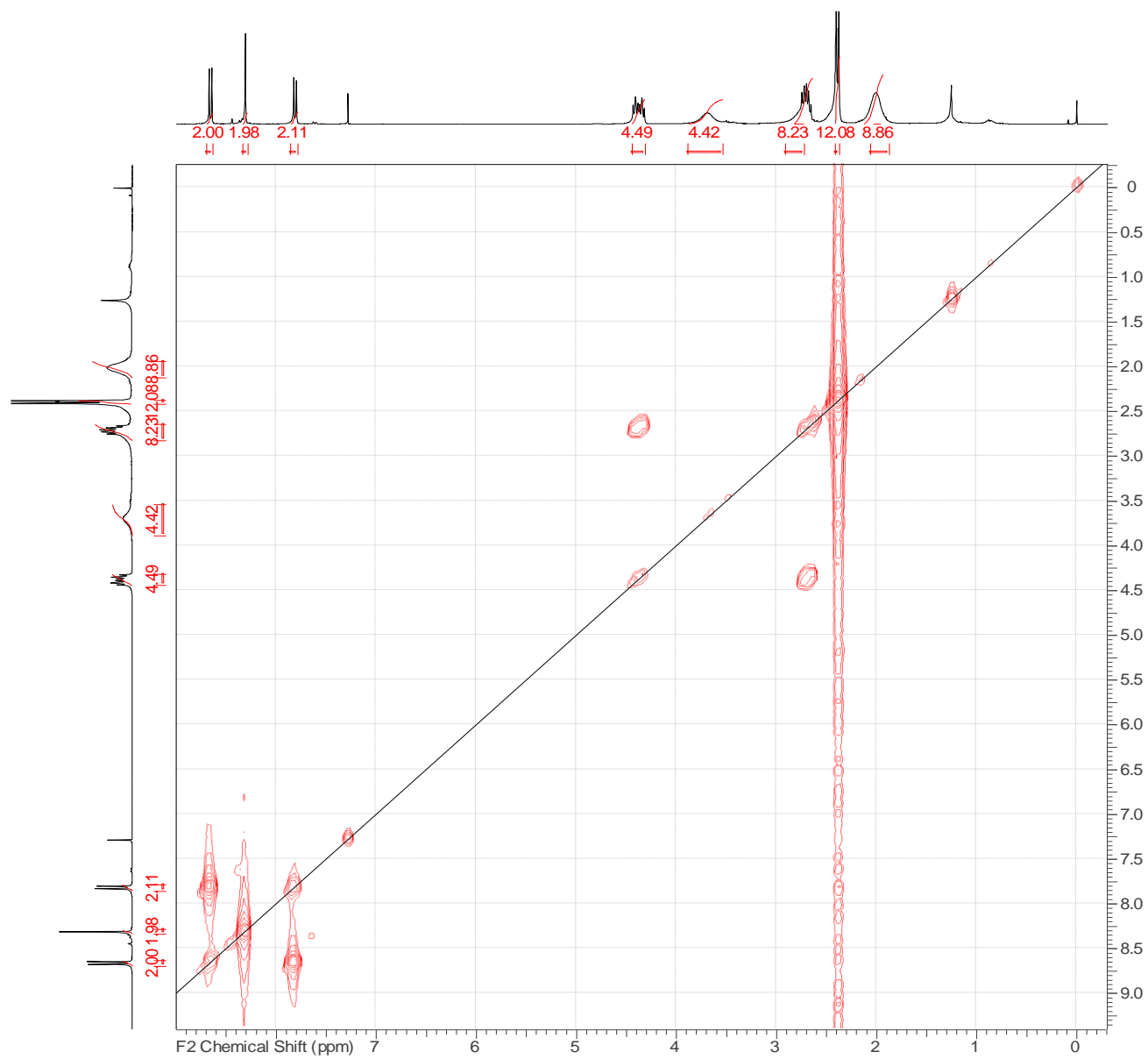


¹H NMR spectrum of compound 19

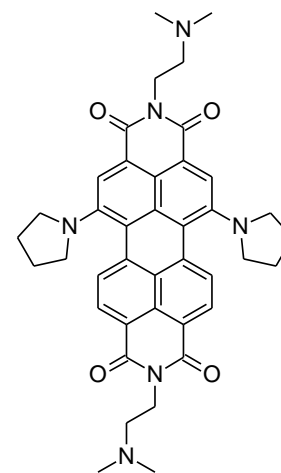
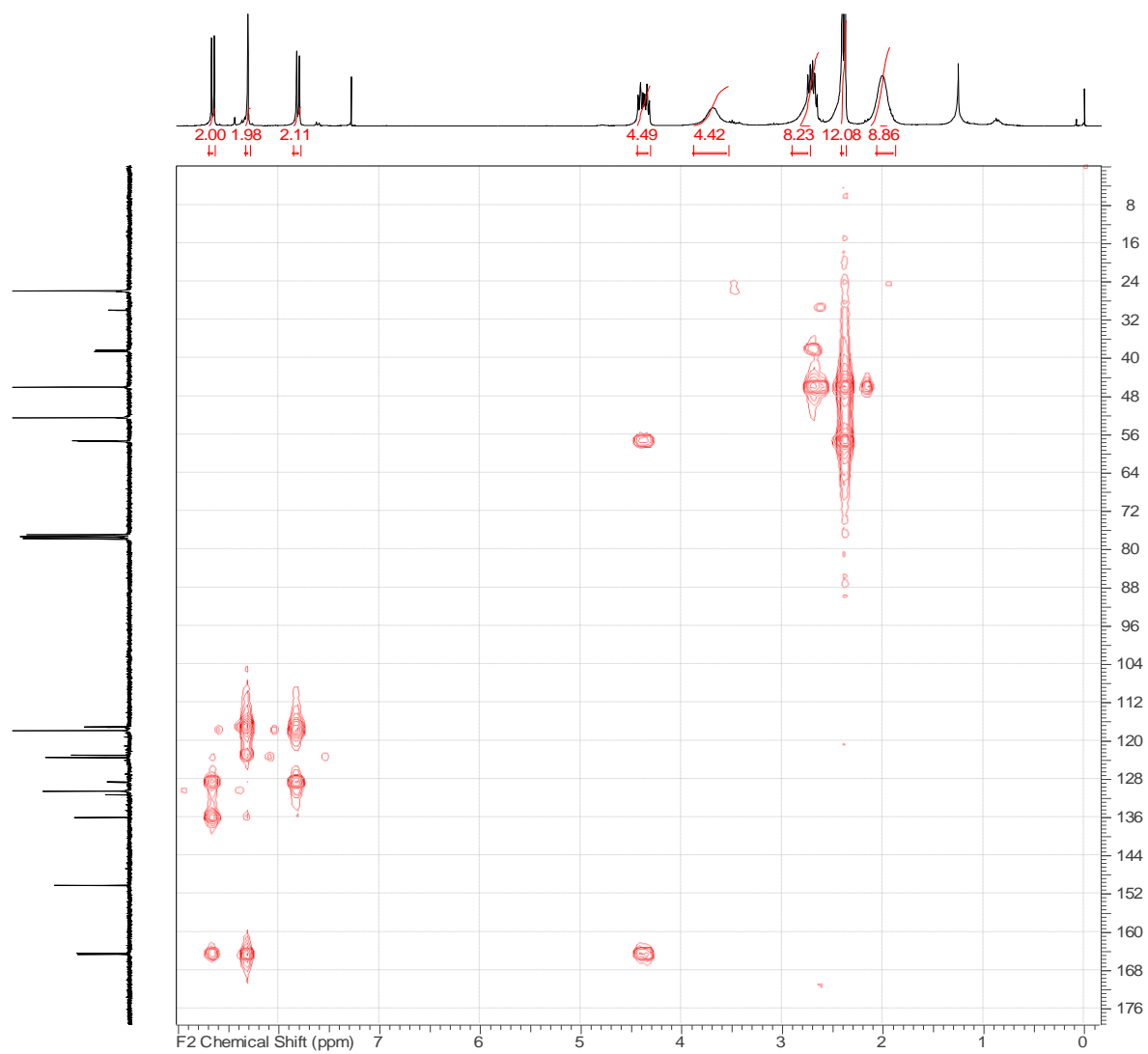


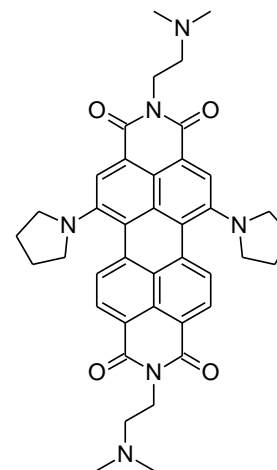
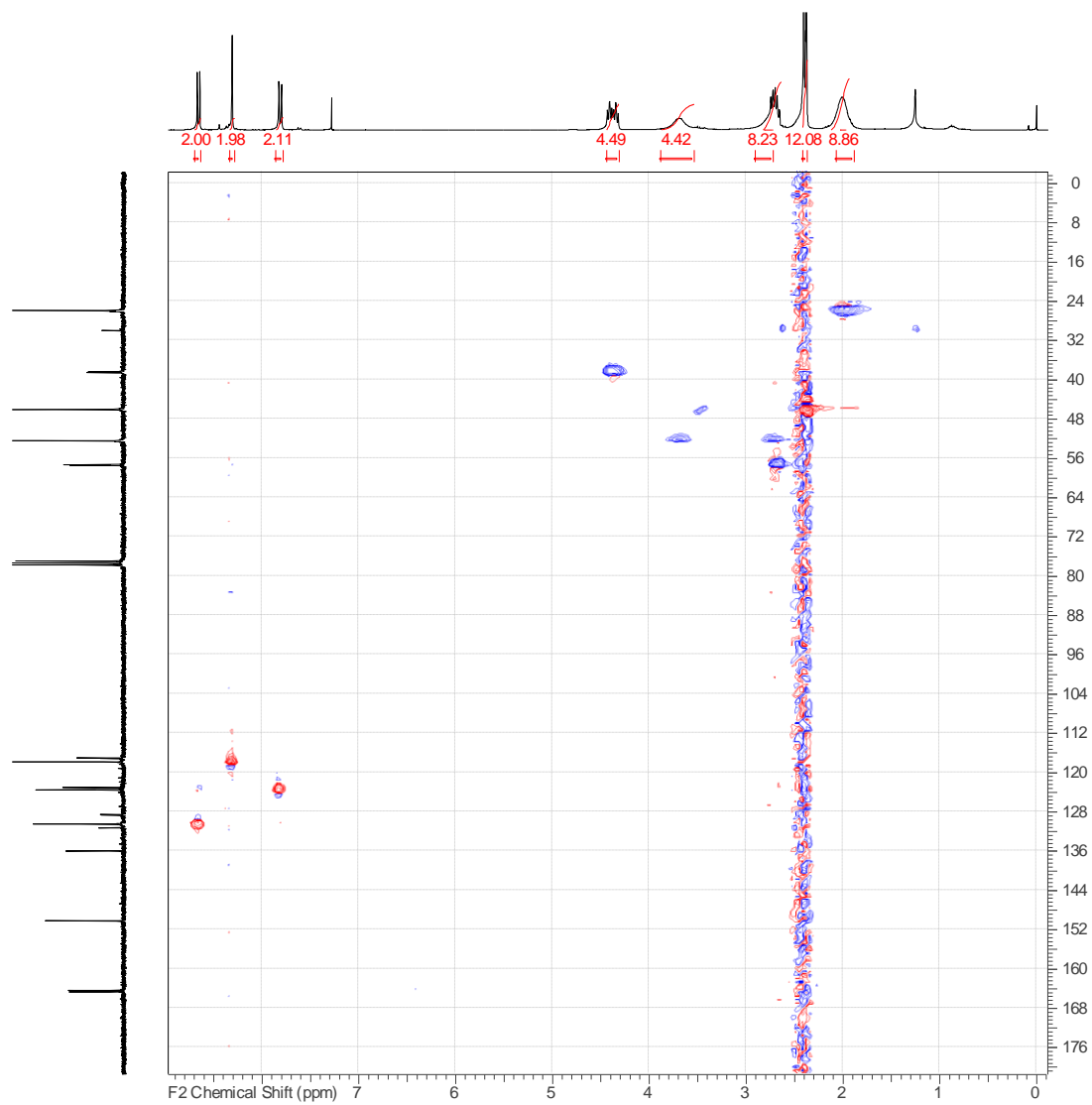
¹³C NMR Spectrum of compound 19



COSY spectrum of compound 19

gHMBC spectrum of compound 19

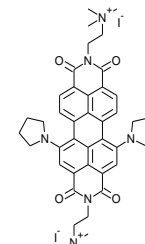


gHSQC spectrum of compound 19

MS spectrum of compound 20

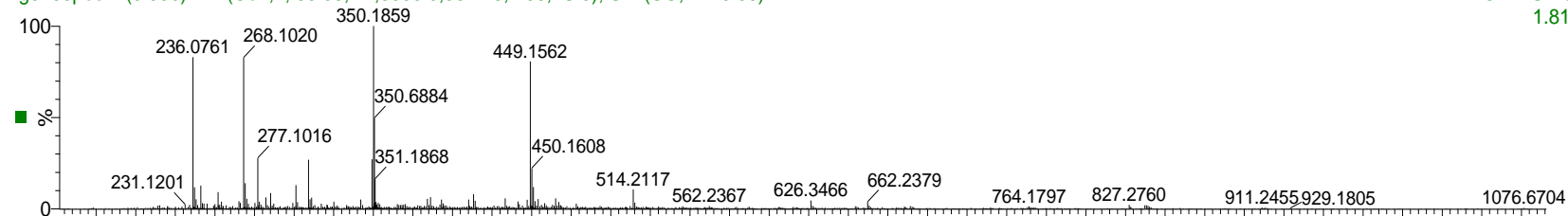
Ig0269pos in Clf/MeOH

Ig0269pos (0.036) Is (1.00,1.00) C₄₂H₄₆N₆O₄



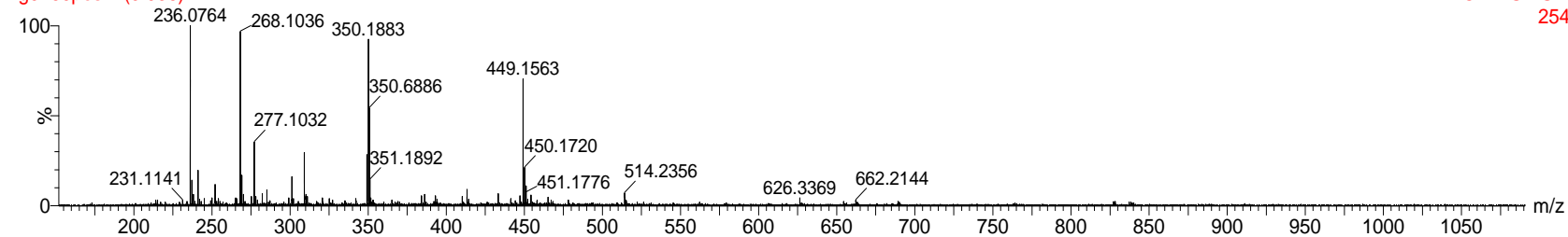
1: TOF MS ES+
6.05e12

Ig0269pos 1 (0.036) AM (Cen,4, 80.00, Ar,8000.0,557.28,1.00,LS 5); Sm (SG, 2x10.00)

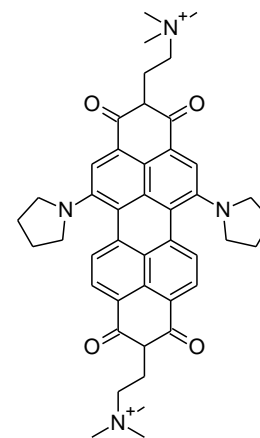
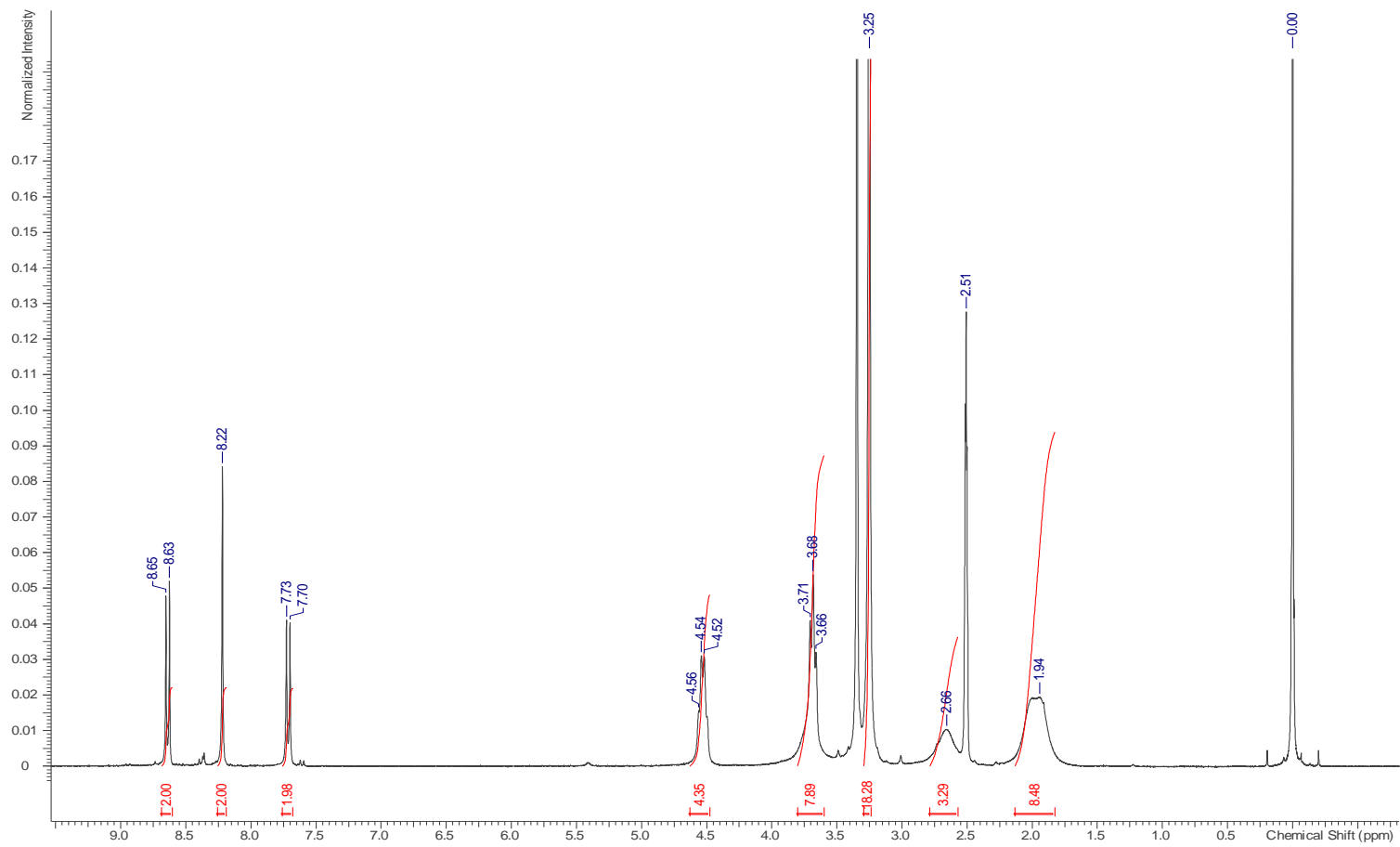


1: TOF MS ES+
1.81e3

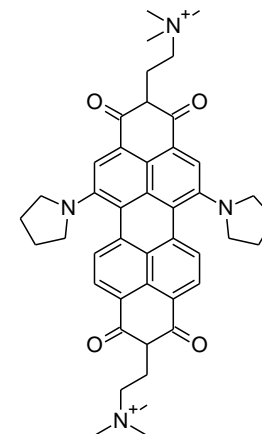
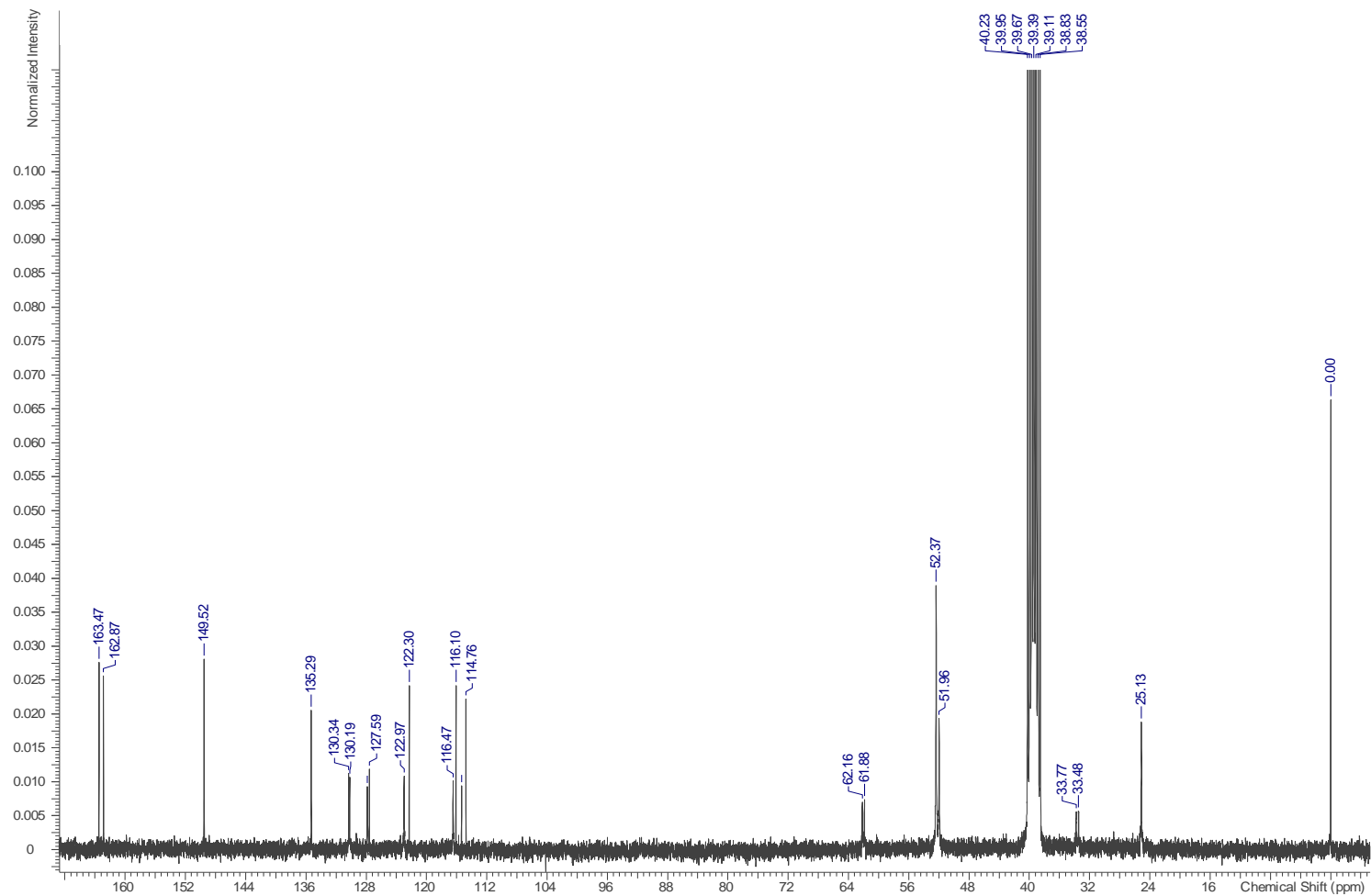
Ig0269pos 1 (0.036)

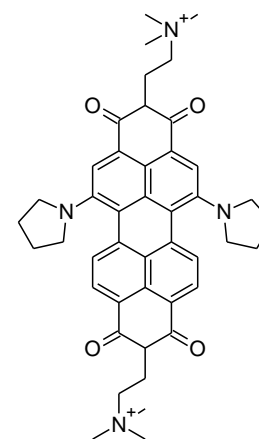
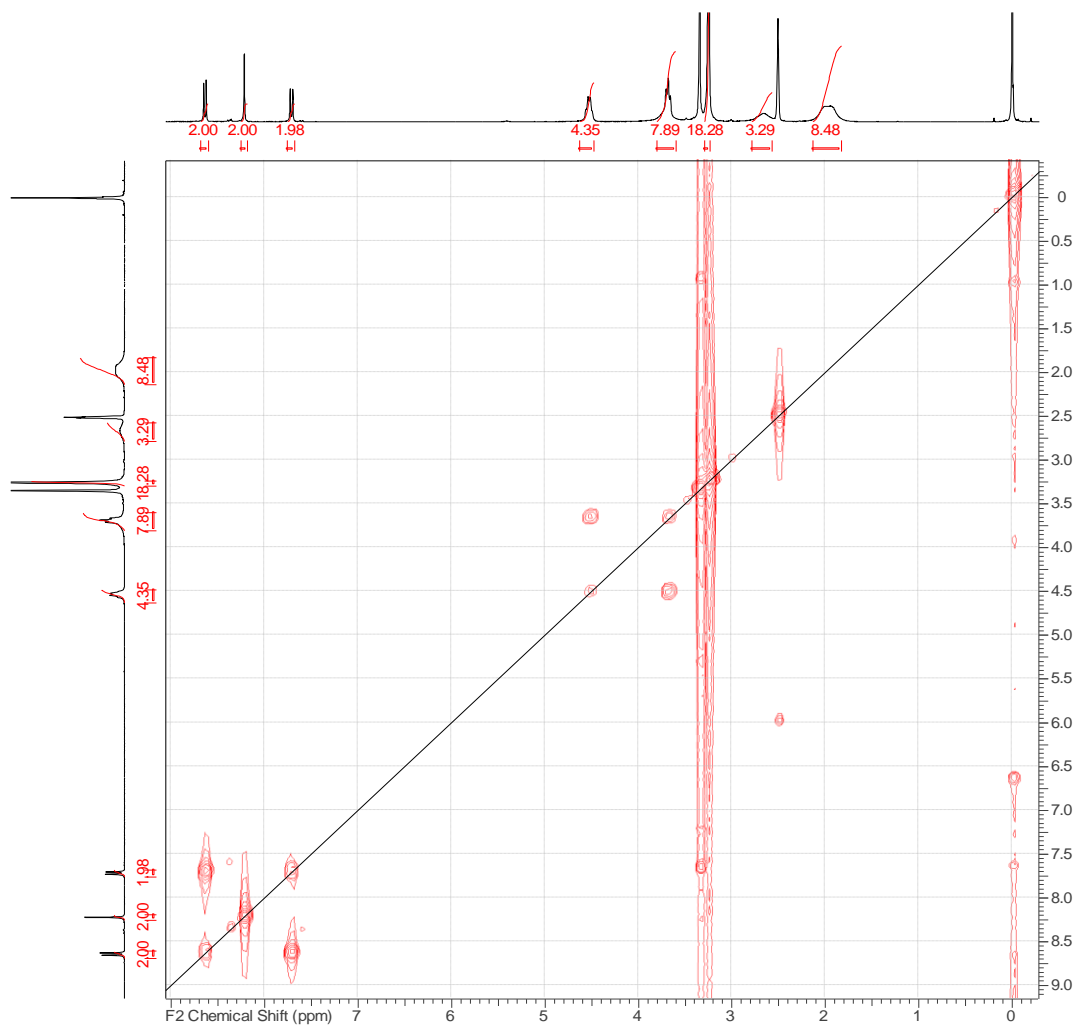


1: TOF MS ES+
254

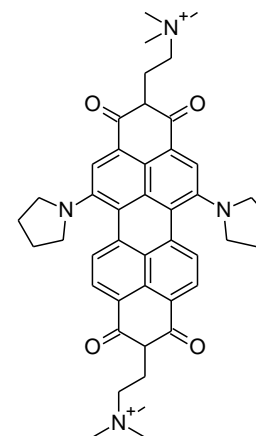
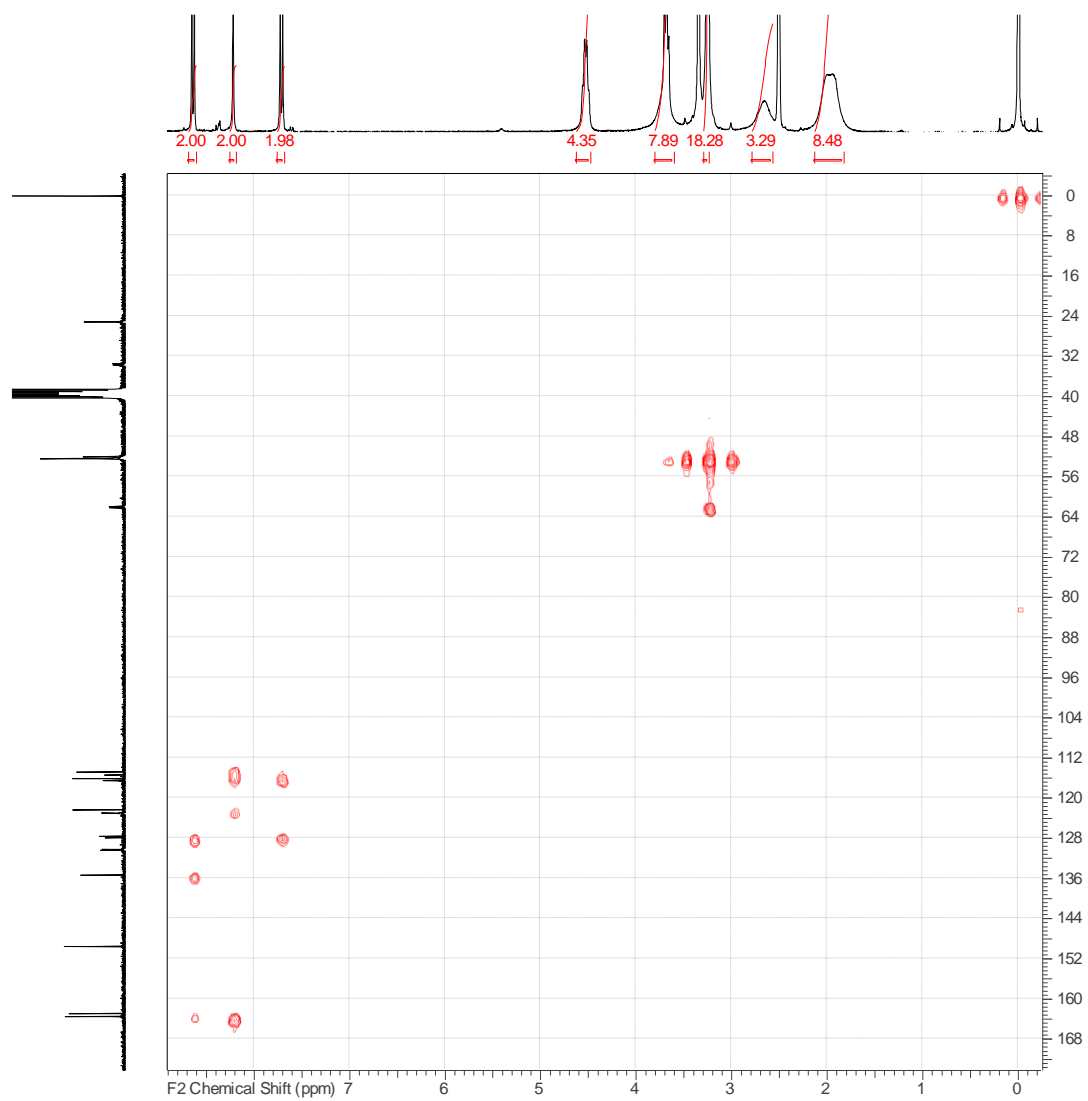
^1H NMR spectrum of compound 20

¹³C NMR Spectrum of compound 20



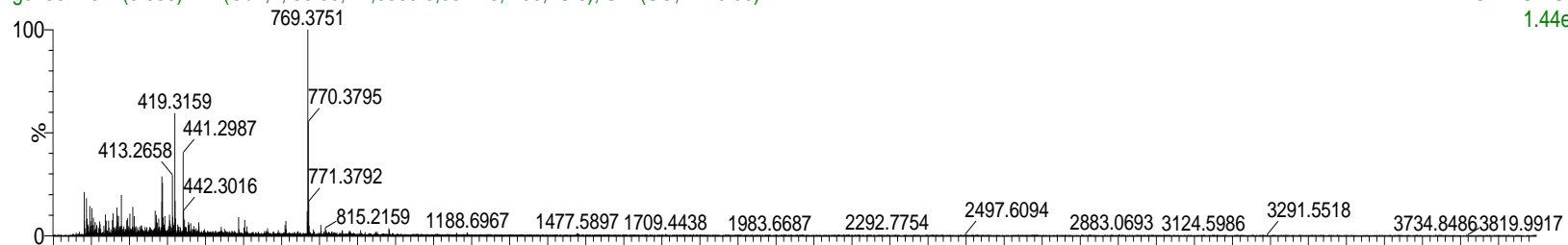
COSY spectrum of compound 20

gHMBC spectrum of compound 20

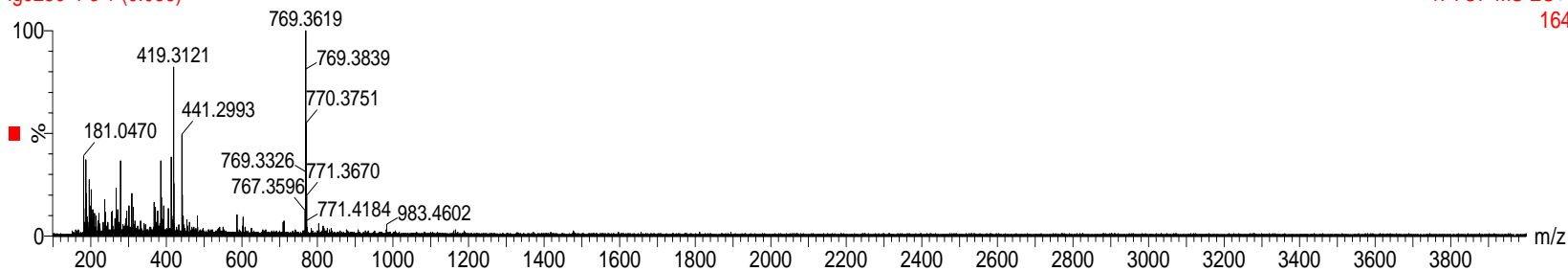


MS spectrum of compound 22**Ig0250-4-3 in clf/MeOH**Ig0250-4-3 (0.036) Is (1.00,1.00) C₅₀H₄₈N₄O₄

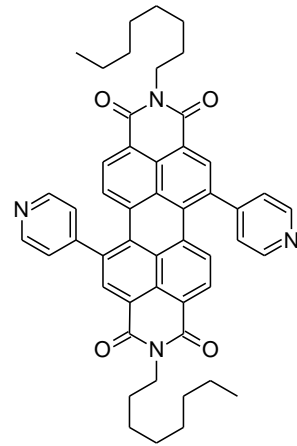
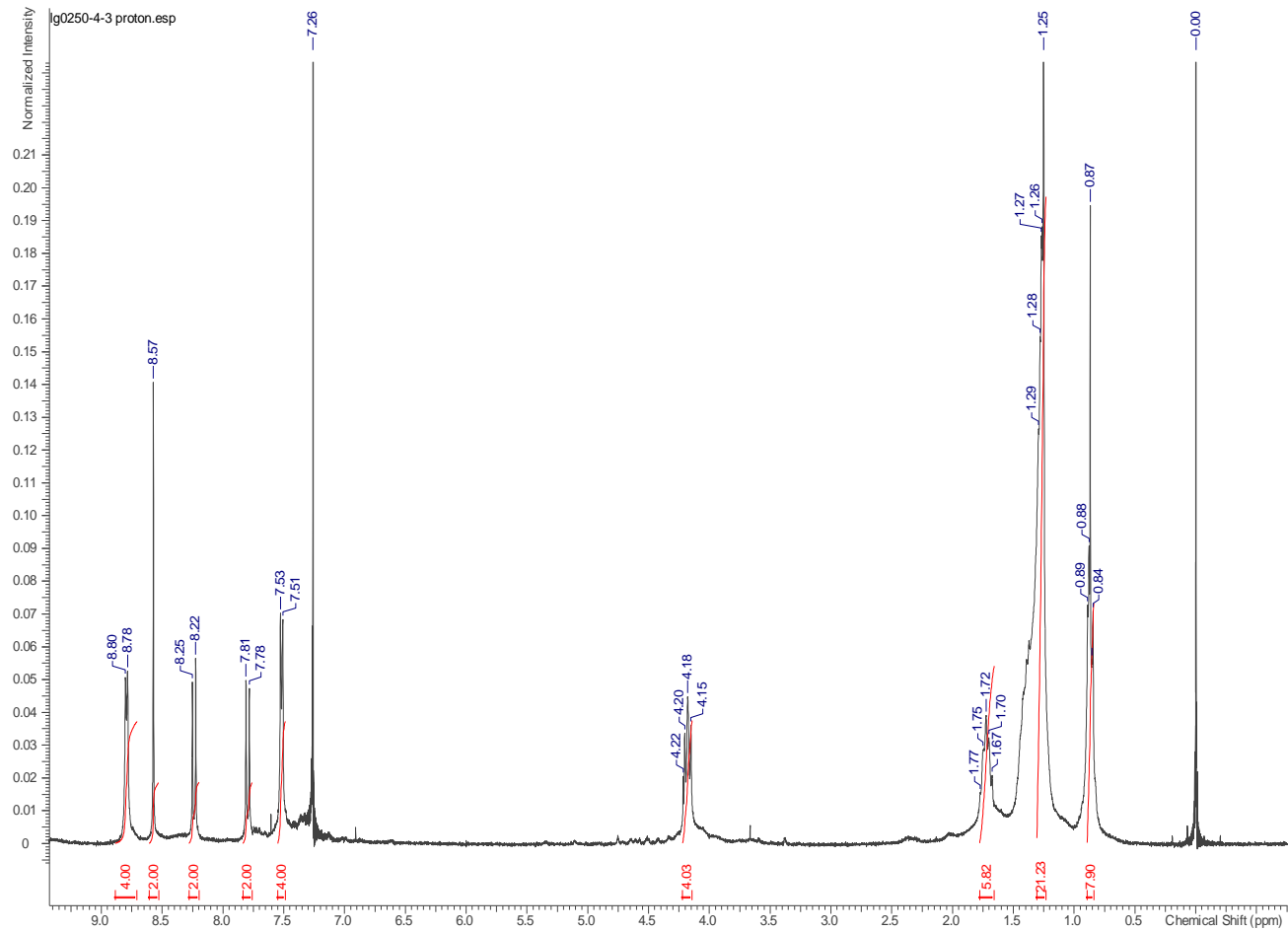
Ig0250-4-3 1 (0.036) AM (Cen,4, 80.00, Ar,8000.0,557.28,1.00,LS 5); Sm (SG, 2x10.00)

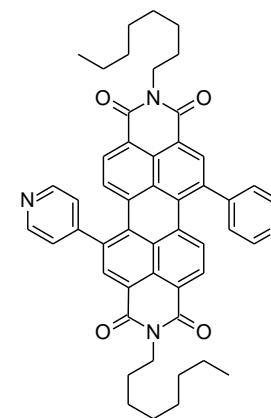
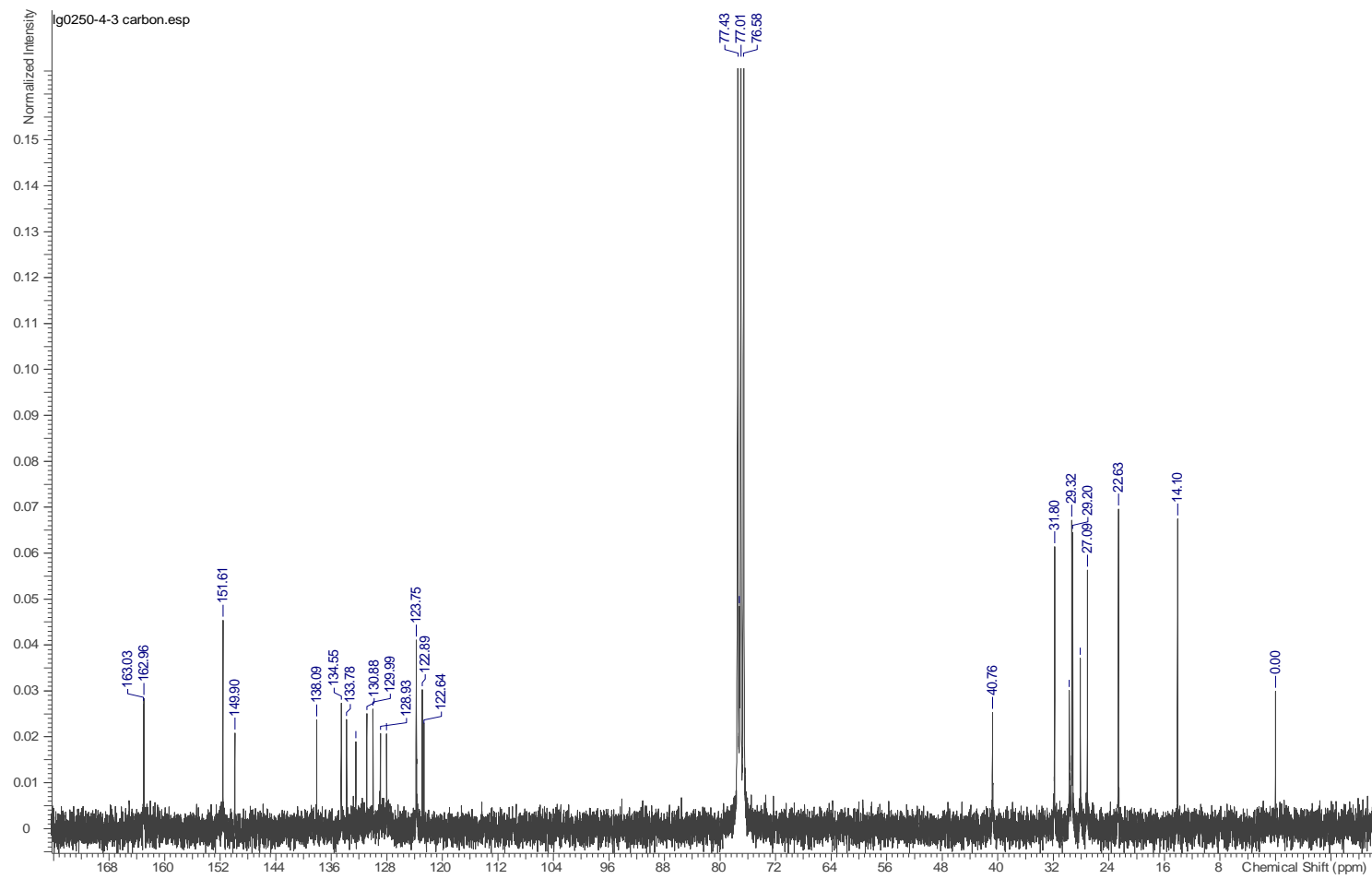
1: TOF MS ES+
1.44e3

Ig0250-4-3 1 (0.036)

1: TOF MS ES+
164

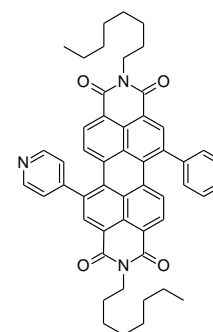
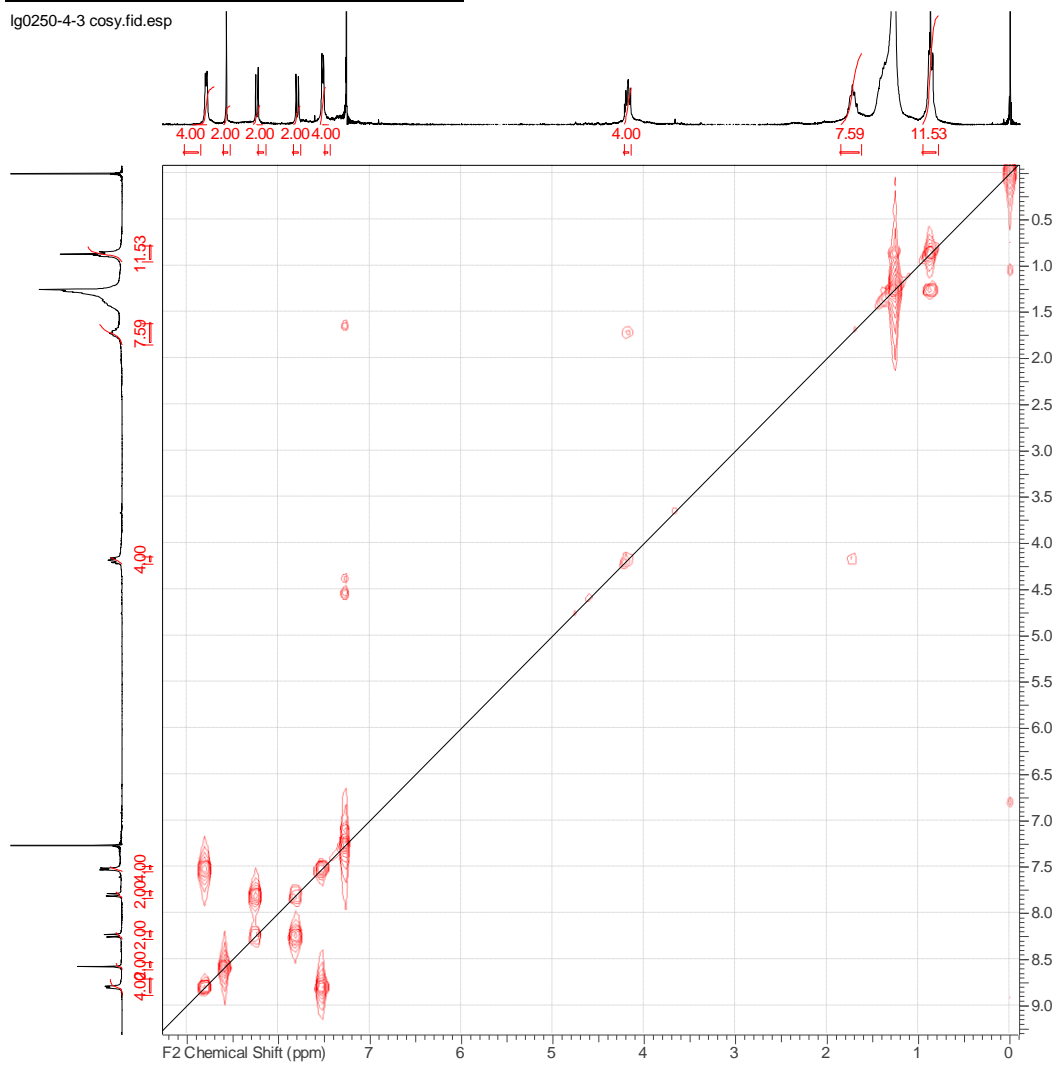
¹H NMR spectrum of compound 22



^{13}C NMR Spectrum of compound 22

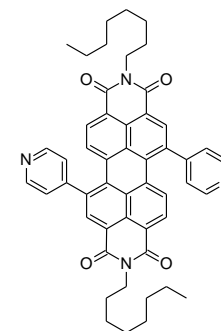
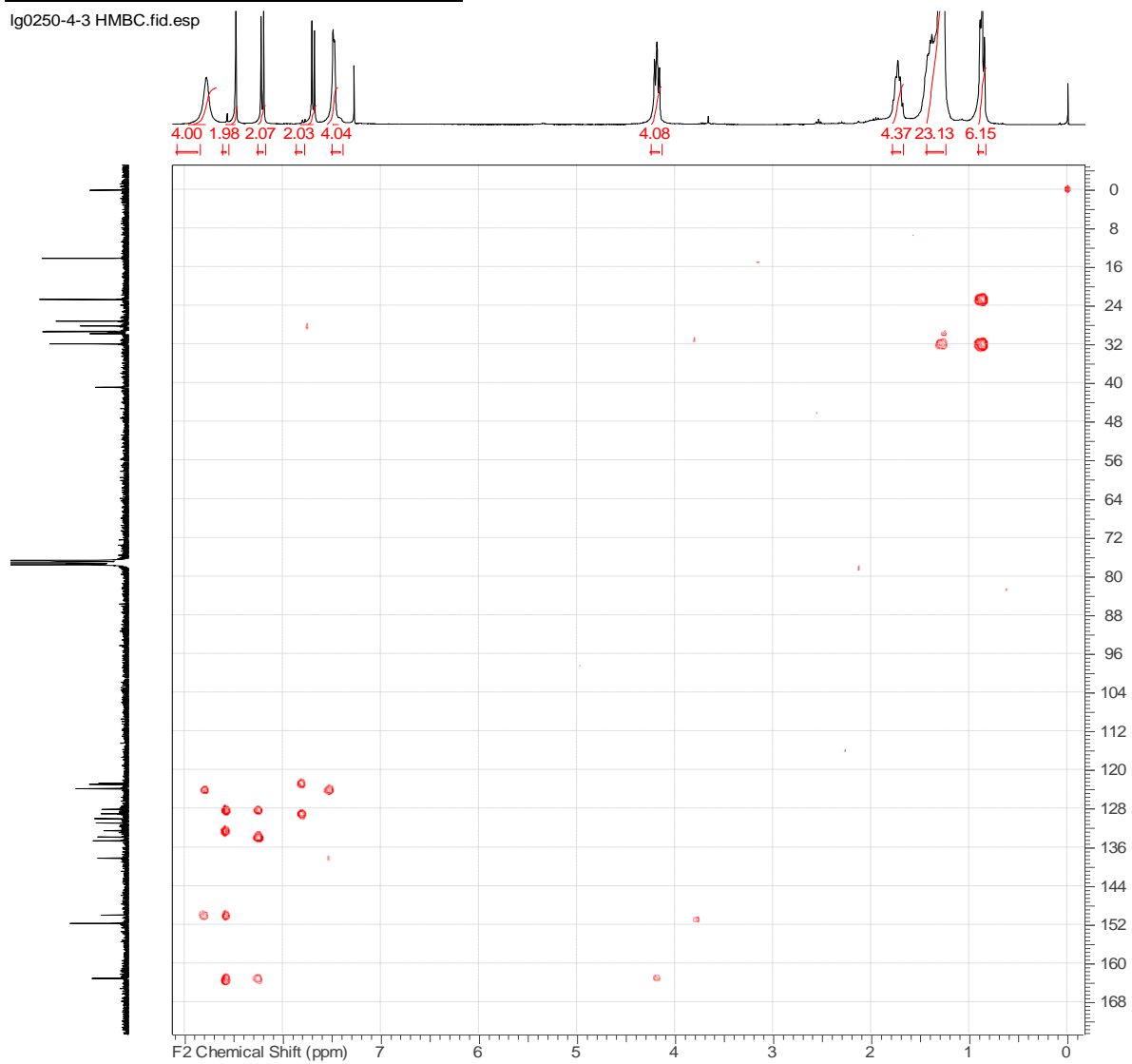
COSY spectrum of compound 22

lg0250-4-3 cosy.fid.esp



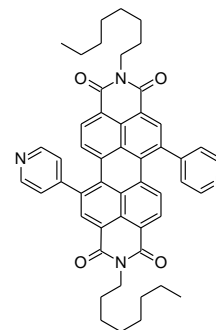
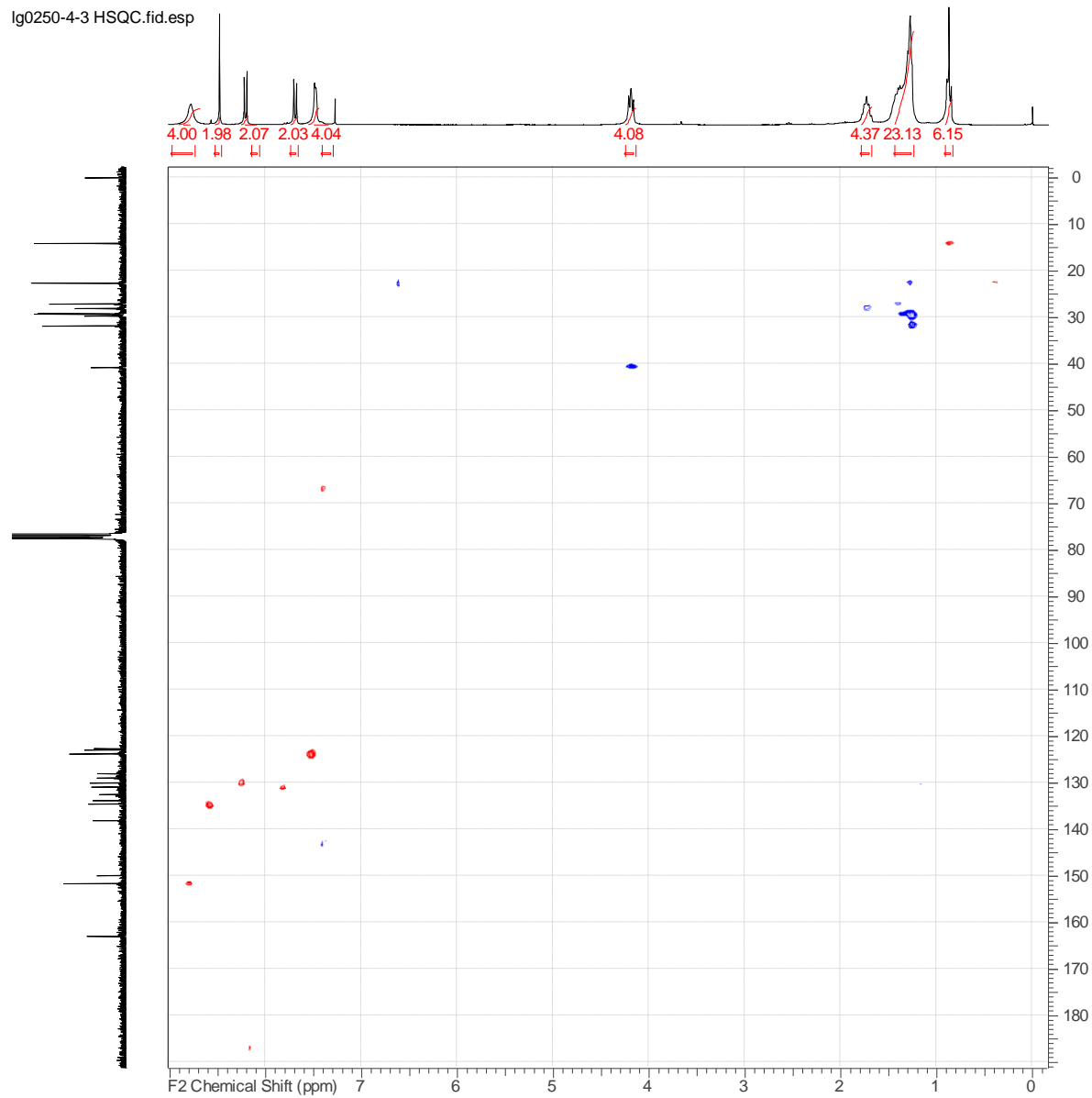
gHMBC spectrum of compound 22

lg0250-4-3 HMBC.fid.esp



gHSQC spectrum of compound 22

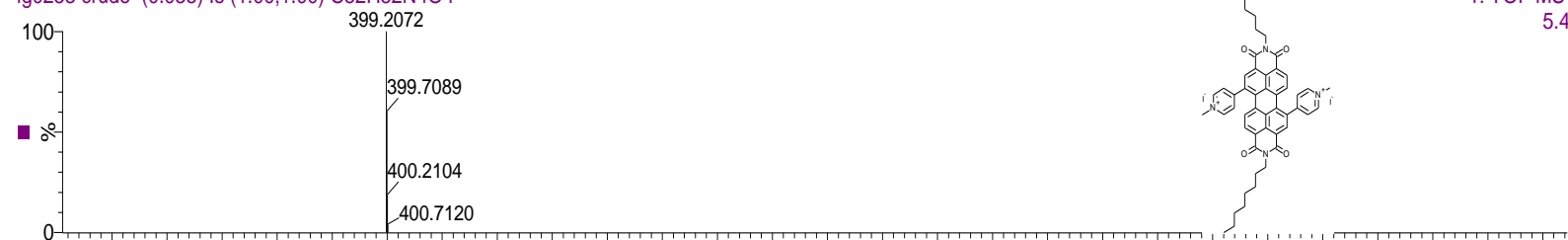
lg0250-4-3 HSQC.fid.esp



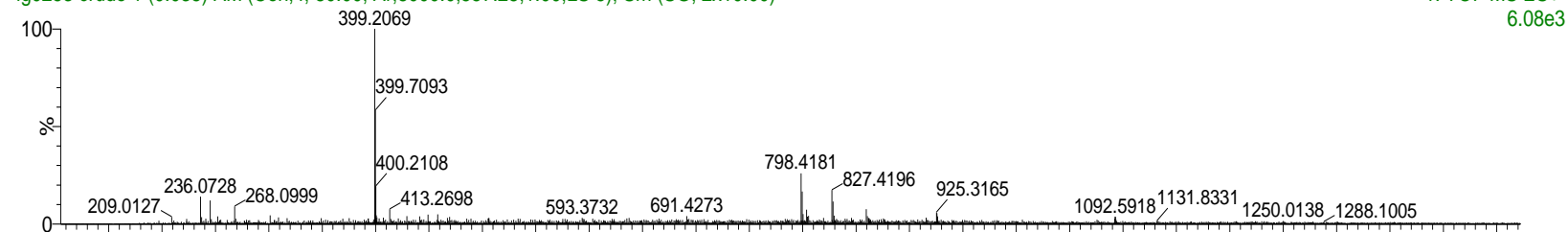
MS spectrum of compound 23

Ig0252 crude in chl/MeOH

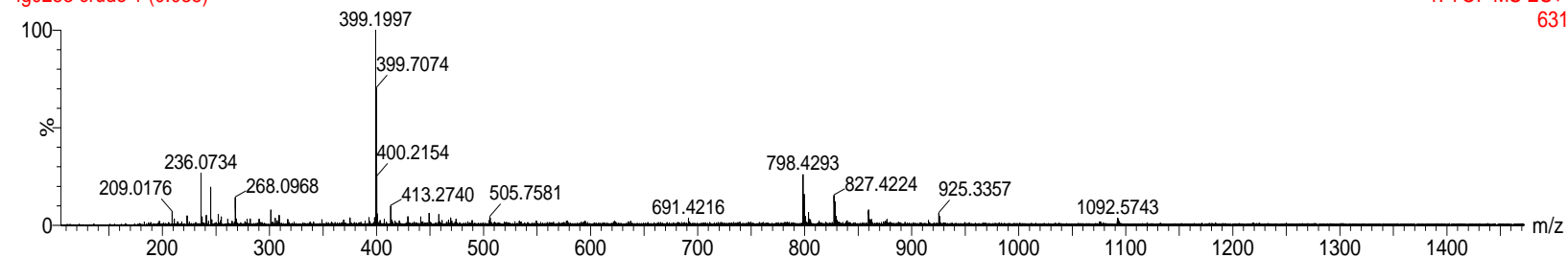
Ig0253 crude (0.035) Is (1.00,1.00) C₅₂H₅₂N₄O₄



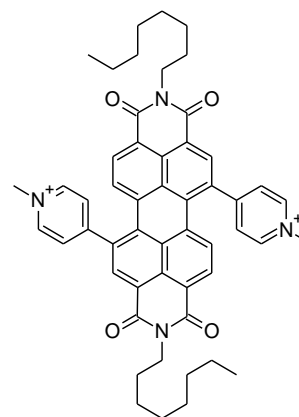
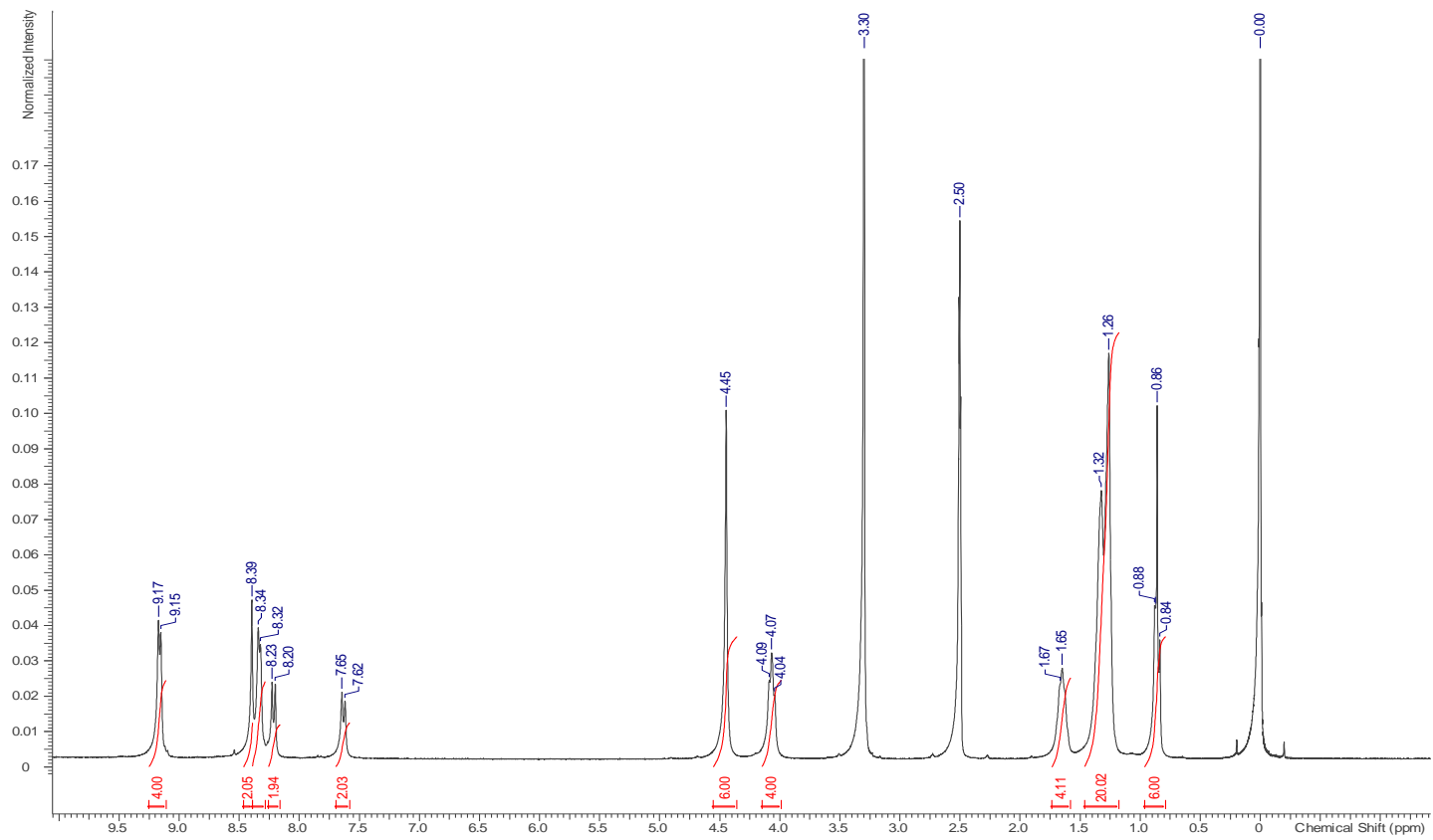
Ig0253 crude 1 (0.035) AM (Cen,4, 80.00, Ar,8000.0,557.28,1.00,LS 5); Sm (SG, 2x10.00)

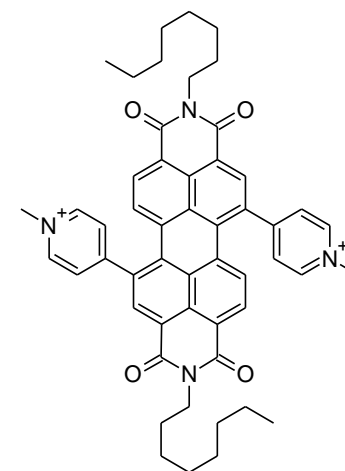
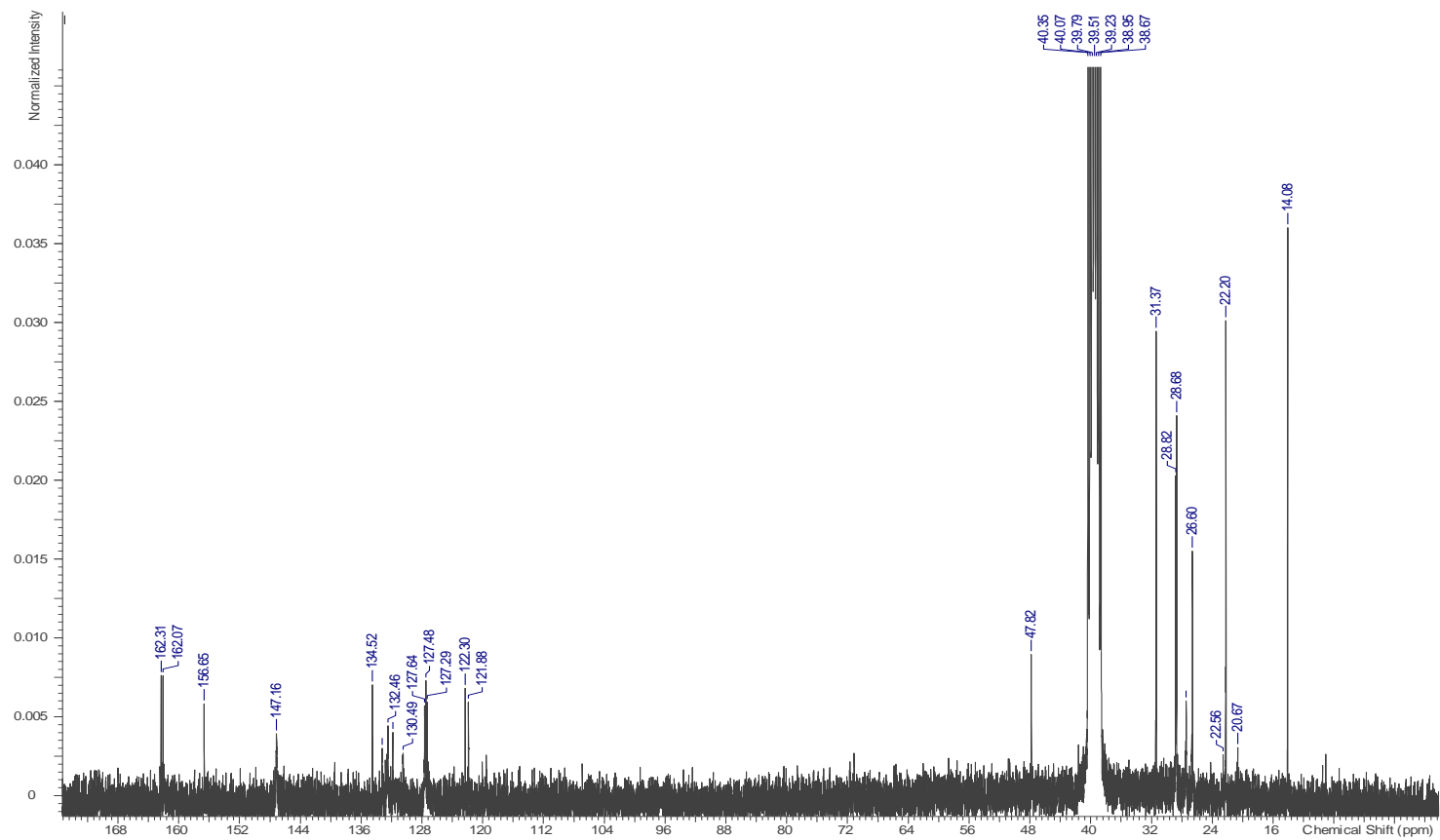


Ig0253 crude 1 (0.035)

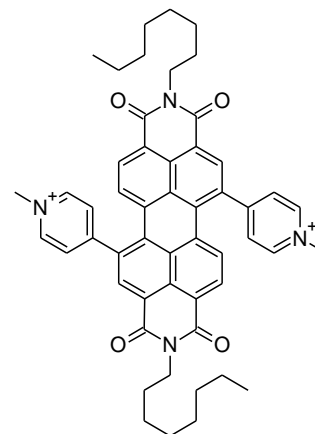
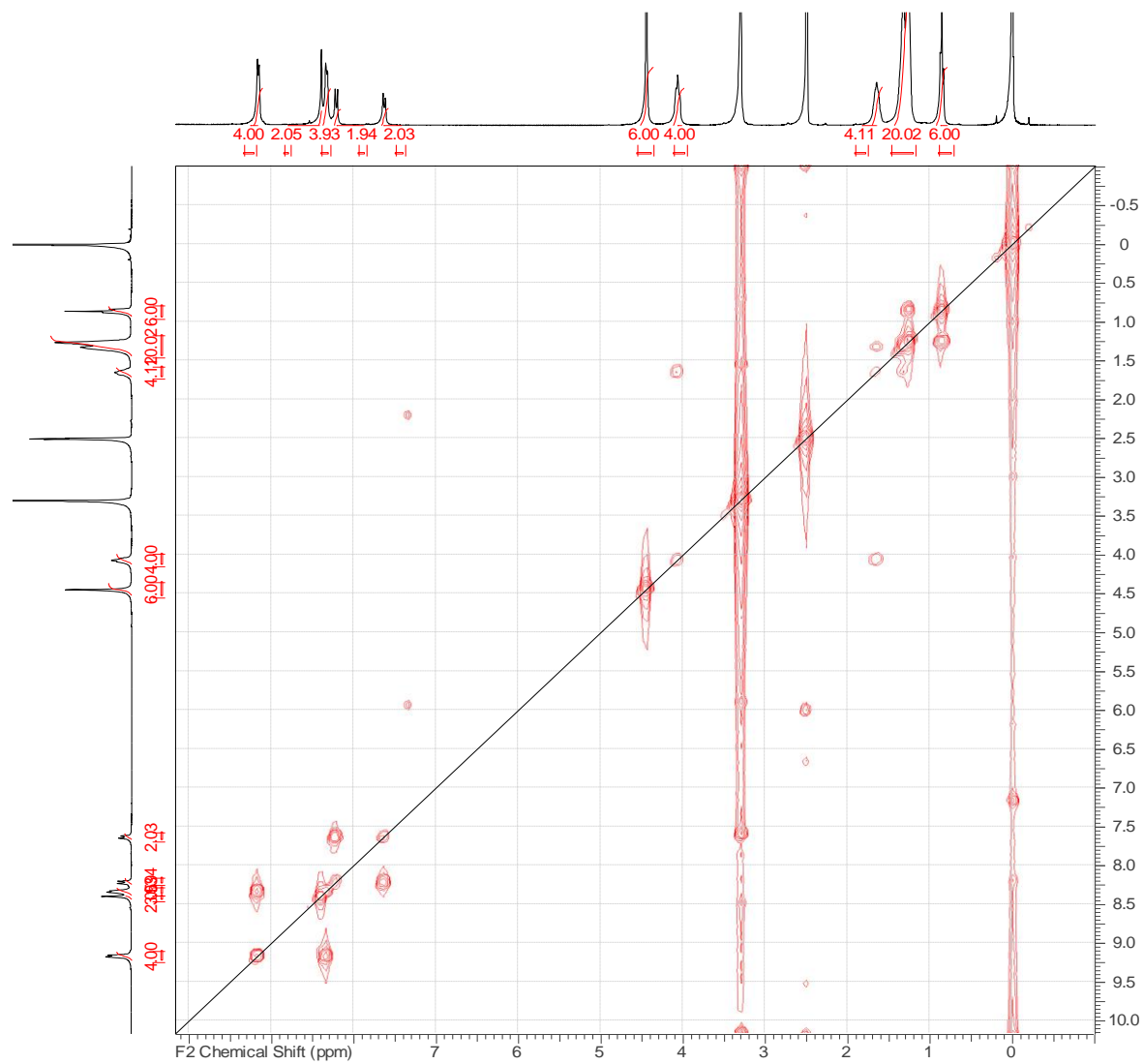


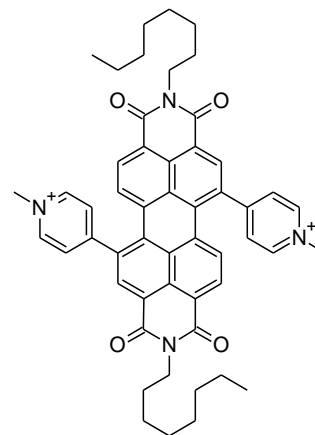
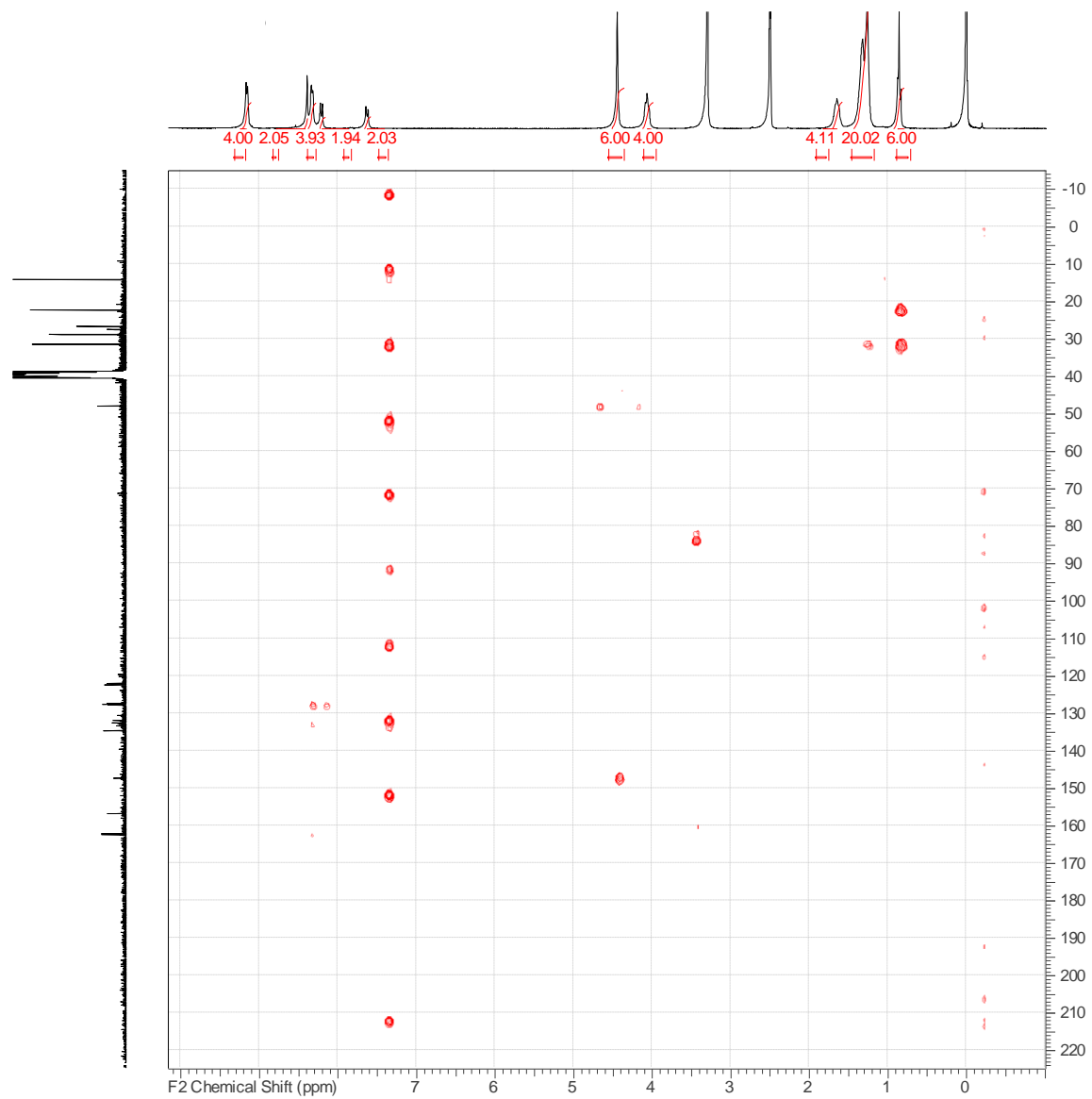
¹H NMR spectrum of compound 23



^{13}C NMR Spectrum of compound 23

COSY spectrum of compound 23



gHSBC spectrum of compound 23

I

**CONTROLLED REGIOSELECTIVE AMINATION OF PERYLENE-
IMIDES**

by

Lijo George, Zafar Ahmed, Helge Lemmetyinen, and Alexander Efimov
Eur. J. Org. Chem. 2015, 584–590
Reproduced with kind permission from WILEY.

Controlled Regioselective Amination of Peryleneimides

Lijo George,^[a] Zafar Ahmed,^[a] Helge Lemmetyinen,^[a] and Alexander Efimov*^[a]

Keywords: Amination / Perylenes / Polycycles / Regioselectivity / Radical anions / Imides

Perylenediimides (PDIs) and perylenemonoimide diesters (PMIs) can be selectively substituted at the 1,6- or 7,12- positions of the bay region, respectively, by direct amination reactions. The reactions proceed by the formation of a perylene radical anion and its subsequent oxidation, and the yields range from 20–97%. The amination can be tuned to obtain

either mono- or disubstituted perylenes by varying the oxidants involved. The presence of the imide cycle is crucial for the transformation, although the amination occurs regioselectively at the bay-region positions distant from the imide cycle.

Introduction

Since their discovery, perylenetetracarboxylic diimides (PDIs) have attracted the interest of industry and academia. Good thermal and photostability, high fluorescence quantum yields, high molar absorption, and excellent redox properties are a few characteristics that have inspired chemists to focus their attention on these versatile organic molecules.^[1,2] PDIs have been utilized extensively in a variety of high-tech applications such as photovoltaics,^[3] field-effect transistors,^[4] biosensors,^[5] organic solar cells,^[3b] organic light-emitting diodes,^[6] optical switches,^[7] and molecular wires.^[8] PDIs have also been used in several other applications, such as artificial photosynthetic systems,^[9] with controlled supramolecular architectures through their high tendency for π - π stacking.^[10] Similarly, perylenemonoimides (PMIs) are useful precursors for asymmetric perylene dyes. Their syntheses from commercially available perylene-3,4,9,10-tetracarboxylic dianhydride (PTCDA) as well as their halogenation and substitution have been described.^[11] PMI dyes had been used in molecular photonic switches and light-harvesting studies.^[12] The major hurdle in the use of perylenemonoimide dyes had been their poor solubility in organic solvents. Various approaches such as the introduction of alkylated *N*-aryl groups or aryloxy substituents at the perimeter of perylene have been used to improve solubility.^[11c] The solubility of PMI dyes can be increased dramatically by the introduction of a diester moiety to the perimeter of the molecule.^[13] The incorporation of a diester moiety not only resolves the solubility issue but also makes the dyes more versatile. For example, the diester

moiety can later be hydrolyzed through an acidic hydrolysis to form a second anhydride group,^[14] which can be used to prepare new asymmetric PDIs with two different *N*-substituted groups.^[11c] The diester groups can also be hydrolyzed to dicarboxylic acids, which can in turn be used to prepare self-assembled monolayers (SAMs) for organic solar cells.

Similarly, despite the established significance and potential of PTCDA, a lack of solubility in organic solvents has kept its usage somewhat restricted. In a BASF patent (1997), Böhm et al. reported a procedure for the 1,7-dibromination, imidation, and subsequent replacement of “bay-region” bromine atoms with alkyne or phenoxy groups.^[15] This method was extensively used in many labs to synthesize bay-functionalized PDIs until 2004 when Wuerthner et al. pointed out the presence of a regioisomeric impurity, namely, the 1,6-isomer, in ca. 20–25%.^[16] Later, many research groups isolated and characterized 1,6- and 1,7-regioisomers of dipiperidinyl-, diphenoxy-, and dipyrrolidinyl-substituted PDIs^[17a,17b] and demonstrated that the 1,6- and 1,7-isomers might have significantly different photochemical properties.^[17c–17f]

Much effort has been paid to the isolation of individual isomers, mostly 1,7-substituted, but no approaches to the synthesis of isomerically pure PDIs were proposed.^[18a–18j] Furthermore, as there was no method to synthesize preferentially the 1,6-isomers of peryleneimides, the knowledge of their properties and potential applications was poor. This situation changed dramatically in 2013 when the direct amination of PDIs was reported.^[19a] Very recently, Rauch et al. reported the synthesis of a regioisomerically pure 1,6-isomer by a Cu-catalyzed amination.^[19b] However, these two reports are somewhat controversial in terms of their reaction mechanisms and product structures.

Herein, we report the controlled highly regioselective amination of perylene mono- and diimides; isomerically pure 7-pyrrolidinyl and 1,6-dipyrrolidinyl derivatives are synthesized, and the substitution reaction can either be cat-

[a] Department of Chemistry and Bioengineering, Tampere University of Technology, Tampere, Finland
E-mail: alexandre.efimov@tut.fi
www.tut.fi/keb

Supporting information for this article is available on the WWW under <http://dx.doi.org/10.1002/ejoc.201403299>.

alyzed by metal complexes or run catalyst-free. Depending on the substrates and the desired product (mono- or disubstituted), the reaction can be performed either at room temperature with KMnO_4 or atmospheric oxygen as an in situ oxidant or as a one-pot, two-step process with subsequent oxidation by pyridinium dichromate (PDC). In either case, the method is highly attractive as it does not require any halogen (or other) leaving group for the substitution to occur, and the reaction conditions are mild. Unlike the previously reported work, in our case, the substitution occurs at the bay region instead of the 2,5-positions of perylene^[19a] and can also proceed without catalyst.^[19b]

Results and Discussion

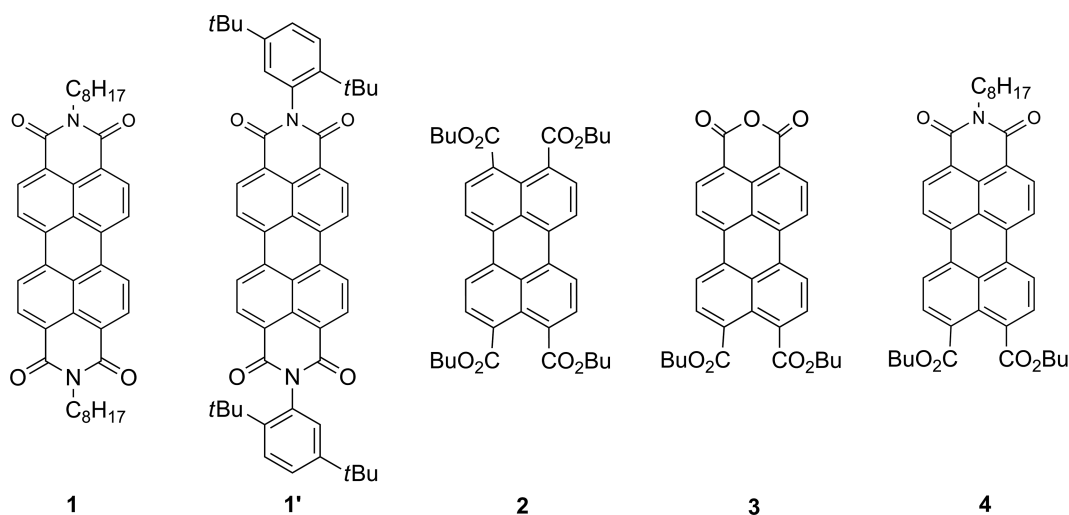
Synthesis of Precursors

The precursors **1**, **1'**, and **4** were synthesized from commercially available PTCDA by slight modification of procedures reported previously.^[18g,20] The treatment of PTCDA with imidazole and the desired amine at elevated temperature yielded the *N*-alkylated PDIs **1** and **1'** in good yields. The perylene tetraester (PTE) **2** was obtained by esterification of PTCDA with an alkanol and alkyl halide in a homogeneous solution.^[18g] The PTE was then selectively hydrolyzed by *p*-toluenesulfonic acid (*p*TsOH) to yield the monoanhydride–diester **3** as a precipitate, which upon imidization with *n*-octylamine and imidazole produced the PMI diester **4** as a dark red solid in 68% yield.^[18g,20] The crucial step in the synthesis of **4** was the selective hydrolysis with *p*TsOH, as even a slight excess of *p*TsOH, the wrong reaction temperature, or an inappropriate solvent resulted in the formation of PTCDA. A mixture of toluene and hexane (5:1 v/v), 1.2 equiv. of *p*TsOH, and a reaction temperature of 100 °C were the optimal conditions, which prevented the second hydrolysis.

Amination of PDIs

While studying different substitution reactions, we noticed that a solution of dioctyl PDI **1** in neat pyrrolidine under argon slowly turned from red to blue upon heating. After the vial was opened and the solution was exposed to air, the color changed rapidly from blue to reddish, and green monopyrrolidine PDI **5a** was recovered from the reaction mixture along with the starting material **1**. Our attempts to isolate “the blue intermediate” for NMR spectroscopy analysis were unsuccessful, as the compound proved to be very air sensitive. However, in situ detection by UV/Vis spectroscopy was possible. A small amount of PDI in thoroughly argon-purged pyrrolidine was heated at 60 °C in a sealed cuvette, and the gradual changes in the absorption spectra were recorded. As can be seen in Figure 1, the two peaks of PDI **1** at $\lambda = 450$ and 550 nm decreased with time and were completely gone after 5 h. Instead, the newly formed compound had distinct absorption maxima at $\lambda = 720$ and 800 nm. A very similar absorption profile was reported for the chemically and electrochemically generated perylenediimide radical anion by different groups.^[21a–21d] After exposure of the solution to air, the bands at $\lambda = 720$ and 800 nm disappeared, the bands at $\lambda = 450$ and 550 nm were partly restored, and a broad absorbance of monopyrrolidyl PDI **5a** appeared in the spectrum. This observation allowed us to suggest that the reaction proceeds by a radical anion pathway with separate stages for the formation of the intermediate and its oxidation to the final product.

To the best of our knowledge, the direct amination of an unsubstituted aromatic core is not very common in organic chemistry. Similar reactions on smaller aromatic rings are described as “oxidative amination” and have received limited attention.^[22a,22b] In the work of Verbeek et al.,^[22a] the amination is thought to proceed by a two-step mechanism: σ^{H} -adduct formation followed by an oxidative rearomatization. For the direct aminations of perylenes at



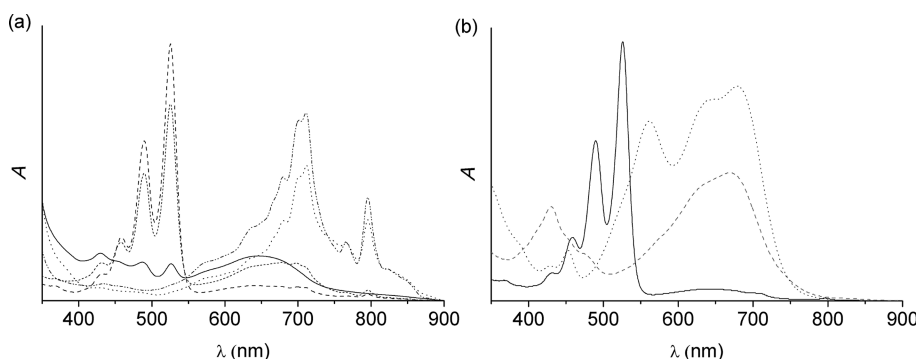
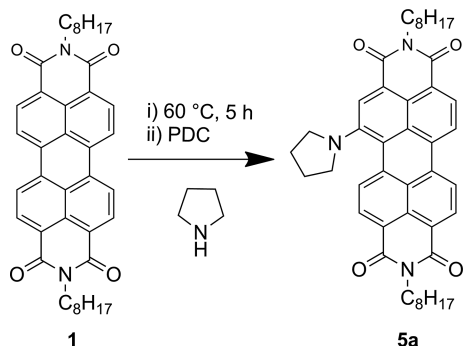


Figure 1. (a) Absorption profile for radical anion formation and oxidation of diocetyl PDI **1** in pyrrolidine. (black dashes: 0 h, short dark gray dashes: 1 h, dark gray dash dot dot: 5 h, black dots: 48 h, black solid line: vial opened). (b) Absorption of unsubstituted **1** (black solid line), monopyrrolidyl **5a** (gray dashes), and dipyrrolidyl **5b** (dark gray dots) diocetyl PDIs.

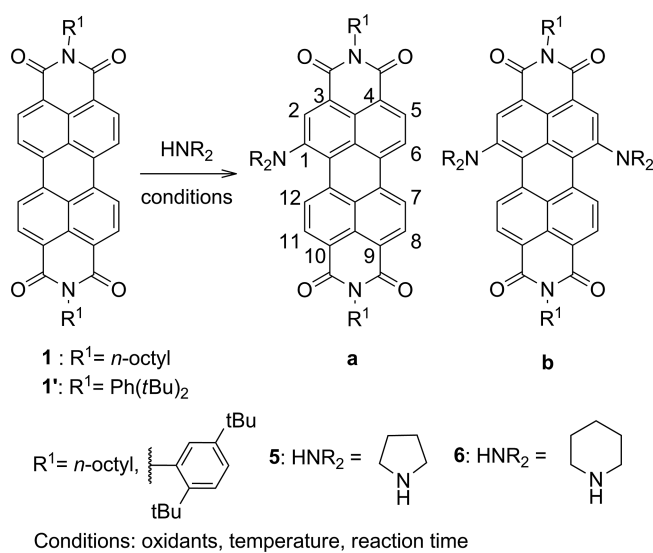
the bay region reported by Langhals and Rauch, two different reaction mechanisms have been proposed, namely, a Chichibabin-like^[19a] reaction resulting in a perisubstitution of PDI or a Cu-catalyzed radical cycle, which produces bay-substituted derivatives.^[19b]

First, we decided to test the catalyst-free reaction (Scheme 1) by preparation of an intermediate under an inert atmosphere and subsequent oxidation. PDI **1** was heated in pyrrolidine under an inert atmosphere for 5 h at 60 °C, and a subsequent oxidation with pyridinium dichromate (PDC) gave 20–70% yield of **5a**. The formation of product **5a** proves that the reaction proceeds through the radical anion. However, the disubstituted compound **5b** appeared only in a trace amount in this case.



Scheme 1. Amination of diocetyl PDI **1** without catalyst.

The radical anion generated was highly sensitive to air, and as a result the yield of the reaction varied greatly. Hence, the amination of the aromatic ring of PDI **1** through in situ oxidation with various oxidizing agents was explored. To our delight, pyrrolidination of diocetyl PDI **1** with $\text{KMnO}_4/\text{AgNO}_3$ as the oxidant, as reported Verbeeck et al.,^[22] proceeded regioselectively to afford exclusively the 1,6-dipyrrolidinyl isomer **5b** in 65% yield (Scheme 2). The yield and the substitution sites are in good agreement with the results published by Rauch et al.^[19b] However, in our case, the substitution occurred without Cu^{II} catalysis and heating.



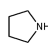
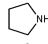
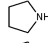
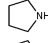
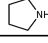
Scheme 2. Regioselective amination of PDIs.

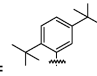
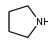
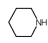
The effect of the oxidizing agent was studied next. When PDC was used as the in situ oxidant, the yield of monopyrrolidyl PDI **5a** was 41%, and a mixture of 1,6- and 1,7-dipyrrolidyl PDIs was also isolated in 25% total yield. When a combination of PDC/AgNO_3 was used for in situ oxidation, the formation of dipyrrolidyl PDI **5b** was greatly enhanced, and the yields reached 60% for the 1,6-isomer and 22% for the 1,7-isomer. The monopyrrolidyl PDI **5a** was obtained only in 15% yield in this case. However, the reaction times were as long as 6 and 4 d, respectively. Surprisingly, the use of CuCl_2 in the amination of PDI **1** with pyrrolidine yielded only a trace amount of dipyrrolidyl PDI **5b** after overnight stirring at room temperature. It should also be noted that we have compared the NMR spectra of the synthesized compounds with the spectra of those prepared by the traditional bromination–pyrrolidination method^[17a,17b] and we have not observed perisubstituted compounds, as described by Langhals.^[19a]

According to our observations, the reactivity of PDIs with different amido substituents in amination reactions,

which was also reported by Rauhe et al.,^[19b] is mostly guided by the solubility. Thus, a mixture of PDI **1** with piperidine produced only a trace amount of the product even after prolonged stirring at room or elevated temperatures owing to the poor solubility of **1** in piperidine. In contrast, the reaction of much more soluble PDI **1'** with pyrrolidine or piperidine and $\text{KMnO}_4/\text{AgNO}_3$ proceeded smoothly toward the disubstituted products **5b'** and **6b'**. A complete set of reactions with $\text{KMnO}_4/\text{AgNO}_3$ and different substrates and nucleophiles is shown in Table 1. The products were isolated by preparative TLC, and the yields are given relative to the starting materials **1** and **1'**. It should be noted that the removal of the residual PTCDA from **1** and **1'** is not an easy task owing to its poor solubility, and the apparent yields might be affected by that.

Table 1. Reactions of PDIs.

I		1 R ¹ = <i>n</i> -Octyl			
Amine	Oxidant	T [°C]	Time	a	b
1	 PDC (oxidation after radical anion generation)	60 °C	5 h	5a (20–70%)	–
2	 PDC	r.t.	6 d	5a (41%)	5b (25%) ^[a]
3	 PDC/AgNO ₃	r.t.	4 d	5a (15%)	5b (60%)
4	 KMnO ₄ /AgNO ₃	r.t.	24 h	–	5b (65%)
5	 KMnO ₄ /AgNO ₃	85 °C	24 h	trace amount ^[b]	trace amount ^[b]

II		1' R ¹ = 			
Amine	Oxidant	T [°C]	Time	a	b
1	 KMnO ₄ /AgNO ₃	r.t.	24 h	–	5b' (69%)
2	 KMnO ₄ /AgNO ₃	r.t.	24 h	–	6b' (60%)

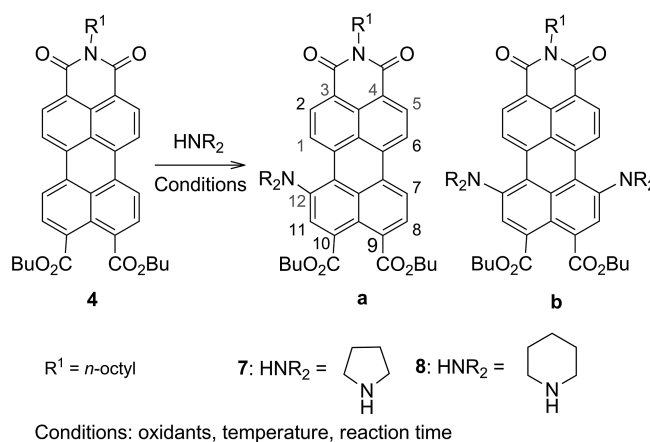
[a] Mixture of 1,6- and 1,7-dipyrrolyl PDI. [b] Observed by TLC and confirmed by MS. Mostly starting material remained in the reaction.

Amination of PMIs

We decided to screen the applicability of the reaction to other perylene derivatives. To our surprise, the presence of the imide cycle played a crucial role in the amination of perylenes. The reactions of perylenetetracarboxylic ester **2** and perylene monoanhydride diester **3**^[18a] under similar reaction condition failed to produce the desired products, and mostly unreacted starting compounds were recovered.

The most interesting results were obtained for the perylenemonoimide diester (PMI diester) **4**, as shown in Scheme 3. When **4** was subjected to pyrrolidination, the reaction produced a mixture of mono- and dipyrrolidinated products in 60 and 20% yield, respectively. However, most surprisingly, the substitution occurred exclusively at the bay 7- and 12-positions of the aromatic ring, which are distant from the imide cycle. This conclusion was unambiguously derived from the NMR spectroscopic data. The gradient

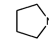
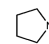
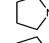
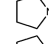

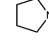
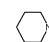
HMBC (gHMBC) spectra of **7a** and **7b** (see Supporting Information, S24 and S28) show that the singlets of protons 8-H and 11-H at $\delta = 7.82$ ppm (disubstituted compound **7b**) and 8-H at 8.0 ppm (compound **7a**) correlate to the C-9' and C-10' carbonyl carbon atoms at $\delta = 169$ and 168 ppm, respectively. The latter two were identified by their cross-peaks with the α -butoxy protons at $\delta = 4.33$ ppm. Simultaneously, the doublet of 2-H and 5-H correlates to the carbonyl atoms of the imide cycle, which were in turn identified by their cross-peaks with the α -amido methylene group of the octyl tail.



Scheme 3. Regioselective amination of PMI diester.

The described reaction is truly unique as it offers regio-directed substitution of perylene derivatives. The amination of PMI diester **4** with piperidine as a nucleophile works similarly and results in the formation of the mono- and disubstituted PMI diester derivatives **8a** and **8b** in 64 and 31% yield, respectively. The regiospecificity of the substitution was also preserved in this case, as confirmed by NMR spectroscopy analysis. The reaction of PMI diester **4** was screened under different conditions and with different oxidants, and the results are summarized in Table 2. Unlike the

Table 2. PMI reactions and yield.

I		1 R ¹ = <i>n</i> -Octyl			
Amine	Oxidant	T [°C]	Time	a	b
1	 CuCl ₂	r.t.	1 h	7a (96%)	7b (2%)
2	 CuCl ₂	r.t.	24 h	7a (31%)	7b (47%)
3	 KMnO ₄	r.t.	24 h	7a ^[a]	7b ^[a]
4	 PDC/AgNO ₃	r.t.	3 d	7a (97%)	–
5	 KMnO ₄ /AgNO ₃	r.t.	24 h	7a (60%)	7b (20%)
1	 KMnO ₄ /AgNO ₃	r.t.	24 h	7a (60%)	7b (42%)
2	 KMnO ₄ /AgNO ₃	r.t.	24 h	8a (60%)	8b (31%)

[a] The major spot was identified as **7a** by TLC. A trace amount of **7b** also formed.

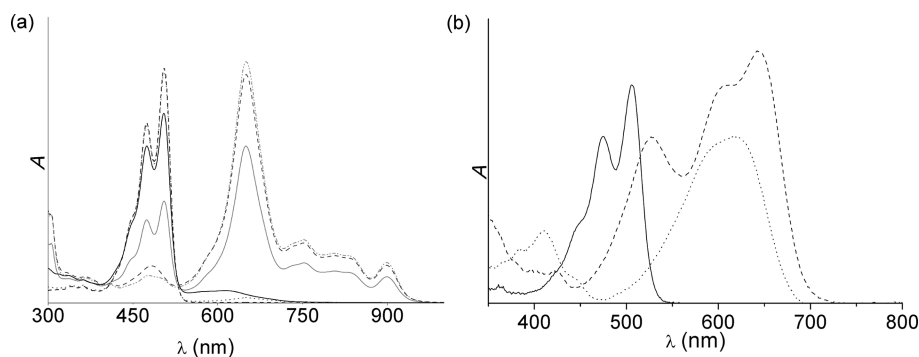


Figure 2. (a) Absorption profile for the progress of reaction of PMI diester **4** in pyrrolidine under an argon atmosphere (black dashes: 0 h, dark gray dots: 4 h, gray solid line: 20 h, gray dash dot dot: 21 h, dark gray dashes: 23 h, black solid line: vial opened). (b) Absorption of unsubstituted **4** (solid black), monopyrrolidyl **7a** (dot black), and dipyrroliidyl **7b** (dash black) PMI diesters.

reaction with the PDI, this reaction proceeds much faster in the presence of CuCl_2 . Under copper catalysis, the reaction can either be stopped at a monosubstitution step or pushed further to the disubstituted product simply by controlling the reaction time. On the other hand, in the presence of PDC and AgNO_3 under argon, the reaction also led to the monosubstituted product **7a** in good yield and gave practically no disubstitution.

The absorption spectra for the reaction of PMI diester **4** and pyrrolidine under argon and the absorption spectra of the products after the exposure of the reaction mixture to ambient air are shown in Figure 2. The spectrum of the intermediate is similar to that observed for the diimide radical anion intermediate (Figure 1) and shows a distinct absorption in the near-IR region. Therefore, we suggest that the reaction also proceeds via a radical anion intermediate. The process does not necessarily require a catalyst, at least to obtain monosubstituted compounds (Table 2, Entry 3). However, the catalyst is needed for the preparation of disubstituted molecules in reasonable yields. The Cu-catalyzed reaction did not show the anion radical species by UV/Vis spectroscopy, most probably because of their fast oxidation upon formation.^[19b] Silver nitrate alone may also serve as a catalyst for the amination. The results of the amination of PMI diester **4** are shown in Table 2.

Conclusions

We have found that the direct amination of peryleneimides proceeds as a stepwise substitution via a perylene radical anion and its subsequent oxidation. The substitution predominantly occurs regioselectively at the 1,6- and 7,12-positions of the bay region for perylenediimide and perylenemonoimide diester, respectively. The imide cycle directs the substitution to the distant position of the bay region; however, the presence of the imide is essential for the reaction to occur. The substitution occurs as a one-pot reaction with yields of 20–97% and can be controlled to produce selected products (mono or disubstituted perylenes) by variation of the oxidant.

Experimental Section

General: All commercially available reagents and solvents were purchased either from Sigma–Aldrich or from VWR and used without further purifications unless otherwise mentioned. The products were purified either by column chromatography with silica gel 60 (Merck) mesh size 40–63 μm or by preparative TLC with neutral aluminium oxide 60 F₂₅₄ plates (Merck). The NMR spectra were recorded with a Varian Mercury 300 MHz spectrometer with tetramethylsilane (TMS) as the internal standard. HRMS measurements were performed with a Waters LCT Premier XE ESI-TOF bench-top mass spectrometer. Lock-mass correction (leucine enkephalin as reference compound), centering, and calibration were applied to the raw data to obtain accurate masses.

General Procedure for the Direct Amination of Peryleneimides: Silver nitrate (1–10 equiv.) was added to a stirred solution of peryleneimide (1 equiv.) in the amine (1.5–5 mL), and the mixture was stirred for 10 min. Powdered KMnO_4 (1–10 equiv.) was added to this reaction mixture in portions over a period of 30 min, and stirring was continued for another 16 h. On completion, the reaction mixture was concentrated under reduced pressure, and the residue was dissolved in chloroform (20 mL). The organic phase was washed with water (2×50 mL) and dried with Na_2SO_4 , and the solvents were evaporated. The crude product was purified by TLC (neutral aluminum oxide 60 F₂₅₄ TLC plates with dichloromethane as eluent) to yield the pure compound.

2,9-Dioctylisoquinolino[4',5',6':6,5,10]anthra[2,1,9-def]isoquinoline-1,3,8,10(2H,9H)-tetrone (1) and 2,9-Bis(2,5-di-tert-butylphenyl)-isoquinolino[4',5',6':6,5,10]anthra[2,1,9-def]isoquinoline-1,3,8,10(2H,9H)-tetrone (1'): Compounds **1** and **1'** were prepared from perylenetetracarboxylic anhydride (PTCDA) according to the literature procedure described by Langhals.^[20]

Tetrabutyl Perylene-3,4,9,10-tetracarboxylate (2) and Dibutyl 1,3-Dioxo-1H,3H-benzo[5,10]anthra[2,1,9-def]isochromene-8,9-dicarboxylate (3): These compounds were prepared from perylenetetracarboxylic anhydride (PTCDA) according to the procedure described by Wang et al.^[18g]

Dibutyl 2-Octyl-1,3-dioxo-2,3-dihydro-1H-benzo[5,10]anthra[2,1,9-def]isoquinoline-8,9-dicarboxylate (4): A mixture of **3** (0.193 mmol, 101 mg), imidazole (1.0 g), and *n*-octylamine (1.15 mmol, 191 μL) was stirred at 140 °C for 4 h. On completion, the reaction mixture was cooled to 60 °C, and ethanol (5 mL) was added. The mixture was neutralized by the dropwise addition of HCl (2 M) and extracted with toluene (three times). The organic phase was washed

with water (twice), dried with Na₂SO₄, and concentrated. The crude product was purified through silica gel with dichloromethane as the eluent to yield **4** (83 mg, 68%) as a dark red solid. ¹H NMR (300 MHz, CDCl₃, TMS): δ = 8.36–8.39 (d, *J* = 7.92 Hz, 2 H), 8.13 (t, *J* = 8.50 Hz, 4 H), 7.95–7.97 (d, *J* = 7.92 Hz, 2 H), 4.36 (t, *J* = 6.74 Hz, 4 H), 4.16 (t, *J* = 7.62 Hz, 2 H), 1.67–1.94 (m, 6 H), 1.20–1.64 (m, 15 H), 1.02 (t, *J* = 7.33 Hz, 6 H), 0.88 (s, 3 H) ppm. ¹³C NMR (75 MHz, CDCl₃, TMS): δ = 168.44, 163.58, 135.24, 132.04, 132.00, 131.27, 130.39, 129.24, 129.03, 128.99, 122.59, 125.83, 122.16, 121.77, 65.81, 56.56, 40.80, 32.08, 30.86, 29.60, 29.51, 28.37, 27.45, 22.89, 19.51, 14.36, 14.06, 9.60, 0.23 ppm. HRMS (ESI-TOF): calcd. for C₄₀H₄₃NO₆ [M]⁺ 633.3085; found 633.3068.

2,9-Dioctyl-5-(pyrrolidin-1-yl)isoquinolino[4',5',6':6,5,10]anthra[2,1,9-def]isoquinoline-1,3,8,10(2H,9H)-tetrone (5a): Pyrrolidine (20 mL) was bubbled with argon for 5 min, and **1** (0.0138 mmol, 8.5 mg) was added. The resultant mixture was again purged with argon for 1 min and heated at 60 °C for 5 h. A pyridinium dichromate solution (0.138 mmol, 5.3 mg dissolved in pyrrolidine and purged with argon for 5 min) was added to the reaction mixture, which was then stirred for 5 min. The reaction was quenched with water (20 mL), extracted with chloroform (three times), dried with Na₂SO₄, and concentrated. The crude product was purified by TLC (neutral aluminum oxide 60 F₂₅₄ TLC plates with dichloromethane as eluent) to yield **5a** as a green solid (7.2 mg, 70%). ¹H NMR (300 MHz, CDCl₃, TMS): δ = 8.57–8.64 (m, 2 H), 8.29–8.49 (m, 4 H), 7.39–7.57 (m, 1 H), 4.09–4.31 (m, 4 H), 3.58–3.83 (m, 2 H), 2.74 (br s, 2 H), 1.88–2.23 (m, 4 H), 1.65–1.86 (m, 4 H), 1.23–1.52 (m, 21 H), 0.88 (t, *J* = 6.74 Hz, 6 H) ppm. ¹³C NMR (75 MHz, CDCl₃, TMS): δ = 163.87, 163.81, 163.71, 163.65, 148.40, 135.42, 135.18, 132.59, 130.95, 130.68, 128.93, 128.59, 127.11, 124.19, 126.56, 123.68, 122.98, 122.56, 122.33, 121.62, 120.41, 118.96, 115.83, 52.42, 40.67, 40.58, 31.86, 31.85, 29.42, 29.37, 29.28, 29.25, 28.18, 27.24, 27.18, 25.78, 22.66, 14.12 ppm. HRMS (ESI-TOF): calcd. for C₄₄H₄₉N₃O₄ [M]⁺ 683.3718; found 683.3740.

2,9-Dioctyl-5,13-di(pyrrolidin-1-yl)isoquinolino[4',5',6':6,5,10]anthra[2,1,9-def]isoquinoline-1,3,8,10(2H,9H)-tetrone (5b): The compound was prepared by following the general procedure for the direct amination of peryleneimides. Compound **1** (0.0325 mmol, 20 mg) was stirred with silver nitrate (0.0516 mmol, 8.7 mg) in pyrrolidine (5 mL). Powdered KMnO₄ (0.0516 mmol, 8.2 mg) was added to the reaction mixture, which was then stirred for 24 h to afford **5b** (65%, 15.8 mg) as a dark blue solid. ¹H NMR (300 MHz, CDCl₃, TMS): δ = 8.68 (d, *J* = 7.92 Hz, 2 H), 8.34 (s, 2 H), 7.86 (d, *J* = 8.21 Hz, 2 H), 4.13–4.36 (m, 4 H), 3.56–3.91 (m, 4 H), 2.77 (br s, 3 H), 1.87–2.23 (m, 8 H), 1.67–1.86 (m, 4 H), 1.13–1.53 (m, 30 H), 0.87 (t, *J* = 6.74 Hz, 9 H) ppm. ¹³C NMR (75 MHz, CDCl₃, TMS): δ = 164.65, 164.35, 150.24, 135.94, 131.28, 130.45, 128.73, 128.47, 123.52, 123.11, 117.99, 117.80, 117.19, 117.10, 52.40, 40.87, 40.69, 32.09, 32.06, 29.93, 29.68, 29.59, 29.49, 29.46, 28.49, 28.44, 27.49, 27.38, 25.90, 22.89, 14.34 ppm. HRMS (ESI-TOF): calcd. for C₄₈H₅₆N₄O₄ [M]⁺ 752.4296; found 752.4291.

2,9-Bis(2,5-di-tert-butylphenyl)-5,13-di(pyrrolidin-1-yl)isoquinolino[4',5',6':6,5,10]anthra[2,1,9-def]isoquinoline-1,3,8,10(2H,9H)-tetrone (5b'): The general procedure for the direct amination was followed by stirring **1'** (0.026 mmol, 20 mg), AgNO₃ (0.26 mmol, 44 mg), and powdered KMnO₄ (0.26 mmol, 41 mg) in pyrrolidine (3 mL) for 24 h at room temperature to give **5b'** (69%, 16.3 mg) as a dark blue solid. ¹H NMR (300 MHz, CDCl₃, TMS): δ = 8.76 (d, *J* = 8.21 Hz, 2 H), 8.41 (s, 2 H), 7.92 (dd, *J* = 8.21 Hz, 2 H), 7.63–7.59 (m, 2 H), 7.49–7.44 (m, 2 H), 7.03–7.00 (m, 2 H), 3.77 (br, 3 H), 2.86 (br, 3 H), 2.05 (br, 8 H), 1.36–1.33 (m, 36 H) ppm. ¹³C NMR (75 MHz, CDCl₃, TMS): δ = 165.38, 165.17, 150.08, 150.03,

150.01, 149.95, 143.88, 143.86, 136.05, 136.03, 133.59, 133.56, 132.96, 132.93, 131.45, 130.93, 130.67, 128.87, 128.83, 128.73, 128.68, 127.79, 127.67, 126.19, 126.01, 123.34, 123.24, 118.08, 117.93, 117.36, 117.12, 52.21, 35.58, 35.56, 34.23, 31.86, 31.83, 31.25, 31.23, 29.69, 25.72 ppm. HRMS (ESI-TOF): calcd. for C₆₀H₆₄N₄O₄ [M]⁺ 904.4922; found 904.4949.

2,9-Bis(2,5-di-tert-butylphenyl)-5,13-di(piperidin-1-yl)isoquinolino[4',5',6':6,5,10]anthra[2,1,9-def]isoquinoline-1,3,8,10(2H,9H)-tetrone (6b'): The general procedure for the direct amination was followed by stirring **1'** (0.013 mmol, 10 mg), AgNO₃ (0.13 mmol, 22 mg), and powdered KMnO₄ (0.13 mmol, 21 mg) in piperidine (1.5 mL) for 24 h at room temperature to give **6b'** (60%, 7.3 mg) as a dark blue solid. ¹H NMR (300 MHz, CDCl₃, TMS): δ = 9.81 (d, *J* = 8.50 Hz, 2 H), 8.68 (d, *J* = 8.50 Hz, 2 H), 8.46 (s, 2 H), 7.62–7.59 (m, 2 H), 7.49–7.44 (m, 2 H), 7.02–6.98 (m, 2 H), 3.48–3.38 (m, 4 H), 2.98–2.87 (m, 4 H), 1.92–1.74 (m, 12 H), 1.35–1.32 (m, 36 H) ppm. ¹³C NMR (75 MHz, CDCl₃, TMS): δ = 164.80, 164.69, 153.45, 150.09, 150.01, 143.91, 143.82, 136.42, 136.39, 133.21, 132.74, 132.09, 131.17, 129.35, 128.77, 128.72, 128.30, 127.74, 127.58, 126.26, 126.15, 123.87, 123.57, 123.46, 122.86, 121.16, 120.58, 53.20, 53.08, 35.56, 34.25, 33.70, 31.93, 31.83, 31.25, 31.23, 30.16, 29.71, 29.37, 26.70, 25.87, 23.77, 22.70 ppm. HRMS (ESI-TOF): calcd. for C₆₂H₆₈N₄O₄ [M]⁺ 932.5235; found 932.5287.

Dibutyl 2-Octyl-1,3-dioxo-6-(pyrrolidin-1-yl)-2,3-dihydro-1H-benzo[5,10]anthra[2,1,9-def]isoquinoline-8,9-dicarboxylate (7a) and Dibutyl 2-Octyl-1,3-dioxo-6,11-di(pyrrolidin-1-yl)-2,3-dihydro-1H-benzo[5,10]anthra[2,1,9-def]isoquinoline-8,9-dicarboxylate (7b): The general procedure for the direct amination was followed by stirring **4** (0.0946 mmol, 60 mg), AgNO₃ (0.945 mmol, 160 mg), and powdered KMnO₄ (0.945 mmol, 150 mg) in pyrrolidine (1.5 mL) for 24 h at room temperature to give **7a** (40 mg, 60%) and **7b** (14.2 mg, 20%) as dark solids.

Data for 7a: ¹H NMR (300 MHz, CDCl₃, TMS): δ = 8.68–8.49 (m, 2 H), 8.46–8.27 (m, 2 H), 8.00 (s, 1 H), 7.95 (d, *J* = 8.05 Hz, 1 H), 7.15 (d, *J* = 8.05 Hz, 1 H), 4.44–4.29 (m, 4 H), 4.26–4.16 (m, 2 H), 3.83–3.67 (m, 2 H), 3.67–3.61 (m, 2 H), 2.87–2.65 (m, 2 H), 2.18–2.00 (m, 2 H), 2.00–1.88 (m, 2 H), 1.87–1.69 (m, 6 H), 1.60–1.39 (m, 8 H), 1.39–1.21 (m, 10 H), 1.02 (t, *J* = 7.24 Hz, 3 H), 0.98 (t, *J* = 7.24 Hz, 3 H), 0.91–0.84 (m, 3 H) ppm. ¹³C NMR (75 MHz, CDCl₃, TMS): δ = 169.07, 168.10, 164.29, 164.16, 147.91, 136.52, 131.43, 131.26, 131.15, 131.02, 130.46, 129.26, 127.03, 126.17, 123.47, 122.69, 121.96, 120.73, 119.60, 117.58, 111.76, 70.77, 65.72, 65.66, 52.73, 40.68, 32.09, 30.92, 30.82, 29.92, 29.66, 29.50, 28.43, 27.48, 25.93, 22.89, 19.50, 19.48, 14.34, 14.06, 14.04 ppm. HRMS (ESI-TOF): calcd. for C₄₄H₅₀N₂O₆ [M]⁺ 702.3663; found 702.3704.

Data for 7b: ¹H NMR (300 MHz, CDCl₃, TMS): δ = 8.65 (t, *J* = 7.92 Hz, 2 H), 7.83 (s, 2 H), 7.51 (t, *J* = 7.92 Hz, 2 H), 4.33 (t, *J* = 7.04 Hz, 4 H), 4.24 (t, *J* = 7.33 Hz, 2 H), 3.90–3.50 (m, 4 H), 3.02–2.52 (m, 4 H), 1.84–1.71 (m, 6 H), 1.55–1.40 (m, 8 H), 0.99 (t, *J* = 7.33 Hz, 6 H), 0.93–0.79 (m, 3 H) ppm. ¹³C NMR (75 MHz, CDCl₃, TMS): δ = 168.65, 164.57, 149.95, 136.62, 132.95, 131.30, 130.34, 128.61, 128.46, 122.89, 116.45, 116.34, 115.89, 112.60, 65.63, 52.61, 40.61, 32.11, 30.88, 29.93, 29.70, 29.51, 28.52, 27.51, 25.97, 22.89, 19.49, 14.35, 14.07 ppm. HRMS (ESI-TOF): calcd. for C₄₈H₅₇N₃O₆ [M]⁺ 771.4242; found 771.4203.

Dibutyl 2-Octyl-1,3-dioxo-6-(piperidin-1-yl)-2,3-dihydro-1H-benzo[5,10]anthra[2,1,9-def]isoquinoline-8,9-dicarboxylate (8a) and Dibutyl 2-Octyl-1,3-dioxo-6,11-di(piperidin-1-yl)-2,3-dihydro-1H-benzo[5,10]anthra[2,1,9-def]isoquinoline-8,9-dicarboxylate (8b): The general procedure for the direct amination was followed by stirring **4** (0.032 mmol, 20.5 mg), AgNO₃ (0.32 mmol, 53 mg), and powdered KMnO₄ (0.32 mmol, 50 mg) in piperidine (3 mL) for 24 h at

room temperature to give **8a** (15 mg, 64%) and **8b** (8 mg, 31%) as dark solids.

Data for 8a: ^1H NMR (300 MHz, CDCl_3 , TMS): δ = 9.29 (d, J = 8.21 Hz, 2 H), 8.54–8.46 (m, 2 H), 8.29 (d, J = 7.92 Hz, 2 H), 8.00 (s, 1 H), 7.94 (d, J = 7.92 Hz, 1 H), 4.38–4.31 (m, 4 H), 4.22 (t, J = 7.33 Hz, 2 H), 3.41–3.37 (m, 2 H), 2.97–2.89 (m, 2 H), 1.85–1.71 (m, 11 H), 1.57–1.25 (m, 20 H), 1.03–0.07 (m, 6 H), 0.90–0.85 (m, 3 H) ppm. ^{13}C NMR (75 MHz, CDCl_3 , TMS): δ = 168.91, 168.32, 164.16, 163.83, 151.31, 137.11, 136.16, 131.90, 131.74, 131.71, 131.57, 131.53, 131.17, 129.26, 129.06, 127.71, 126.89, 124.44, 124.27, 123.53, 123.17, 121.39, 120.51, 119.82, 118.4, 65.75, 65.68, 52.80, 40.70, 32.08, 30.90, 30.80, 29.93, 29.63, 29.48, 28.42, 27.45, 25.93, 24.08, 22.88, 19.49, 14.33, 14.05 ppm. HRMS (ESI-TOF): calcd. for $\text{C}_{45}\text{H}_{52}\text{N}_2\text{O}_6\text{Na}$ [$\text{M} + \text{Na}$] $^+$ 739.3718; found 739.3747.

Data for 8b: ^1H NMR (300 MHz, CDCl_3 , TMS): δ = 9.39 (d, J = 8.21 Hz, 2 H), 8.58 (d, J = 8.21 Hz, 2 H), 7.85 (s, 2 H), 4.34 (t, J = 7.04 Hz, 4 H), 4.23 (t, J = 7.62 Hz, 2 H), 3.35–3.31 (m, 4 H), 2.90–2.82 (m, 4 H), 1.82–1.72 (m, 16 H), 1.51–1.43 (m, 7 H), 1.28–1.25 (m, 15 H), 1.01 (t, J = 7.33 Hz, 6 H), 0.90–0.85 (m, 4 H) ppm. ^{13}C NMR (75 MHz, CDCl_3 , TMS): δ = 168.66, 164.15, 152.31, 137.36, 134.14, 131.66, 131.02, 129.02, 128.2, 123.12, 121.22, 119.77, 119.4, 119.06, 65.66, 53.06, 40.63, 32.09, 30.82, 29.92, 29.65, 29.48, 28.47, 27.48, 25.99, 24.16, 22.88, 19.47, 14.33, 14.03 ppm. HRMS (ESI-TOF): calcd. for $\text{C}_{50}\text{H}_{61}\text{N}_3\text{O}_6$ [M] $^+$ 799.4555; found 799.4553.

Supporting Information (see footnote on the first page of this article): NMR spectra of all the compounds synthesized for the current work.

Acknowledgments

The authors gratefully acknowledge the financial support from the Academy of Finland.

- [1] a) C. Huang, S. Barlow, S. R. Marder, *J. Org. Chem.* **2011**, *76*, 2386–2407, and references cited therein; b) A. Ajayaghosh, S. J. George, A. P. H. Schenning, *Top. Curr. Chem.* **2005**, *258*, 83–118; c) F. Wuerthner, *Chem. Commun.* **2004**, 1564–1579, and references cited therein; d) B. A. Jones, M. J. Ahrens, M. H. Yoon, A. Facchetti, T. J. Marks, M. R. Wasielewski, *Angew. Chem. Int. Ed.* **2004**, *43*, 6363–6366; *Angew. Chem.* **2004**, *116*, 6523; e) C. D. Dimitrakopoulos, P. R. L. Malenfant, *Adv. Mater.* **2002**, *14*, 99–177.
- [2] M. R. Wasielewski, *J. Org. Chem.* **2006**, *71*, 5051.
- [3] a) C. W. Tang, *Appl. Phys. Lett.* **1986**, *48*, 183–185; b) L. Schmidt-Mende, A. Fechtenkotter, K. Mullen, E. Moons, R. Friend, J. Mackenzie, *Science* **2001**, *293*, 1119–1122.
- [4] Z. Chen, M. G. Debije, T. Debaerdemaeker, P. Osswald, F. Wuerthner, *ChemPhysChem* **2004**, *5*, 137–140.
- [5] B. Wang, C. Yu, *Angew. Chem. Int. Ed.* **2010**, *49*, 1485–1488; *Angew. Chem.* **2010**, *122*, 1527.
- [6] M. A. Angadi, D. Gosztola, M. R. Wasielewski, *Mater. Sci. Eng. B* **1999**, *63*, 191–194.
- [7] M. P. O'neil, M. P. Niemczyk, W. A. Svec, D. Gosztola, G. L. Gaines III, M. R. Wasielewski, *Science* **1992**, *257*, 63–65.
- [8] J. A. A. W. Elemans, R. Van Hameren, R. J. M. Nolte, A. E. Rowan, *Adv. Mater.* **2006**, *18*, 1251–1266.
- [9] M. S. Rodrigues-Morgado, T. Torres, C. Atienza-Castellanos, D. M. Guldi, *J. Am. Chem. Soc.* **2006**, *128*, 15145–15154.
- [10] F. Wuerthner, T. E. Kaiser, C. R. Saha-Möller, *Angew. Chem. Int. Ed.* **2011**, *50*, 3376–3410; *Angew. Chem.* **2011**, *123*, 3436.
- [11] a) L. Feiler, H. Langhals, K. Polborn, *Liebigs Ann.* **1995**, 1229–1244; b) H. Quante, K. Mullen, *Angew. Chem. Int. Ed. Engl.* **1995**, *34*, 1323–1235; *Angew. Chem.* **1995**, *107*, 1487; c) F. O. Holtrup, G. R. J. Muller, H. Quante, S. De Feyter, F. C. De Schryver, K. Mullen, *Chem. Eur. J.* **1997**, *3*, 219–225; d) G. R. J. Muller, C. Meiners, V. Enkelmann, Y. Geerts, K. Mullen, *J. Mater. Chem.* **1998**, *8*, 61–64; e) S. Sengupta, R. K. Dubey, R. W. M. Hoek, S. P. P. van Eeden, D. D. Gunbas, F. C. Grozema, E. J. R. Sudhölter, W. F. Jager, *J. Org. Chem.* **2014**, *79*, 6655–6662.
- [12] a) S. I. Yang, R. K. Lammi, S. Prathapan, M. A. Miller, J. Seth, J. R. Diers, D. F. Bocian, J. S. Lindsey, D. Holten, *J. Mater. Chem.* **2001**, *11*, 2420–2430; b) C. Kirmaier, S. I. Yang, S. Prathapan, M. A. Miller, J. R. Diers, D. F. Bocian, J. S. Lindsey, D. Holten, *Res. Chem. Intermed.* **2002**, *28*, 719–740; c) D. Gosztola, M. P. Niemczyk, M. R. Wasielewski, *J. Am. Chem. Soc.* **1998**, *120*, 5118–5119; d) M. J. Fuller, M. R. Wasielewski, *J. Phys. Chem. B* **2001**, *105*, 7216–7219; e) E. M. Just, M. R. Wasielewski, *Superlattices Microstruct.* **2000**, *28*, 317–328; f) R. T. Hayes, M. R. Wasielewski, D. Gosztola, *J. Am. Chem. Soc.* **2000**, *122*, 5563–5567; g) A. S. Lukas, Y. Zhao, S. E. Miller, M. R. Wasielewski, *J. Phys. Chem. B* **2002**, *106*, 1299–1306.
- [13] X. Mo, H. Z. Chen, M. M. Shi, M. Wang, *Chem. Phys. Lett.* **2006**, *417*, 457–460.
- [14] S. Asir, A. S. Demir, H. Icil, *Dyes Pigm.* **2010**, *84*, 1–13.
- [15] A. Böhm, H. Arms, G. Henning, P. Blaschka (BASF AG), DE 19547209 A1, **1997**.
- [16] F. Wuerthner, V. Stepanenko, Z. Chen, C. R. Saha-Möller, N. Kocher, D. Stalke, *J. Org. Chem.* **2004**, *69*, 7933–7939.
- [17] a) R. K. Dubey, A. Efimov, H. Lemmetyinen, *Chem. Mater.* **2011**, *23*, 778–788; b) H. Y. Tsai, C. W. Chang, K. Y. Chen, *Tetrahedron Lett.* **2014**, *55*, 884–888; c) H. Y. Tsai, K. Y. Chen, *J. Lumin.* **2014**, *149*, 103–111; d) R. K. Dubey, M. Niemi, K. Kauristo, A. Efimov, N. V. Tkachenko, H. Lemmetyinen, *Chem. Eur. J.* **2013**, *19*, 6791–6806; e) A. Keerthi, S. Valiyaveetil, *J. Phys. Chem. B* **2012**, *116*, 4603–4614; f) N. V. Handa, K. D. Mendoza, L. D. Shirtcliff, *Org. Lett.* **2011**, *13*, 4724–4727.
- [18] a) A. G. Slater, E. S. Davies, S. P. Argent, W. Lewis, A. J. Blake, J. McMaster, N. R. Champness, *J. Org. Chem.* **2013**, *78*, 2853–2862; b) S. Nagarajan, C. Barthes, N. K. Girdhar, T. T. Dang, A. Gourdon, *Tetrahedron* **2012**, *68*, 9371–9375; c) T. Fukaminato, T. Doi, N. Tamaoki, K. Okuno, Y. Ishibashi, H. Miyasaka, M. Irie, *J. Am. Chem. Soc.* **2011**, *133*, 4984–4990; d) Á. J. Jiménez, M. J. Lin, C. Burschka, J. Becker, V. Settels, B. Engels, F. Würthner, *Chem. Sci.* **2014**, *5*, 608–619; e) T. Heek, F. Würthner, R. Haag, *Chem. Eur. J.* **2013**, *19*, 10911–10921; f) M. H. Luo, K. Y. Chen, *Dyes Pigm.* **2013**, *99*, 456–464; g) R. Wang, Z. Shi, C. Zhang, A. Zhang, J. Chen, W. Guo, Z. Sun, *Dyes Pigm.* **2013**, *98*, 450–458; h) M. J. Lin, Á. J. Jiménez, C. Burschka, F. Würthner, *Chem. Commun.* **2012**, *48*, 12050–12052; i) M. Bagui, T. Dutta, H. Zhong, S. Li, S. Chakraborty, A. Keightley, Z. Peng, *Tetrahedron* **2012**, *68*, 2806–2818; j) L. Perrin, P. Hudhomme, *Eur. J. Org. Chem.* **2011**, *28*, 5427–5440.
- [19] a) H. Langhals, S. Christian, A. Hofer, *J. Org. Chem.* **2013**, *78*, 9883–9891; b) G. Rauch, S. Höger, *Chem. Commun.* **2014**, *50*, 5659–5661.
- [20] H. Langhals, *Heterocycles* **1995**, *40*, 477–500.
- [21] a) D. Gosztola, M. P. Niemczyk, W. Svec, A. S. Lukas, M. R. Wasielewski, *J. Phys. Chem. A* **2000**, *104*, 6545–6551; b) S. Brochsztain, R. O. Marcon, *Langmuir* **2007**, *23*, 11972–11976; c) M. D. Miguel, M. Alvaro, H. Garcia, F. J. C. Guirao, F. F. Lazaro, A. S. Santos, *J. Photochem. Photobiol. A: Chem.* **2012**, *231*, 28–32; d) F. S. Goodson, D. K. Panda, S. Ray, A. Mitra, S. Guha, S. Saha, *Org. Biomol. Chem.* **2013**, *11*, 4797–4803.
- [22] a) S. Verbeeck, W. A. Herrebut, A. A. Gulevskaya, B. A. Van der Veken, B. U. W. Maes, *J. Org. Chem.* **2010**, *75*, 5126–5133; b) F. Doria, M. di Antonio, M. Benotti, D. Verga, M. Freccero, *J. Org. Chem.* **2009**, *74*, 8616–8625.

Received: October 13, 2014

Published Online: December 12, 2014

II

SYNTHESIS AND STUDY OF ELECTROCHEMICAL AND OPTICAL PROPERTIES OF SUBSTITUTED PERYLENEMONOIMIDES IN SOLUTIONS AND ON SOLID SURFACES

by

Zafar Ahmed, Lijo George, Arto Hiltunen, Helge Lemmetyinen, Terttu Hukka
and Alexander Efimov

J. Mater. Chem. A, 2015, 3, 13332–13339

Reproduced with kind permission from The Royal Society of Chemistry (RSC).

CrossMark
click for updatesCite this: *J. Mater. Chem. A*, 2015, 3,
13332

Synthesis and study of electrochemical and optical properties of substituted perylenemonoimides in solutions and on solid surfaces†

Zafar Ahmed, Lijo George, Arto Hiltunen, Helge Lemmetyinen, Terttu Hukka and Alexander Efimov*

A new and efficient methodology towards the synthesis of 7-pyrrolidinyl and 7,12-bispyrrolidinyl perylenemonoimide monoanhydrides (PMI monoanhydrides) and their corresponding dicarboxylic acids is devised. The high yields (70–96%) and facile synthesis of PMI monoanhydrides, as compared to traditional methodologies, make the method attractive and versatile. The reported 7,12-bispyrrolidinyl PMI monoanhydrides are a new family of peryleneimides, where both the bay-substituents are located towards the anhydride cycle. The electrochemical and optical properties of target molecules and their precursors were investigated using UV-Vis spectroscopy and differential pulse voltammetry. Atomic charges and electronic properties were calculated using density functional theory (DFT). In addition, self-assembling monolayers of the PMI monoanhydrides and their corresponding diacids were successfully formed over ZnO and TiO₂ films. The results of the current study indicate that these molecules are potentially good candidates for various applications in the fields of organic electronics and solar cells.

Received 27th March 2015
Accepted 13th May 2015

DOI: 10.1039/c5ta02241j

www.rsc.org/MaterialsA

Introduction

Perylene dyes are one of the most versatile and robust chromophores known to be thermally and photophysically stable. Their discovery almost a century ago has not limited the interest of chemists in developing new synthetic methods for improving their applications.^{1a,b} Initially used as vat dyes,² their applications gradually spread to several high-tech fields like sensitizers in organic solar cells,³ photovoltaics,⁴ biosensors,⁵ artificial photosynthesis,⁶ and several other optical devices.⁷

The functionalization of the perylene core at *peri*-, *bay*- and *ortho*-positions greatly influences the solubility, and electronic and morphological properties of the dyes.⁸ The substitution at the *peri*-position and its effect on the morphology, solubility and chrysalochromic properties of PDI dyes have been reported.⁹ Similarly, the functionalization at the *bay*-position via halogenation,¹⁰ Pd coupling,¹¹ and catalytic or catalyst free oxidation¹² has also been published. The alkylation,¹³ arylation,¹⁴ borylation¹⁵ and halogenation¹⁶ at *ortho*-positions are well documented.

Since the substitution pattern greatly influences the chemical and physical properties of perylene dyes, it is crucial to keep these properties in mind while devising the molecules for

specific applications. For example, it is known that when perylene derivatives are used as sensitizers in DSSCs, the molecule should have an anchoring group through which it can bind to the substrate surface and the presence of electron donating groups on the perylene core increases the photoconversion efficiency.^{17–19} All these molecules carry either aryloxy or thiophenolic substituents in the *bay*-region. In their work, Imahori *et al.* have reported the synthesis and application of electron donating 1,7-substituted perylene tetracarboxylic acid derivatives.²⁰ Recently, Sengupta and co-workers have described the synthesis of 1,7-dibromo perylene monoimide anhydride.²¹ All these synthetic strategies are heavily dependent on the presence of good leaving groups at the *bay*-positions. This results in either an isomeric mixture of 1,7- and 1,6-substituted products or involves tedious purification steps and yield losses.^{21,22} Additionally, selective conversion of imide to anhydride through saponification produces low yields and a mixture of mono and bisanhydride.^{23a,b}

Despite established knowledge about differences in the properties of isomeric perylene diimides,^{23f,24} efforts have been mostly focused on the synthesis or purification of 1,7-substituted isomers of PDIs.^{22a,b,25} This has resulted in poor knowledge about the properties and potential applications of 1,6-isomers. Only very recently, the synthesis of the 1,6-isomer of perylene imide has been reported.^{12a,b} So far, only the 1,7-isomer of the PMI anhydride or its derivatives have been studied as sensitizers in DSSCs¹⁵ leaving 7,12-substituted perylene monoimides with an anchoring group virtually unknown.

Department of Chemistry and Bioengineering, Tampere University of Technology, Tampere, Finland. E-mail: alexandre.efimov@tut.fi

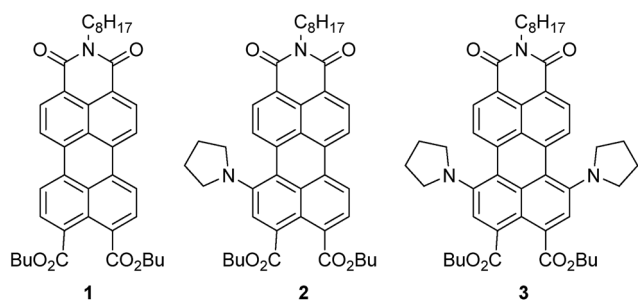
† Electronic supplementary information (ESI) available. See DOI: 10.1039/c5ta02241j

We have recently published, first of this kind, the synthesis of isomerically pure 7- and 7,12-aminated perylene monoimide diesters (PMI diesters), both under catalytic and catalyst free conditions.^{12a} Herein, we report further extension of our methodology towards the synthesis of novel 7- and 7,12-substituted perylene derivatives having strong electron donating groups in the *bay*-region and anchoring groups at *peri*-positions. The electrochemical and photophysical properties of these compounds were studied both experimentally and computationally in detail and self-assembling monolayers (SAMs) were prepared over ZnO films and TiO₂ nanoparticles. The results of our studies suggest that these compounds can be good candidates for their potential use as sensitizers in DSSCs and related applications.

Results and discussion

Synthesis

We have recently reported the synthesis of precursors 1–3 in 47–96% yields.^{12a} A treatment of perylene-3,4,9,10-tetracarboxylic acid bisanhydride (PTCDA) with an alkanol and alkyl halide in a homogeneous solution produced perylene tetraester (PTE).²⁶ Selective hydrolysis and subsequent imidization with octylamine resulted in the formation of perylene monoimide diester PMI (diester) 1.^{12a} The regioselective amination of PMI 1 at 7-, or 7,12-positions was performed under catalytic or catalyst free conditions.



With precursors in hand, the hydrolysis of these PMI diesters to dicarboxylic acids was attempted under different conditions. Ester hydrolysis has been reported under acidic, basic and neutral conditions.²⁷ The most widely used method for the said purpose is the basic hydrolysis carried out in the presence of aqueous hydroxides and co-solvents at different temperatures. Khurana *et al.* have reported the facile hydrolysis of esters with potassium hydroxide in methanol at ambient temperature.²⁸ However, a treatment of PMI diester 2 with KOH in methanol failed to produce the desired diacid product. Similarly, the use of trimethylsilyl iodide (TMSI) in various solvents resulted in either partial hydrolysis or decarboxylation of diesters. The same problem was encountered while attempting ester cleavage using sulfuric acid at elevated temperatures. A prolonged treatment of PMI diesters with KOH in a mixture of THF : EtOH : H₂O at room temperature or at 50 °C again resulted in a monoacid along with several other spots on TLC. Therefore, we decided to use the procedure described by Terunuma *et al.*²⁹ PMI diester 1 was heated at reflux for 24 hours

with a 6 M aqueous solution of KOH in a 2 : 1 mixture of THF : EtOH. The removal of solvents and treatment with 3 M HCl gave the desired PMI diacid 5 in 96% yield (Scheme 1).

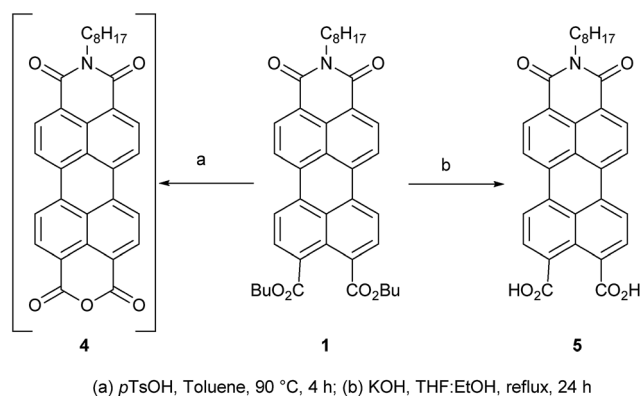
However, when 7-, or 7,12-pyrrolidyl PMI diesters 2 and 3 were subjected to similar reaction conditions, it was observed that the pyrrolidinyl substituents at the *bay*-positions greatly influenced the dealkylation process. For example, even a longer reaction time did not fully convert the starting material to diacid products. The reaction mixtures contained by-products, which proved to be challenging to separate from the desired compounds. The close vicinity of the two carboxylic groups resulted in the formation of an anhydride during purification with an acidic mixture of organic solvents. In addition, decomposition of product spots was also observed on the HPTLC plates.

Keeping all the above mentioned limitations in mind, an alternate approach toward the desired diacids was needed and a ring closing–opening method was adopted. Acid hydrolysis of PMI diesters 2 and 3 with *p*-toluenesulfonic acid in toluene at elevated temperature²¹ yielded novel 7- and 7,12-substituted PMI monohydrides 6 and 7 in 93 and 75% yields, respectively.

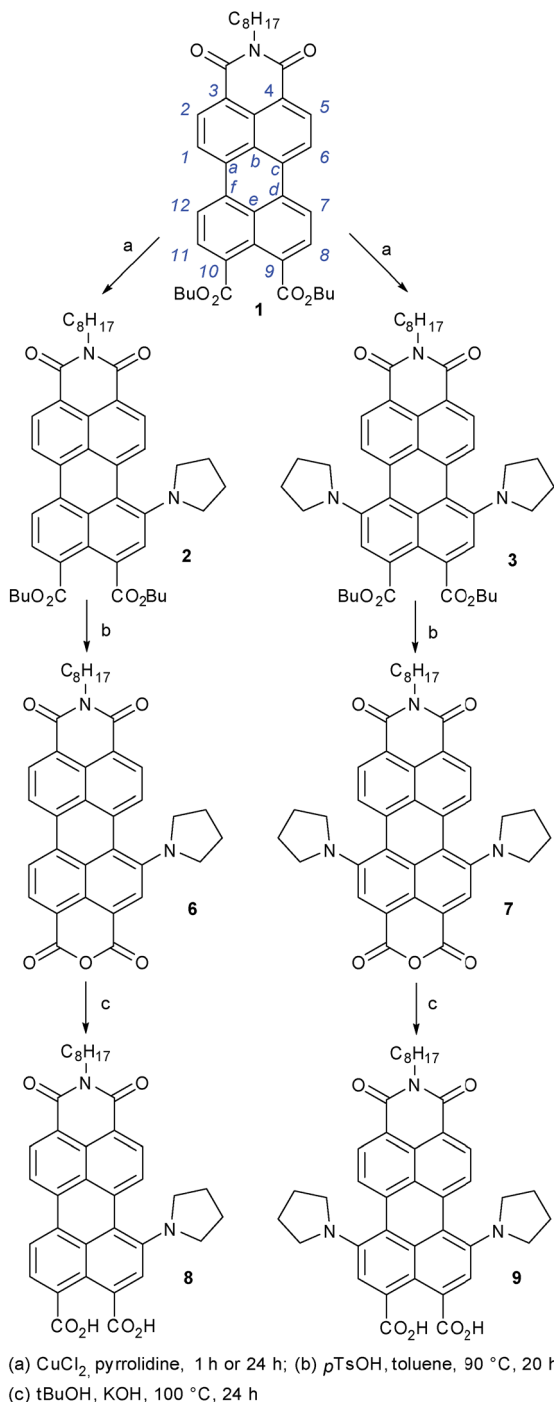
It is well established that this anhydride moiety opens up on adsorption over TiO₂, providing strong chemical interactions with TiO₂ surfaces and effective electronic coupling.³⁰ This property of the anhydride moiety makes it an excellent anchoring group for sensitizers in DSSCs. The same dicarboxylate functionality was achieved when compounds 6 and 7 were heated at 100 °C with 2 equiv. of KOH in *t*BuOH. The desired diacids 8 and 9 were obtained in 70 and 76% yields, respectively (Scheme 2).

Theoretical calculations

In order to clarify the possible reasons for the selectivity of substitution, we have performed the quantum chemical calculations. In our previous paper we suggested that the reaction goes through an anion radical intermediate, and the specificity of the substitution is guided by the charge distribution pattern in the PMI anion radical.^{12a} The atomic charges were calculated using two different levels of theory. The calculations predict that the negative charge is mostly localized on the ester side of

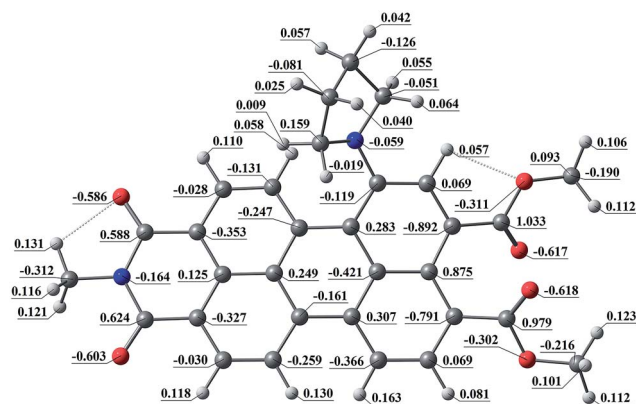


Scheme 1 Synthesis of PMI anhydride 4 and diacid 5.



Scheme 2 Synthesis of PMI anhydrides and acids.

both the neutral and radical anion species of **1** and **2** and especially on the four carbon atoms: *d*, *7*, *8* and *9* or *10*, *11*, *12* and *f* (see Scheme 2, comp. **1**). This makes the ester side rings prone to electrophilic attack by the pyrrolidine moiety. Calculations predict that for ester **2**, once the radical anion has formed, carbon 12 becomes the most electronegative in the *bay*-region (-0.366 , at both levels of theory; compared with -0.261 or -0.259 for carbon 1). This makes carbon 12 more attractive to the approaching electrophile (Fig. 1).

Fig. 1 MK charges of a radical anion of **2** calculated at the M062X/6-311++G(d,p)//M062X/6-311++G(d,p) level of theory.

The required level of theory for the quantum chemical calculations has been verified by predicting HOMO/LUMO energies for compounds **1**–**3**. The theoretical values are in good agreement with the experimental data ($-3.6/-5.9$ vs. $-3.6/-6.1$ for **1**, $-3.1/-5.2$ vs. $-3.1/-5.5$ for **2**, and $-3.3/-5.0$ vs. $-2.8/-5.2$ for **3**). More details on calculations can be found in the ESI.†

Absorption/emission studies

The UV-vis absorption and emission spectra of compounds **1**–**3** and **5**–**9** are shown in Fig. 2. The spectra of perylene monoimide diesters **1**–**3** were recorded in CHCl_3 while for the corresponding PMI anhydrides **6**, **7** and diacids **5**, **8** and **9**, measurements were made in ethanol.

It is very informative and evident to note the effect of the pyrrolidiny substituents at the 7- and 12-positions. In the case of unsubstituted PMI diester **1**, two distinct absorption bands at 506 nm and 476 nm are visible (Fig. 2a, comp. **1**). One pyrrolidiny substituent at the 7-position shifts the absorption maximum towards *ca.* 620 nm, and a second absorption band appears at 410 nm (Fig. 2a, comp. **2**). In the case of di-substitution, *i.e.* 7,12-pyrrolidiny PMI diester **3**, the absorption region becomes wider with a maximum at 642 nm and a second absorption band at 528 nm. These features allow us to conclude that the enhanced interaction between the pyrrolidiny substituents and the perylene core greatly influences the optical properties of the compounds. It is visible from the spectra that the substituted PMI anhydrides **6** and **7** (Fig. 2c) and their corresponding carboxylic acids **8** and **9** (Fig. 2e) retain the absorptive features of their corresponding PMI diesters **2** and **3** (Fig. 2a). They absorb light in the visible region and cover a large part of the spectrum from 475 up to 750 nm. Though substituted PMI diesters, anhydrides and carboxylic acids show similar absorption bands in the visible region, the PMI anhydrides **6** and **7** and acids **8** and **9** have molar extinction coefficients almost two folds higher than those of the diesters **2** and **3** at low energy (Fig. 2).

The emission properties of the substituted PMI diesters, anhydrides, and diacids are almost identical, showing the

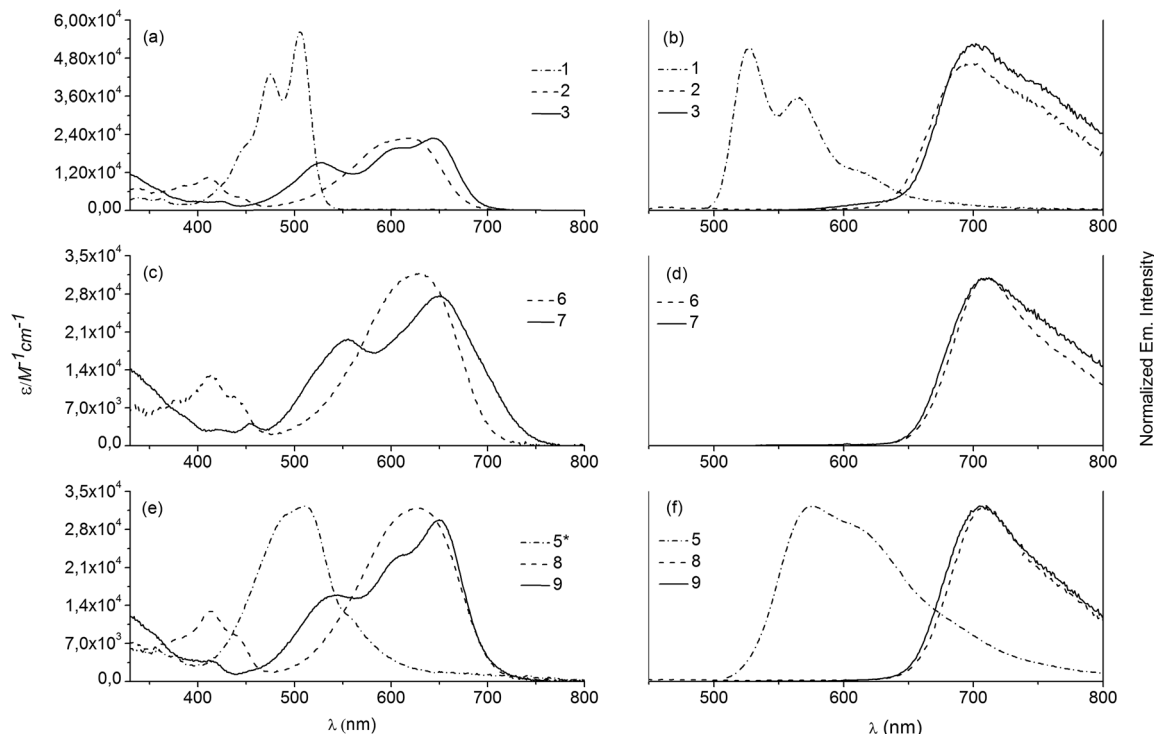


Fig. 2 Absorption (a, c, and e), and emission (b, d, and f) spectra of PMI diesters 1–3 in CHCl_3 , anhydrides 6, 7, and acids 5, 8, 9 in ethanol. Abs. of 5* is normalised due to poor solubility.

emission maxima around 700 nm. The normalized emission spectra of PMI diesters 1–3, anhydrides 6 and 7 and diacid 5, 8 and 9 are shown in Fig. 2b, d and f.

Electrochemical properties

Several properties and field of applications of peryleneimides and their derivatives depend on the energies of the frontier orbitals, HOMO and LUMO. These energies and relative donor–acceptor capabilities of perylenemonoimide diesters 1–3, PMI monoimide anhydride 6, and diacid 5 were investigated by differential pulse voltammetry (DPV) in benzonitrile containing 0.1 M tetrabutylammonium tetrafluoroborate as a supporting electrolyte. The obtained redox potentials (V vs. ferrocene) are shown in Table 1 while the calculated HOMO–LUMO energy levels are plotted in Fig. 4 (along with the data for TiO_2 (ref. 31) and fullerene³² for comparison). The IV curves can be found in the ESI, pages S9–S13.†

Table 1 Redox potentials (V vs. ferrocene) of PMIs obtained by DPV and HOMO and LUMO (eV) calculated against vacuum

Com	$E_{1\text{red}}$	$E_{2\text{red}}$	$E_{1\text{ox}}$	$E_{2\text{ox}}$	HOMO	LUMO
1	−1.2	−1.5	1.1	—	−5.9	−3.6
2	−1.4	−1.6	0.4	—	−5.2	−3.4
3	−1.5	−1.8	0.25	—	−5.0	−3.3
5	−0.9	−1.2	1.1	1.3	−5.9	−3.9
6	−1.1	−1.3	0.6	1.0	−5.4	−3.7

The unsubstituted PMI diester 1 and the 12-pyrrolidinyl PMI diester 2 exhibit very similar redox characteristics. Similarly, both compounds show a single one-step irreversible oxidation, where the oxidation peak was detected at around +1.1 V and +0.45 V, respectively. The higher value of the oxidation potential for compound 1 (Fig. 3) compared to the 12-substituted PMI diester 2 means that the unsubstituted PMI diester 1 is a weaker electron donor compared to 2.

Similarly, the 7,12-pyrrolidinyl PMI diester 3 undergoes a two-step reduction and a single-step oxidation. The reduction occurs at around −1.5 V and −1.8 V, whereas the oxidation peak appears at +0.25 V. The oxidation potentials of the 7-pyrrolidinyl PMI diester 2 and 7,12-pyrrolidinyl diester 3 are quite similar. The unsubstituted PMI diacid 5, on the other hand, undergoes a three-step reversible reduction, reflecting the first, second and third one-electron reductive processes. The reversible reductions occur at −0.9 V, −1.2 V, and −1.5 V. The diacid 5 shows two irreversible oxidation peaks at higher oxidation potentials of 1.52 and 1.73 V (spectra in the ESI†). The voltammograms of the 12-pyrrolidinyl PMI monoanhydride 6 show two reversible reductions at −1.1 V and −1.3 V. For the oxidative potentials, it shows two reversible oxidation peaks around 0.6 V and 1.0 V.

Self-assembling monolayers

Commercially available indium-tin-oxide (ITO) coated glass substrates were used to prepare ZnO layers using zinc acetate and were fabricated according to the literature procedure.³³ Self-assembling monolayers (SAMs) were prepared in a single step. The substrate plates were annealed at 150 °C for 1.5 hours,

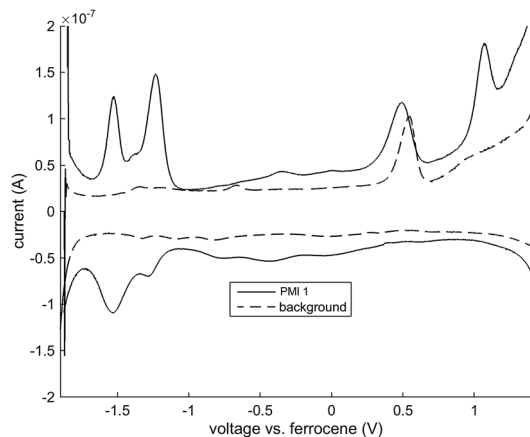


Fig. 3 DPV curve of compound 1 vs. ferrocene.

cooled, and immersed in 0.1 mM solutions of PMI diacid 5, 7,12-pyrrolidinyl PMI monoanhydride 7, and 7,12-pyrrolidinyl PMI dicarboxylic acid 9 in ethanol. After 60 minutes, the plates were taken out, thoroughly washed with ethanol, dried and the absorption spectra were measured. The spectra for SAMs were obtained by subtracting the absorbance of clean substrates from that of SAMs.

The absorption spectra of SAMs of both diacids 5 and 9 and 7,12-substituted anhydride 7 (Fig. 5) differ from those in solution form (Fig. 2b and c). Particularly interesting are the absorption features of 7,12-substituted PMI anhydride 7 and its corresponding diacid 9. In solution, 7,12-substituted PMI anhydride 7 shows two major absorption bands at 652 nm and 555 nm plus a weak band at *ca.* 453 nm (Fig. 2b). On solid substrates, the major absorption bands shift towards the blue region and a new band in the higher energy region (*ca.* 364 nm) appears (Fig. 5). Similarly 7,12-substituted PMI diacid 9, in solution, exhibits two absorption bands at 545 nm and 652 nm together with a shoulder at 612 nm. After immobilization on a solid substrate, diacid 9 shows blue shifted absorptions at 588 nm and 514 nm together with a high energy region absorption band at 364 nm. It's important to note that the absorption shape of SAMs of both the 7,12-substituted PMI anhydride 7 and its corresponding diacid 9 are essentially imitations of each other. This can be explained by their mode of binding to the

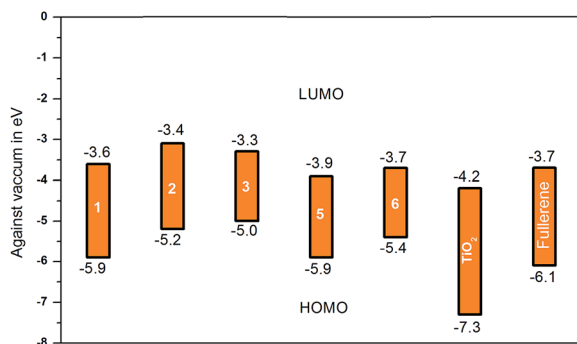


Fig. 4 HOMO and LUMO levels of PMIs against TiO_2 and fullerene.

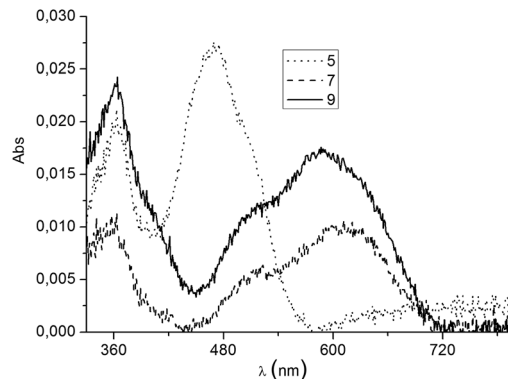


Fig. 5 Absorption spectra of SAMs of PMI diacid 5, monoanhydride 7, and dicarboxylic acid 9 on ITO/ZnO plates.

substrate surface. The dicarboxylic acid 9 reacts strongly with the ZnO surface and forms the desired monolayer. Whereas in the case of 7,12-substituted PMI anhydride 7, the anhydride moiety does the anchoring role *via* ring opening and the resultant dicarboxylate groups bind to the substrate surface, as proved by absorption.³²

SAM layer formation was also studied on TiO_2 as a substrate. Annealed TiO_2 -coated glass plates were immersed in 0.1 mM solutions of PMI diacids 5, 8, and 9, and 7,12-substituted PMI anhydride 7. In the case of compounds 7, 8 and 9, the plates were taken out after 3 hours, washed, dried and absorption spectra were recorded. For the PMI diacid 5, the deposition time was 24 hours due to its poor solubility and therefore a low concentration of the deposition solution. The absorption spectra showed the formation of monolayers (Fig. 6).

All in all, the formation of monolayers was fast, efficient and simple. Due to the asymmetric structure of PMIs, namely the 7,12-substitution, the formed layers have an intrinsically anisotropic structure, which might have a beneficial effect in photovoltaic applications. Also, it should be noted that a versatility of substitution in the *bay*-region and distant from the imide side, along with the two possibilities for an anchor (anhydride or bis-acid) makes the proposed PMI template an attractive target for future studies in self-assembled molecular films.

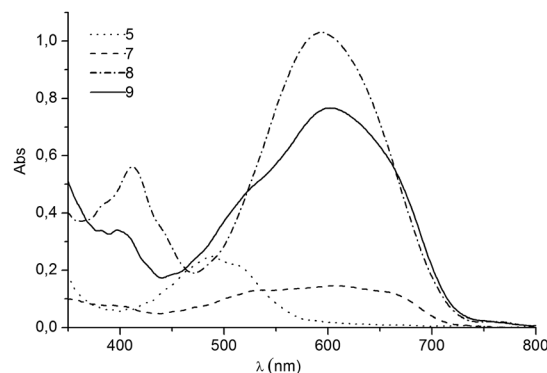


Fig. 6 Absorption spectra of SAMs of PMI diacids 5, 8, and 9 and PMI anhydride 7 over glass/ TiO_2 plates.

Conclusions

A new and facile route towards the synthesis of novel 7- and 7,12-bispyrrolidinyl PMI monoanhydride and their dicarboxylic acids is developed. The traditional synthesis of the PMI monoanhydrides heavily depends upon selective saponification of PDIs resulting in low yields due to the absence of selectivity. Our methodology is free of selective saponification and thus good to excellent yields for the substituted PMI monoanhydrides are obtained in a few steps. These substituted PMI monoanhydrides are easily transformed into either corresponding dicarboxylic acids or unsymmetrical PDIs by introducing a second imide functionality on the anhydride cycle. Also, this is the first report of this kind of synthesis, where PMI monoanhydrides carry both the amine substituents at 7,12-positions, distant from the imide cycle. The investigation of their optical and electrochemical properties indicates that these kinds of perylene derivatives can be applied in various fields of materials chemistry and device preparations. The immobilization studies of the PMI monoanhydrides and diacids clearly indicate their usefulness as building blocks for SAMs. The presence of the electron donating pyrrolidine substituents in the *bay*-region and the presence of the anchoring groups in the form of anhydride/carboxylic acids make them attractive candidates for DSSCs and other types of solar cells.

Experimental section

General

All commercially available reagents and solvents were purchased either from Sigma Aldrich Co. or from VWR and were used without further purification unless otherwise mentioned. Purification of the products was carried out either by column chromatography on silica gel 60 (Merck) mesh size 40–63 μm or on preparative TLC plates (Merck) coated with neutral aluminum oxide 60 F254. NMR spectra were recorded using a Varian Mercury 300 MHz spectrometer using TMS as the internal standard. HRMS measurements were done with a Waters LCT Premier XE ESI-TOF bench top mass spectrometer. Lock-mass correction (leucine enkephaline as the reference compound), centering and calibration were applied to the raw data to obtain the accurate mass.

Computational methods

Density functional theory (DFT) was applied in all calculations using the Gaussian 09 (Revision D.01) suite of programs.³⁴ The *n*-octyl and *n*-butyl side chains of the molecules **1**, **2** and **3** were replaced by methyl (CH_3) groups in the modelling of the molecular structures. The geometries were optimized and electronic properties were calculated using the B3LYP and M062X functionals and the 6-311++G(d,p) basis set. The atomic charges were computed using the same levels of theories by the Merz–Kollman method^{35,36} for the neutral and radical ion models of **1** and **2**.

Synthesis of precursors **1**, **2** and **3**

Synthesis and characterization of precursors **1**, **2** and **3** have been reported in our previous article.^{12a}

General procedure for synthesis of PMI anhydrides

Perylene monoimide diesters **1**, **2** or **3** (1.0 equiv.) and *p*-toluenesulfonic acid (5.0 equiv.) were taken in toluene (33 mL mmol^{-1} PMI diester). The resultant mixture was stirred at 90 °C for 18 hours (in the case of precursor **1**, only 4 hours). After cooling to room temperature, the solvent was evaporated. The crude was dissolved in CHCl_3 and washed with water (2 \times). The organic phase was dried over Na_2SO_4 , filtered and concentrated on a rotary evaporator. The residue was taken in methanol and refluxed for 2 hours. The precipitates were filtered and washed with methanol to obtain pure products.

Synthesis of 2-octyl-1,3-dioxo-2,3-dihydro-1H-benzo[10,5]-anthra[2,1,9-def]isoquinoline-8,9-dicarboxylic acid **5.** PMI diester **1** (0.157 mmol, 100 mg) was taken in a 2.53 mL mixture of THF : EtOH (2 : 1 v/v). To this mixture, 0.835 mL of aq. KOH (6 M) was added and the resultant mixture was heated at 80 °C for 24 hours. The reaction mixture was cooled to room temperature and solvents were removed on a rotary evaporator. The pH was adjusted to *ca.* 4 by adding 3 M HCl over an ice bath. The precipitates were filtered and dried. The desired PMI diacid **5** was obtained as a red solid (80 mg, 97%).

Data for **5**: ^1H NMR (300 MHz, DMSO): δ = 8.69 (d, J = 8.21 Hz, 2H), 8.63 (d, J = 7.92 Hz, 2H), 8.45 (d, J = 8.21 Hz, 2H), 4.04 (t, J = 7.33 Hz, 2H), 1.69–1.57 (m, 2H), 1.39–1.18 (m, 10H), 0.86–0.81 (m, 3H) ppm. Due to poor solubility, ^{13}C NMR data could not be recorded. MS (ESI-TOF): $[\text{M}^+]$ calcd for $\text{C}_{32}\text{H}_{27}\text{NO}_6^+$, 520.1777; found, 520.1760.

9-Octyl-5-(pyrrolidin-1-yl)-1H-isochromeno[6',5',4':10,5,6]anthra[2,1,9-def]isoquinoline-1,3,8,10(9H)-tetraone **6.** Starting from 7-pyrrolidinyl PMI diester **2** (0.096 mmol, 68 mg) and *p*-TsOH \cdot H_2O (0.483 mmol, 91 mg), 7-pyrrolidinyl PMI anhydride **6** was obtained as blue solids (51 mg, 91%).

Data for **6**: ^1H NMR (300 MHz, CDCl_3 , TMS): δ = 8.62 (t, J = 8.21 Hz, 2H), 8.45–8.33 (m, 4H), 7.47 (d, J = 8.21, 1H), 4.19 (t, J = 7.62, 2H), 3.74 (br, 2H), 2.75 (br, 2H), 2.12–2.02 (m, 4H), 1.74–1.70 (m, 2H), 1.44–1.25 (m, 6H), 0.89–0.84 (m, 3H) ppm. ^{13}C NMR (75 MHz, CDCl_3 , TMS): δ = 163.80, 163.69, 148.32, 134.95, 134.71, 134.35, 131.18, 131.00, 129.06, 128.55, 127.62, 125.35, 124.86, 124.68, 123.99, 122.54, 121.34, 119.91, 118.89, 118.26, 117.19, 52.83, 40.82, 32.05, 29.91, 29.59, 29, 45, 28.38, 27.41, 25.98, 22.86, 14.30 ppm. MS (ESI-TOF): $[\text{M}^+]$ calcd for $\text{C}_{36}\text{H}_{32}\text{N}_2\text{O}_5^+$, 572.2350; found, 572.2311.

9-Octyl-5,13-di(pyrrolidin-1-yl)-1H-isochromeno[6',5',4':10,5,6]anthra[2,1,9-def]isoquinoline-1,3,8,10(9H)-tetraone **7.** Starting from 7,12-pyrrolidinyl PMI diester **3** (0.216 mmol, 167 mg) and *p*-TsOH \cdot H_2O (1.08 mmol, 205 mg), 7,12-pyrrolidinyl PMI anhydride **7** was obtained as a dark blue solid (105 mg, 75%).

Data for **7**: ^1H NMR (300 MHz, CDCl_3 , TMS): δ = 8.70 (d, J = 7.92 Hz, 2H), 8.30 (s, 2H), 7.80 (d, J = 8.21 Hz, 2H), 4.24 (t, J = 7.62 Hz, 2H), 3.70 (br, 4H), 2.74 (br, 4H), 1.83–1.73 (m, 2H), 1.49–1.25 (m, 10H), 0.90–0.85 (m, 3H) ppm. ^{13}C NMR (75 MHz, CDCl_3 , TMS): δ = 164.21, 161.30, 150.01, 135.29, 131.44, 130.41,

129.15, 128.33, 123.89, 119.37, 118.79, 118.60, 117.95, 52.57, 40.74, 32.09, 29.67, 29.48, 28, 47, 27.47, 25.91, 22.89, 14.34 ppm. MS (ESI-TOF): $[M^+]$ calcd for $C_{40}H_{39}N_3O_5^+$, 641.2897; found, 641.2890.

2-Octyl-1,3-dioxo-6-(pyrrolidin-1-yl)-2,3-dihydro-1H-benzo[10,5]anthra[2,1,9-def]isoquinoline-8,9-dicarboxylic acid 8. 7-Pyrrolidinyl PMI anhydride **6** (0.050 mmol, 29 mg) and KOH (0.101 mmol, 6 mg) were taken in 3 mL of *t*BuOH. The reaction mixture was heated at 100 °C for 3 hours. After cooling to room temperature, the pH of the mixture was adjusted to *ca.* 6–6.5 by adding aqueous NH_4Cl . Precipitates were formed which were filtered and dried to yield the desired product as a blue solid (23 mg, 76%).

Data for **8**: 1H NMR (300 MHz, CD_3OD): δ = 8.58 (d, J = 8.21 Hz, 1H), 8.52–8.46 (m, 3H), 7.97 (s, 1H), 7.90 (d, J = 7.92 Hz, 1H), 7.11 (d, J = 7.92 Hz, 1H), 4.19 (t, J = 7.92 Hz, 2H), 3.81 (br, 2H), 2.81 (br, 2H), 1.77–1.72 (m, 2H), 1.43–1.31 (m, 10H), 0.93–0.87 (m, 3H) ppm. Due to poor solubility, ^{13}C NMR data could not be recorded. MS (ESI-TOF): $[M^+]$ calcd for $C_{36}H_{34}N_2O_6^+$, 641.2897; found, 641.2890.

2-Octyl-1,3-dioxo-6,11-di(pyrrolidin-1-yl)-2,3-dihydro-1H-benzo[10,5]anthra[2,1,9-def]isoquinoline-8,9-dicarboxylic acid 9. 7,12-Pyrrolidinyl PMI anhydride **7** (0.109 mmol, 70 mg) and KOH (0.201 mmol, 12 mg) were taken in 6 mL of *t*BuOH. The reaction mixture was heated at 100 °C for 3 hours. After cooling to room temperature, the pH of the mixture was adjusted to *ca.* 6–6.5 by adding aqueous NH_4Cl . Precipitates were formed which were filtered and dried to yield the desired product as a blue solid (55 mg, 76%).

Data for **9**: 1H NMR (300 MHz, CD_3OD): δ = 8.52 (d, J = 7.92 Hz, 2H), 8.30 (s, 2H), 7.54 (d, J = 8.21 Hz, 2H), 4.21 (t, J = 7.92 Hz, 2H), 3.74 (br, 4H), 2.75 (br, 4H), 1.79–1.66 (m, 2H), 1.41–1.29 (m, 10H), 0.92–0.88 (m, 3H) ppm. ^{13}C NMR (75 MHz, CD_3OD): δ = 164.57, 150.86, 137.70, 137.68, 137.66, 132.20, 130.17, 129.76, 122.02, 121.99, 114.82, 114.14, 111.20, 52.10, 39.98, 31.83, 29.30, 29.19, 27.98, 27.06, 25.48, 22.54, 13.26 ppm. MS (ESI-TOF): $[M^+]$ calcd for $C_{40}H_{41}N_3O_6^+$, 659.3008; found, 659.2996.

Acknowledgements

The authors gratefully acknowledge the financial support from the Academy of Finland. The authors are grateful to Ms Tuuva Kastinen for helping with the analysis of the molecular modelling calculations. Computing resources provided by the CSC – IT Center for Science Ltd., administered by the Finnish Ministry of Education, are acknowledged.

Notes and references

- (a) K. Grice, H. Lu, P. Atahan, M. Asif, C. Hallmann, P. Greenwood, E. Maslen, S. Tulipani, K. Williford and J. Dodson, *Geochim. Cosmochim. Acta*, 2009, **73**, 6531–6543; (b) M. Kardos, Deutsches Reichspatent No. 276357, 1913.
- H. Zollinger, *Color Chemistry*, Wiley-VCH GmbH & Co. KGaA, 3rd edn, 2003.
- (a) L. Schmidt-Mende, A. Fechtenkötter, K. Müllen, E. Moons, R. H. Friend and J. D. MacKenzie, *Science*, 2001, **293**, 1119–1122; (b) J. J. Dittmer, E. A. Marseglia and R. H. Friend, *Adv. Mater.*, 2000, **12**, 1270–1274; (c) J. J. Dittmer, R. Lazzaroni, P. Leclère, P. Moretti, M. Granström, K. Petritsch, E. A. Marseglia, R. H. Friend, J. L. Brédas, H. Rost and A. B. Holms, *Sol. Energy Mater. Sol. Cells*, 2000, **61**, 53–61; (d) K. Petritsch, J. J. Dittmer, E. A. Marseglia, R. H. Friend, A. Lux, G. G. Rozenberg, P. Moretti and A. B. Holmes, *Sol. Energy Mater. Sol. Cells*, 2000, **61**, 63–72; (e) S.-B. Rim, R. F. Fink, J. C. Schöneboom, P. Erk and P. Peumans, *Appl. Phys. Lett.*, 2007, **91**, 173504; (f) S. Erten, F. Meghdadi, S. Gunes, R. Koeppel, N. S. Sariciftci and S. Icli, *Eur. Phys. J.: Appl. Phys.*, 2006, **36**, 225–229; (g) A. K. Pandey and J.-M. Nunzi, *Appl. Phys. Lett.*, 2007, **90**, 263508; (h) Y. Ooyama and Y. Harima, *Eur. J. Org. Chem.*, 2009, **18**, 2903–2934; (i) C. Li, M. Liu, N. G. Pschirer, M. Baumgarten and K. Müllen, *Chem. Rev.*, 2010, **110**, 6817–6855; (j) Y. Lin, Y. Li and X. Zhan, *Chem. Soc. Rev.*, 2012, **41**, 4245–4272; (k) M. Sommer, S. Hüttner, M. Thelakkat, in *Ideas in Chemistry and Molecular Sciences, Advances in Nanotechnology, Materials and Devices*, ed. B. Pig-nataro, Wiley-VCH, Weinheim, Germany, 2010, pp. 317–338; (l) H. Qian, Z. Wang, W. Yue and D. Zhu, *J. Am. Chem. Soc.*, 2007, **129**, 10664–10665; (m) C. Li and H. Wonneberger, *Adv. Mater.*, 2012, **24**, 613–636.
- C. W. Tang, *Appl. Phys. Lett.*, 1986, **48**, 183–185.
- B. Wang and C. Yu, *Angew. Chem., Int. Ed.*, 2010, **49**, 1485–1488.
- M. S. Rodrigues-Morgade, T. Torres, C. Atienza-Castellanos and D. M. Guldi, *J. Am. Chem. Soc.*, 2006, **128**, 15145–15154.
- (a) C. Ego, D. Marsitzky, S. Becker, J. Zhang, A. C. Grimsdale, H. Muellen, J. D. MacKenzie, C. Silva and R. H. Friend, *J. Am. Chem. Soc.*, 2003, **125**, 437–443; (b) S. Alibert-Fouet, S. Dardel, H. Bock, M. Oukachmih, S. Archambeau, I. Seguy, P. Jolinat and P. Destruel, *ChemPhysChem*, 2003, **4**, 983–985; (c) Y. Liu, Y. Li, L. Jiang, H. Gan, H. Liu, Y. Li, J. Zhuang, F. Lu and D. Zhu, *J. Org. Chem.*, 2004, **69**, 9049–9054; (d) W. S. Shin, H. H. Jeong, M. K. Kim, S. H. Jin, M. R. Kim, J. K. Lee, J. W. Lee and Y. S. Gal, *J. Mater. Chem.*, 2006, **16**, 384–390; (e) M. P. O'Neil, M. P. Niemczyk, W. A. Svec, D. Gosztola, G. L. Gaines and M. R. Wasielewski, *Science*, 1992, **257**, 63–65; (f) L. Zang, R. Liu, M. W. Holman, K. T. Nguyen and D. M. Adams, *J. Am. Chem. Soc.*, 2002, **124**, 10640–10641.
- C. Li and H. Wonneberger, *Adv. Mater.*, 2012, **24**, 613–636.
- (a) P. Erwin and M. E. Thompson, *Appl. Phys. Lett.*, 2011, **98**, 223305; (b) F. Gaser and E. Hädicke, *Liebigs Ann. Chem.*, 1980, **1980**, 1994–2011; (c) E. Hädicke and F. Graser, *Acta Crystallogr., Sect. A: Cryst. Phys., Diffr., Theor. Gen. Crystallogr.*, 1986, **42**, 189–195.
- (a) A. Böhm, H. Arms, G. Henning and P. Blaschka, (BASF AG) Ger. Pat., DE 19547209 A1, 1997; (b) F. Würthner, *Chem. Commun.*, 2004, 1564–1579.
- (a) B. Pagoaga, L. Giraudet and N. Hoffmann, *Eur. J. Org. Chem.*, 2014, **24**, 5178–5195; (b) S. Dey, A. Efimov and H. Lemmetyinen, *Eur. J. Org. Chem.*, 2012, **12**, 2367–2374.
- (a) L. George, Z. Ahmed, H. Lemmetyinen and A. Efimov, *Eur. J. Org. Chem.*, 2015, **3**, 584–590; (b) H. Langhals, S. Christian

- and A. Hofer, *J. Org. Chem.*, 2013, **78**, 9883–9891; (c) G. Rauch and S. Höger, *Chem. Commun.*, 2014, **50**, 5659–5661.
- 13 S. Nakazono, Y. Imazaki, H. Yoo, J. Yang, T. Sasamori, N. Tokitoh, T. Cédric, H. Kageyama, D. Kim, H. Shinokubo and A. Osuka, *Chem.–Eur. J.*, 2009, **15**, 7530–7533.
- 14 S. Nakazono, S. Easwaramoorthi, D. Kim, H. Shinokubo and A. Osuka, *Org. Lett.*, 2009, **11**, 5426–5429.
- 15 (a) T. Teraoka, S. Hiroto and H. Shinokubo, *Org. Lett.*, 2011, **13**, 2532–2535; (b) G. Battagliarin, C. Li, V. Enkelmann and K. Müllen, *Org. Lett.*, 2011, **13**, 3012–3015.
- 16 G. Battagliarin, Y. Zhao, C. Li and K. Müllen, *Org. Lett.*, 2011, **13**, 3399–3401.
- 17 (a) S. Ferrere and B. A. Gregg, *J. Phys. Chem.*, 2001, **105**, 7602–7605; (b) S. Ferrere and B. A. Gregg, *New J. Chem.*, 2002, **26**, 1155–1160.
- 18 T. Edvinsson, C. Li, N. Pschirer, J. Schöneboom, F. Eickemeyer, R. Sens, G. Boschloo, A. Herrmann, K. Müllen and A. Hagfeldt, *J. Phys. Chem.*, 2007, **111**, 15137–15140.
- 19 C. Li, J.-H. Yum, S.-J. Moon, A. Herrmann, F. Eickemeyer, N. G. Pschirer, P. Erk, J. Schöneboom, K. Müllen, M. Grätzel and M. K. Nazeeruddin, *ChemSusChem*, 2008, **1**, 615–618.
- 20 Y. Shibano, T. Umeyama, Y. Matano and H. Imahori, *Org. Lett.*, 2007, **9**, 1971–1974.
- 21 S. Sengupta, R. K. Dubey, R. W. M. Hoek, S. P. P. van Eden, D. D. Gunbas, F. C. Grozema, E. J. R. Sudhölter and W. F. Jager, *J. Org. Chem.*, 2014, **79**, 6655–6662.
- 22 (a) R. K. Dubey, A. Efimov and H. Lemmetyinen, *Chem. Mater.*, 2011, **23**, 778–788; (b) H. Y. Tsai, C. W. Chang and K. Y. Chen, *Tetrahedron Lett.*, 2014, **55**, 884–888; (c) H. Y. Tsai and K. Y. Chen, *J. Lumin.*, 2014, **149**, 103–111; (d) R. K. Dubey, M. Niemi, K. Kaunisto, A. Efimov, N. V. Tkachenko and H. Lemmetyinen, *Chem.–Eur. J.*, 2013, **19**, 6791–6806; (e) A. Keerthi and S. Valiyaveetil, *J. Phys. Chem. B*, 2012, **116**, 4603–4614; (f) N. V. Handa, K. D. Mendoza and L. D. Shirlcliff, *Org. Lett.*, 2011, **13**, 4724–4727.
- 23 (a) T. Ren, P. K. Mandal, W. Erker, Z. Liu, Y. Avlasevich, L. Puhl, K. Muellen and T. Bosche, *J. Am. Chem. Soc.*, 2008, **130**, 17242–17243; (b) J. Fortage, M. Severac, C. H. Rassin, Y. Pellegrin, E. Blart and F. Odobel, *J. Photochem. Photobiol., A*, 2008, **197**, 156–169.
- 24 (a) H. Y. Tsai and K. Y. Chen, *J. Lumin.*, 2014, **149**, 103–111; (b) R. K. Dubey, M. Niemi, K. Kaunisto, A. Efimov, N. V. Tkachenko and H. Lemmetyinen, *Chem.–Eur. J.*, 2013, **19**, 6791–6806; (c) A. Keerthi and S. Valiyaveetil, *J. Phys. Chem. B*, 2012, **116**, 4603–4614.
- 25 (a) X. Guo, D. Zhang and D. Zhu, *Adv. Mater.*, 2004, **16**, 125–130; (b) Y. Zhao and M. R. Wasielewski, *Tetrahedron Lett.*, 1999, **40**, 7047–7050; (c) M. J. Ahrens, M. J. Fuller and M. R. Wasielewski, *Chem. Mater.*, 2003, **15**, 2684–2686; (d) Y. Liu, Y. Li, L. Jiang, H. Gan, H. Liu, Y. Li, J. Zhuang, F. Lu and D. J. Zhu, *J. Org. Chem.*, 2004, **69**, 9049–9054; (e) F. Wurthner, C. Thalacker, S. Diele and C. Tschierske, *Chem.–Eur. J.*, 2001, **7**, 2247–2253; (f) J. M. Serin, D. W. Brousmiche and J. M. J. Frechet, *J. Am. Chem. Soc.*, 2002, **124**, 11848–11849.
- 26 R. Wang, Z. Shi, C. Zhang, A. Zhang, J. Chen, W. Guo and Z. Sun, *Dyes Pigm.*, 2013, **98**, 450–458.
- 27 (a) F. A. Carey and R. J. Sundberg, *Advanced Organic Chemistry*, Plenum Press, New York, 3rd edn, 1990, p. 465; (b) J. March, *Advanced Organic Chemistry, Reaction Mechanisms and Structure*, John Wiley & Sons, New York, 4th edn, 2001, p. 378 and references cited therein; (c) K. Sisido, Y. Kazama, H. Kodama and H. Nozaki, *J. Am. Chem. Soc.*, 1959, **81**, 5817; (d) C. S. Marvel, J. Dec, H. G. Cooke Jr and J. C. Cowan, *J. Am. Chem. Soc.*, 1940, **62**, 3495; (e) B. Dayal, G. Salen, B. Toome, G. S. Tint, S. Shefer and J. Padia, *Steroids*, 1990, **55**, 233; (f) G. Blay, M. L. Cardona, M. B. Garcia and J. R. Pedro, *Synthesis*, 1989, 438–439; (g) M. F. Jung and M. A. Lyster, *J. Am. Chem. Soc.*, 1977, **99**, 968–969.
- 28 J. M. Khurana, S. Chauhan and G. Bansal, *Monatsh. Chem.*, 2004, **135**, 83–87.
- 29 K. Tojo, T. Arisawa, M. Yasutake, Y. Aoki and D. Terunuma, *Chem. Lett.*, 2008, 930–931.
- 30 S. Wang, L. Dössel, A. Mavrinskiy, P. Gao, X. Feng, W. Pisula and K. Muellen, *Small*, 2011, **7**, 2841–2846.
- 31 M. Grätzel, *Nature*, 2001, **414**, 338–344.
- 32 J. Y. Kim, S. H. Kim, H.-H. Lee, K. Lee, W. Ma, X. Gong and A. J. Heeger, *Adv. Mater.*, 2006, **18**, 572–576.
- 33 M. S. White, D. C. Olson, S. E. Shaheen, N. Kopidakis and D. S. Ginley, *Appl. Phys. Lett.*, 2006, **89**, 143517–143520.
- 34 M. J. Frisch, G. W. Trucks, H. B. Schlegel, G. E. Scuseria, M. A. Robb, J. R. Cheeseman, G. Scalmani, V. Barone, B. Mennucci, G. A. Petersson, H. Nakatsuji, M. Caricato, X. Li, H. P. Hratchian, A. F. Izmaylov, J. Bloino, G. Zheng, J. L. Sonnenberg, M. Hada, M. Ehara, K. Toyota, R. Fukuda, J. Hasegawa, M. Ishida, T. Nakajima, Y. Honda, O. Kitao, H. Nakai, T. Vreven, J. A. Montgomery Jr, J. E. Peralta, F. Ogliaro, M. Bearpark, J. J. Heyd, E. Brothers, K. N. Kudin, V. N. Staroverov, R. Kobayashi, J. Normand, K. Raghavachari, A. Rendell, J. C. Burant, S. S. Iyengar, J. Tomasi, M. Cossi, N. Rega, J. M. Millam, M. Klene, J. E. Knox, J. B. Cross, V. Bakken, C. Adamo, J. Jaramillo, R. Gomperts, R. E. Stratmann, O. Yazyev, A. J. Austin, R. Cammi, C. Pomelli, J. W. Ochterski, R. L. Martin, K. Morokuma, V. G. Zakrzewski, G. A. Voth, P. Salvador, J. J. Dannenberg, S. Dapprich, A. D. Daniels, Ö. Farkas, J. B. Foresman, J. V. Ortiz, J. Cioslowski, and D. J. Fox, *Gaussian 09, Revision D.01*, Gaussian, Inc., Wallingford CT, 2009.
- 35 U. C. Singh and P. A. Kollman, *J. Comput. Chem.*, 1984, **5**, 129–145.
- 36 B. H. Besler, K. M. Merz Jr and P. A. Kollman, *J. Comput. Chem.*, 1990, **11**, 431–439.

III

PHOTODYNAMIC SELF-DISINFECTING SURFACE USING PYRIDINIUM PHTHALOCYANINE

by

Lijo George , Alexander Müller , Beate Röder, Ville Santala , Alexander Efimov.
Dyes and Pigments 147 (2017) 334-342
Reproduced with kind permission from Elsevier.



Photodynamic self–disinfecting surface using pyridinium phthalocyanine



Lijo George ^a, Alexander Müller ^b, Beate Röder ^b, Ville Santala ^a, Alexander Efimov ^{a,*}

^a Laboratory of Chemistry and Bioengineering, Tampere University of Technology, P. O. Box 541, 33101 Tampere, Finland

^b AG Photobiophysik, Humboldt-Universität zu Berlin, MNF, Institut für Physik, Newtonstrasse 15, 12489 Berlin, Raum 1'519, Germany

ARTICLE INFO

Article history:

Received 12 May 2017

Received in revised form

16 June 2017

Accepted 14 August 2017

Available online 17 August 2017

Keywords:

Antimicrobial

Self-disinfecting surface

Pyridinium phthalocyanine

Singlet oxygen

Photodynamic antimicrobial chemotherapy

ABSTRACT

We have synthesized novel phthalocyanine with four pyridyl substituents connected to α -phthalopositions via direct C–C bond. The Zn complex and tetracationic derivatives of phthalocyanine were also synthesized and the dyes were impregnated into filter paper to prepare photoactive antimicrobial surface. The photodynamic antimicrobial efficacy of the dyed paper samples was evaluated by a simple and fast setup using bioluminescent microbes. *Escherichia coli* and *Acinetobacter baylyi* ADP1 strains carrying bacterial luciferase genes were used in the screening experiment. The most efficient compound, tetracationic zinc derivative **8**, was investigated further. The compound was highly water soluble, had high molar absorptivity and exhibited good adhesion to the filter paper without leaching into the solution. The singlet oxygen quantum yield of tetracationic zinc derivative **8** in water was found out to be $30 \pm 20\%$. According to the cell viability assay test performed on *E. coli* wild type in solution, the molecule had similar or better photo toxicity as the reference photosensitizer, tetrakis (1-methyl-pyridinium-4-yl) porphyrin (TMPyP). Antimicrobial efficacy of the dye **8** on photoactive surface was studied by live cell assessment through colony forming unit (CFU) counting. The colored surface demonstrated 3 log reduction in CFU against *E. coli* and *A. baylyi* ADP1 just after 1 h of illumination with the white light of low intensity.

© 2017 Elsevier Ltd. All rights reserved.

1. Introduction

One of the major challenges of the 21st century is how to prevent the spread of life threatening epidemics. Nosocomial or Healthcare associated infections (HAI) account for the major source of transmission of infectious disease. Contaminated surfaces play a significant role in the spread of microbes. The contamination leads to the formation of biofilms, which facilitate microbial proliferation [1–6]. Together with the emergence of drug resistant bacteria, the risk is multiplied several times [7–13]. The so called “ESKAPE”-pathogens (*Enterococcus faecium*, *Staphylococcus aureus*, *Klebsiella pneumoniae*, *Acinetobacter baumannii*, *Pseudomonas aeruginosa* and *Enterobacter* strains) survive almost any individual antibiotic treatment [14]. Hence, in order to control the transmission of the pathogenic microorganism, new approaches are required.

One such approach is photodynamic antimicrobial chemotherapy (PACT), which has been found to be effective against drug

resistant bacteria and biofilms [15–19]. The term “photodynamic reaction” was introduced by Hv Tappeiner for inactivation of microbes by dyes in the presence of light; he also demonstrated the involvement of oxygen in the process [20,21]. Inactivation is achieved via the oxidative action of singlet oxygen produced by an organic dye upon light irradiation. Since the singlet oxygen can diffuse in liquids and air, as well as through cell wall [22,23], its applications are extended in the preparation of photoactive self-disinfecting surfaces such as coatings, films, polymers, paints for controlling microbial contamination [24–33], and to water sanitation [34]. Whether or not an organic dye is suitable for the purpose, depends first of all on the quantum yield of singlet oxygen generation, on extinction coefficient, photo- and thermal stability and appropriate wavelength absorptions. Additional properties, such as dark toxicity, redox potentials of excited states, lipophilicity and ionization degree must also be taken into consideration while selecting the photosensitizer [35–39].

Many organic dyes such as methylene blue, toluidine blue O, acridine, rose bengal, and various macrocyclic structures are capable of generating singlet oxygen [23,40,41]. In particular

* Corresponding author.

E-mail address: alexandre.efimov@tut.fi (A. Efimov).

porphyrins, such as haematoporphyrin and protoporphyrin and their various derivatives are excellent photosensitizers for treatment of microbes and malignant cells [42,43]. Complexes of phthalocyanines and naphthalocyanines also exhibit considerable photobiological activity against tumors [44]. The level of photo toxicity is strongly related to the size, charge, and hydrophobicity balance of the dye molecule [16,39]. It was found that cationic photosensitizers have higher activity than anionic or neutral ones against both Gram-negative and Gram-positive bacteria [45–48]. Such difference can be explained by the fact that even though photosensitizers are not required to penetrate into the cells, the electrostatic interaction between cationic dye and poly-anionic lipopolysaccharide layer of the cell wall structure of the bacteria may result in its destabilization and thus facilitates the subsequent photosensitization [33,49,50]. On the other hand, testing the photosensitizers is a long and time-consuming procedure. To the best of our knowledge, there is no fast and simple procedure for screening of potential photoactive molecules; this fact considerable restricts their development.

Inspired by the above observations, we synthesized novel tetrakis(α -phthalopyridyl) substituted phthalocyanine, its zinc complex and their tetracationic salts, which can serve as a potent photosensitizer for antimicrobial treatment. In our present work, a photoactive self-disinfecting surface was prepared by immobilizing the photosensitizer on to the filter paper by a simple technique. The surface hence prepared was found to be stable without any leaching into water. We also propose a simple and fast method to evaluate the antimicrobial efficacy of the surface using bioluminescent microbes. In addition, photo inactivation of the surface was also confirmed by conventional CFU counting method using two different microbes. However, we have also tested the phototoxic action of the dye in solutions.

2. Materials and methods

2.1. General methods

Reagents and solvents were purchased from TCI Europe, Sigma Aldrich Co. or from VWR and were used without further purifications unless otherwise mentioned. Purification of the products was carried out either by column chromatography on Silica gel 60 or Silica gel 100 (Merck) or on preparative TLC plates (Merck) coated with neutral aluminum oxide 60 F₂₅₄. NMR spectra were recorded using Varian Mercury 300 MHz spectrometer using TMS as internal standard. HRMS measurements were done with Waters LCT Premier XE ESI-TOF bench top mass spectrometer. Lock-mass correction (leucine enkephaline as a reference compound), centering and calibration were applied to the raw data to obtain accurate mass. UV-Vis absorption spectra were recorded using Shimadzu spectrophotometer.

2.2. Synthesis

The compounds 3-hydroxyphthalonitrile **1**, 2,3-dicyanophenyl trifluoromethanesulfonate **2** and 4-(5,5-dimethyl-1,3,2-dioxaborinan-2-yl) pyridine **3** were synthesized according to the literature procedure [51,52]. The synthetic route for compounds **2–8** were described in Scheme 1.

2.2.1. Synthesis of 3-(pyridin-4-yl) phthalonitrile **4**

Pyridine boronate ester **3** (120 mg, 0.628 mmol), triflate phthalonitrile **2** (174 mg, 0.628 mmol), PdCl₂(dppf)·DCM (26 mg, 0.0314 mmol), K₃PO₄ (400 mg, 1.884 mmol) was dissolved in a mixture of 7.5 ml water and 7.5 ml of toluene, and was heated at vigorous stirring at 90 °C for 2 h. The reaction mixture was

extracted with CHCl₃ and washed with brine, and dried over anhydrous Na₂SO₄. The solvent was evaporated under reduced pressure to yield 105 mg of a crude product. The pure product **4** was isolated by re-precipitating from CHCl₃/hexane. Yield 75 mg, 60%.

MS (ESI-TOF): [M+H]⁺ calcd for C₁₃H₇N₃, 206.0718; found, 206.0719. ¹H NMR (300 MHz, CDCl₃, TMS): δ = 8.83 (d, *J* = 5.86 Hz, 2 H), 7.93–7.77 (m, 3 H), 7.50 (d, *J* = 5.86 Hz, 2 H); ¹³C NMR (75 MHz, CDCl₃, 25 °C, TMS): δ = 150.65, 144.35, 143.77, 133.72, 133.26, 123.03, 117.81, 115.24, 114.54 ppm.

2.2.2. Synthesis of 1, 8, 15, 22-tetra(pyridin-4-yl)-29H,31H-phthalocyanine **5**

Freshly cut lithium shots (57 mg, 8.212 mmol) were dissolved in *n*-butanol (5.7 ml) at 90 °C under argon atmosphere. The reaction mixture was allowed to cool to room temperature and pyridine phthalonitrile **2** (80 mg, 0.3898 mmol) was added to the above solution under argon atmosphere. The mixture was stirred at 90 °C for 18 h. The product was extracted with CHCl₃ and washed with water several times until the pH of the aqueous layer was neutral. The organic layer was evaporated under reduced pressure to get a crude residue. The residue was washed with acetonitrile and purified by column chromatography (neutral alumina, 1% EtOH in CHCl₃) to yield free base phthalocyanine **5** (40 mg, 50%).

MS (ESI-TOF): [M+H]⁺ calcd for C₅₂H₃₀N₁₂, 823.2795; found, 823.2832. ¹H NMR (300 MHz, CDCl₃, TMS): δ = 9.01–8.95 (m, 5 H), 8.86–8.84 (m, 2 H), 8.60–8.59 (m, 6 H), 8.55–8.53 (m, 1 H), 8.35–8.33 (m, 1 H), 8.28–8.26 (m, 2 H), 8.11–8.08 (m, 1 H), 8.02–7.96 (m, 3 H), 7.86–7.80 (m, 8 H), 7.67–7.61 (m, 5 H), 7.57–7.51 (m, 7 H), 7.44–7.42 (m, 2 H), 1.65 (br, 1 H), 2.21 (br, 1 H). UV/Vis (CHCl₃): λ (ϵ) = 715 (100000), 680 nm (87037), 650 nm (31481), 615 nm (20370 L mol⁻¹cm⁻¹).

2.2.3. Synthesis [1,8,15,22-tetra(pyridin-4-yl)-29H,31H-phthalocyaninato(2-)- κ 4N29,N30,N31,N32]zinc **6**

Tetrapyrrolyl phthalocyanine free base **5** (12 mg, 0.0146 mmol) was dissolved in CHCl₃ (1.5 ml) and ZnOAc·2H₂O (12 mg, 0.0547 mmol) in 120 μ l H₂O was added into it. The reaction mixture was stirred at 60 °C for 2 h. The product was extracted with CHCl₃ (20 ml) and washed with water (25 ml x 3), dried over anhydrous Na₂SO₄ and evaporated under reduced pressure to yield crude residue. The product was purified with column chromatography. (Neutral alumina, 10% EtOH in CHCl₃) and later washed with diethyl ether and acetonitrile to yield a pure compound **6** (11 mg, 85%).

MS (ESI-TOF): [M+H]⁺ calcd for C₅₂H₂₈N₁₂Zn⁺, 885.1929; found, 885.1970. ¹H NMR (300 MHz, DMSO d₆, TMS): δ = 9.52–9.50 (m, 1 H), 9.10–9.06 (m, 2 H), 8.62 (br, 8 H), 8.45 (br, 2 H), 8.31 (br, 2 H), 8.16–8.14 (m, 1 H), 7.78–7.58 (m, 19 H). UV/Vis (CHCl₃): λ (ϵ) = 695 (113077), 634 nm (24615 L mol⁻¹cm⁻¹).

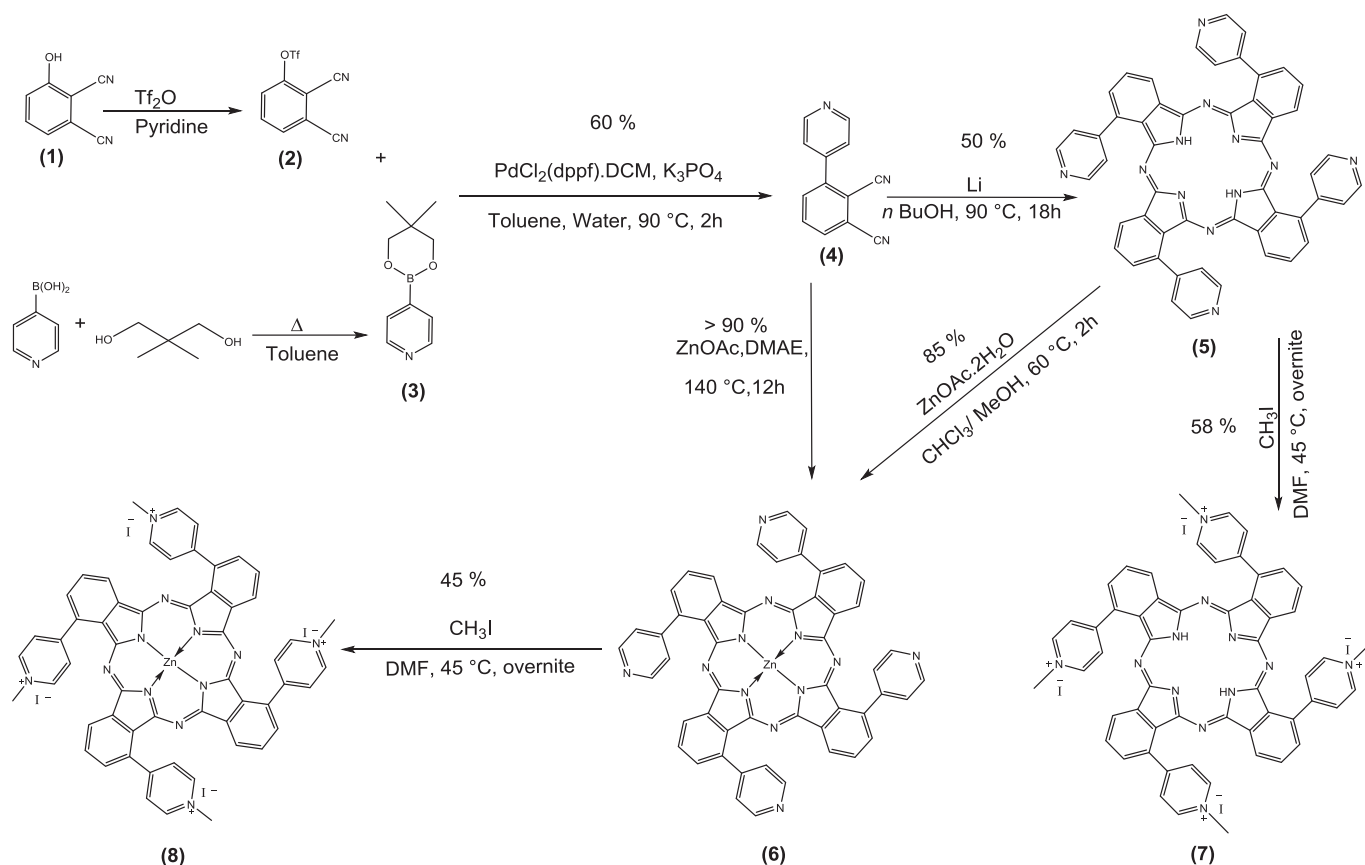
2.2.4. Synthesis of [1,8,15,22-tetra(pyridin-4-yl)-29H,31H-phthalocyaninato(2-)- κ 4N29,N30,N31,N32]zinc **6** (direct method)

A mixture of pyridine phthalonitrile **4** (77 mg, 0.3752 mmol) and anhydrous zinc acetate (84.67 mg, 0.4615 mmol) in dimethylaminoethanol (DMAE, 810 μ l) was heated at reflux at 140 °C for 12 h. The reaction mixture was cooled to room temperature and the product was precipitated by adding a mixture of MeOH/H₂O (9:1). The green solid was filtered and washed with methanol to yield the product **6** (80 mg, 96%).

MS (ESI-TOF): [M+H]⁺ calcd for C₅₂H₂₈N₁₂Zn⁺, 885.1929; found, 885.1904.

2.2.5. Synthesis of 4,4',4'',4'''-(29H,31H-phthalocyanine-1,8,15,22-tetra-yl)tetrakis(1-methylpyridinium) tetraiodide **7**

Phthalocyanine **5** (15 mg, 0.0182 mmol) was dissolved in DMF (3 ml) and methyl iodide (1 ml, 16.0642 mmol) was added into



Scheme 1. Synthetic route for the preparation of pyridine substituted phthalocyanine.

solution. The reaction mixture was stirred at 45 °C for 18 h. The reaction mixture was cooled in an ice bath and product was precipitated with diethyl ether (15 ml). The solid was filtered, washed with diethyl ether several times and later with acetone/diethyl ether to yield pure product **7** (14.8 mg, 58.32%).

MS (ESI-TOF): $[M-4I]^{4+}$ calcd for $C_{56}H_{38}N_{12}Zn^{4+}$, 220.5914; found, 220.5889; $[M-3I]^{3+}$ calcd for $C_{56}H_{39}IN_{12}Zn^{3+}$, 336.4233; found, 336.4204. 1H NMR (300 MHz, DMSO D_6 , TMS): δ = 9.69–9.55 (m, 5 H), 9.14–9.07 (m, 8 H), 8.77–8.69 (m, 6 H), 8.46–8.32 (m, 9 H), 4.88–4.61 (m, 12 H). UV/Vis (DMF): λ (ϵ) = 702 (141250), 635 nm ($28750 \text{ L mol}^{-1}\text{cm}^{-1}$).

2.2.6. Synthesis of $\{4,4',4'',4'''-(29H,31H\text{-phthalocyanine-1,8,15,22-tetrayl-}\kappa^4N29,N30,N31,N32)\text{tetraakis}[1\text{-methylpyridiniumato}(2-)]\}\text{zinc}(4+)\text{ tetraiodide } 8$

Tetrapyrindyl phthalocyanine zinc **6** (20 mg, 0.0225 mmol) was dissolved in DMF (3 ml), and methyl iodide (1 ml, 16.0642 mmol) was added to solution. The reaction mixture was stirred at 45 °C for 18 h. The reaction mixture was cooled in an ice bath and product was precipitated by adding diethyl ether (15 ml). The solid was filtered and washed several times with diethyl ether and later with mixture of acetone/ H_2O (1:1) to yield the product **8** (15 mg, 45.71%).

MS (ESI-TOF): $[M-4I]^{4+}$ calcd for $C_{56}H_{36}N_{12}Zn^{4+}$, 236.0698; found, 236.0692; $[M-3I]^{3+}$ calcd for $C_{56}H_{37}IN_{12}Zn^{3+}$, 357.0612; found, 357.0617. 1H NMR (300 MHz, DMSO D_6 , TMS): δ = 9.77–9.70 (m, 1 H), 9.95–9.54 (m, 5 H), 9.21–9.04 (m, 8 H), 8.76 (br, 3 H), 8.62 (br, 2 H), 8.46–8.35 (m, 6 H), 8.25–8.19 (m, 1 H), 4.85–4.59 (m, 12 H). UV/Vis (DMF): λ (ϵ) = 692 (128500), 625 nm ($22000 \text{ L mol}^{-1}\text{cm}^{-1}$).

2.3. Singlet oxygen measurement

Singlet oxygen kinetics were monitored in aqueous solution via time-correlated multi-photon counting (TCMPC) at $1270 \pm 15 \text{ nm}$, the characteristic singlet oxygen luminescence wavelength. For sample excitation, a LMD-405D diode laser (Omikron-Laserage, Rodgau-Dudenhofen, Germany) was used: excitation wavelength 405 nm, pulse width 120 ns, channel width 20 ns, average power 1.2 W, duration of measurement 60 s. A TCMPC-1270 Singlet Oxygen Luminescence Detection System by SHB Analytics (Berlin, Germany) was used for luminescence signal detection. Singlet oxygen quantum yields were determined indirectly from fitting the luminescence signal and using TMPyP, optical density adjusted for the excitation wavelength, as reference. [41] Fits of the data were conducted following the standard bi-exponential model for singlet oxygen kinetics and an additional mono-exponential phosphorescence term for TMPyP [53]. The goodness of the fit is indicated by the reduced χ^2 -test.

2.4. Antimicrobial tests

2.4.1. Screening test on dyed paper

The efficiency of dyes was screened by conducting antimicrobial test with bioluminescent bacterial strains *Escherichia coli* (XL1-Blue, Stratagene, USA) pBAV1C-T5-lux and *Acinetobacter baylyi* ADP1 (DSM 24193) carrying plasmid pBAV1C-T5-lux. The plasmid was constructed by replacing *gfp* with *lux* in pBAV1C-T5-GFP [54]. The lux operon was cloned from the pBAV1K-T5-lux plasmid, kind gift from Ichiro Matsumura (Addgene plasmid # 55800) [55] using standard BioBrick cloning. Whatman 1 filter papers (area

12.25 cm²) were soaked in solutions of dyes 5–8 (0.9 mg dye in 200 µl solvent) and allowed to dry out. After drying, three discs 0.5 cm in diameter were cut from each dyed paper and pasted on the LA agar gel plate (15 g/l agar, 10 g/l tryptone, 5 g/l yeast extract, 5 g/l NaCl, 0.2 % glucose, 25 µg/ml chloramphenicol) in a 3 × 4 grid. As shown in Fig. 1, each column contains 4 disks with dyes 5–8, while the rows contain disks of the same dye. A dark screen with a square hole was placed over the agar plate in such a way that, one column of the four dyes was under the dark area while the two other columns would be accessible for light. Blank control samples were prepared by cutting neat uncoloured filter papers of the same size and placing them in the dark and illuminated areas of LA agar plate. Background luminescence arising from the setup was recorded (Xenogen IVIS Lumina, Caliper Life Sciences, USA). Microbial strains were inoculated in 5 ml of LB medium (10 g/l tryptone, 5 g/l yeast extract, 5 g/l NaCl) containing 0.5% glucose and 25 µg/ml of chloramphenicol and incubated at 30 °C 300 rpm. After overnight cultivation, 100 µl of the culture was diluted with 5 ml of LB medium containing 0.5% glucose and 25 µg/ml of chloramphenicol and incubated for 3 h at 30 °C 300 rpm. Microbial solution thus prepared, was pipetted over the paper discs (5 µl per disk). To check the influence of filter paper on the bioluminescence of bacteria the microbial solution was pipetted as well straight on the agar in the dark region of the plate. Luminescence of the plate with microbes deposited was recorded by IVIS and the plate was subjected to illumination. The whole plate was placed inside solar simulator (Luzchem, Canada) and the light intensity was adjusted to 18 mW·cm⁻² by lifting the plate up/down. Two filters [KG3 band pass with 315–750 nm transmittance and YG-17 filter with transmittance > 485 nm] were placed over the square hole to remove the infrared and UV radiation. After 1 h of illumination, the luminescence was measured again, and the antimicrobial efficacy of dyes was compared.

2.4.2. Cell viability assay

For relative cell viability tests a resazurin assay was used [56]. Two different sample sets with *E. coli* wild type (ATCC 25922) cell suspension in PBS (approx. 4 × 10⁸ cfu/ml) were incubated for 2 h under standard ambient temperature in the dark and under low white-light illumination conditions (fluence rate of 8 ± 2 mW cm⁻²). First set: 200 µl cell suspension on M9-minimal-agar substrate in 24-well-plates. Second set: 1 ml cell suspension without any agar in 24-well-plates. A photosensitizer

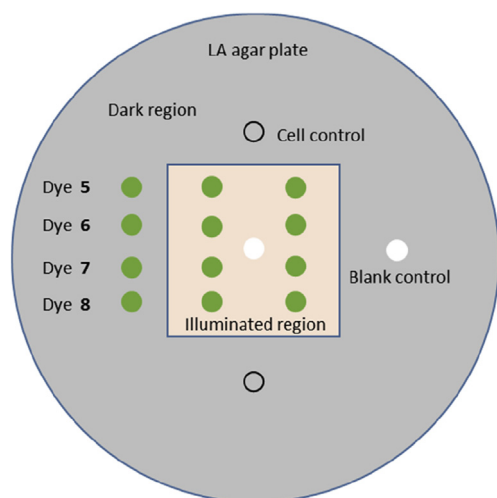


Fig. 1. Schematic diagram of the setup for screening dyes.

concentration of 5 µM was used. After addition of the resazurin reactant (for each well 900 µl of 0.05 g/l Resazurin sodium salt, Sigma-Aldrich, Germany) all samples were incubated for another 4 h in the dark under gentle stirring. The relative viability was then determined from resorufin fluorescence using a VICTOR³ plate reader, PerkinElmer Inc., USA. Per sample, three wells were used measuring each well nine times.

2.4.3. Determination of optimal dye loading on filter paper

The filter papers with different dye loading of were prepared in the following way. First four solutions of phthalocyanine 8 (1 mg, 0.5 mg, 0.25 mg and 0.1 mg) in 200 µl milli Q water was prepared in 4 different vials. Whatman 1 filter paper of size 3.5 cm × 3.5 cm (12.25 cm²) soaked in the solution containing 1 mg dye gives 0.081 mg/cm² dye loading. The filter paper of same size soaked in 0.5 mg dye solution gives loading of 0.04 mg/cm². Similarly, 0.25 mg dye solution and 0.1 mg dye solution gives dye loading of 0.02 mg/cm² and 0.008 mg/cm² respectively. A filter paper of same size without dye was kept as a control.

Antimicrobial efficiency of the filter papers was confirmed by live cell assessment through CFU counts using microbe *Acinetobacter baylyi* ADP1 (ATCC 33305). Microbial strain was inoculated in a solution of 5 ml of LB medium and supplemented with 1% glucose at 30 °C and 300 rpm overnight. The overnight-cultivated solution (100 µl) was diluted with 5 ml of LB medium and 1% glucose and shaken (300 rpm) at 30 °C for 3 h. The optical density of culture was measured at 600 nm. The microbial solution was centrifuged for 5 min at 6500 rpm and the LB medium was decanted out from the vial. The residual microbes were suspended in 5 ml of PBS (phosphate-buffered saline) buffer. Circular discs (cut from filter papers of different dye loading and control paper) were placed in the wells of a microplate and microbial solution (25 µl) was pipetted over the disks. The microplate was illuminated in the solar simulator for 1 h. UV and IR radiations were cut off using a combination of KG3 band pass filter (315–750 nm transmittance) and YG-17 filter (transmittance > 485 nm) and the overall light intensity kept at 18 mW cm⁻². After 1 h of illumination, the microbes were extracted from wells with 975 µl of LB medium and serial dilutions (up to two times) were made from each extract. The dilutions were then plated on LA agar plates (15 g/l agar, 10 g/l tryptone, 5 g/l yeast extract, 5 g/l NaCl, 0.2 % glucose) and incubated at 30 °C overnight. The number of colonies grown on the agar plate were counted and CFUs per milliliter were calculated from it and the filter paper with optimal dye loading was determined from it.

2.4.4. Determination of antimicrobial efficacy of dyed-filter paper

The *E. coli* MG1655 (*E. coli* Genetic Resources at Yale) and *Acinetobacter baylyi* ADP1 (ATCC 33305) strains were used in determining antimicrobial efficacy. The cultivations and resuspensions were carried out as described above. Two sets of paper discs (original and duplicate), with phthalocyanine 8 and an uncoloured blank control, were placed in the wells of a microplate and microbial solution (25 µl) was pipetted over the disks. The microplate was illuminated in the solar simulator for 1 h. UV and IR radiations were cut off using a combination of KG3 band pass filter (315–750 nm transmittance) and YG-17 filter (transmittance > 485 nm) and the overall light intensity kept at 18 mW cm⁻². Dark control samples were prepared by depositing microbial medium over dyed and uncoloured disks and keeping the microplate in dark for 1 h at room temperature inside the laminar hood. After 1 h of illumination or incubation, the microbes were extracted from wells with 975 µl of LB medium (10 g/l tryptone, 5 g/l yeast extract, 5 g/l NaCl) and serial dilutions (up to 10⁻⁶) were made from each extract. The dilutions were then plated on LA agar plates (15 g/l agar, 10 g/l tryptone, 5 g/l yeast extract, 5 g/l NaCl, 0.2

% glucose) and incubated at 30 °C overnight. The number of colonies grown on the agar plate was counted and CFUs per milliliter were calculated to determine the antimicrobial efficacy.

3. Results and discussion

3.1. Synthesis

Photodynamic antimicrobial activities of pyridine substituted phthalocyanines are already known [57,58]. However most of these compounds describe substitution in beta-phthalo position via oxy or thio-bridge. In the present work, we give a first example of direct C-C link between the α -phthalo position and pyridine unit. Novel pyridine-containing phthalocyanine and its zinc complex were synthesized according to Scheme 1. The triflate phthalonitrile **2** was prepared from 3-hydroxy phthalonitrile **1** which in turn synthesized from commercially available 3-nitro phthalonitrile by following the literature procedures reported elsewhere [51,52]. Pyridine phthalonitrile **4** was prepared with 80% yield by coupling pyridine boronate ester **3** and triflate phthalonitrile **2**. It should be mentioned that the coupling reaction between commercially available pyridine boronic acid and triflate phthalonitrile **2** did not produce reasonable yield of pyridine phthalonitrile. Therefore, pyridine boronic acid was converted into boronate ester **3** by reacting with neopentyl glycol. When the reaction was accomplished in the presence of molecular sieves, the ester **3** precipitated in 1,4-dioxane at room temperature and its separation from the molecular sieves was difficult. Therefore, we used the azeotropic distillation in the synthesis and obtained boronic ester **3** with high yield (ca. 80%). Free base phthalocyanine **5** was prepared by the tetramerization of pyridine phthalonitrile **4** with 50% yield. The zinc complex **6** was synthesized by reacting free base phthalocyanine **5** with zinc acetate in a mixture of chloroform and methanol with a yield of around 85%. Nonetheless, direct synthesis of zinc complex **6** produced better overall yield than converting free base phthalocyanine **5** [58].

The free base **5** and phthalocyanines zinc complex **6** were converted into cationic salts **7** and **8** respectively by methylation with iodomethane in DMF. High-resolution MS spectrometry was used to identify the molecules. The 0.25 Da separation between the peaks in the MS signals confirmed the tetra cationic charge of the molecule. However, since the substance was a mixture of regioisomers, NMR spectra were rather broad and difficult to interpret (see SI).

UV-visible absorption spectra were measured in chloroform (for **5** and **6**) and DMF (**7** and **8**) and shown in Fig. 2. The Q band peak for

free base phthalocyanine **5** was split into two when compared to corresponding zinc phthalocyanine **6** [59]. However, broadening of the peaks after methylation for the free base cationic phthalocyanine **7** indicates the aggregation.

Overall, we synthesized a novel phthalocyanine with pyridyl substituents at α phthalo positions through direct C-C linkage. Cationic tetra salts were found to be soluble in water, ethanol, could be easily precipitated into a solid, and gave a clear mass-spectrum, which suggests good degree of quaternization. Integrals of $^1\text{H-NMR}$ signals support a good purity of the obtained salt, though the signals are broad indeed.

3.2. Singlet oxygen quantum yield

Quantitative measurement of singlet oxygen for cationic zinc phthalocyanine **8** was done in water (shown in Fig. 3). The singlet oxygen quantum yield of phthalocyanine **8** was calculated to be $30 \pm 20\%$ by comparing the phosphorescence signal intensity at 1270 nm of with that of TMPyP as reference with a quantum yield of 74% [41]. This value was reasonably good since water was known to quench the singlet oxygen [60]. However, cationic pyridine free base phthalocyanine **7** did not produce any signal for singlet oxygen in water. Most probable reason may be the aggregation of the molecule in water as previously explained in the discussion of UV-visible absorption spectra.

3.3. Screening of dyes' efficiency

In our search for surfaces with photodynamic antimicrobial effect, we decided to identify the most efficient dye from the set of synthesized phthalocyanines, by comparing its antimicrobial capability on a solid support. In particular, the dyes **7** and **8** were highly soluble in water and readily adsorbed to the filter paper to form stable and permanent color. The leaching of the dyes to the medium was tested in by sonicating a piece of the filter paper impregnated with cationic phthalocyanines (**7** and **8**) in 3 ml of milli Q water for 30 min. The UV visible absorption measurement of the resultant water sample did not show any indication of the dye in the water nor the color of the filter paper faded out after 30 min of sonication. Moreover, even an overnight incubation of filter paper in milli Q water at room temperature did not induce leaching of the dye into water. Leaching was observed only after acidifying the extraction water down to pH 2. In this case, phthalocyanine tetra salts were obviously extracted into water, however not completely.

As we had four dyes to test, we needed a simple and rapid way of

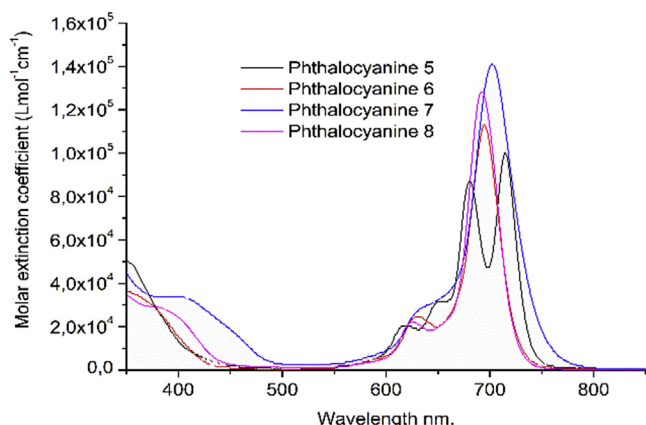


Fig. 2. UV-visible absorption spectra of phthalocyanines.

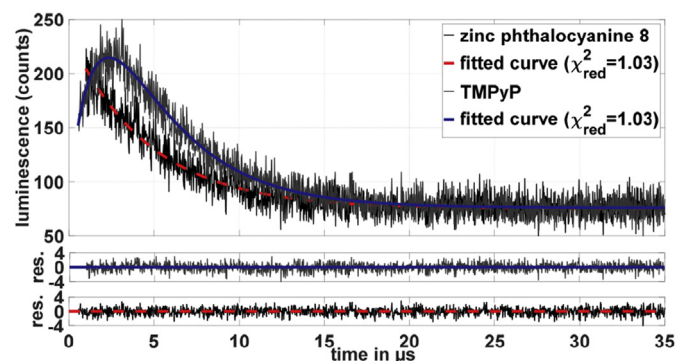


Fig. 3. Time resolved singlet oxygen measurement of TMPyP and cationic zinc phthalocyanine **8**. The optical density of TMPyP is adjusted for the excitation wavelength at 405 nm. Pearson residuals illustrate the goodness of the fit (reduced chi-squared below 1.04 for both fits). No distinct signal for cationic free base phthalocyanine **7** could be observed.

evaluation of the phototoxic effect. One possibility to identify the efficient photosensitizer was to use bioluminescent bacteria as reporter cells. The bioluminescence-based screening method has been applied in multiple studies [61] as it allows a growth-independent and sensitive monitoring of toxic effects of different agents on the cells. The intensity of bioluminescence arising from the bacteria on a surface is directly related to the metabolic status of the bioluminescent bacteria [58]. In other words, when an efficient dye effectively inactivates bioluminescent microbes, we expect a sharp decrease in the signal intensity. The bioluminescence arising from surface of filter paper soaked with bioluminescent *E. coli* cell solution was recorded before and after illumination as shown in Fig. 4a. As expected, surfaces with cationic derivatives **7** and **8** were more effective against *E. coli*. Moreover, cationic zinc derivative **8** had shown higher efficacy than free base phthalocyanine **7**. It should be noted that the bioluminescence from the paper with dye **8** incubated in the dark region of the plate was also reduced. However, this decrease may not necessarily arise from the dark toxicity of the substance, but rather can be attributed to the photo toxicity induced by the stray light, since the incubation was done in the same plate.

Similar test was conducted using filter paper soaked with more resistant bacteria - bioluminescent *Acinetobacter baylyi* ADP1 carrying plasmid pBAV1C-T5-lux. In this case, the phthalocyanines (**6**, **7** and **8**) showed much activity (Fig. 5). However, the cationic zinc derivative was far more efficient in inactivation of microbes. This time also the signal from the filter paper incubated in the dark region was absent probably due to the stray light exposure. These experiments concluded that tetra cationic derivatives of pyridine phthalocyanines (**7** and **8**) are more efficient dyes compared to the neutral ones. The extra cationic charges of the molecules might have played an important role in binding the gram negative bacteria towards the surface of the filter paper there by ensuring a better photodynamic inactivation.

3.4. Cell viability assay

In order to understand the antimicrobial efficacy of the

photosensitizers directly in a medium without substrate support, the cell viability assay of both cationic derivatives (**7** and **8**) were tested in M9-agar medium and PBS suspension. The results concluded that cationic zinc phthalocyanine **8** was highly phototoxic towards *E. coli* wild type upon 2 h of illumination. The antimicrobial efficacy of the compound was found to be superior to that of the reference photosensitizer tetrakis(methylpyridinium iodide) porphyrin TMPyP. However, the free base cationic phthalocyanine **7** had comparable phototoxicity to that of reference photosensitizer. The results are presented in Fig. 6.

3.5. Live cell assessment through colony forming unit (CFU) counting

All the above-mentioned tests pointed out that cationic zinc derivative **8** was best among the set of phthalocyanines synthesized. Therefore, antimicrobial efficacy of the filter paper impregnated with phthalocyanine **8** was determined by CFU counting. In order to control the growth of microbes during the illumination experiment and on serial dilution, the LB medium was replaced with PBS before the deposition on the filter paper. It must be mentioned that the paper impregnated with the photosensitizer **8** was highly toxic towards both *E. coli* and *A. baylyi*. If the dye loading was higher than 0.008 mg/cm^2 , no any single bacterial colony could be found on LA plates plated with the microbial extracts from the illuminated filter papers even after overnight incubation (Table 1).

Hence, the filter paper with dye loading 0.008 mg/cm^2 was found to be optimal for activity testing and was used for further experiments. The optical densities of the microbial solutions measured before deposition on the filter paper was 0.2 and 0.1 for *E. coli* and *A. baylyi* respectively. Thus, the higher number of colonies of *E. coli* compared to *A. baylyi* grown after plating agree with the absorbance values. We have found that photo inactivation against *E. coli* was as high as 2.7 log reduction in CFU, whereas the phototoxic effect against *A. baylyi* demonstrated 3.4 log reduction in CFU (Fig. 7).

These values are very well comparable with the best results reported in literature for the dyes immobilized on similar surfaces.

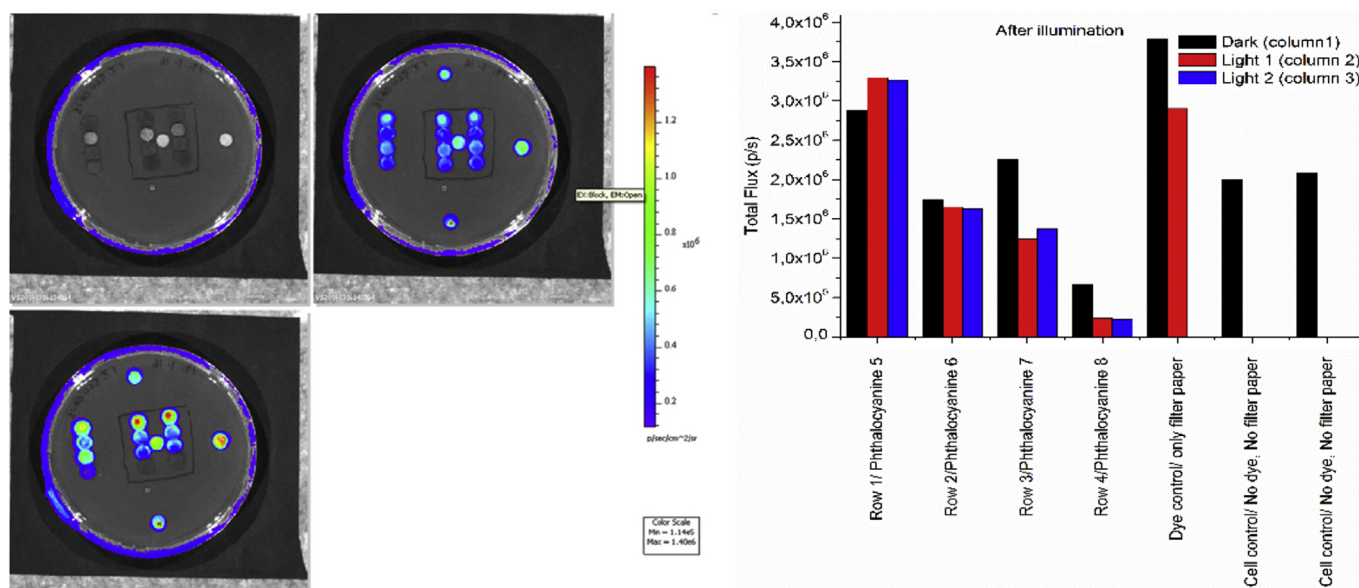


Fig. 4. (a) Bioluminescent images of *E. coli* (carrying pBAV1C-T5-lux plasmid) on surface, before and after illumination (clock wise direction: background image, before illumination, after illumination). (b) Graph showing the antibacterial activity of the phthalocyanine after illumination for 1 h with light of intensity 18 mW cm^{-2} and wavelength 485–750 nm. The data and graphs for back ground luminescence and before illumination were shown in supplementary information.

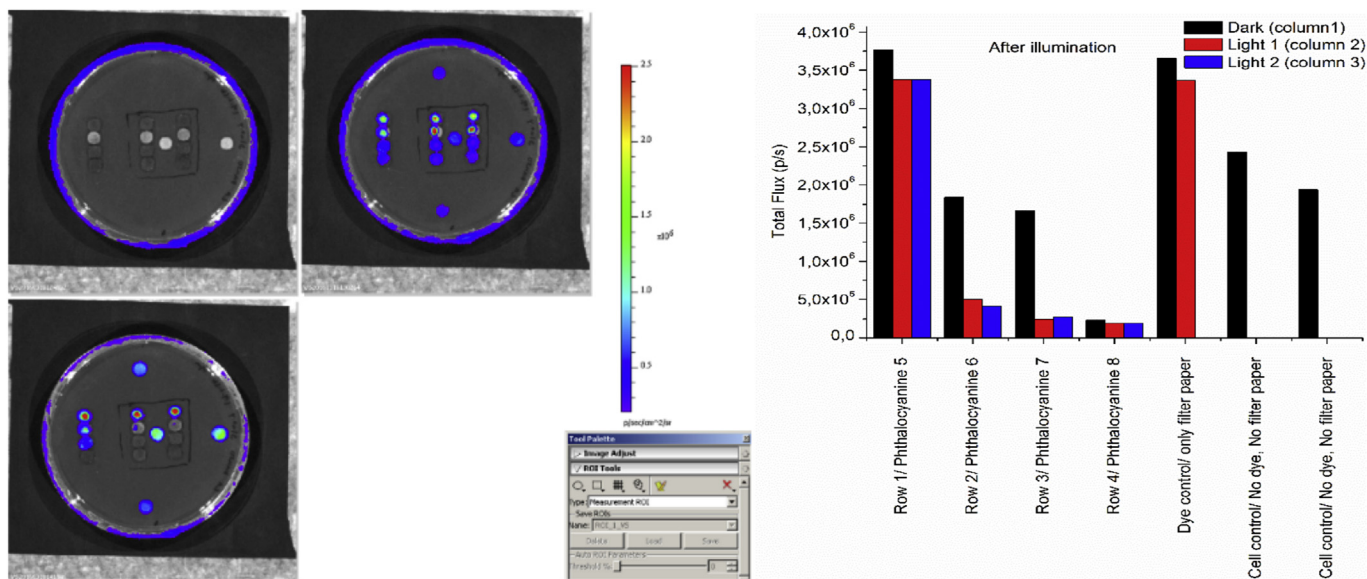


Fig. 5. (a) Bioluminescent images of *Acinetobacter baylyi* ADP1 (carrying plasmid pBAVIC-T5-lux) on surface, before and after illumination (clock wise direction: background image, before illumination, after illumination). (b) Graph showing the antibacterial activity of the phthalocyanine after illumination for 1 h with light of intensity 18 mW cm^{-2} and wavelength 485–750 nm. The data and graphs for back ground luminescence and before illumination were shown in supplementary information.

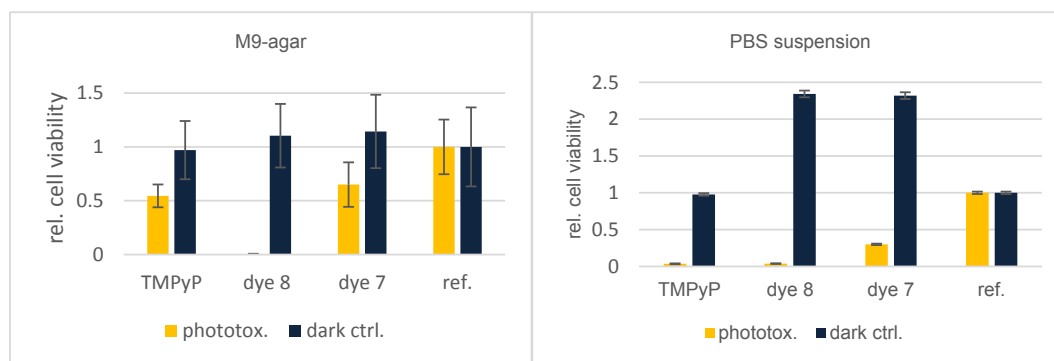


Fig. 6. Relative cell viability was measured on M9-Agar (minimal medium for *E. coli*) and directly in PBS suspension. The values are normalized with the reference (bacteria without any photosensitizers) fluorescence. The photosensitizer concentration is $5 \mu\text{M}$. Error bars result from standard deviation and error propagation. Phototox.: illuminated samples, dark ctrl.: dark controls.

Table 1
Photoinactivation of *A. baylyi* under illumination.

Dye loading	Number of Colonies	
	1st dilution	2nd dilution
0.08 mg/cm ²	0	0
0.04 mg/cm ²	0	0
0.02 mg/cm ²	0	0
0.008 mg/cm ²	20	1
Control	Too many to count	Too many to count

Ringot et al. prepared photoactive cotton fabrics by covalently grafting anionic, neutral, and cationic amino porphyrins on cotton fabric via 1,3,5-triazine linker (dye load 18 mg/g of substrate). When subjected to light irradiation of 0.16 mW/cm^2 for 24 h (total light dose 13.8 J/cm^2), the cationic fabric exhibited 100% photo inactivation against gram-positive bacteria (*Staphylococcus aureus*) while did not show any activity against gram-negative bacteria (*E. coli*) [62]. Porphyrin-grafted filter paper through 1,3,5-triazine linker was prepared by Mbakidi et al. The substrate demonstrated antimicrobial activity of 4 and 2 log decrease in CFU against both

S.aureus and *E.coli* respectively under same illumination condition as mentioned above [63]. In these experiments the dye load was 19 mg/g of substrate ($0.03 \mu\text{mol/mg}$, MW = 672). Similarly Carpenter et al. was able to achieve photo inactivation of 4 log CFU reduction against different types of bacterial strains using porphyrin linked covalently to cellulose paper with the dye load ca. 8 mg/g (12.4 nmol/mg , MW = 672), and with the illumination intensity of $65 \pm 5 \text{ mW/cm}^2$ for 30 min (total light dose 117 J/cm^2) [64]. In our case, similar activity was achieved with the white light dose 64.8 J/cm^2 (1 h at 18 mW/cm^2) and the dye load of 1.2 mg/g of substrate (0.008 mg/cm^2 , paper density 68.8 g/m^2 , Fig. S16) prepared by a simple method without any complex chemical modifications.

4. Conclusions

Novel phthalocyanine with pyridine substitution at α -position, its zinc complexes and cationic derivatives were synthesized in high yield. The dyes exhibited good dyeing ability on filter paper, good stability against leaching, and good photostability. We have elaborated a fast and simple screening setup for testing the

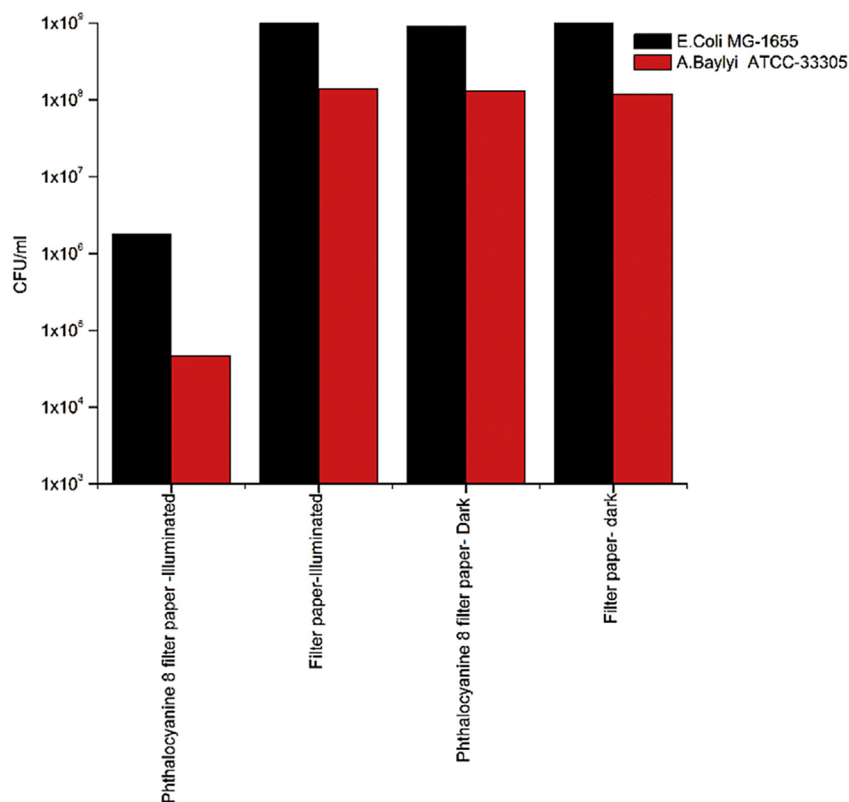


Fig. 7. Antimicrobial efficacy of filter paper dyed with phthalocyanine 8 against *E. coli* and *A. baylyi* after illumination for 1 h with light of intensity 18 mW cm⁻² and wavelength 485–750 nm.

photodynamic antimicrobial substances using bioluminescent bacteria *E. coli* and *A. baylyi*. We applied the method to study the antimicrobial efficacy of self-disinfecting surfaces prepared from the dyes. The tetracationic derivatives were found to be the most efficient. Cell viability assay in M9 agar medium and PBS suspension clearly demonstrated the superior photo toxicity of cationic zinc derivative of pyridine phthalocyanine **8**. Finally, the antimicrobial activity using the filter paper dyed with the photosensitizer **8** was studied by CFU counting method. We have achieved 2.7 log CFU reduction against *E. coli* and 3.4 log CFU reduction against *A. baylyi*, respectively, which is comparable with the best results reported to date.

Further study using different metal complexes of pyridine phthalocyanine and substrates for immobilization of the photosensitizer are under progress.

Acknowledgements

This research was funded by the Graduate School of Tampere University of Technology.

Appendix A. Supplementary data

Supplementary data related to this article can be found at <http://dx.doi.org/10.1016/j.dyepig.2017.08.021>.

References

- [1] Cloutier M, Mantovani D, Rosei F. Antibacterial Coatings: challenges, perspectives, and opportunities. *Trends Biotechnol* 2015;33:637–52. <http://dx.doi.org/10.1016/j.tibtech.2015.09.002>.
- [2] Fijan S, Turk SS. Hospital textiles, are they a possible vehicle for healthcare-associated infections? *Int J Environ Res Public Health* 2012;9:3330–43. <http://dx.doi.org/10.3390/ijerph9093330>.
- [3] Donlan RM. Biofilm formation: a clinically relevant microbiological process. *Clin Infect Dis* 2001;33:1387–92. <http://dx.doi.org/10.1086/322972>.
- [4] Bazaka K, Jacob MV, Crawford RJ, Ivanova EP. Efficient surface modification of biomaterial to prevent biofilm formation and the attachment of microorganisms. *Appl Microbiol Biotechnol* 2012;95:299–311. <http://dx.doi.org/10.1007/s00253-012-4144-7>.
- [5] Chung KK, Schumacher JF, Sampson EM, Burne RA, Antonelli PJ, Brennan AB. Impact of engineered surface microtopography on biofilm formation of *Staphylococcus aureus*. *Biointerphases* 2007;2:89–94. <http://dx.doi.org/10.1116/1.2751405>.
- [6] Knetsch MLW, Koole LH. New strategies in the development of antimicrobial coatings: the example of increasing usage of silver and silver nanoparticles. *Polym (Basel)* 2011;3:340–66. <http://dx.doi.org/10.3390/polym3010340>.
- [7] Grundmann H, Aires-de-Sousa M, Boyce J, Tiemersma E. Emergence and resurgence of methicillin-resistant *Staphylococcus aureus* as a public-health threat. *Lancet* 2006;368:874–85. [http://dx.doi.org/10.1016/S0140-6736\(06\)68853-3](http://dx.doi.org/10.1016/S0140-6736(06)68853-3).
- [8] Klein E, Smith DL, Laxminarayan R. Hospitalizations and deaths caused by methicillin-resistant *Staphylococcus aureus*, United States, 1999–2005. *Emerg Infect Dis* 2007;13:1840–6. <http://dx.doi.org/10.3201/eid1312.070629>.
- [9] Rossolini GM, Mantengoli E. Antimicrobial resistance in Europe and its potential impact on empirical therapy. *Clin Microbiol Infect* 2008;14:2–8. <http://dx.doi.org/10.1111/j.1469-0691.2008.02126.x>.
- [10] Healy MA. “slow catastrophe” unfolds as the golden age of antibiotics comes to an end. *Los Angl Times* 12.07.2016:A7. <http://www.latimes.com/science/sciencenow/la-sci-antibiotic-resistance-20160711-snap-story.html>.
- [11] Van Duin D, Van Delden C. Multidrug-resistant gram-negative bacteria infections in solid organ transplantation. *Am J Transpl* 2013;13:31–41. <http://dx.doi.org/10.1111/ajt.12096>.
- [12] Cervera C, van Delden C, Gavaldd?? J, Welte T, Akova M, Carratala?? J. Multidrug-resistant bacteria in solid organ transplant recipients. *Clin Microbiol Infect* 2014;20:49–73. <http://dx.doi.org/10.1111/1469-0691.12687>.
- [13] Lewis JD, Sifri CD. Multidrug-resistant bacterial donor-derived infections in solid organ transplantation. *Curr Infect Dis Rep* 2016;18. <http://dx.doi.org/10.1007/s11908-016-0526-9>.
- [14] Maisch T. Strategies to optimize photosensitizers for photodynamic inactivation of bacteria. *J Photochem Photobiol B Biol* 2015;150:2–10. <http://dx.doi.org/10.1016/j.jphotobiol.2015.05.010>.
- [15] Wainwright M. Photodynamic antimicrobial chemotherapy (PACT). *J Antimicrob Chemother* 1998;42:13–28. <http://dx.doi.org/10.1093/jac>

- 42.1.13.
- [16] Maisch T. Resistance in antimicrobial photodynamic inactivation of bacteria. *Photochem Photobiol Sci* 2015;14:1518–26. <http://dx.doi.org/10.1039/c5pp00037h>.
- [17] Cieplik F, Tabenski L, Buchalla W, Maisch T. Antimicrobial photodynamic therapy for inactivation of biofilms formed by oral key pathogens. *Front Microbiol* 2014;5:1–17. <http://dx.doi.org/10.3389/fmicb.2014.00405>.
- [18] Wainwright M. Photodynamic medicine and infection control. *J Antimicrob Chemother* 2012;67:787–8. <http://dx.doi.org/10.1093/jac/dkr562>.
- [19] Maisch T, Hackbarth S, Regensburger J, Felgenträger A, Bäuml W, Landthaler M, et al. Photodynamic inactivation of multi-resistant bacteria (PIB) – a new approach to treat superficial infections in the 21st century. *JDDG - J Ger Soc Dermatol* 2011;9:360–6. <http://dx.doi.org/10.1111/j.1610-0387.2010.07577.x>.
- [20] Maisch T. Anti-microbial photodynamic therapy: useful in the future? *Lasers Med Sci* 2007;22:83–91. <http://dx.doi.org/10.1007/s10103-006-0409-7>.
- [21] Rajesh S, Koshi E, Philip K, Mohan A. Antimicrobial activity of nanoparticle calcium hydroxide against enterococcus faecalis: an in vitro study. *J Indian Soc Periodontol* 2011;15:323–7. <http://dx.doi.org/10.4103/0972>.
- [22] Redmond RW, Kochevar IE. Spatially resolved cellular responses to singlet oxygen. *Photochem Photobiol* 2006;82:1178–86. <http://dx.doi.org/10.1562/2006-04-14-1R-874>.
- [23] DeRosa MC, Crutchley RJ. Photosensitized singlet oxygen and its applications. *Coord Chem Rev* 2002;233–234:351–71. [http://dx.doi.org/10.1016/S0010-8545\(02\)00034-6](http://dx.doi.org/10.1016/S0010-8545(02)00034-6).
- [24] Wilson M. Light-activated antimicrobial coating for the continuous disinfection of surfaces. *Infect Control Hosp Epidemiol* 2003;24:782–4. <http://dx.doi.org/10.1086/502136>.
- [25] Decraene V, Pratten J, Wilson M. Cellulose acetate containing toluidine blue and rose bengal is an effective antimicrobial coating when exposed to white light. *Appl Environ Microbiol* 2006;72:4436–9. <http://dx.doi.org/10.1128/AEM.02945-05>.
- [26] Decraene V, Pratten J, Wilson M. An assessment of the activity of a novel light-activated antimicrobial coating in a clinical environment. *Infect Control Hosp Epidemiol* 2008;29:1181–4. <http://dx.doi.org/10.1086/592413>.
- [27] Decraene V, Pratten J, Wilson M. Novel light-activated antimicrobial coatings are effective against surface-deposited *Staphylococcus aureus*. *Curr Microbiol* 2008;57:269–73. <http://dx.doi.org/10.1007/s00284-008-9188-7>.
- [28] Felgenträger A, Maisch T, Späth A, Schröder J a, Bäuml W. Singlet oxygen generation in porphyrin-doped polymeric surface coating enables antimicrobial effects on *Staphylococcus aureus*. *Phys Chem Chem Phys* 2014;16:20598–607. <http://dx.doi.org/10.1039/c4cp02439g>.
- [29] Ballatore MB, Durantini J, Gsponer NS, Suarez MB, Gervaldo M, Otero L, et al. Photodynamic inactivation of bacteria using novel electrogenerated porphyrin-fullerene C60 polymeric films. *Environ Sci Technol* 2015;49:7456–63. <http://dx.doi.org/10.1021/acs.est.5b01407>.
- [30] Brovko L, Anany H, Bayoumi M, Giang K, Kunkel E, Lim E, et al. Antimicrobial light-activated materials: towards application for food and environmental safety. *J Appl Microbiol* 2014;117:1260–6. <http://dx.doi.org/10.1111/jam.12622>.
- [31] Noimark S, Dunnill CW, Parkin IP. Shining light on materials – a self-sterilising revolution. *Adv Drug Deliv Rev* 2013;65:570–80. <http://dx.doi.org/10.1016/j.addr.2012.07.003>.
- [32] Spagnul C, Turner LC, Boyle RW. Immobilized photosensitizers for antimicrobial applications. *J Photochem Photobiol B Biol* 2015;150:11–30. <http://dx.doi.org/10.1016/j.jphotobiol.2015.04.021>.
- [33] Preuß A, Bornhütter T, Färber A, Schaller C, Röder B. Photodynamic inactivation of biofilm building microorganisms by photoactive facade paints. *J Photochem Photobiol B Biol* 2016;160:79–85. <http://dx.doi.org/10.1016/j.jphotobiol.2016.04.008>.
- [34] Bonnett R, Krysteva MA, Lalov IG, Artarsky SV. Water disinfection using photosensitizers immobilized on chitosan. *Water Res* 2006;40:1269–75. <http://dx.doi.org/10.1016/j.watres.2006.01.014>.
- [35] Huang ZA. Review of progress in clinical photodynamic therapy. *Technol Cancer Res Treat* 2005;4:283–93. <http://dx.doi.org/10.1016/j.immuni.2010.12.017.Two-stage>.
- [36] Siraj N, Kolic PE, Regmi BP, Warner IM. Strategy for tuning the photophysical properties of photosensitizers for use in photodynamic therapy. *Chem - A Eur J* 2015;21:14440–6. <http://dx.doi.org/10.1002/chem.201501686>.
- [37] Benov L. Photodynamic therapy: current status and future directions. *Med Princ Pract* 2015;24:14–28. <http://dx.doi.org/10.1159/000362416>.
- [38] Mantareva V, Kussovski V, Angelov I, Borisova E, Avramov L, Schnurpfel G, et al. Photodynamic activity of water-soluble phthalocyanine zinc(II) complexes against pathogenic microorganisms. *Bioorg Med Chem* 2007;15:4829–35. <http://dx.doi.org/10.1016/j.bmc.2007.04.069>.
- [39] Castano AP, Demidova TN, Hamblin MR. Mechanisms in photodynamic therapy: part one-photosensitizers, photochemistry and cellular localization. *Photodiagnosis Photodyn Ther* 2004;1:279–93. [http://dx.doi.org/10.1016/S1572-1000\(05\)00007-4](http://dx.doi.org/10.1016/S1572-1000(05)00007-4).
- [40] Redmond RW, Gamlin JN. A compilation of singlet oxygen yields from biologically relevant molecules. *Photochem Photobiol* 1999;70:391–475. <http://dx.doi.org/10.1111/j.1751-1097.1999.tb08240.x>.
- [41] Wilkinson F, Helman WP, Ross AB. Quantum yields for the photosensitized formation of the lowest electronically excited singlet state of molecular oxygen in solution. *J Phys Chem Ref Data* 1993;22:113–262. <http://dx.doi.org/10.1063/1.555934>.
- [42] Stojiljkovic I, Evavold BD, Kumar V. Antimicrobial properties of porphyrins. *Expert Opin Investig Drugs* 2001;10:309–20. <http://dx.doi.org/10.1517/13543784.10.2.309>.
- [43] La Penna M, Alvarez MG, Yslas EI, Rivarola V, Durantini EN. Photodynamic activity of 5,10,15,20-tetrakis(4-methoxyphenyl)porphyrin on the Hep-2 human carcinoma cell line: effect of light dose and wavelength range. *Bioorg Chem* 2001;29:130–9. <http://dx.doi.org/10.1006/bioo.2001.1204>.
- [44] Staicu A, Pascu A, Nuta A, Sorescu A, Raditoiu V, Pascu ML. Studies about phthalocyanine photosensitizers to be used in photodynamic therapy. *Rom Rep Phys* 2013;65:1032–51.
- [45] Carvalho CMB, Gomes ATPC, Fernandes SCD, Prata ACB, Almeida MA, Cunha MA, et al. Photoinactivation of bacteria in wastewater by porphyrins: bacterial β -galactosidase activity and leucine-uptake as methods to monitor the process. *J Photochem Photobiol B Biol* 2007;88:112–8. <http://dx.doi.org/10.1016/j.jphotobiol.2007.04.015>.
- [46] Alves E, Costa L, Carvalho CMB, Tomé JPC, Faustino MA, Neves MGPMS, et al. Charge effect on the photoinactivation of Gram-negative and Gram-positive bacteria by cationic meso-substituted porphyrins. *BMC Microbiol* 2009;9:70. <http://dx.doi.org/10.1186/1471-2180-9-70>.
- [47] Osifeko OL, Nyokong T. Applications of lead phthalocyanines embedded in electropun fibers for the photoinactivation of *Escherichia coli* in water. *Dye Pigment* 2014;111:8–15. <http://dx.doi.org/10.1016/j.dyepig.2014.05.010>.
- [48] Milanesio ME, Alvarez MG, Silber JJ, Rivarola V, Durantini EN. Photodynamic activity of monocationic and non-charged methoxyphenylporphyrin derivatives in homogeneous and biological media. *Photochem Photobiol Sci* 2003;2:926–33. <http://dx.doi.org/10.1039/b212890j>.
- [49] Preuß A, Zeugner L, Hackbarth S, Faustino MAF, Neves MGPMS, Cavaleiro JAS, et al. Photoinactivation of *Escherichia coli* (SURE2) without intracellular uptake of the photosensitizer. *J Appl Microbiol* 2012;114:36–43. <http://dx.doi.org/10.1111/jam.12018>.
- [50] Hamblin MR, Hasan T. Photodynamic therapy: a new antimicrobial approach to infectious disease? *Photochem Photobiol Sci* 2004;3:436–50. <http://dx.doi.org/10.1039/b311900a>.
- [51] Ranta J, Kumpulainen T, Lemmetyinen H, Efimov A. Synthesis and characterization of monoisomeric 1,8,15,22-substituted (a 3 B and A 2 B 2) phthalocyanines and Phthalocyanine–Fullerene dyads. *J Org Chem* 2010;75:5178–94. <http://dx.doi.org/10.1021/jo100766h>.
- [52] Maki T, Ishihara K, Yamamoto H. N-Alkyl-4-boronopyridinium salts as thermally stable and reusable amide condensation catalysts. *Org Lett* 2005;7:5043–6. <http://dx.doi.org/10.1021/OL052060L>.
- [53] Preuß A, Saltsman I, Mahammed A, Pfützner M, Goldberg I, Gross Z, et al. Photodynamic inactivation of mold fungi spores by newly developed charged corroles. *J Photochem Photobiol B Biol* 2014;133:39–46. <http://dx.doi.org/10.1016/j.jphotobiol.2014.02.013>.
- [54] Santala S, Karp M, Santala V. Rationally engineered synthetic coculture for improved biomass and product formation. *PLoS One* 2014;9:e113786. <http://dx.doi.org/10.1371/journal.pone.0113786>.
- [55] Bryklyn AV, Matsumura I. Rational design of a plasmid origin that replicates efficiently in both gram-positive and gram-negative bacteria. *PLoS One* 2010;5:e13244. <http://dx.doi.org/10.1371/journal.pone.0013244>.
- [56] Sarker SD, Nahar L, Kumarasamy Y. Microtitre plate-based antibacterial assay incorporating resazurin as an indicator of cell growth, and its application in the in vitro antibacterial screening of phytochemicals. *Methods* 2007;42:321–4. <http://dx.doi.org/10.1016/j.ymeth.2007.01.006>.
- [57] Liu JY, Li J, Yuan X, Wang WM, Xue JP. In vitro photodynamic activities of zinc(II) phthalocyanines substituted with pyridine moieties. *Photodyn Ther* 2016;13:341–3. <http://dx.doi.org/10.1016/j.pdpdt.2015.07.003>.
- [58] Pereira JB, Carvalho EFA, Faustino MAF, Fernandes R, Neves MGPMS, Cavaleiro JAS, et al. Phthalocyanine thio-pyridinium derivatives as antibacterial photosensitizers. *Photochem Photobiol* 2012;88:537–47. <http://dx.doi.org/10.1111/j.1751-1097.2012.01113.x>.
- [59] Okura I. Photosensitization of porphyrins and phthalocyanines. *Photosensit. Porphyrins phthalocyanines*. Kodansha Ltd and Gordon and Breach Sciences Publishers; 2000. p. 45–51.
- [60] Ogunsipe A, Chen J-Y, Nyokong T. Photophysical and photochemical studies of zinc(II) phthalocyanine derivatives—effects of substituents and solvents. *New J Chem* 2004;28:822–7. <http://dx.doi.org/10.1039/B315319C>.
- [61] Karp M, Galluzzi L. Whole cell strategies based on lux genes for high throughput applications toward new antimicrobials. *Comb Chem High Throughput Screen* 2006;9:501–14. <http://dx.doi.org/10.2174/13862070677935351>.
- [62] Ringot C, Sol V, Barrière M, Saad N, Bressollier P, Granet R, et al. Triazinyl porphyrin-based photoactive cotton fabrics: preparation, characterization, and antibacterial activity. *Biomacromolecules* 2011;12:1716–23. <http://dx.doi.org/10.1021/bm200082d>.
- [63] Mbakidi JP, Herke K, Alvé S, Chaleix V, Granet R, Krausz P, et al. Synthesis and photobiocidal properties of cationic porphyrin-grafted paper. *Carbohydr Polym* 2013;91:333–8. <http://dx.doi.org/10.1016/j.carbpol.2012.08.013>.
- [64] Carpenter BL, Scholle F, Sadeghifar H, Francis AJ, Boltersdorf J, Wear W, et al. Synthesis, characterization, and antimicrobial efficacy of photomicrobical cellulose paper. *Biomacromolecules* 2015;16:2482–92. <http://dx.doi.org/10.1021/acs.biomac.5b00758>.

IV

PHOTO-ANTIMICROBIAL EFFICACY OF ZINC COMPLEXES OF PORPHYRIN AND PHTHALOCYANINE ACTIVATED BY INEXPENSIVE CONSUMER LED LAMP.

by

Lijo George , Arto Hiltunen, Ville Santala, Alexander Efimov.
Journal of Inorganic Biochemistry 183 (2018) 94–100
Reproduced with kind permission from Elsevier.



Photo-antimicrobial efficacy of zinc complexes of porphyrin and phthalocyanine activated by inexpensive consumer LED lamp

Lijo George, Arto Hiltunen, Ville Santala, Alexander Efimov*

Laboratory of Chemistry and Bioengineering, Tampere University of Technology, P.O. Box 541, 33101 Tampere, Finland

ABSTRACT

The properties and antimicrobial efficacies of zinc complexes of tetrakis(*N*-methylpyridinium-4-yl) tetraiodide porphyrin and tetrakis(*N*-methylpyridinium-4-yl) tetraiodide phthalocyanine impregnated to paper were evaluated. Photo-inactivation of microbes using inexpensive consumer light-emitting diode lamp was assessed on surface of dyed papers. Antimicrobial experiments of phthalocyanine-dyed paper by live cell assessment through colony forming units counting demonstrated 3.72 and 4.01 log reduction against *Escherichia coli* (*E. coli*) and *Acinetobacter baylyi* (*A. baylyi*) respectively after 1 h of illumination with 35 mW/cm² light. The porphyrin-dyed paper exhibited 1.66 and 2.01 log reduction in colony forming units against *E. coli* and *A. baylyi* respectively after 1 h exposure with 4 mW/cm² light. Both dyed papers were photo-stable after 64 h of continuous exposure with 42 mW/cm² light, while phthalocyanine-dyed paper exhibited superior leaching stability in phosphate-buffered saline.

1. Introduction

Light-activated antimicrobial substances are gaining new momentum and attract more and more attention of researchers. State of the art is covered in a recent series of excellent reviews, which demonstrate that significant success has been achieved in photodynamic treatment of bacteria [1–4], fungi [4–7], and biofilms [8]. Considerable application field is dentistry and treatment of carious infections in particular [9,10]. Applicability of Photodynamic antimicrobial chemotherapy (PACT) is not limited with the above-mentioned examples [4,11,12], but extends from fish farming [13] to blood sterilization [14].

Most commonly, the derivatives of phenothiazine, porphyrin and phthalocyanine are used as photosensitizers for PACT [15]. Regarding the latter two, porphyrinoid ligand is usually employed to chelate an inorganic ion, which improves dramatically the efficiency of photodynamic action. The choice between porphyrin and phthalocyanine ligand is a matter of debate, with both macrocycles having their advantages. However, it is commonly accepted that the ligand should bear cationic species, preferably quaternized amino groups, which renders the molecule much more active against microorganisms compare to neutral or anionic substances [16]. Among the most popular, zinc(II) ions [1,17–26] along with silicon [27–29] and aluminium [9] complexes have demonstrated best efficacies.

Photosensitizers are mostly used in form of solutions against

planktonic microbes or biofilms. Examples of photoactive surfaces with chromophores immobilized on solid a support are however quite rare [30]. Immobilization requires significant synthetic efforts since both the substrate and the chromophore should be modified to create a covalent link between them. This in turn requires synthesis of asymmetric porphyrinoids, which is laborious and proceeds with lower yields. Indeed, there are very good examples of substances with high activity, however their preparation is challenging [26,29,31,32].

As has been mentioned by Cieplik et al. [8], comparing different reports to each other is very difficult a task because of very different concentrations, microbial strains, and cultivation and illumination conditions employed by different groups. One of the least standardized parameters is the choice of light source. In recent publications, some have used quartz lamps, near-infrared (NIR) lamps, halogen lamps, slide projector lamps [18,26,28,29,31,33–36], or special photodynamic therapy (PDT) light sources [21,22,37]. Another popular option is to employ the laser light, mostly from diode lasers with the wavelength selected close to the absorption maxima of the photosensitizer (650–720 nm) [17,23,38,39]. Third option is to employ special light-emitting diode (LED) lights [61] or non-coherent red light-emitting diodes, which represent a less expensive alternative to lasers [2,20,31,34,40–43].

When a new photosensitizer needs to be compared against already existing benchmark substance, the lack of commonly accepted standard conditions leads to a complication. However, the situation has

* Corresponding author.

E-mail address: alexandre.efimov@tut.fi (A. Efimov).

improved with recent reports, which present the data about the light dose instead of just the wavelength range and light power of the source. Typical light doses are varied between 20 and 70 J/cm², and sometimes can be very modest 10 J/cm² in antifungal action [44] or even 6 J/cm² in successful antibacterial treatment [17].

It is also important to remember that photodynamic treatment is inherently dependent on the light source, and implementing PACT in everyday life would not be possible without providing an accessible, economical and long-lasting illumination device. Speaking about PACT as a way of disinfection of large surfaces e.g. in public places, households or air/water filter systems, one need to find an affordable source of irradiation which can be used in consumer scale.

In this work, a comparison between two Zn(II) porphyrinoid ligands, a well known tetrakis(*N*-methylpyridinium-4-yl) tetraiodide porphyrin and novel, recently synthesized tetrakis(*N*-methylpyridinium-4-yl) tetraiodide phthalocyanine is presented. Both the substances can be easily immobilized on a cellulose substrate (filter paper) and have demonstrated significant antimicrobial activity against model microorganisms *E. coli* and *A. baylyi* upon illumination with inexpensive consumer LED lamp. Moreover, phthalocyanine has shown superior stability against leaching and photobleaching.

2. Materials and methods

2.1. General methods

All commercial reagents and solvents were purchased from TCI Europe, SigmaAldrich Co. or from VWR and were used without further purifications unless otherwise mentioned. Purification of the products was carried out either by column chromatography on Silica gel 60 or Silica gel 100 (Merck). NMR spectra were recorded using Varian Mercury 300 MHz spectrometer using TMS as internal standard. High-resolution mass spectrometry (HRMS) measurements were done with Waters LCT Premier XE electrospray ionization time-of-flight (ESI-TOF) bench top mass spectrometer. Lock-mass correction (leucine enkephaline as a reference compound), centering and calibration were applied to the raw data to obtain accurate mass. UV-Vis absorption spectra were recorded using Shimadzu UV-2501PC spectrophotometer and emission spectra were recorded on a Fluorolog Yobin Yvon-SPEX spectrofluorometer. All solutions, culture mediums, vials and pipette tips used for microbial tests were sterilized before the experiments and all operations were conducted inside the laminar hood to prevent any contamination. Qualitative filter paper 413 (medium filtration rate, particle retention 5–13 μm) used for preparation of photoantimicrobial surfaces was purchased from VWR (cat. No. 516-0813).

2.2. Photosensitizers and light source

Two photosensitizers used for the experiments were Zn(II) tetrakis(*N*-methylpyridinium-4-yl) tetraiodide phthalocyanine (**ZnPc**) and Zn(II) tetrakis(*N*-methylpyridinium-4-yl) tetraiodide porphyrin (**ZnPf**) [45] (Fig. 1). The synthesis and characterization of **ZnPc** were discussed in our previous work [24]. Phthalocyanine papers used for antimicrobial test were prepared by soaking filter paper (3.5 cm × 3.5 cm) in the aqueous solution containing 0.1 mg **ZnPc**. Porphyrin **ZnPf** was synthesized in-house according to the literature procedure reported elsewhere. Porphyrin papers were prepared by following the above-mentioned procedure using **ZnPf**. The light absorption of the papers was examined with Shimadzu UV-3600 UV-VIS-NIR spectrophotometer using an integrating sphere attachment (ISR-3100). Transmittance (T) and reflectance (R) spectra of papers were recorded. From these two, the absorbance **a**, which is the fraction of incident light absorbed by sample was calculated according to equation $a = 1 - T - R$, where R is reflectance and T transmittance of the sample at given wavelength. Commercially available indoor lighting LED lamp (LED lamp OSRAM Star PAR16 80 W 575 lm GU10) was used as an illumination source. The

spectrum of the LED lamp was recorded with AvaSpec-2048 fiber optics spectrometer. Intensity of the lamp emission was measured using Coherent LM10 power meter.

2.3. Determination of antimicrobial efficacy of dyed paper

Microbial strains, *E. coli* MG1655 (*E. coli* Genetic Resources at Yale) and *A. baylyi* ADP1 (ATCC 33305) were used in determining antimicrobial efficacy. Microbial strains were inoculated in 5 mL of Lysogeny broth (LB) medium (10 g/L tryptone, 5 g/L yeast extract, 5 g/L NaCl) containing 1% glucose and cultivated at 30 °C and at 300 rpm in temperature-controlled incubator shaker (IKA® KS 4000 i control). After overnight cultivation, 100 μL of the culture was diluted with 4.9 mL of LB medium containing 1% glucose and cultivated for 3 h at 30 °C and at 300 rpm in temperature controlled incubator shaker (IKA® KS 4000 i control). The optical density of culture was recorded at 600 nm. The microbial solution was centrifuged for 5 min at 6500 rpm and the LB medium was decanted out from the vial. The residual microbes were suspended in 5 mL of phosphate-buffered saline (PBS) buffer. Two sets (original and duplicate) of circular discs (5 mm in diameter) were cut from phthalocyanine-dyed paper and control paper and placed in the wells of a microplate. 25 μL of microbial solution was pipetted over the disks. The microplate was covered with a transparent lid and was illuminated with LED lamp for 1 h with a light intensity of 35 mW/cm². Dark control samples and their duplicates were prepared by depositing 25 μL of microbial medium over dyed and uncolored paper disks in a separate microplate, which was incubated in dark for 1 h at room temperature inside the laminar hood. After 1 h of illumination or incubation, the microbes were extracted from wells with 975 μL of PBS buffer and serial dilutions (up to 10⁻⁶) were made from each extract. The dilutions were then plated on LA agar plates (15 g/L agar, 10 g/L tryptone, 5 g/L yeast extract, 5 g/L NaCl, 0.2% glucose) and incubated at 30 °C overnight in a laboratory incubator (Termaks). The number of colonies grown on the agar plates was counted and colony forming units (CFUs) per milliliter were calculated to determine the antimicrobial efficacy. The same procedure was used to estimate the antimicrobial efficacy for porphyrin paper. The scheme presenting the procedure is shown in Fig. 2.

2.4. Leaching test of phthalocyanine and porphyrin papers

28 mg of each dyed paper was soaked in 4 mL of PBS buffer in a glass vial for 1 h at room temperature. Absorbance and emission of PBS buffer from each vial was measured after 1 h to check the leaching of dyes from papers.

2.5. Photostability of phthalocyanine and porphyrin papers

Phthalocyanine and porphyrin papers were illuminated for 64 h using LED lamp with the intensity of 42 mW/cm². Absorbance of the papers was measured before and after the illumination and difference in the values were used to calculate the photostability of dye on paper.

3. Results and discussion

In our previous work, we have demonstrated that the paper dyed with Zn(II) tetrakis(*N*-methylpyridinium-4-yl) tetraiodide phthalocyanine (**ZnPc**) had antimicrobial efficacy of 2.7 and 3.4 log reduction in CFU against *E. coli* and *A. baylyi* respectively after 1 h of illumination with light intensity 18 mW/cm² [24]. However, these experiments were conducted using a solar simulator, which is not suitable for practical applications. In order to implement PACT in everyday life, a simple and affordable illumination source should be found. Use of commercially available indoor lighting system such as consumer LED lamp would be much beneficial for this purpose. In the present study, the phototoxic effect of paper impregnated with **ZnPc** illuminated using a consumer

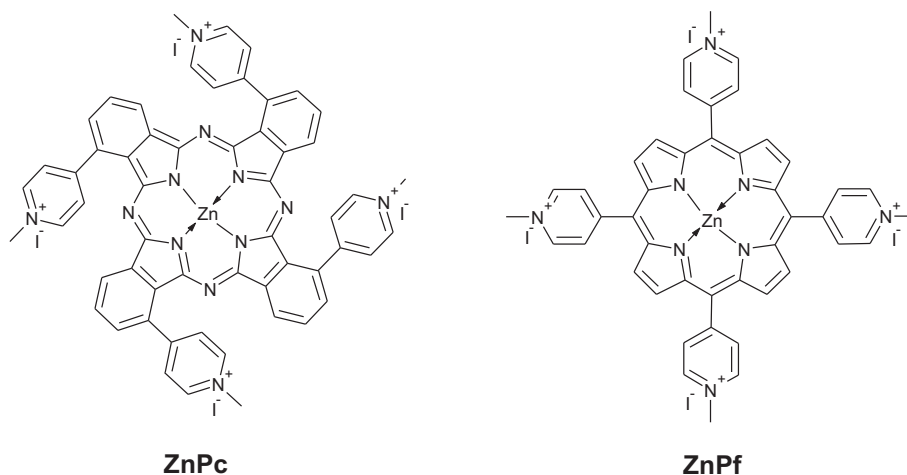


Fig. 1. Cationic phthalocyanine and porphyrin used in the study.

LED lamp is reported and compared against the paper dyed with well-known zinc porphyrin photosensitizer **ZnPf** [46]. Important parameters such as photostability and stability against leaching are also compared.

3.1. Dyeing of paper

The filter papers used in laboratory are pure cellulose, which is described in the literature as being “very hydrophilic and slightly anionic with low negative surface charge density” [47]. It is established that cellulose is able to strongly bind cationic molecules and polymers with positively charged fragments, even from water solutions [47–49]. In our experiments, when the filter paper was immersed in an aqueous solution of cationic dye, the chromophore was fully absorbed by paper in a few minutes, leaving behind the colourless water. Thus, we suggest that electrostatic interactions bind porphyrinoid tetracations onto the paper thereby giving it a stable colour. Due to the low amount of dye used for the immobilization with respect to weight of the paper (0.12 wt %) and the non-transparent character of the samples, the most reliable way to monitor the dye impregnation was the UV–Vis absorption measurements using integrating sphere.

3.2. Lamp profile and absorbance of the dyes

Even though light-emitting diodes are largely used in photodynamic therapy, the use of consumer LED lamps remains very limited. However, accessible and economical light source is a keystone in successful implementation of PACT. Typically, no spectral data are available for consumer bulbs, which makes their selection and comparison difficult. For the work, a “warm white” OSRAM LED lamp was selected, and its emitted spectrum was measured prior to the experiments. The wavelength of lamp emission spans from 400 to about 750 nm with a maximum at 594 nm (Fig. 3a). In order to correctly quantify the photoactivation results the power density of the lamp was also measured at different illumination distances. Total light intensities were found to be 4 mW/cm² at a distance 28 cm, 8 mW/cm² at 20 cm, 15 mW/cm² at 14 cm and 35 mW/cm² at distance 9 cm away from the lamp front window.

The absorbance of phthalocyanine- and porphyrin-dyed papers were calculated from reflectance (R) and transmittance (T) spectra measured using integrating sphere (IS) detector. The absorbance profiles were similar to the absorbance spectra in solutions, though with some changes in relative intensities. Wavelengths corresponding to the

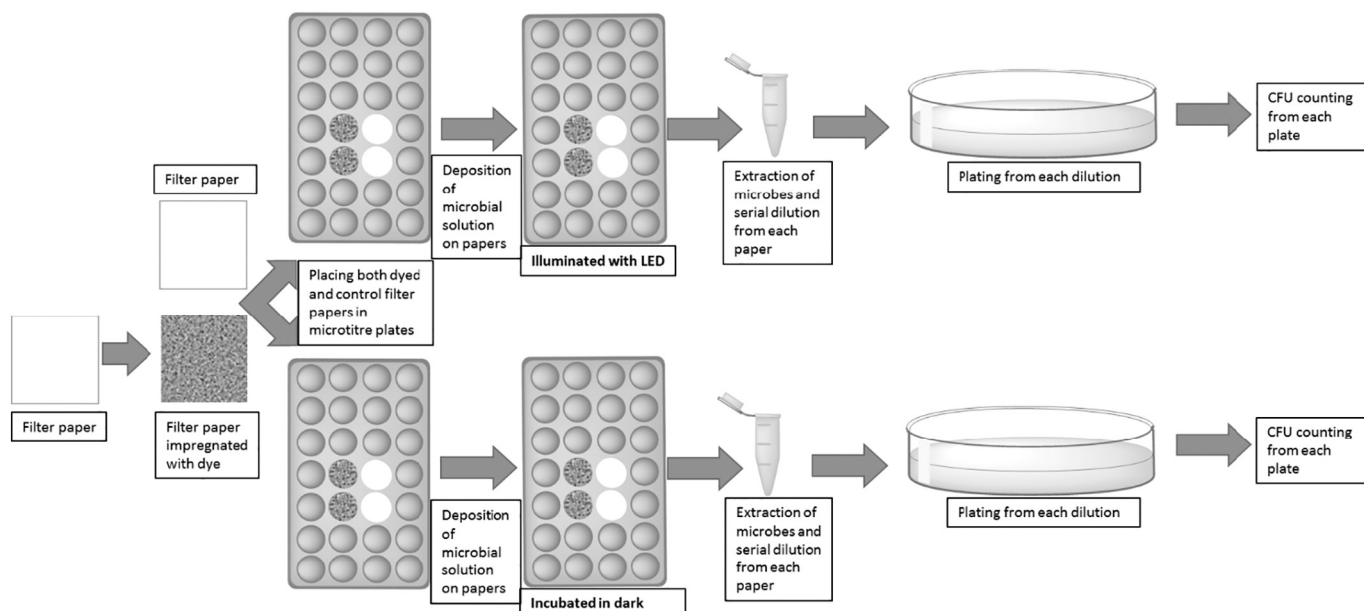


Fig. 2. Scheme to determine antimicrobial efficacy by CFU counting.

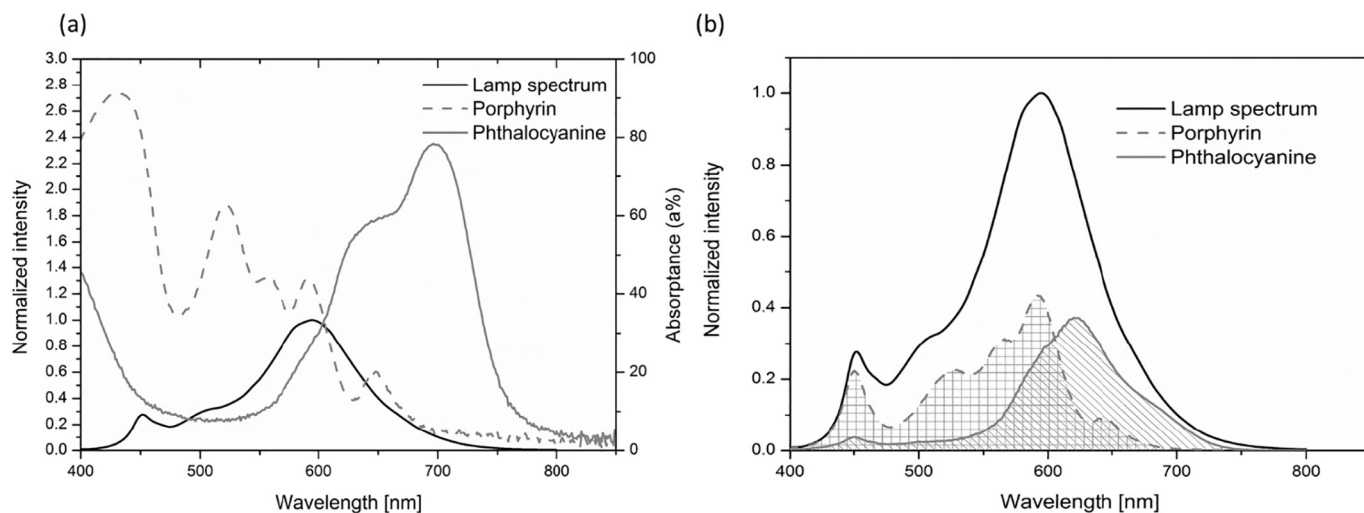


Fig. 3. (a) The lamp profile and absorbance of zinc phthalocyanine and porphyrin papers (b) light dose calculated for phthalocyanine and porphyrin papers.

maximum absorption are 430 nm for porphyrin and 696 nm for phthalocyanine, respectively. Since the two dyes absorb differently at different wavelengths and the lamp profile is not flat either, the dyes' absorbance profiles were recalculated according to the eq. $I(\lambda) = L(\lambda) \times a(\lambda) / 100$, where $I(\lambda)$ is the recalculated light absorbance at certain wavelength, $L(\lambda)$ is the relative light intensity of the lamp, and $a(\lambda)$ is the absorbance value as measured with the integrating sphere. The resulting spectra are present in Fig. 3b. The absorbed light power densities for porphyrin and phthalocyanine were calculated from the ratio between the area under recalculated spectra for respective dyes to the total area of the lamp spectrum. The absorbed light power density for porphyrin was found to be 1.2 times greater than that of phthalocyanine. Hence for the lamp intensity 35 mW/cm^2 , the light doses calculated were 45 J/cm^2 and 37 J/cm^2 for porphyrin and phthalocyanine respectively. This difference in light doses was taken into consideration while setting the illumination conditions for photoinactivation. Thus for porphyrin paper the total light intensity of the lamp would be decreased to 29 mW/cm^2 to match the light doses.

3.3. Photostability of papers

The photostability of photosensitizers is a very important factor for practical application. Therefore, the photostability of phthalocyanine and porphyrin papers was measured from the difference in the absorbance values before and after the illumination in air. The absorbance of papers were calculated from the reflectance and transmittance measurements (Fig. 4). The absorbance of phthalocyanine paper (at 696 nm) before the illumination was 81.88% and after illumination was 71.30%. Therefore, the photodegradation of the ZnPc dye on paper was 12.9% while, the shape of the spectra remained same even after 64 h of illumination. For porphyrin, the absorbance of the main peak around 430 nm before illumination was 90.50% and after illumination was 81.28%. Hence, the photodegradation of porphyrin paper calculated was 10.18%. However, peaks around 520 nm and 590 nm almost disappeared after exposure to light. These results show that there was no significant photodegradation of phthalocyanine on paper even after 64 h of continuous illumination with light intensity of 42 mW/cm^2 . The porphyrin dye also preserved its absorbance quite well, though the changes in the shape of the spectrum were noticeable.

3.4. Leaching test

In order to check the leaching of dyes, the dyed papers were incubated in a 4 mL volume of PBS buffer at pH 7.4. The amount of the zinc complexes extracted into the PBS buffer was determined by

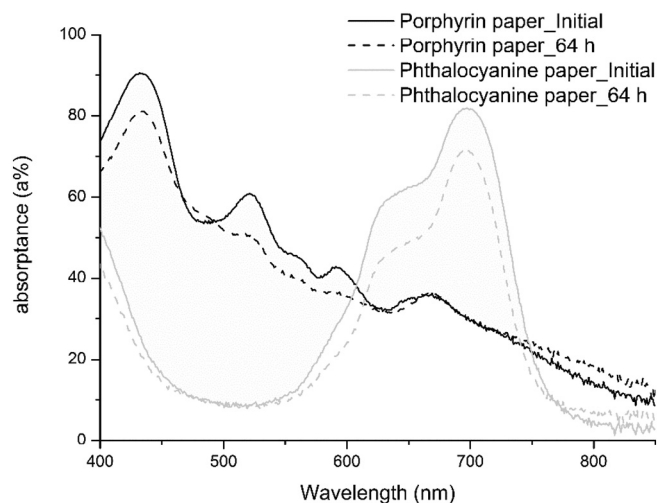


Fig. 4. Absorbance of dyed papers before and after illumination for 64 h.

measuring the UV-Vis absorption spectra of the extract. The fluorescence spectra of the extracts were recorded in order to detect the minute concentrations of extracted dyes, which could not be reliably observed by absorption measurements. The PBS extract of porphyrin paper had shown a strong absorption peak at 422 nm that confirmed the leaching of porphyrin into the solution. The emission spectrum of PBS extract of porphyrin paper excited at 422 nm displayed a broad intense peak with maximum around 720 nm. Remarkably, the PBS extract of phthalocyanine paper did not show any absorption peak corresponding to the dye in UV-Vis spectrum even after 20 h of incubation at room temperature (Fig. 5a). In emission measurements, upon excitation at 694 nm it produced a signal, however very faint. (Fig. 5b). Obviously, the amount of extracted zinc phthalocyanine was negligible. Such a strong binding ability of ZnPc is a beneficial property, which is very important for practical applications.

3.5. Antimicrobial efficacy by colony forming unit (CFU) counting

In general, incorporation of metals such as Zn [50,51], Al [52,53], Si [54–56], Pb [57], In [34,51,58], Pd [59] into porphyrinoid core improves the phototoxicity of the compounds towards microbes. Skwor et al. [46] reported 2.6 log CFUs reduction in methicillin-resistant strains of *S. aureus* (MRSA) by using ZnPf with light dose 2.5 J/cm^2 . The activity of the corresponding free base porphyrin was however

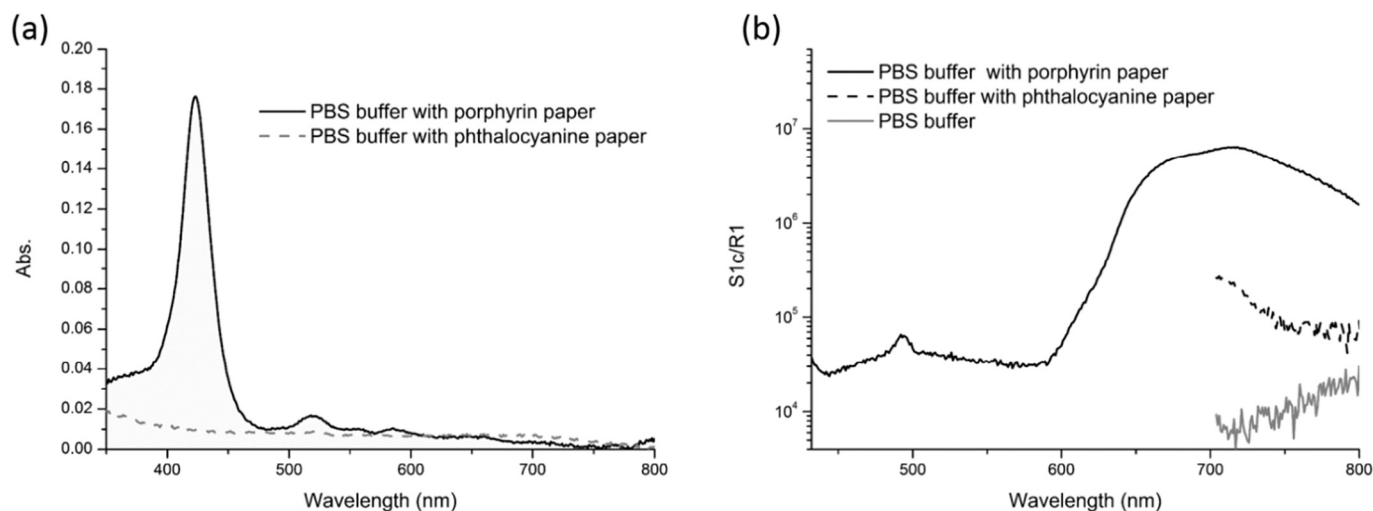


Fig. 5. (a) Absorbance measurements (b) emission measurements of PBS extracts.

lower. Higher phototoxicity of cationic zinc phthalocyanine towards microbes was also reported in our previous work [24].

For the immobilization of photosensitizers on polymer matrix, few strategies are commonly employed. One method is a covalent attachment of photosensitizer to polymer [60–65]. Other methods rely on incorporation of photosensitizers into polymer matrix during electrospinning of polymer fiber [57,66–72], or employ binding of the dye through electrostatic interactions [73–75]. Cationic zinc porphyrin covalently bonded to cellulose nanocrystals exhibited 1–2 log reduction in *E. coli* CFUs with 20 μM dye concentration and light dose 108 J/cm^2 [65]. Cationic zinc porphyrin embedded into polyacrylonitrile nanofiber (10 wt% with respect to the mass of polymer) prepared by electrospinning has shown 6 log photoinactivation against *E. coli* when exposed to light dose of 118 J/cm^2 [72]. Polystyrene nanofibers with embedded tetracationic lead phthalocyanine exhibited significant photo inactivation against *E. coli* [57]. Porphyrin-nanofiber material prepared by electrostatic interaction of tetracationic porphyrin (TMPyP) and modified polystyrene (molar ratio TMPyP/ $\text{SO}^{3-} = 2.5 \times 10^{-3}$) demonstrated phototoxicity towards *E. coli* after illumination for 2 min with a 400 W solar simulator [74]. Similar results were reported on the inactivation *E. coli* with cationic porphyrin TMPyP (dye concentration 180 mg/m^2) attached electrostatically to regenerated cellulose upon 24 h of illumination [75].

In our previous publication, a strong dependence of the efficiency of antimicrobial surface on the dye load was observed. The inactivation rate for ZnPc dye loads 800 mg/m^2 , 400 mg/m^2 and 200 mg/m^2 was so high that it could not be calculated reliably. Simply, there were no microbes survived after 1 h of illumination. The only dye load which allowed to obtain reliable and reproducible inactivation rate was 80 mg/m^2 , at which some surviving colonies still could be observed, counted and compared to dark controls [24].

In the present study, 80 mg/m^2 load was selected as a starting point for experiments. The antimicrobial effects of our phthalocyanine and porphyrin papers against Gram-negative microbial strains such as *E. coli* and *A. baylyi* were evaluated. For zinc phthalocyanine paper, the total light intensity of the lamp was set at 35 mW/cm^2 . Hence ZnPc paper would be exposed to light intensity 10.3 mW/cm^2 (calculated from area under the spectrum for phthalocyanine with that of lamp spectrum) and light dose of 37 J/cm^2 after 1 h of illumination.

For the illumination of porphyrin paper, total light intensity of lamp was set at 29 mW/cm^2 to obtain the same light dose as that of phthalocyanine paper. Hence calculated intensity of light for porphyrin from the area under the spectrum is 10.3 mW/cm^2 and light dose 37 J/cm^2 . However, the tested microbes could not survive on porphyrin papers after 1 h of illumination with this intensity. The reason is the extraction

of porphyrin from paper into PBS buffer as observed in the leaching studies. This in turn increased the concentration of photosensitizer in liquid and its accessibility for bacteria, thereby enhancing inactivation of microbes. In order to obtain a countable number of colonies of bacteria after illumination, the total light intensity of lamp had to be reduced to 4 mW/cm^2 (absorbed light power density calculated from the area under the spectrum for porphyrin paper = 1.4 mW/cm^2 , light dose = 5.04 J/cm^2). With this light dose, porphyrin-dyed paper demonstrated 1.66 and 2.01 log reduction of CFU against *E. coli* and *A. baylyi*, respectively.

The paper dyed with tetracationic phthalocyanine ZnPc exhibited 3.72 and 4.01 log reduction in CFU units against *E. coli* and *A. baylyi*, respectively after 1 h of illumination. Such a high efficiency proves that the photodynamic effect can be achieved with a consumer LED bulb. The results are shown in Fig. 6. It must be underlined, that no dark toxicity of the dye was observed during the experiments. Light activity of the dye ZnPc is high indeed, and it compares very well to the efficiencies published in literature. As advantages of our approach, we can underline high photostability, strong binding capacity and significant photoinactivation of microbes.

In this work, filter paper was selected as a substrate to prepare the photoactive self-disinfecting surface because it can easily immobilize tetracationic phthalocyanine via electrostatic interactions. Further studies using polymer substrates other than filter paper should be done in future. This would greatly expand the range of possible PACT materials.

4. Conclusions

We have recently synthesized Zn(II) tetrakis(*N*-methylpyridinium-4-yl) tetraiodide phthalocyanine which binds onto a paper substrate strongly and efficiently from water solution via simple dipping procedure. Even at the dye load as low as 80 mg/m^2 this novel phthalocyanine has strong phototoxicity against Gram negative bacteria *E. coli* and *A. baylyi*. Phthalocyanine-impregnated paper has very good photostability with no significant degradation after 64 h of continuous exposure to the light. The phthalocyanine-dyed paper also demonstrated remarkable stability in the leaching tests in PBS buffer.

We have shown that a consumer LED lamp can serve as an economical and efficient light source for photodynamic inactivation of microbes. These results give a promising direction for implementing PACT in real life applications. More studies using antibiotic-resistant pathogens are under progress and will be reported in due time.

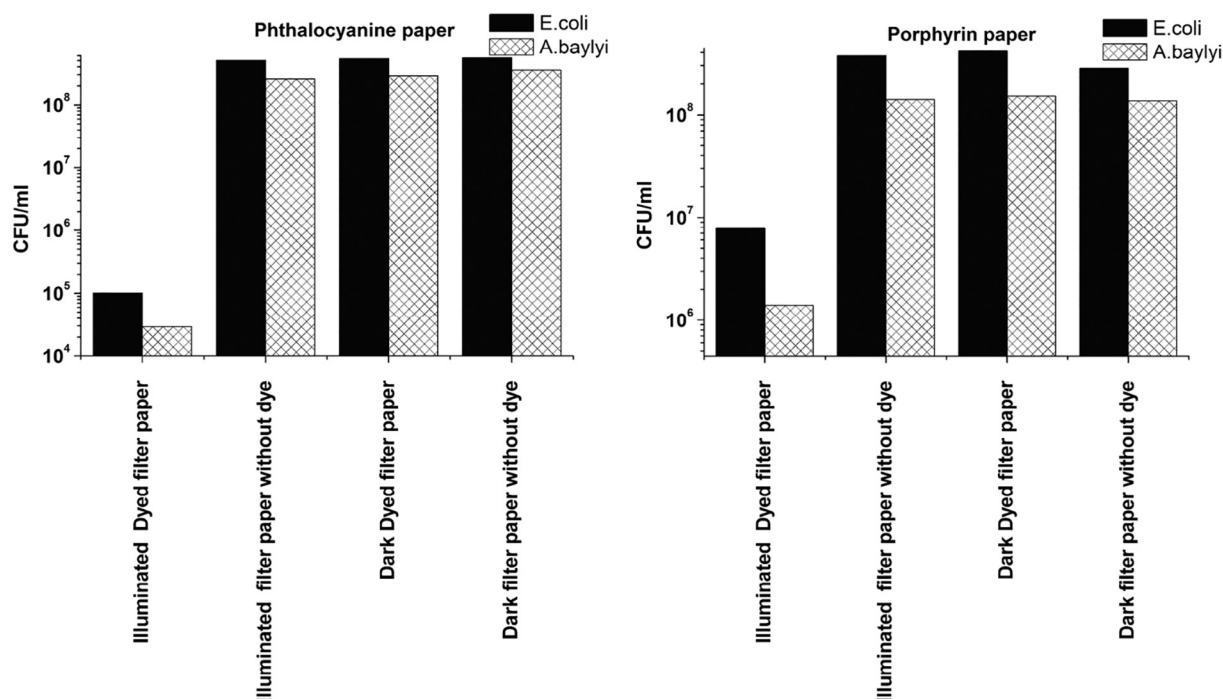


Fig. 6. Antimicrobial efficacy of zinc phthalocyanine and porphyrin papers against *E. coli* and *A. baylyi* after illumination for 1 h.

Acknowledgement

Financial support from the Graduate School of Tampere University of Technology is gratefully acknowledged.

References

- J. Chen, W. Wang, P. Hu, D. Wang, F. Lin, J. Xue, Z. Chen, Z. Iqbal, M. Huang, Dyes Pigments 140 (2017), <http://dx.doi.org/10.1016/j.dyepig.2017.01.032>.
- C.C.C. Quishida, E.G. de Oliveira Mima, L.N. Dovigo, J.H. Jorge, V.S. Bagnato, A.C. Pavarina, Lasers Med. Sci. 30 (2015), <http://dx.doi.org/10.1007/s10103-015-1811-9>.
- X. Fu, Y. Fang, M. Yao, Biomed. Res. Int. 2013 (2013) 1–9, <http://dx.doi.org/10.1155/2013/159157>.
- M. Wainwright, T. Maisch, S. Nonell, K. Plaetzer, A. Almeida, G.P. Tegos, M.R. Hamblin, Lancet Infect. Dis. 17 (2017) e49–e55, [http://dx.doi.org/10.1016/S1473-3099\(16\)30268-7](http://dx.doi.org/10.1016/S1473-3099(16)30268-7).
- L.M. Baltazar, A. Ray, D.A. Santos, P.S. Cisalpino, A.J. Friedman, J.D. Nosanchuk, Front. Microbiol. 6 (2015) 1–11, <http://dx.doi.org/10.3389/fmicb.2015.00202>.
- P. Calzavara-Pinton, M.T. Rossi, R. Sala, M. Venturini, Photochem. Photobiol. 88 (2012) 512–522, <http://dx.doi.org/10.1111/j.1751-1097.2012.01107.x>.
- J.P. Lyon, L.M. Moreira, P.C.G. de Moraes, F.V. dos Santos, M.A. de Resende, Mycoses 54 (2011) e265–e271, <http://dx.doi.org/10.1111/j.1439-0507.2010.01966.x>.
- F. Cieplik, L. Tabenski, W. Buchalla, T. Maisch, Front. Microbiol. 5 (2014) 1–17, <http://dx.doi.org/10.3389/fmicb.2014.00405>.
- F. Cieplik, W. Buchalla, E. Hellwig, A. Al-Ahmad, K.A. Hiller, T. Maisch, L. Karygianni, Photodiagn. Photodyn. Ther. 18 (2017) 54–62, <http://dx.doi.org/10.1016/j.pdpdt.2017.01.005>.
- M. Wilson, Photochem. Photobiol. Sci. 3 (2004) 412, <http://dx.doi.org/10.1039/b211266c>.
- T. Dai, Y.-Y. Huang, M.R. Hamblin, Photodiagn. Photodyn. Ther. 6 (2009) 170–188, <http://dx.doi.org/10.1016/j.pdpdt.2009.10.008>.
- M. Wainwright, Int. J. Antimicrob. Agents 44 (2014), <http://dx.doi.org/10.1016/j.ijantimicag.2014.02.013>.
- A. Almeida, Á. Cunha, N.C.M. Gomes, E. Alves, L. Costa, M.A.F. Faustino, Mar. Drugs 7 (2009) 268–313, <http://dx.doi.org/10.3390/md7030268>.
- M. Wainwright, Curr. Med. Chem. 9 (2002).
- M. Tim, J. Photochem. Photobiol. B Biol. 150 (2015), <http://dx.doi.org/10.1016/j.jphotochem.2015.05.010>.
- A. Martínez De Pinillos Bayona, P. Mroz, C. Thunshelle, M.R. Hamblin, Chem. Biol. Drug Des. 89 (2017) 192–206, <http://dx.doi.org/10.1111/cbdd.12792>.
- Z. Zhao, Y. Li, S. Meng, S. Li, Q. Wang, T. Liu, Lasers Med. Sci. 29 (2014), <http://dx.doi.org/10.1007/s10103-013-1488-x>.
- M.-R. Ke, J.M. Eastel, K.L.K. Ngai, Y.-Y. Cheung, P.K.S. Chan, M. Hui, D.K.P. Ng, P.-C. Lo, Eur. J. Med. Chem. 84 (2014) 278–283, <http://dx.doi.org/10.1016/j.ejmech.2014.07.022>.
- M.B. Spesia, E.N. Durantini, J. Photochem. Photobiol. B Biol. 125 (2013) 179–187, <http://dx.doi.org/10.1016/j.jphotochem.2013.06.007>.
- Z. Chen, D. Wang, Y. Zhang, S. Yan, Z. Chen, Y. Deng, P. Xu, J. Chen, W. Liu, P. Hu, M. Huang, J. Porphyrins Phthalocyanines 21 (2017), <http://dx.doi.org/10.1142/S1088424617500298>.
- D.K. Muli, B.L. Carpenter, M. Mayukh, R.A. Ghiladi, D.V. McGrath, Tetrahedron Lett. 56 (2015) 3541–3545, <http://dx.doi.org/10.1016/j.tetlet.2015.01.076>.
- M. Grinholc, A. Rodziewicz, K. Forsy, A. Rapacka-Zdonczyk, A. Kawiak, A. Domachowska, G. Golunski, C. Wolz, L. Mesak, K. Becker, K.P. Bielawski, Appl. Microbiol. Biotechnol. 99 (2015) 9161–9176, <http://dx.doi.org/10.1007/s00253-015-6863-z>.
- M. Li, B. Mai, A. Wang, Y. Gao, X. Wang, X. Liu, S. Song, Q. Liu, S. Wei, P. Wang, RSC Adv. 7 (2017), <http://dx.doi.org/10.1039/c7ra06073d>.
- L. George, A. Müller, B. Röder, V. Santala, A. Efimov, Dyes Pigments 147 (2017) 334–342, <http://dx.doi.org/10.1016/j.dyepig.2017.08.021>.
- L. Ryskova, V. Buchta, M. Karaskova, J. Rakusan, J. Cerny, R. Slezak, Open Life Sci. 8 (2013), <http://dx.doi.org/10.2478/s11535-013-0118-0>.
- T. Tempesti, M.G. Alvarez, C. Gómez, M. Strumia, E.N. Durantini, Polym.-Plast. Technol. Eng. (2017), <http://dx.doi.org/10.1080/03602559.2017.1315643>.
- G.C. Taşkın, M. Durmuş, F. Yüksel, V. Mantareva, V. Kussovski, I. Angelov, D. Atilla, J. Photochem. Photobiol. A Chem. 306 (2015), <http://dx.doi.org/10.1016/j.jphotochem.2015.03.010>.
- E. van de Winckel, B. David, M.M. Simoni, J.A. González-Delgado, A. de la Escosura, Á. Cunha, T. Torres, Dyes Pigments 145 (2017) 239–245, <http://dx.doi.org/10.1016/j.dyepig.2017.06.004>.
- A. Galstyan, R. Schiller, U. Dobrindt, Angew. Chem. Int. Ed. 56 (2017) 10362–10366, <http://dx.doi.org/10.1002/anie.201703398>.
- C. Spagnul, L.C. Turner, R.W. Boyle, J. Photochem. Photobiol. B Biol. 150 (2015), <http://dx.doi.org/10.1016/j.jphotochem.2015.04.021>.
- N. Masilela, P. Kleyi, Z. Tshentu, G. Priniotakis, P. Westbroek, T. Nyokong, Dyes Pigments 96 (2013) 500–508, <http://dx.doi.org/10.1016/j.dyepig.2012.10.001>.
- V. Mantareva, V. Kussovski, I. Angelov, D. Wöhrle, R. Dimitrov, E. Popova, S. Dimitrov, Photochem. Photobiol. Sci. 10 (2011) 91–102, <http://dx.doi.org/10.1039/B9PP00154A>.
- L. Marciel, L. Teles, B. Moreira, M. Pacheco, L.M.O. Lourenço, M.G.P.M.S. Neves, J.P.C. Tomé, M.A.F. Faustino, A. Almeida, Future Med. Chem. 9 (2017), <http://dx.doi.org/10.4155/fmc-2016-0217>.
- O.L. Osifeko, I. Uddin, P.N. Mashazi, T. Nyokong, New J. Chem. 40 (2016) 2710–2721, <http://dx.doi.org/10.1039/C5NJ01922B>.
- Y. Gerasymchuk, A. Lukowiak, A. Wedzynska, A. Kedziora, G. Bugla-Ploskonska, D. Piatek, T. Bachanek, V. Chernii, L. Tomachynski, W. Strek, J. Inorg. Biochem. 159 (2016) 142–148, <http://dx.doi.org/10.1016/j.jinorgbio.2016.02.019>.
- E. Feese, R.A. Ghiladi, J. Antimicrob. Chemother. 64 (2009) 782–785, <http://dx.doi.org/10.1093/jac/dkp278>.
- Ü. İçi, M. Beyreis, N. Tortik, S.Z. Topal, M. Glueck, V. Ahsen, F. Dumoulin, T. Kiesslich, K. Plaetzer, Photodiagn. Photodyn. Ther. 13 (2016) 40–47, <http://dx.doi.org/10.1016/j.pdpdt.2015.10.010>.
- I. Maliszewska, W. Kałas, E. Wysockińska, W. Tylus, N. Pietrzyk, K. Popko, K. Palewska, Lasers Med. Sci. (2017), <http://dx.doi.org/10.1007/s10103-017->

- 2337-0.
- [39] E. Mannucci, S. Genovese, M. Monami, G. Navalesi, F. Dotta, R. Anichini, F. Romagnoli, G. Gensini, *Acta Diabetol.* 51 (2014) 435–440, <http://dx.doi.org/10.1007/s00592-013-0533-3>.
- [40] J. Długaszewska, W. Szczolko, T. Koczorowski, P. Skupin-Mrugalska, A. Teubert, K. Konopka, M. Kucinska, M. Murias, N. Düzgüneş, J. Mielcarek, T. Gosliński, J. *Inorg. Biochem.* 172 (2017), <http://dx.doi.org/10.1016/j.jinorgbio.2017.04.009>.
- [41] Y. Zhang, K. Zheng, Z. Chen, J. Chen, P. Hu, L. Cai, Z. Iqbal, M. Huang, *Appl. Microbiol. Biotechnol.* 101 (2017), <http://dx.doi.org/10.1007/s00253-017-8133-8>.
- [42] A.P.D. Ribeiro, M.C. Andrade, J. de Fátima, J.H. da Silva, F.L. Jorge, A.C. Primo, A.C. Pavarina Tedesco, *Photochem. Photobiol.* 89 (2013) 111–119, <http://dx.doi.org/10.1111/j.1751-1097.2012.01198.x>.
- [43] A.P.D. Ribeiro, M.C. Andrade, V.S. Bagnato, C.E. Vergani, F.L. Primo, A.C. Tedesco, A.C. Pavarina, *Lasers Med. Sci.* 30 (2015) 549–559, <http://dx.doi.org/10.1007/s10103-013-1354-x>.
- [44] G.B. Rodrigues, F.L. Primo, A.C. Tedesco, G.U.L. Braga, *Photochem. Photobiol.* 88 (2012) 440–447, <http://dx.doi.org/10.1111/j.1751-1097.2011.01055.x>.
- [45] K. Kalyanasundaram, M. Neumann-Spallart, *J. Phys. Chem.* 86 (1982) 5163–5169, <http://dx.doi.org/10.1021/j100223a022>.
- [46] T.A. Skwor, S. Klemm, H. Zhang, B. Schardt, S. Blaszczyk, M.A. Bork, *J. Photochem. Photobiol. B Biol.* 165 (2016) 51–57, <http://dx.doi.org/10.1016/j.jphotobiol.2016.10.016>.
- [47] R. Pelton, *TrAC Trends Anal. Chem.* 28 (2009) 925–942, <http://dx.doi.org/10.1016/j.trac.2009.05.005>.
- [48] R. Pelton, *Nord. Pulp Pap. Res. J.* 8 (1993) 113–119, <http://dx.doi.org/10.3183/NPPRJ-1993-08-01-p113-119>.
- [49] J. Su, C.J. Garvey, S. Holt, R.F. Tabor, B. Winther-Jensen, W. Batchelor, G. Garnier, *J. Colloid Interface Sci.* 448 (2015) 88–99, <http://dx.doi.org/10.1016/j.jcis.2015.02.008>.
- [50] E.I. Yslas, E.N. Durantini, V.A. Rivarola, *Bioorg. Med. Chem.* 15 (2007) 4651–4660, <http://dx.doi.org/10.1016/j.bmc.2007.03.079>.
- [51] M. Pişkin, *Polyhedron* 104 (2016) 17–24, <http://dx.doi.org/10.1016/j.poly.2015.11.017>.
- [52] M.A. Griffiths, B.W. Wren, M. Wilson, *J. Antimicrob. Chemother.* 40 (1997) 873–876, <http://dx.doi.org/10.1111/j.1601-5223.1959.tb03062.x>.
- [53] N. Masilela, T. Nyokong, *J. Lumin.* 130 (2010) 1787–1793, <http://dx.doi.org/10.1016/j.jlumin.2010.04.011>.
- [54] J.D. Huang, W.P. Fong, E.Y.M. Chan, M.T.M. Choi, W.K. Chan, M.C. Chan, D.K.P. Ng, *Tetrahedron Lett.* 44 (2003) 8029–8032, <http://dx.doi.org/10.1016/j.tetlet.2003.07.007>.
- [55] J.D. Huang, P.C. Lo, Y.M. Chen, J.C. Lai, W.P. Fong, D.K.P. Ng, *J. Inorg. Biochem.* 100 (2006) 946–951, <http://dx.doi.org/10.1016/j.jinorgbio.2005.12.004>.
- [56] P.-C. Lo, S.C.H. Leung, E.Y.M. Chan, W.-P. Fong, W.-H. Ko, D.K.P. Ng, *Photodiagn. Photodyn. Ther.* 4 (2007) 117–123, <http://dx.doi.org/10.1016/j.pdpdt.2007.03.001>.
- [57] O.L. Osifeko, T. Nyokong, *Dyes Pigments* 111 (2014) 8–15, <http://dx.doi.org/10.1016/j.dyepig.2014.05.010>.
- [58] M. Durmuş, T. Nyokong, *Tetrahedron* 63 (2007) 1385–1394, <http://dx.doi.org/10.1016/j.tet.2006.11.089>.
- [59] C. Spagnol, L.C. Turner, F. Giuntini, J. Greenman, R.W. Boyle, J. Mater. Chem. B 5 (2017) 1834–1845, <http://dx.doi.org/10.1039/C6TB03198F>.
- [60] C. Ringot, V. Sol, R. Granet, P. Krausz, *Mater. Lett.* 63 (2009) 1889–1891, <http://dx.doi.org/10.1016/j.matlet.2009.06.009>.
- [61] C. Ringot, V. Sol, M. Barrière, N. Saad, P. Bressollier, R. Granet, P. Couleaud, C. Frochot, P. Krausz, *Biomacromolecules* 12 (2011) 1716–1723, <http://dx.doi.org/10.1021/bm200082d>.
- [62] B.L. Carpenter, F. Scholle, H. Sadeghifar, A.J. Francis, J. Boltersdorf, W.W. Weare, D.S. Argyropoulos, P.A. Maggard, R.A. Ghiladi, *Biomacromolecules* 16 (2015) 2482–2492, <http://dx.doi.org/10.1021/acs.biomac.5b00758>.
- [63] B.L. Carpenter, E. Feese, H. Sadeghifar, D.S. Argyropoulos, R.A. Ghiladi, *Photochem. Photobiol.* 88 (2012) 527–536, <http://dx.doi.org/10.1111/j.1751-1097.2012.01117.x>.
- [64] J.P. Mbakidi, K. Herke, S. Alvès, V. Chaleix, R. Granet, P. Krausz, S. Leroy-Lhez, T.S. Ouk, V. Sol, *Carbohydr. Polym.* 91 (2013) 333–338, <http://dx.doi.org/10.1016/j.carbpol.2012.08.013>.
- [65] E. Feese, H. Sadeghifar, H.S. Gracz, D.S. Argyropoulos, R.A. Ghiladi, *Biomacromolecules* 12 (2011) 3528–3539, <http://dx.doi.org/10.1021/bm200718s>.
- [66] J. Mosinger, O. Jirsák, P. Kubát, K. Lang, B. Mosinger, *J. Mater. Chem.* 17 (2007) 164, <http://dx.doi.org/10.1039/b614617a>.
- [67] J. Mosinger, K. Lang, P. Kubát, J. Sýkora, M. Hof, L. Plíštil, B. Mosinger, *J. Fluoresc.* 19 (2009) 705–713, <http://dx.doi.org/10.1007/s10895-009-0464-0>.
- [68] S. Jesenská, L. Plíštil, P. Kubát, K. Lang, L. Brožová, Š. Popelka, L. Szatmáry, J. Mosinger, *J. Biomed. Mater. Res. A* 99 A (2011) 676–683, <http://dx.doi.org/10.1002/jbm.a.33218>.
- [69] M. Arenbergerova, P. Arenberger, M. Bednar, P. Kubat, J. Mosinger, *Exp. Dermatol.* 21 (2012) 619–624, <http://dx.doi.org/10.1111/j.1600-0625.2012.01536.x>.
- [70] Y. Lhotáková, L. Plíštil, A. Morávková, P. Kubát, K. Lang, J. Forstová, J. Mosinger, *PLoS One* 7 (2012) e49226, <http://dx.doi.org/10.1371/journal.pone.0049226>.
- [71] A. Goethals, T. Mugadza, Y. Arslanoglu, R. Zugle, E. Antunes, S.W.H. Van Hulle, T. Nyokong, K. De Clerck, *J. Appl. Polym. Sci.* 131 (2014) 1–7, <http://dx.doi.org/10.1002/app.40486>.
- [72] S. Stanley, F. Scholle, J. Zhu, Y. Lu, X. Zhang, X. Situ, R. Ghiladi, *Nano* 6 (2016) 77, <http://dx.doi.org/10.3390/nano6040077>.
- [73] J. Dolansky, P. Henke, P. Kubat, A. Fraix, S. Sortino, J. Mosinger, *ACS Appl. Mater. Interfaces* 7 (2015) 22980–22989, <http://dx.doi.org/10.1021/acsami.5b06233>.
- [74] P. Henke, K. Lang, P. Kubát, J. Sýkora, M. Šlouf, J. Mosinger, *ACS Appl. Mater. Interfaces* 5 (2013) 3776–3783, <http://dx.doi.org/10.1021/am4004057>.
- [75] R. Bonnett, A. Galia, *Biotechnol. Biotechnol. Equip.* 8 (1994) 68–74, <http://dx.doi.org/10.1080/13102818.1994.10818756>.

Tampereen teknillinen yliopisto
PL 527
33101 Tampere

Tampere University of Technology
P.O.B. 527
FI-33101 Tampere, Finland

ISBN 978-952-15-4156-8

ISSN 1459-2045